Intracellular peptide library screening to derive inhibitors of Parkinson's disease associated α-synuclein aggregation

Harish Cheruvara

A thesis submitted for the degree of Doctor of Philosophy

Department of Biological Sciences

University of Essex

September 2015

Acknowledgements

First of all, I would like to extend my deepest gratitude to my supervisors Dr. Jody Mason and Dr. Neil Kad, for their valuable support, understanding, patience, advice and guidance without whom this PhD could not have been achieved. I am very thankful to them for getting me the scholarship and giving me an opportunity to fulfil my dream. I would like to thank the Parkinson's UK for funding my PhD program.

I would like to extend my sincere thanks to the members of Jody's and Neil's lab, with whom I have shared many of my PhD hurdles and fun times. My deepest gratitude goes to Dr. Nicola Acerra, Dr. Michelle Simons, Dr. Miao Yu and Dr. Victoria Allen Baume for their valuable advices and guidance. Special thanks to all my friends from other labs, teaching staffs and technical members of Biological Sciences department for their support.

I am expressing my sincere thanks and love to my beloved wife, Mrs. Madhavi Harish for her support, love and caring throughout my tough times. I also thank my Parents and brother who have always been the greatest support and guidance for me. I would like to thank all my friends, cousins, and extended relatives back home.

Publications

Cheruvara, H., Allen-Baume, V.L., Kad, N.M., and Mason, J.M. (2015) Intracellular screening of a peptide library to derive a potent inhibitor of α-synuclein aggregation. *The Journal of Biological Chemistry* 290 (12), 7426-7435.

Acerra, N., Kad, N.M, Cheruvara, H., and Mason, J.M. (2014) Intracellular selection of peptide inhibitors that target disulphide-bridged $A\beta_{42}$ oligomers. *Protein Science* 23, 1262-1274.

Poster presentation

1. Graduate Forum at University of Essex, Colchester, September 2012- won best poster prize.
2. Parkinson's UK conference, York, November 2012- 'Combining semi rational design and intracellular selection to generate peptide antagonists of α-synuclein aggregation' - Harish Cheruvara and Jody Mason

Oral presentation

1. Graduate Forum at University of Essex, Colchester, September 2013-
2. Parkinson's UK local branch, Ipswich, September 2014- 'Are Lewy bodies the bad guys in Parkinson's?'- Harish Cheruvara and Jody Mason.
3. 3 Minute competition, University of Essex, Colchester, April 2015- 'Parkinson's Disease'

Abstract

Aggregation of α-synuclein (α-syn) into toxic fibrils is a pathogenic hallmark of Parkinson's disease (PD). This research aimed to develop peptides capable of inhibiting α-syn aggregation using a semi-rational design combined with a multiplexed intracellular Protein-fragment Complementation Assay (PCA) library screening system. Successfully selected peptides must bind to full length α-syn and lower its toxicity to confer bacterial growth. PCA selected peptides were characterized using several biophysical assays and a cell viability assay. The peptides were screened using library templates based on α-syn$_{71-82}$ initially and later on the α-syn$_{45-54}$ region in which many key mutations associated with early onset PD are found. In both cases we targeted the peptide libraries at the wild type protein or again by using mutated versions of α-syn. Results demonstrate that some of those selected peptides had the effect of delaying or even preventing the aggregation process, with others providing more subtle effects in reversing the fully formed amyloid fibrils. PCA peptides selected against 71-82 region of wild type α-syn showed a moderate level of efficacy whereas against mutants, it showed a low level of efficacy in inhibiting amyloid fibril formation. In the final part of the study, the peptide selected against 45-54 region of wild type α-syn was capable of preventing the aggregation and reducing the amyloid cytotoxicity at an equimolar ratio. We have thus demonstrated that the PCA strategy can be used as a generalised method for deriving peptide antagonists of α-syn aggregation, together with a new region; α-syn$_{45-54}$ as an inhibitor target and produced a peptide inhibitor expected to provide a scaffold for future drug candidates to slow or even prevent the onset of PD.

List of abbreviations

PD	Parkinson's disease
AFM	Atomic Force Microscopy
α-syn	Alpha-synuclein
Amp	Ampicillin
APS	Ammonium per sulphate
CD	Circular Dichroism
Cm	Chloramphenicol
ddH_2O	Double distilled water
DMSO	Dimethylsulfoxide
DNA	Deoxyribonucleic acid
dNTPs	Deoxynucleotide Triphosphate
DTT	Dithiothreitol
EDTA	Ethylenediaminetetraacetic acid
EtOH	Ethanol
FBS	Fetal bovine serum
FDU	Fast digest unit
HFIP	Hexofluoro-2-propanol
HRP	Horseradish Peroxidase
IPTG	Isopropylthiogalactoside
Kan	Kanamycine
kDa	Kilo Dalton

KPP	Potassium Phosphate buffer
LA	LB-Agar
LB	Luria Bertani
LBs	Lewy Bodies
L-DOPA	Levodopa
LN	Lewy Neurites
M9	M9 Minimal Media
M9A	M9-Agar
MAO-B	Monoamine oxidase-B
MAP	Microtubule associated protein
mAu	Milli Absorbance unit
mdeg	Millidegrees
mDHFR	Murine dihyrdofolate reductase
MetOH	Methanol
µl	Microliter
mg	Milligram
ml	Milliliter
MTT	3-(4, 5-dimethylthiazol-2-yl)-2, 5-diphenyltetrazolium bromide
NAC	Non-amyloid β component
NMR	Nuclear Magnetic Resonance
OD	Optical Density
PBS	Phosphate buffered saline

PCA	Protein-fragment Complementation Assay
PCR	Polymerase Chain Reaction
PPI	Protein-protein interaction
rpm	Rotations per minute
SDS	Sodium dodecyl sulfate
SDS PAGE	Sodium dodecyl sulfate polyacrylamide gel electrophoresis
TAE	Tris-Acetate EDTA
TEMED	Tetramethylethylenediamine
Tet	Tetracycline
ThT	Thioflavin T
Tmp	Trimethoprim
Tris	Tris (hydroxymethyl)-aminomethan
2XYT	2X Yeast Extract Tryptone medium

Aminoacids

Ala (A)	Alanine
Arg (R)	Arginine
Asn (N)	Asparagine
Asp (D)	Aspartic acid
Cys (C)	Cysteine
Gln (Q)	Glutamine
Glu (E)	Glutamic acid
Gly (G)	Glycine

His (H)	Histidine
Ile (I)	Isoleucine
Leu (L)	Leucine
Lys (K)	Lysine
Met (M)	Methionine
Phe (F)	Phenylalanine
Pro (P)	Proline
Ser (S)	Serine
Thr (T)	Threonine
Trp (W)	Tryptophan
Tyr (Y)	Tyrosine
Val (V)	Valine

Contents

Chapter 2: Materials and Methods

List of Figures

Chapter 1

Chapter 3

Chapter 4

Chapter 5

List of Tables

Chapter 2

Chapter 3

Chapter 4

List of Equations

Chapter 2

Chapter 1: Introduction

1.1 Parkinson's disease

Parkinson's disease (PD) is a neurodegenerative disorder that is caused by the loss of dopamine producing neurons. The symptoms of PD include movement disorders, tremor (involuntary shaking of particular parts of the body), rigidity due to stiff and inflexible muscles, slowness of movement, walking difficulty and gait. Neuropsychiatric (cognitive, behavioural, sensory, sleep, emotional) problems may also arise in the advanced stages of the disease which eventually leads to dementia. It has been estimated that one in every 500 individuals has PD, leading to about 127,000 cases in the UK (Parkinson's UK, 2015). The average age of onset for PD is 50 or over, but it is also found in younger people, with one in 20 patients under the age of 40. In particular, PD is caused by the death of dopaminergic neurons in the ventral component of pars compacta region within the substantia nigra of the mid brain. The substantia nigra plays an important role in reward, addiction and movement. It consists of two parts, the pars compacta and the pars reticulata, in which the former serves as input to the basal ganglia circuit, supplying the dopamine and the latter serves as output, conveying signals to other brain structures (Damier *et al*., 1999). The most important function of the pars compacta is motor control. The depletion of dopaminergic neurons in this region causes PD symptoms which usually do not appear until up to 50-80 % of neuronal death occurs (Parkinson's UK, 2015). PD is one among many age related disorders that are thought to be caused by amyloid fibrils. There is a growing body of evidence that suggests that neuronal death in PD is due to amyloid fibrils comprising a protein known as α-synuclein (α-syn) (Gallea and Celej., 2015; Chiti and Dobson., 2006; Yagi *et al*., 2005; Conway *et al*., 2000; Takeda *et al*., 1998; Spillantini *et al*., 1997). Misfolding and

loss of function of this normally soluble functional protein leads to the formation of thread-like, well-defined amyloid structures. Amyloid fibrils are composed of β-sheets with intermolecular interactions, oriented perpendicularly to the fibril axis (Serpell, 2000). Most proteins fold as they are being synthesised on the ribosome. A wide range of molecular chaperones in the ER and Golgi apparatus are involved in the guidance of the folding process in order to avoid the untimely interaction of protein in the cell environment. If a protein misfolds by chance, it will be directed into the ubiquitin-proteasome degradation system and autophagy (Pirkkala *et al*., 2000). Some proteins with a high tendency to misfold are able to bypass all these protective mechanisms and form insoluble aggregates in the tissues. Protein misfolding can give rise to the abnormal functioning of the cell and leads to disease (Knowles *et al*., 2014).

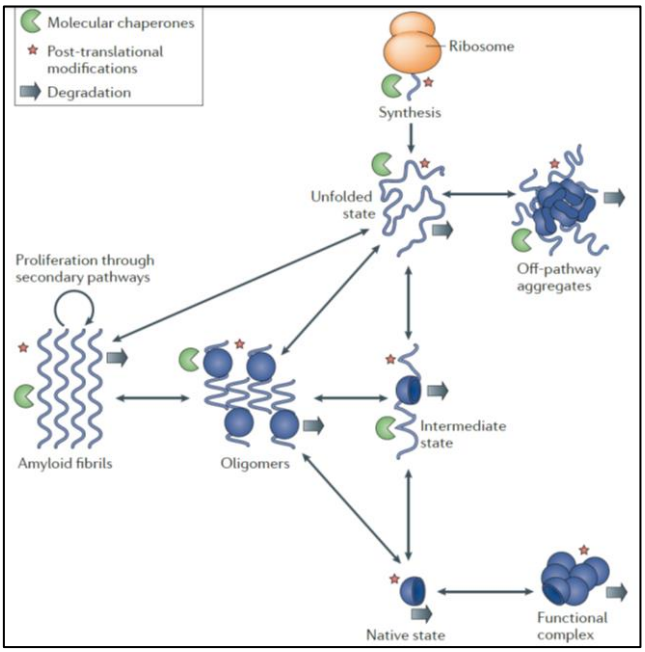

Figure 1.1: The different states in which a protein can exist during its synthesis-degradation mechanism. Inter-conversion rates are determined by various thermodynamic factors and free energy barriers thereby determining the rate of synthesis and degradation (Image source: Knowles *et al*., 2014).

PD is one of a collection of α-synucleinopathies, with others including dementia with Lewy bodies (LBs), and multiple system atrophy (McCann *et al*., 2014). All these diseases are characterized by misfolding and aggregation of α-syn in the dopaminergic neurons. α-syn aggregation causes neuronal inclusion deposits known as 'Lewy bodies' (LBs) which are the most distinctive neuropathological feature of PD. 'Lewy neurites' (LNs) also coexist with LBs in PD, which are abnormal neurites (projections from the axons or dendrites) containing α-syn filaments (Spillantini *et al*., 1998; Kanazawa *et al*.,2008). The deposition of LBs or LNs leads to neuronal cell death in PD.

1.2 Genetics of PD and Parkinsonism

Studies estimate that only 5 % of PD cases may be inherited which is rare compared to idiopathic PD (Parkinson's UK, 2015). However, the mutations found in the ***SNCA*** gene [α-syn (PARK 1/4)] that cause familial PD are typically mis-sense in which single nucleotides are changed, or are duplications and triplications of the ***SNCA*** containing locus. The known ***SNCA*** mutations lead to protein aggregation, LB/LN formation and neuronal cell death which are a significant in the early onset of PD symptoms in patients carrying familial α-syn mutants (Giasson *et al.,* 2000; Singleton *et al*., 2003; Berg *et al*., 2005; Lesage *et al.*, 2009). A clinical definition of a variety of movement related disorders of which PD is just one is known as Parkinsonism. The other genes involved in Parkinsonism are: ***LRRK2*** [Leucine rich repeat kinase 2/ dardarin (PARK8)], ***PRKN*** [parkin (PARK2)], ***PINK1*** (PARK6), ***DJ-1*** (PARK7) (Hardy *et al.*, 2006). The LRRK2 gene encodes two distinct enzymes, a protein kinase and a GTPase. The mutations (G2019S, R1441G and I2020T) on LRRK2 enhance its kinase activity relative to the wild type protein. An increase in the kinase activity leads to neuronal toxicity, but in some cases the cell death is not identified as a result of inclusion body formation

(Khan *et al*., 2005; Mata *et al.*, 2006; Masso *et al*., 2015). The natural known function of parkin is as an E3 ligase that can control protein turnover via ubiquitin chain addition, whereas PINK1 functions as a mitochondrial serine/threonine kinase, and the DJ1 functions as anti-oxidant thereby protecting cells against mitochondrial damage. The mutations in these genes which cause its loss of function lead to early onset of Parkinsonism (Hardy *et al.*, 2006). When the substantia nigra is severely affected it can lead to Parkinsonism whereas when Lewy pathology and associated cell loss are seen in any other parts of the brain (e.g.: the cortex), the predominant symptoms would lead to dementia (Hardy *et al.*, 2006). The mutations in the parkin gene are known to be linked to some forms of early onset of PD (diagnosed under the age of 40). The mutation in DJ-1 is found to be linked with some inherited forms of PD. The parkin, PINK1, and DJ-1 gene mutations are related with Parkinsonism with limited evidence of protein inclusion body formation (Lucking *et al*., 2000; Bonifati *et al*., 2002; Mata *et al.*, 2006).

1.3 Structure and Role of α-syn

α-syn is a neuronal protein with a molecular weight of 14 kDa, containing 140 amino acids, encoded by the ***SNCA*** gene (Serpell *et al*., 2000; Baba *et al*., 1998; Spillantini *et al*., 1997). The structure of α-syn has three domains; the N-terminal region consists of ***(i)*** an amphipathic region (1-60) and ***(ii)*** a hydrophobic non amyloid component (NAC) region (61-95). The C-terminal comprises of ***(iii)*** an acidic proline rich region (96-140) (Fig 1.2).

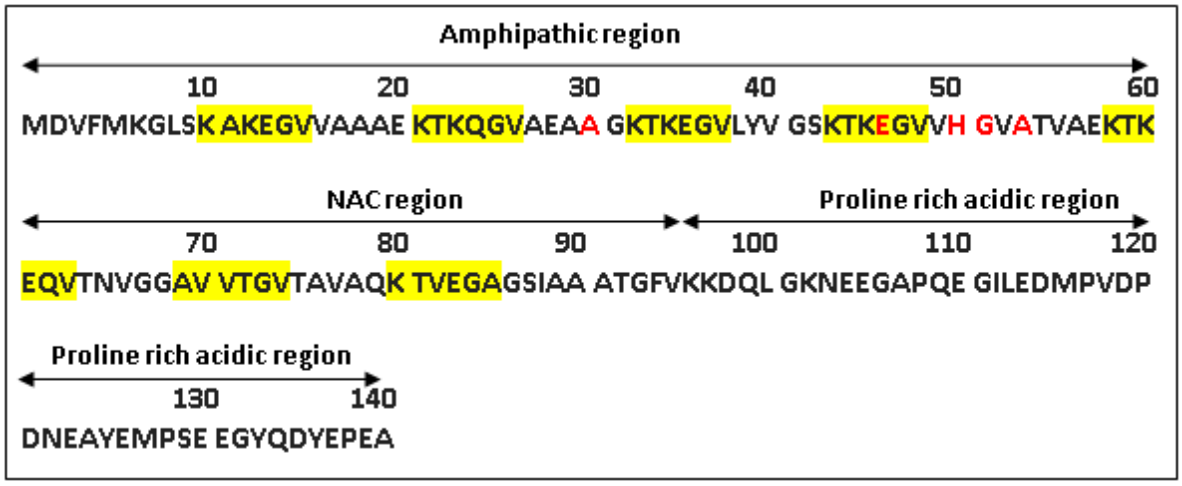

Figure 1.2: α-syn residues: consisting of three overlapping regions, N-terminal amphipathic and hydrophobic NAC region along with acidic C-terminal region. The seven 11-mer imperfect sequences (XKTKEGVXXXX) containing highly conserved KTKEGV hexameric motif (highlighted in yellow) are believed to be involved in lipid interaction, NAC region in aggregation and C-terminal region for binding of different ions and proteins. The residues highlighted in red are where point mutations (A30P, E46K, H50Q, G51D and A53T) identified associated with the early onset of PD.

The 12 amino acid sequence (^{71}VTGVTAVAQKTV^{82}) found in the middle of the hydrophobic region is widely identified to be responsible for the fibril formation (Bedard *et al*., 2014; Waxman *et al*., 2009; Giasson *et al.*, 2001). Structural studies show that α-syn is monomeric and natively unfolded in the solution (Vilar *et al*., 2008; Lundvig *et al*., 2005; Uversky et al., 2002). The N-terminal region forms an α-helical conformation upon interaction with phospholipid membranes. α-syn forms cross β-amyloid structures spontaneously when exposed to various physical and chemical factors. In the cross β structure, the central spine of fibril is formed by stacking of intermolecular β-sheets. The hydrogen bonds that connect β-strands into a pleated β-structure are aligned parallel to the fibril axis and the side chains define the intra-intermolecular interactions within the plane of the fibril cross-section

(Fandrich *et al*., 2009). This structural conversion of a natively unfolded structure to cross-β amyloid structure leads to α-syn toxicity in PD.

There are some structural ambiguities of native α-syn which remain as a critical challenge to understand PD pathology. Recent studies suggested that, α-syn is able to form a stable helically folded tetrameric structure which is able to resist aggregation (Wang *et al*., 2011; Bartels *et al*., 2011). According to their studies, the higher lipid binding capacity of α-syn confirms that the monomer species is not fully functional and is found less abundant in the normal cells. According to Wang (2011), the tetrameric structure does not perforate membranes unlike oligomeric α-syn. The proposed tetramer is believed to undergo destabilization before the formation of α-syn aggregates as abnormal oligomeric and fibrillar assemblies that induce cytotoxicity in PD. Thus the stabilisation of tetrameric structure and prevention of α-syn from aggregation and toxicity, may lead to a significant therapeutic strategy against PD. In addition, the structure of α-syn depends on subunit concentration and environmental factors. Perturbations caused by physical factors or disease associated mutations enhance its aggregation propensity.

1.4 Expression and Normal Function of α-syn in the Brain

α-syn is predominantly expressed in the neocortex, hippocampus, substantia nigra, thalamus and cerebellum of the brain. In mammalian neurons, it is extensively localized in the nucleus (Yu *et al.,* 2007) and in the pre-synaptic termini in both free or membrane bound forms (Lee *et al.,* 2002). Recent studies showed that α-syn has been localized in neuronal mitochondria found in olfactory bulb, hippocampus, striatum, and thalamus. However, the cerebral cortex and cerebellum have more cytosolic, but less mitochondrial α-syn (Liua *et al.,* 2009). α-syn located in the synaptic nerve terminals, functions mainly in the

vesicular homeostasis and neurotransmission. It exists as monomeric form in cytosolic pool where as both monomeric and oligomeric species in the pool associated with synaptic vesicle. The protein dissociates from the vesicles and re-associates slowly during synaptic activity when there is an electrical stimulation inside the neurons. α-syn concentration is also a key factor in determining the complex I activity of mitochondrial respiratory chain (Fortin *et al.,* 2005). It can also bind to lipids and is associated with plasma membrane interactions (Jo *et al*., 2000; Eliezer *et al*., 2001). The impairment in the folding/unfolding mechanisms of α-syn due to several factors lead to the formation and accumulation of LB inside the dopaminergic neurons. Thus its unavailability during the formation of synaptic vesicles (for the storage of dopamine) at pre-synaptic terminal leads to the mis-regulation of dopamine pathway (Fig 1.3) and finally to the movement related symptoms of PD (Mizuno *et al.* 2008).

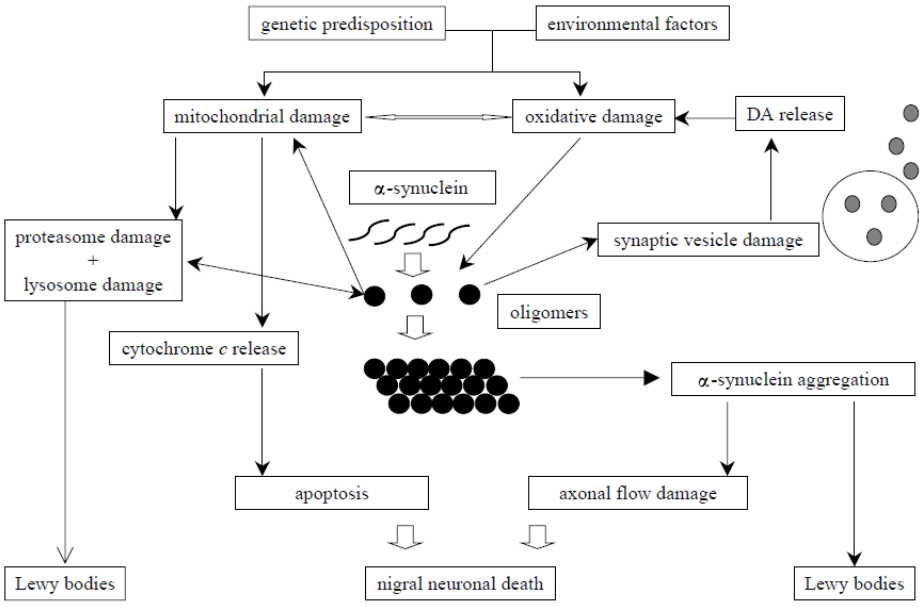

Figure 1.3: Schematic representation of substantia nigral neuronal death in PD. The various genetic and environmental risk factors initiate the pathological sporadic PD while the SNCA point mutations lead to mutant α-syn causes familial PD. DA: dopamine (Image source: Mizuno *et al.* 2008)

1.5 Aggregation of α-syn

α-syn aggregation *in vitro* is found to be a nucleation dependent process which demands a minimum concentration of monomers required under which there would be no aggregation. The aggregation is characterized by; ***(i)*** a slow nucleation phase or lag phase where the protein undergoes various thermodynamically unfavourable steps to oligomeric nuclei, ***(ii)*** a growth phase or an elongation phase where rapid association of monomers into the cross-β structure nuclei when the monomeric concentration reaches a threshold, and ***(iii)*** a saturation/stationary phase where there exists an equilibrium between soluble α-syn species and insoluble aggregates (Fig 1.4). A recent study shows that once a critical concentration of small amyloid fibrils seen to be accumulated, the further toxic species are primarily formed by a fibril-mediated secondary nucleation reaction rather than classical primary nucleation mechanism (Cohen *et al*., 2013). Thus an addition of nucleation competent filaments to α-syn reaction mixture above the critical concentration can reduce the lag phase, so called '*seeding'* in which monomers can attach, and elongate into fibrils (Lundvig *et al.*, 2005).

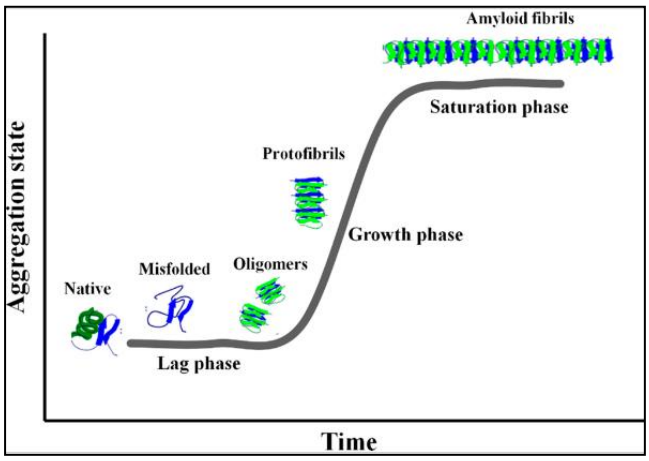

Figure 1.4: Nucleation dependent α-syn fibrillisation process showing three phases ***(i)*** lag phase (aggregation of misfolded monomers into intermediate oligomeric species) ***(ii)*** growth phase (re-

arrangement oligomers into an organized cross-β conformation), and ***(iii)*** a saturation phase (formation of proto-fibrils and finally into fibrils). Several factors can reduce the lag phase and stimulate the aggregation (Image source: Iannuzzi *et al.*, 2015).

Oligomers which can dissociate into monomers and simultaneously re-associate into larger assemblies are formed during the aggregation progresses. These oligomers which are more likely to be unfolded, with a lower amount of secondary structure are also identified to re-associate as toxic cross-β structure. Along with fibrils, the assembly of these toxic oligomers are also found to be involved in the pathogenesis of PD (Roberts *et al*., 2015; Kalia *et al*., 2013; Winner *et al*., 2011; Outeiro *et al*. 2008). The oligomeric species can be stabilized through covalent cross linking techniques; and it can be analysed using SDS PAGE or size exclusion chromatography. Studies have been undertaken using novel proximity ligation assay (PLA) which selectively detects oligomeric forms of α-syn in neuro-anatomical areas relevant to early PD pathology (Roberts *et al*., 2015). The *in vitro* transition of oligomers into amyloid fibrils occurs during a maturation process. α-syn can form fibrils with 5-10 nm in height, 10-20 nm wide and ~500 nm to 2.5 μm length as characterised by atomic force microscopy and electron microscopy (Khurana *et al*., 2003). The fibril structure can be studied by dye binding assays, microscopic and spectroscopic studies. The filaments formed *in vitro* are usually found to be straight, unbranched (homo-aggregate) similar to that found in LB and glial cytoplasmic inclusions. Although in some cases due to the association of α-syn aggregate binding proteins, the filaments can form mesh like structures possessing frequent branching. It shows that several protein factors could have been involved in the α-syn aggregation *in vivo* (Lundvig *et al.*, 2005).

The functional effect of α-syn aggregation includes dysregulation of the microtubule network which is very important for the long transport pathways in the axons. The microtubule-associated proteins, such as MAP-1A, MAP-1B, tau, and p25α have been identified in LB along with α-syn. An increased concentration of MAP-1B, tau and p25α enhances α-syn aggregation. The mis-functioning of α-syn expression causes its interaction with p25α and leads to their co-localization as oligodendroglial cytoplasmic inclusions which are commonly seen in neuronal LB in PD. The transcriptional factors NF-kB and Elk-1 have been also found in LB. High Mobility Group B-1 protein (HMGB-1) has been found to bind directly with α-syn *in vitro* and also found as a component in LB. α-syn oligomers result an increased permeability of calcium ions in liposomes. The membrane permeabilisation *in vivo* is still not clear, but it may be due to the existence of its structural similarity with the bacterial pore forming toxins. It disturbs the ionic homeostasis inside the cells by forming pores in the membrane and thus leads to the cell lysis (Lundvig *et al.*, 2005). The accumulation of ubiquitinated proteins found in the LB shows an imbalance between the proteasome production and its catabolic capacity. Dysregulated ubiquitin-proteasome system is found in most α-synucleinopathies. A decreased level of certain proteasomal subunits and an impaired function of chymotrypsin-, trypsin-, and caspase- like activities of proteasomes have been investigated in PD. In contrast, some studies show that the ubiquitinated α-syn in LB pathology is found to have partly phosphorylated and not complete impairment of proteolytic activity of proteasome occurs (Tofaris *et al.*, 2003). The misfolded α-syn also shows resistance to proteinase-K digestion in PD (Neumann *et al.*, 2002).

1.6 Factors causing α-syn aggregation

Various chemical and physical factors such as mis-sense mutations in the N-terminal regions, a number of post translational modifications in the 20 residue C-terminal region (truncation, nitration, phosphorylation or methionine oxidation), concentration, pH, temperature, ionic strength, metals, lipids, pesticides, and other proteins are found to have important roles in controlling α-syn in its membrane binding, aggregation and toxicity properties.

The N-terminal region is relatively inaccessible to the post translational modifications due to its interaction with the membranes. Rare familial point mutations such as A53T, A30P, E46K along with recently identified H50Q and G51D have been recognized in the formation of amyloid fibrils that contribute to the early onset of PD. These mutations are seen to increase the β–sheet propensity of α-syn (Spira *et al*., 2001; Zarrenz *et al*., 2004; Greenbaum *et al.*, 2005; Ki *et al*., 2007; Seidel *et al*., 2010; Cresswell *et al*., 2013; Proukakis *et al*., 2013; Lesage *et al*., 2013; Rutherford *et al*., 2014). Though the wild type α-syn and all mutants possess identical structural properties and conformational behaviour, the propensity to form aggregates is strongly enhanced by the familial PD point mutations (Scira *et al*., 2013; Li *et al*., 2001). Hydrophobic interactions are observed to play an important role in aggregation as a decreased hydrophobicity leads to an increased aggregation propensity. For instance, A30P and A53T cause the reduction of hydrophobicity relative to the wild type α-syn (Li *et al*., 2001). Some mutations like E46K can cause a change in the net charge of α-syn and the replacement of an existing residue that stabilizes the structure which can lead to increased β-sheet propensity (Scira *et al*., 2013; Rospigliosi *et al*., 2009; Uversky *et al*., 2000). The point mutations can reduce α-helical propensity of N-terminal region which actively participates in lipid binding makes the mutants more likely to form β-sheet structure. The point

mutations might not be involved in conformational change but can affect the nature and rate of α-syn aggregation.

A wide range of post translational modifications of α-syn in the pathological nerve cell lesions and brain tissue have been identified which increases its β-sheet propensity. Some modifications are found in the C-terminal region of α-syn. In oxidatively stressed neurons, Tyr-125 in α-syn is found to be phosphorylated, nitrated or aminated suggesting that this residue is highly susceptible to different modifications. In addition, Tyr-133 is identified to be never phosphorylated but nitrated or aminated indicating it is not targeted by kinases (Mirzaei *et al*., 2006). Nitrating agents such as nitric oxide, nitrogen dioxide and peroxynitrite are strong oxidants which induce α-syn aggregation by promoting Tyr oxidation (Periquet *et al*., 2007). A recent study suggests that Tyr-125 phosphorylation functions as a primary step leads to the phosphorylation of Ser-129 by CK-1 *in vitro* (Kosten *et al*., 2014).

Oxidative stress is believed to aggravate PD pathogenesis. α-syn undergoes enhanced methionine oxidation in oxidatively stressed neurons with impaired mitochondrial complex-I activity (Uversky *et al*., 2002). According to their findings, since α-syn doesn't have Trp or Cys residues, all four Met residues get oxidised to corresponding sulphoxides. The fibrillisation of such oxidised α-syn is inhibited by facilitating the formation of soluble stable oligomers at normal physiological conditions. Though in the presence of a high number of oxidatively stressed neurons along with some environmental metal pollution leads to an enhanced fibrillisation process. In addition to that, the met- oxidized forms of α-syn would not get repaired by methionine sulfoxide reductases leads to its accumulation (Glaser *et al*., 2005; Hald *et al*., 2005; Mirzaei *et al.*, 2006). There is an increase in evidence that calcium

dysregulation and lysosome dysfunction plays an important role in PD pathogenesis. Thus, it may be therapeutic strategy to design calcium channel blockers that may reduce the risk of PD (Pasternak *et al*., 2012; Tofaris, 2012; Mattson, 2012).

Considering the physical factors that influence α-syn aggregation, most *in vitro* investigations are carried out at much higher concentrations in order to reduce the lag phase, under physiological temperature and ionic strength. The lowering of pH enhances the fibrillisation rate as it decreases the lag phase due to the shielding of negative charges by protonation. But a neutral pH is better for *in vitro* studies since the acidic pH may affect the structure of aggregates. An increase in temperature causes the filaments to differ morphologically from that in physiological conditions but it is found to affect the aggregation process (Ariesandi *et al*., 2013). The binding of metals to the acidic residues region corresponding 116 to 136 of α-syn is found to favour the oxidative modifications and thereby increases its aggregation. Various metals are found to influence α-syn aggregation *in vitro*, such as Al^{3+}, Fe^{3+}, Co^{3+}, Mn^{2+}, Ca^{2+}, and Cu^{2+} (Uversky *et al*., 2001). The interaction of Al^{3+} to the acidic C- terminus induces structural perturbations in α-syn which leads to an increased aggregation rate. Some metals are found to inhibit the aggregation effect induced by other metals, for example Mg^{2+} inhibits the iron induced α-syn aggregation (Mirzaei *et al.*, 2006; Uversky *et al*., 2001). Various fatty acids, anionic detergents and anionic lipids are found to enhance the α-syn fibrillisation *in vitro*. Amorphous aggregates and small filaments are formed as a result of interaction between soluble α-syn and planar bi-lipid layers. The recombinant α-syn when exposed to poly unsaturated fatty acids, leads to the formation of SDS resistant multimers. Pesticides induce conformational changes in α-syn and accelerate the formation of α-syn inclusions in the nerve cells. For instance, the effect of paraquat; a

herbicide and rotenone inducing inhibition of mitochondrial complex I, due to oxidative stress and following death of neurons have been studied on various animal models (Maturana *et al*., 2015; Lundvig *et al.*, 2005). α-syn is identified to have high capacity to form non-specific interactions with other proteins. Many proteins are found to accelerate the α-syn aggregation while some shows inhibitory effect on aggregation rate *in vitro*. Proteins such as tau, histones, brain specific protein p25α, and tubulin are found to accelerate the aggregation (Paytona *et al.*, 2001). Except histones all the other proteins have been identified in LB or glial cytoplasmic inclusion components along with α-syn. These interactions of α-syn with other proteins may have effects in the morphology of α-syn aggregates in their branching and interactions with cellular constituents. The presence of non-fibrillogenic human homologues, β-synuclein and γ-synuclein are found to be inhibiting α-syn aggregation *in vitro* (Karyo *et al.*, 2010; Uversky *et al*., 2002; Hashimoto *et al*., 2001). There are some protective proteins expressed by the cells to lessen the proteasomal inhibitory properties of aggregated α-syn. The heat shock protein-70 (hsp-70) and glyceraldehyde-3-phosphate dehydrogenase that binds to α-syn reduces its anti-proteasomal effects (Pirkkala *et al.*, 2000).

1.7 Therapeutic approaches against PD

A better understanding through wide spread research on structure of α-syn and its role in cellular degeneration are yet to be evolved for developing new therapeutic interventions towards this second most dreadful neurodegenerative disorder. There are many studies going on to identify a potential drug to stop or slow down the aggregation of α-syn and thereby mitigate PD symptoms. Most of the inhibitors are found to attach covalently with α-syn. The structural analysis of inhibitor bound α-syn oligomers is essential for the better understanding of the inhibitory mechanism. There are several mechanisms by which compounds can inhibit α-syn fibrillisation: ***(i)*** stabilizing the native state of amyloid, ***(ii)*** blocking the different intermediates on amyloid pathway from their conversion to fibrils, ***(iii)*** alteration of aggregation pathway and leads to the formation of non-amyloidogenic, non-pathogenic aggregates, ***(iv)*** breakdown of toxic fibrils, and ***(v)*** prevention of prion-like spread.

Levodopa (L-DOPA) which has trade names duodopa™, sinemat, atamet, madopar etc is one of the main drugs used currently to alleviate PD symptoms. L-DOPA is co-administered with benserazide (as co-beneldopa) or carbidopa (as co-careldopa) to cross the blood-brain barrier efficiently. The decarboxylation of L-DOPA converts it into dopamine. Although there are some side effects such as nausea, hypotension, insomnia, auditory-visual hallucinations and many more associated with L-DOPA administration, it is found to be effective in alleviating PD symptoms in the early or later stages of disease progression. The oxidation of dopamine is required to stabilize the soluble oligomeric α-syn intermediates and thereby inhibit fibrillisation. This kinetic stabilization is dependent on the non-covalent interaction between oxidised dopamine and the amino acids ^{125}Tyr-Glu-Met-Pro-Ser^{129} of α-syn. This

interaction induces reversible conformational change of α-syn which prevents it from fibrillisation. Dopamine has the ability to auto-oxidize more rapidly than any other compounds containing catechol ring *in vivo* under physiological pH.

In PD, oxidative or nitrative damage of tyrosine hydroxylase (the catecholamine synthesis rate-limiting enzyme) causes a decrease in its catalytic activity, thereby leads to the decrease in catecholamine levels. Studies show that the intracellular catechol levels are critical in the development of PD. An increased cytosolic catechol level can inhibit the formation of α-syn aggregates *in vitro* (Mazzulli *et al.*, 2006). Some molecules such as Catechol O-methyltransferase inhibitors; entacapone and tolcapone have shown some anti-amyloidogenic property that inhibits the α-syn aggregation (Giovanni *et al.*, 2010). It is now available in the market and being used as drugs to alleviate PD symptoms in the early or later stages of progression. There are some drugs which act as dopamine receptor agonist. It includes apomorphine, bromocriptine, cabergoline, lisuride subcutaneous, ropinirole, rotigotine and pramipexole. These drugs are administered at the early or late stages of PD progression. Case studies showed that pramipexole has neuroprotective properties and found to cause a delay in the disease progression (Schapira *et al*., 2014). Another therapeutic intervention against PD is based on monoamine oxidase (MAO) inhibitors. These inhibitors act upon MAO and prevent the breakdown of monoamine neurotransmitters including dopamine and thereby increasing their availability. The common drugs available under this category are selegiline and rasagiline which specifically acts upon MAO-B. Although these drugs can be used in the early stages of PD and also it delays its progression, MAO inhibitors are reserved as a last line of treatment as it causes lethal dietary side effects (Bartl *et al*., 2014; Am *et al*., 2004; Youdim *et al*., 2001). A recent study developed some

neuro-protective agents; arylalkenylpropargylamines against MAO-B marks the survival of PC-12 cells *in vitro* (Huleatt *et al*., 2015). Other drugs administered are zonisamide; which targets the ion channels, rivastigmine; which is an acetylcholinesterase inhibitor, ropinirole and amantadine; both reduce dyskinesias associated with PD (Chan *et al*., 2013; Murata *et al*., 2001; Emre *et al*., 2004; Rascol *et al*., 2000). The role of human silent information regulator-2 (Sir-2 or sirtuins), a nicotinamide adenine dinulceotide-dependent histone deacetylase (HDAC) enzyme in maintaining neuronal cell protection and cell cycle regulation have been widely studied. It protects the axons from its degeneration from increased NAD^+ biosynthesis. There are seven distinct sirtuin proteins, SIRT1 to SIRT7 identified in humans. The selective inhibition of SIRT2 is found to modulate the α-syn toxicity and rescue the neurons from cell death, by reducing the small LB formation. SIRT2 deacetylates α-tubulin at Lys^{40} and enhances the co-localization of tubulin with α-syn in the LB formation. AGK2 (2-cyano-3-[5-(2, 5-dichlorophenyl)-2-furanyl]-N-5-quinolinyl-2-propenamide) found to be an effective inhibitor of SIRT2. AGK2 inhibits the deacetylation activity of SIRT2 and thereby increases the acetylated α-tubulin concentration in the cell (Chen *et al*., 2014; Outeiro *et al.*, 2007). Some poly-aromatic inhibitors like cyclic tetrapyrrole phthalocyanine tetrasulfonate (PcTS) are found to disassemble tau proteins and inhibit α-syn filament assembly eventually leading to non-toxic aggregates. The tetrapyrrolic ring occupied by different metal cations in phthalocyanine moiety and the negatively charged tetrasulfonate groups are responsible for modulating anti amyloidogenic activity of PcTS on α-syn. The anti-amyloid effect exerted by PcTS on α-syn and its mode of interaction depends on the nature of metal ion (PcTS [Ni(II)], PcTS [Zn(II)], and PcTS [Al(III)]) bound to it and the propensity of PcTS species to self-associate (Lamberto *et al.*, 2011). The molecular interaction between α-syn and β-synuclein were found to reduce both amyloid fibrils and soluble oligomer formation *in vitro*. β-

synuclein lacks the NAC region and does not aggregate into amyloid fibrils. It binds specifically to α-syn in a dose dependent manner and reduces its aggregation propensity (Karyo *et al.*, 2010). Several small polyphenol molecules have been identified to inhibit the formation of amyloid fibrils and its associated cyto-toxicity. Polyphenols act as free radical scavengers and thus possess anti-oxidative property. Polyphenols such as α-tocopherol, β-carotene, curcumin, baicalein, delphinidin, epigallocatechin gallate, exifone, gallo-catechins, gossypetin, hinokiflavone, hypericin, procyanidins, rosmarinic acid, theaflavine, dopamine chloride and many more are found to be strong inhibitors of α-syn assembly (Ahsan *et al*., 2015; Ahmad *et al*., 2012; Caruana *et al*., 2011; Masuda *et al.*, 2006; Porat *et al*., 2006). They were identified to interact with the C-terminal end of α-syn. The structural constraints, adjacent phenolic -OH groups present in polyphenolic compounds and specific aromatic interactions play an important role in the inhibition of α-syn aggregation. The over-expression of Hsp-70 is found to inhibit both oligomeric formation and toxicity of α-syn by preventing the formation of prefibrillar α-syn. The Hsp-70 substrate binding domain is found to interact with the prefibrillar species and causes the C-terminal domain bind to the α-syn nuclei and thereby retarding the fibril elongation (Huang *et al.*, 2006; Pirkkala *et al.*, 2000). Inhibition of prolyl oligopeptidase (PREP) may be an important therapeutic strategy against PD as PREP can accelerate α-syn aggregation in cell models and *in vitro*. PREP inhibitor; KYP-2047 was found to be effective in decreasing α-syn aggregation via increased autophagy and normalizes cell functioning *in vivo* and *in vitro* (Savolainen *et al*., 2014; Myohanen *et al*., 2012). A study shows that antibodies can interfere with α-syn fibrillisation and inhibit amyloid formation by altering the aggregation pathway in a catalytic manner (Breydo *et al*., 2015). Emadi and coworkers (2004 & 2007) showed that the human single chain antibody fragments (scFv's) isolated from phage display antibody libraries decreasing the aggregation

rate of monomeric α-syn and also inhibiting the formation of oligomeric and protofibrillar α-syn structures.

1.7.1 Strategy for developing peptide antagonist

The strategy for developing specific amyloid peptide inhibitors includes the addition of small compounds, groups, or amino acid residues into the α-syn partial sequence. As NAC region is responsible for the aggregation of α-syn into fibrils, peptide fragments ETVK or KTVE based on NAC template was identified as a strong binder to NAC region. The high affinity corresponds to the Val-Thr and Thr-Val motifs repeated amino acid sequence of NAC. An oligopeptide based on template ETVK or KTVE would become an effective inhibitor against α-syn aggregation (Kuroda *et al*., 2004). The N-methylated (at Gly_{73}) analogue species of α-syn is found to be anti-amyloidogenic. The addition of N-methyl group causes the replacement of the amide hydrogen and thereby disrupts the chance of peptide bond formation required for a stable β-sheet structure (Bodles *et al.*, 2004). Madine and colleagues (2008) studied the inhibitory effect of N-methylated peptides on α-syn aggregation. The designed peptides were found to be highly soluble in aqueous and organic solvents, resistant to proteolytic degradation and can diffuse across membranes which are essential along with the inhibitory properties. Seven residues in 71-82 region (four valine, one glycine and two alanine) were considered and has more possibility for introducing N-methyl group to induce inhibitory property to α-syn. But the double methylation found to be unsuitable as an inhibitor of α-syn aggregation due to its increased hydrophobicity and greater size of 1000 nm which leads to the formation of non-amyloid aggregates. Pyrroloquinoline quinine (PQQ) modified α-syn_{36-46}, partial peptide modified with quinine molecules; baicalein and epigallocatechin gallate (EGCG) were reported to prevent α-syn

amyloid fibril formation (Yoshida *et al*., 2013). Some groups used *in silico* panning for screening peptide ligands against α-syn targeting the hydrophobic amyloid core forming α-syn_{68-78} region. The peptides derived such as QSTQ and AQTQ at five fold molar excess were seen to interact with α-syn and found to promote fibrillisation (Abe *et al*., 2007).

Peptide inhibitors against α-syn aggregation can be generated using a multiplexed intracellular Protein-fragment Complementation Assay (PCA) library screening system (Acerra *et al*., 2013; Mason *et al*., 2006; Pelletier *et al*., 1998). The PCA system involves transformation or transfection of cell lines using library containing plasmids to screen and select for peptide antagonists. Successfully selected peptides must bind to the target protein; α-syn, inhibit amyloid growth thereby reducing amyloid cytotoxicity and confer bacterial cell growth. The parameter checked during peptide selection is that, whether the peptides bind to α-syn such that the two halves of a reporter enzyme is recombined and expressed which facilitates the cell survival under selective conditions. The advantage of PCA is that since it is an *in vivo* selection system, only stable, protease resistant, non-aggregating (soluble), non-toxic and target-specific peptides can be selected. In PCA, the possible artifacts are that we will get colonies growing where the peptides does not really bind the target strongly. The problem can be solved by increasing the stringency of the conditions by an increased amount of Tmp which I used is a bit arbitrary. Another artefact is that the GS linkers on the peptide and target could interact with each other which are probably not enough to make a peptide that doesn't bind the target look like it does, but could increase the apparent affinity so that the colony of that peptide grows faster than it should. In this thesis, PCA has been used to screen peptides from a library containing many thousands of members for an interaction with full length wild type α-syn or its mutants.

Antagonistic peptides were designed scaffolding two targets; α-syn$_{71-82}$ (against wild type α-syn and its mutants) and α-syn$_{45-54}$ (against wild type α-syn).

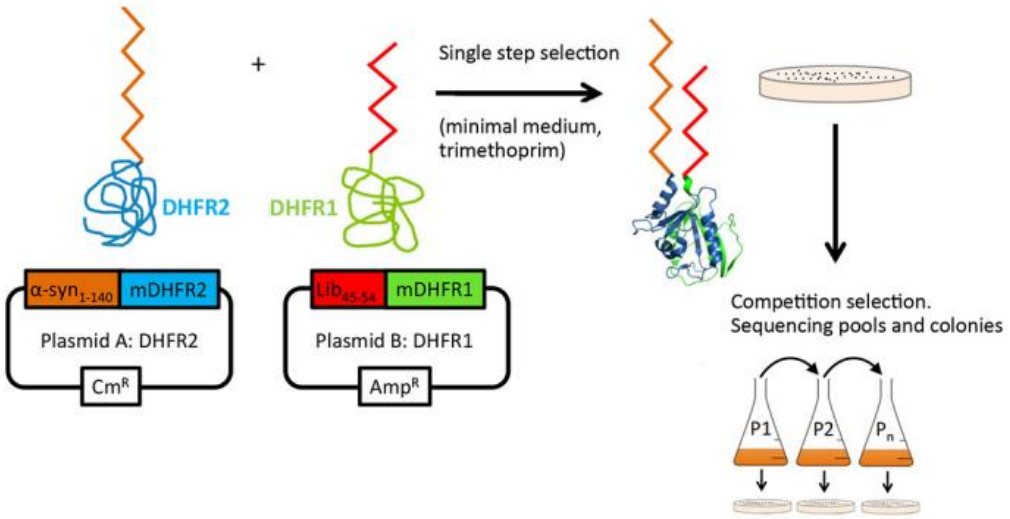

Figure 1.5: Protein fragment complementation assay (PCA). Peptide library members that bind to α-syn reconstitute murine dihydrofolate reductase (mDHFR) activity and induce cell growth under selective condition containing trimethoprim. Subsequent passages in liquid media were undertaken in competition selection process to isolate potential peptides with highest efficacy (Image source: Cheruvara *et al*., 2015).

1.8 Conclusion

Symptomatic treatments like introducing L-DOPA, cell replacement therapies or deep brain stimulations is being provided for the more advanced stages of PD. Some of the events such as oxidative stress, mitochondrial dysfunction, kinase phosphorylation, inflammation, protein handling, and ubiquitin-proteasome pathways appear to be important in the pathogenesis of PD which led to the identification of molecular targets for designing potential drug candidate to slow or reverse the disease progression. PD has been classified as a cell autonomous disease. However some studies reported a prion-like intercellular transfer of misfolded α-syn leads to question the basic understanding of the disease (Olanow *et al*., 2013; Li *et al*., 2008). The knowledge about the genetic cause and different risk factors contributing to the various events that leads to neurodegeneration should provide new targets for developing neuroprotective drugs. The hypothesis of designing small inhibitor molecules is that it can manipulate biochemical pathways, genes or proteins. The strategies for developing such drugs can be designing modulators that can enhance specific pathways for clearance of proteins or degradation of toxic oligomers or aggregates. Phosphorylation pathways are suitable targets for developing peptide drugs as α-syn undergo such pathways in several sites during aggregation process.

In this thesis, I have successfully demonstrated that the PCA strategy can be used as a generalised method for deriving peptide inhibitors against α-syn aggregation. In the future, these newly designed inhibitors can be modified into drugs to slow or even prevent the onset of PD.

Chapter 2: Materials and Methods

2.1 Purification of wild type α-synuclein (α-syn) and mutants

The hexa-His tag containing pET21b expression vector (ampicillin resistance) was used for protein expression. This vector was fused with a 100 residues long 'SUMO' (small ubiquitin related modifier) tag to increase protein solubility (Malakhov *et al*., 2004; Butt *et al*., 2005; Marblestone *et al*., 2006; Lee *et al*., 2008). The inserts terminated with a 'stop' codon were cloned into the vector via NheI and AscI restriction sites. The enzyme SUMO protease (ULP1) was used to remove the His-SUMO tag.

Protein purification overview:

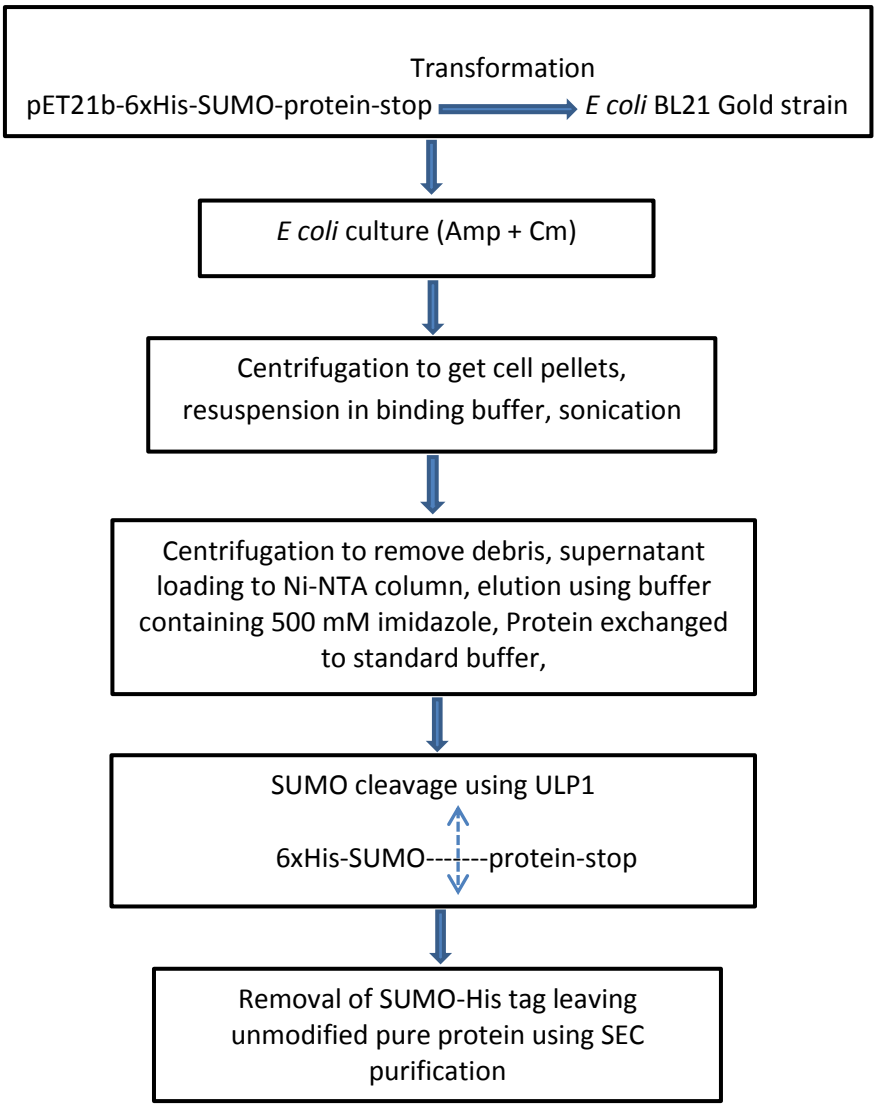

2.1.1 Bacterial strain: *Escherichia coli* (*E coli*)

E coli strain XL1Blu was used for construction and cloning of libraries, BL21-Gold were used for transformation and protein purification protocols. BL21-Gold cells were used as they show high degree efficiency in transformation and protein expression.

***E coli* strain**	**Genotype**
BL21-Gold	*B F- dcm+ Hte ompT hsdS(r_B- m_B-) gal λ (DE3) endA Tet^r*
XL1 Blue	*recA1 endA1 gyrA96 thi-1 hsdR17 supE44 relA1 lac [F´ proAB lacIq ZΔM15 Tn10 (Tetr)]*

Table 2.1 *E coli* strain BL21-Gold and XL1 Blue showing genotype (source: Stratagene).

Antibiotics (Sigma aldrich UK)			
Antibiotics	**Dilution factor**	**Concentration**	**Composition**
Ampicillin (Amp)	1000 X	100 mg/ml	1 g in 10 ml 70 % EtOH
Chloramphenicol (Cm)	1000 X	25 mg/ml	250 mg in 10 ml 70 % EtOH
Kanamycin (Kan)	1000 X	50 mg/ml	500 mg in 10 ml 100 % H_2O
Tetracycline (Tet)	1000 X	25 mg/ml	250 mg in 10 ml 70 % EtOH
Trimethoprim (Tmp)	1000 X	1.0 mg/ml	10 mg in 10 ml 70 % MetOH

Table 2.2 List of antibiotics and its concentrations.

Media and reagents : Protein purification	
Media & reagents	**Composition**
Luria Bertani (LB) broth pH:7.0 (1 liter)	10 g Bacto-tryptone, 5 g NaCl, 5 g Yeast extract.
2xYT media broth (2xYT) pH7.0 (1 liter)	16 g Bacto-tryptone, 5 g NaCl, 10 g Yeast extract.
2xYT-antibiotics media broth	2xYT media autoclaved, cooled to 25^0C, then added appropriate antibiotics ampicillin (100 µg/ml) and chloramphenicol (100 µg/ml)
LB Agar (LA) (1 liter)	LB broth + 15 g granulated bacto-agar (0.15 %)
LA-antibiotics petri plate	LB agar, autoclaved, cooled to 55^0C, then added appropriate antibiotics ampicillin (100 µg/ml) chloramphenicol (100 µg/ml), kanamycin (50 µg/ml).
Transformation buffer I (TBI) pH 5.8	30 mM CH_3CO_2K (2.94 g), 50 mM $MnCl_2.4H_2O$ (9.9 g), 100 mM RbCl (12.09 g), 100 mM $CaCl_2$ (1.1 g), 15 % (w/v) glycerol (pH the solution to 5.8 with acetic acid and filter sterilize).
Transformation buffer II (TBII) pH 5.8	10 mM Na MOPS (2.092 g), 75 mM $CaCl_2$ (8.3 g) 10 mM RbCl (1.209 g), 15 % (w/v) glycerol.
Electroporation salts (100x)	0.25 M KCl, 1 M $MgCl_2$
Isopropylthiogalactoside (IPTG)	1 M (2.4 g in 10 ml ddH_2O)

Table 2.3 Media and reagents used for protein purification.

2.1.2 Protein expression in bacterial culture

The vector containing the peptide sequence was transformed into *E.coli* (BL21-Gold) using electroporation. This was then plated onto LB agar plates with the antibiotics Amp and Cm at 37^0C, non-transformed cells were plated alongside as controls. Single colonies were sent for sequencing to confirm the correct sequence had been introduced.

Colonies were picked and cells were inoculated in 5ml LB broth containing 5µl each of Amp and Cm. 1 ml of overnight culture was inoculated into 1 litre of 2xYT containing appropriate antibiotics. The cells were grown at 37^0C, 220 rpm, in an Innova-43 incubator shaker, until it reached the mid log phase growth ($OD_{600\ nm}$: 0.6). Once the appropriate OD had been reached, cells were induced by 1 mM IPTG for 3 hours at 37^0C.

The cells were harvested by centrifugation at 4^0C, 2988xg for 20 mins in a SLC-6000 rotor using a Sorvall RC superspeed centrifuge. The cell pellets were resuspended in 30 ml binding buffer (Table 2.4). The resuspended cells were homogenised using a magnetic stirrer for 15 mins. The cell suspension was divided into 3x50 ml falcon tubes and stored on ice for lysis by sonication. The cells in the falcon tubes were sonicated using a Diagenode Bioruptor sonicator, keeping in ice cold water at 200 W for 60 cycles. Each cycle consisted of 10 seconds 'on' and 'off'. The viscous lysate was then centrifuged at 40905xg for 20 mins at 4^0C using a SS-34 rotor (Sorvall RC superspeed centrifuge). The supernatant containing the protein was stored at -20^0C.

2.1.3 Nickel-NTA column (Affinity chromatography) purification

Following cell lysis, the hexa-His tagged protein was purified using 5 mL Ni-NTA column (Qiagen). Ni-NTA columns have a capacity to yield up to 50 mg/ml of pure protein without altering the protein structure.

Protein purification buffers	
Buffers	**Composition**
Binding buffer pH 8.0	50 mM NaH_2PO_4, 300 mM NaCl, 10 mM imidazole, 0.1 % tween
Wash buffer pH 8.0	50 mM NaH_2PO_4, 300 mM NaCl, 30 mM imidazole, 0.1 % tween
Elution buffer pH 8.0	50 mM NaH_2PO_4, 300 mM NaCl, 500 mM imidazole
Standard buffer (1x) pH 8.0	20 mM Tris HCl, 0.5 mM DTT
MES buffer pH 8.0	10 mM MES, 150 mM NaCl

Table 2.4 Buffers used for protein purification.

The column was calibrated using 10 ml of ddH_2O, then 10 ml of 0.5 M EDTA (pH 8.0), washed by 10 ml of ddH_2O, followed by 10 ml of 0.45 M NaOH, then 10 ml of ddH_2O again at a flow rate of 5 ml/min to eliminate any residual proteins or nickel from the previous purification processes. The white coloured column was then reloaded with 100mM $NiSO_4$ (approximately 5 ml), washed excess unbound Ni ions using 10 ml of ddH_2O and calibrated using 10 ml of binding buffer at a reduced flow rate of 3 ml/min. Finally the supernatant of sonicated sample was loaded continuously 3 times to ensure the column was bound to its full capacity.

Using an AKTA prime purification system (GE healthcare), the protein loaded column was washed by programming to run in wash buffer (30 mM imidazole) at a flow rate of 1 ml/min until the Abs_{280nm} showed a base line at 0.0 absorbance unit relative to wash buffer. After washing for approximately 30 mins, the inlet filters of AKTA were transferred to elution buffer (500 mM imidazole) and started the run at 1 ml/min. After around 10 mins, a clear peak appeared on the absorbance graph indicating the elution of His-tagged protein which was collected in 1 ml fractions for further purification steps. The high imidazole concentration can adversely affect the SUMO protease activity in the cleavage reaction later. Thus the protein in elution buffer was exchanged to standard buffer using a PD10 desalting column (GE healthcare). The PD10 columns were calibrated using 25 ml of standard buffer which was allowed to flow through 8.5 ml Sephadex resin under gravity. Next, added 2.5 ml of protein sample to the column and discarded the flow through. Finally the protein was eluted by adding 3.5 ml of standard buffer. The diluted protein was concentrated using a centrifugal filter column (Millipore) having molecular weight cut off 3000 daltons. The column was then centrifuged at 1702xg using balanced bench top centrifuge (Eppendorf 5810 R) until desired volume remained in the column filter. The process repeated with newly added buffer to ensure the complete removal of salts before cleavage reaction.

2.1.4 SUMO-tag cleavage reaction

The SUMO conjugated protein eluted from Ni-NTA column underwent cleavage reaction to remove SUMO-His tag using highly specific SUMO protease (ULP1) enzyme leaving the final unmodified protein. 1 mg/ml of purified ULP1 was added at a ratio of 1:4 (enzyme: protein) and cleaved at 30^0C for 16 hours without shaking.

Purification of SUMO protease enzyme: The hexa-His tag containing pET21b expression vector (Amp resistance) was used for ULP1 expression in *E coli* BL21 Gold cells and purified using Ni-NTA column method as described above. The enzyme was stored in standard buffer as aliquots at -80^{0}C.

2.1.5 Cleaved protein purification (G75; Size exclusion chromatography)

After the cleavage reaction the protein, SUMO-His tag, un-cleaved protein and other non-specific proteins were separated by size exclusion chromatography (Sephadex 75, GE healthcare). The G75 has exclusion limit of 70 kDa. The column was attached to an AKTA prime purification system and washed by programming with three column volumes (120 ml) of ddH_2O, and calibrated by 120 ml of MES buffer at a flow rate of 0.8 ml/min. After that 2 ml of protein was injected to the column and eluted by fractionation according to the molecular size. Larger proteins eluted first as they bypass the gel pores, while smaller proteins enter the gel pores and eluted later in the profile. The elution profile was detected as an Abs_{280nm} graph. Samples according to their sizes collected as 1 ml fractions using a programmed sample collector. To standardize the G75, a set of protein standards (67 kDa BSA, 43 kDa CsoR1, 27.2 kDa cytochrome C prime L16I, 12.5 kDa cytochrome C) of known sizes were applied through the column. The molecular weight of protein eluted was calculated using linear plot between log value of mass vs. elution volume. Actual mass was calculated using the equation below:

$$MW = \text{Inverse log}\left(\frac{(Ve-Vo)}{[(Vt-Vo)\text{-intercept}] / \text{slope}}\right) \qquad \text{(Eq: 1)}$$

Where; Ve= elution volume
Vo= void volume
Vt= total gel bed volume

2.1.6 ^{13}C and ^{15}N labelling of α-syn for NMR analysis

Components for NMR minimal media	Amount
Salt solution (1 litre)	
KH_2PO_4	13 g
K_2HPO_4	10 g
Na_2HPO_4	9 g
Na_2SO_4	2.4 g
Trace elements solution (100 ml)	
$FeSO_4.7H_2O$	0.6 g
$CaCl_2.2H_2O$	0.6 g
$MnCl_2.4H_2O$	0.12 g
$CoCl_2.6H_2O$	0.08 g
$ZnSO_4.7H_2O$	0.07 g
$CuCl_2.2H_2O$	0.03 g
H_3BO_3	0.002 g
EDTA	0.5 g
Vitamin mix solution (100 ml)	
Biotin	10 mg
Choline chloride	10 mg
Folic acid	10 mg
Niacinamide	10 mg
Pantothenate	10 mg
Pyridoxal	10 mg
Riboflavin	1 mg

Table 2.5 List of salts, trace elements and vitamins used for the preparation of NMR minimal media.

Minimal media preparation for labelled NMR samples: 1 litre of salt solution prepared in a 2 litre conical flask and autoclaved. Then added 10 ml of filter sterilised trace elements solution along with filter sterilised 10 ml vitamin mix solution. Then added 10 ml of filter sterilised 1 M $MgCl_2$ along with 6 ml of freshly prepared 30 mg Thiamine solution in sterile ddH_2O. Then 5 g of ^{13}C-glucose and 0.8 g of $^{15}NH_4Cl$ was added to the medium. Finally, 1 ml of Amp (100 mg/ml) was added.

Protein was expressed in *E.coli* (BL21-Gold) grown in similar minimal media conditions as described in the above section. Growth in minimal media is slow, needing approximately 6-7 hours to reach an $OD_{600\ nm}$ of 0.6. Finally the protein was purified by affinity and gel chromatography techniques and purity was checked by SDS PAGE. The pure protein was sent for NMR analysis in our collaborator's lab along with the PCA peptides.

2.1.7 Protein characterisation using Sodium dodecyl sulphate poly acrylamide gel electrophoresis (SDS PAGE)

SDS PAGE buffers and reagents	
Gel	**Components**
15 % Resolving gel (5 ml)	2.50 ml 30 % bis acrylamide, 1.30 ml 1.5 M Tris (pH 8.8), 50 µl 10 % SDS, 50 µl 10 % Ammonium per sulphate (APS), 3 µl TEMED, 1.10 ml ddH_2O
5 % Stacking gel (2 ml)	330 µl 30 % bis acrylamide, 250 µl 1 M Tris (pH 6.8), 20 µl 10 % SDS, 20 µl 10 % APS, 2 µl TEMED, 1.40 ml ddH_2O
SDS lysis buffer (1x) pH 6.8	50 mM Tris, 100 mM DTT, 2 % SDS
SDS running buffer (5x) pH 8.3	25 mM Tris, 250 mM glycine, 0.1 % SDS
SDS staining buffer	1.25 g Coomassie R-250, 225 ml methanol, 225 ml H_2O, 50 ml glacial acetic acid
SDS destaining buffer (1 liter)	300 ml methanol, 100 ml acetic acid, 600 ml H_2O

Table 2.6 List of SDS PAGE buffers and reagents.

The SDS PAGE gel was used to determine the purity and expected molecular mass of protein. The samples from G75 column were run on a 15 % acrylamide gel along with a pre-stained protein ladder with a molecular weight range of 250 kDa to 10 kDa (Spectra^{TM} multicolour broad range protein ladder, #SM1841 Fermentas). Before loading to the gel, 10 µl of each sample was mixed with lysis buffer and boiled for 5 mins at 95^{0}C. Gels were set up using glass plates. The resolving gel according to the composition given in the Table 2.6 was made and added between the plates and allowed to set for approximately 20 mins. A layer of ddH_2O was added to get a bubble free top surface. Once the gel is formed the water was removed and added the stacking gel followed by the insertion of a well comb immediately. Gels were polymerised by 0.02 % (v/v) TEMED (Fisher) and 0.05 % (v/v) APS (Fisher). Proteins were denatured with SDS and resolved at 170 V in 1x running buffer.

Protein of interest underwent buffer exchanges and the molecular mass was confirmed by using electro-spray mass spectroscopy. The protein concentration was determined in a spectrophotometer by carrying out an absorbance scan from 200-300 nm or measuring the absorbance at 280 nm using 1 cm path length cuvette and calculated by using molar extinction coefficient of tyrosine 1209 M^{-1} cm^{-1} (Mason *et al,* 2007). The purified protein was transferred to ddH_2O and lyophilized in aliquots using a freeze drier (Christ Alpha 2-4 LO plus) under vacuum at -80^{0}C for approximately 18 hours. Samples were stored at -80^{0}C for long term preservation.

2.2 Cellular and Molecular biology protocols

2.2.1 Preparation of XL1 Blue/ BL21 Gold electro-competent cells

The entire protocol was carried out at 4^0C and each centrifugation step at 2500g for 10 mins. The plasmid containing cells were inoculated in 5 ml LB media with appropriate antibiotics and incubated overnight at 37^0C. The overnight grown culture was added to 500 ml pre-warmed 2xYT and incubated at 37^0C, shaken at 5xg until the cells reached OD_{600}: 0.6-0.8. The culture was transferred to 10x50 ml falcon tubes, then cooled on ice for 15 mins and centrifuged. The pellets were resuspended in pre-cooled ddH_2O and centrifuged to remove residual media and salts in the cells. Pellets were resuspended in 50 ml of ddH_2O and transferred to 8 falcon tubes, and again centrifuged. Pellets were resuspended in 25 ml of ddH_2O and transferred to 4 falcon tubes, and again centrifuged. 25 ml of pre-cooled 10 % DMSO was added to the pellets and the resuspension was allowed to stand on ice for 5 mins and then centrifuged. Pellets were resuspended in 5 ml of 10 % DMSO, allowed to stand for 5 mins and again centrifuged. Thereafter, the pellet was resuspended in 1 ml of 10 % DMSO solution. To ensure the correct concentration needed for transformation, the OD_{600} was measured for 100 fold dilution of the pellet and was continuously diluted using 10 % DMSO until it reached OD_{600}: 0.4. Aliquots of 80 µl were snap frozen in liquid nitrogen and stored at -80^0C

2.2.2 Transformation of XL1 Blue/ BL21 Gold electro-competent cells

80 µl of electro-competent cells was allowed to thaw on ice for 30 mins. 100 ng of plasmid or ligated DNA was added to the thawed cells, mixed gently by tapping or pipetting and was kept on ice for 10 mins. The mixture was transferred to a pre-cooled electroporation cuvette (EQUIBIO) and inserted into a gene pulser. The cell membranes were destabilized for the DNA uptake by introducing a large electric pulse of 1.7 kilovolts, 400 Ω and 25 µFD. Immediately added 920 µl of pre-warmed, antibiotic free 2xYT media (10 µl electroporation salts + 990 µl 2xYT) to the cuvette and transferred to 1.5 ml Eppendorf tube followed by incubation at 37^0C shaken at 209xg for 75 mins. After that, the cells were centrifuged, removed supernatant and pellets resuspended in 50 µl of 2xYT. The entire solution was plated on pre-warmed LB plates containing appropriate antibiotics and incubated overnight at 37^0C.

2.2.3 Preservation of bacterial cell stock containing plasmid of interest

Overnight 5-10 ml cultures were grown in LB or 2xYT broth containing appropriate antibiotics at 37^0C, 5xg by using a bench top shaker (IKA® Incubator Shaker KS 4000) in glass universal tubes. The cell cultures then preserved as glycerol stocks for future uses. The glycerol stocks were prepared by adding 600 µl of 30 % glycerol to 1.4 ml of cell culture, mixed well, snap frozen and stored at -80^0C.

2.2.4 Recombinant DNA protocols

Buffers and solutions: Molecular biology experiments		
Reagent	**Composition**	**Source**
Ethanol (EtOH)	100 %, absolute, extra pure	Fisher Scientific, UK
1-Butanol	100 %	Fisher Scientific, UK
Isopropanol	100 %	Fisher Scientific, UK
Ethidium bromide		Sigma Aldrich, UK
DNA loading buffer (6x)	0.03 % Bromophenol blue, 10 mM Tris HCl (pH 7.6), 0.03 % Xylene Cyanol FF, 60 % glycerol, 60 mM EDTA	Fermentas, UK
TAE buffer (1x)	40 mM Tris, 20 mM Glacial acetic acid, 1 mM EDTA	
Fast Alkaline phosphatase		Fermentas, UK
Fast Digest® enzymes		Fermentas, UK
GeneRuler™ DNA ladder		Fermentas, UK
T4 DNA ligase		Fermentas, UK
GeneJET™ Plasmid miniprep		Fermentas, UK
QIAquick gel extraction kit buffers		Qiagen, UK

Table 2.7 Buffers and solutions used for molecular biology experiments.

2.2.5 Plasmid DNA extraction

Extraction of plasmid DNA from *E. coli* cultures was carried out using GeneJET^{TM} Plasmid Miniprep Kit (Fermentas). Colonies from glycerol stock or single clones were used to inoculate 5 ml LB medium containing appropriate antibiotics and incubated at 37^0C overnight. The cell culture was centrifuged at 6810xg for 2 mins. Supernatant removed and the pellets were resuspended in 250 µl of resuspension solution (RNAse added). Then added 250 µl of lysis buffer and mixed the solution by inverting the tube for 4-6 times. After that, 350 µl of neutralisation buffer added and gently mixed until a white precipitate appeared. The solution was centrifuged at 17982xg for 5 mins. The supernatant containing plasmid DNA was carefully transferred to the supplied GeneJET spin column placed in 2 ml collection tube and centrifuged for 1 min at 13000 rpm. The column was then washed twice with 500 µl of wash buffer (containing ethanol) and centrifuged for 1 min. The flow through discarded and an additional centrifugation of emptied column was performed to remove the residual ethanol from the column. The column was then transferred to a new 1.5 ml eppendorf. 50 µl of elution buffer was added to the centre of the column and allowed it to stand for 2 mins. The column was centrifuged at 17982xg for 2 mins, determined the concentration using NanoDrop 2000/2000c spectrophotometer (Thermo Scientific) and stored at -20^0C.

2.2.6 DNA desalting

Desalting was undertaken by adding 500 µl of butanol to 50 µl of diluted DNA (10 µl of DNA+ 40 µl of ddH_2O), mixed well and centrifuged for 30 mins at 20854xg. After that, the supernatant was aspirated and the pellet was air dried at 30^0C for 30 mins. Finally the pellet was resuspended in 10 µl of sterile ddH_2O and the concentration was determined by using NanoDrop.

2.2.7 Restriction digestion of the plasmid DNA

Approximately 0.5 µg of plasmid DNA was used in a digestion reaction carried out for 1 hour at 37^0C. Following the FastDigest® (Fermentas) protocol, the digestion mixture was prepared as shown in Table 2.8.

Restriction digestion	
Component	**Volume/concentration**
Plasmid DNA	~0.5 µg
Restriction enzyme 1	2 µl
Restriction enzyme 2	2 µl
10x FastDigest® buffer	5 µl
ddH_2O	X µl
Total	50 µl

Table 2.8 Components used for restriction digestion reactions.

2.2.8 Dephosphorylation of the plasmid DNA

Dephosphorylation of the vector is a prerequisite to reduce vector background and also it minimize re-ligation and circularisation of linearized plasmids. The reaction mixture was prepared as shown in Table 2.9.

Dephosphorylation	
Component	**Volume**
Digestion mixture	50 µl
10x buffer	6 µl
Alkaline phosphatase (Fermentas)	2 µl
ddH_2O	2 µl
Total	60 µl

Table 2.9 Components used for dephosphorylation reactions.

The reaction was carried out at 37^0C for 15 mins. The mix was then incubated at 75^0C for 5 mins to deactivate the alkaline phosphatase enzyme.

2.2.9 Agarose gel electrophoresis

Following restriction digestion, the plasmid DNA sizes were determined by using agarose gel electrophoresis. 50 µl of digested DNA was mixed with 10 µl of 6x DNA loading buffer and loaded in to 1 % agarose gel along with GeneRuler^{TM} 6x DNA ladder (Fermentas). The gel was made by boiling standard agarose in 1x TAE buffer until the agarose dissolved completely. The solution was allowed to cool for 5 mins and added 0.5 µg/ml EtBr. The loaded gel was run at 80 V until the dye front reached 3/4th of the gel. Later the gel was examined under UV illumination at wavelength 365 nm.

2.2.10 Purification of DNA from Agarose gel using QIAquick gel extraction kit (Qiagen)

The plasmid of interest identified using a UV transilluminator was excised from the Agarose gel using a clean sharp scalpel and placed in individual eppendorf tubes. The gel slices were weighed. Three times the volume of Buffer QG was added to 1 volume of the gel slice and incubated at 50^0C allowing the gel slice to melt completely. An equal volume of isopropanol was added to the solution and inverted to mix thoroughly. The mixture was transferred to a QIAquick spin column and centrifuged at 17982xg for 1 min. The flow-through was discarded, then added 0.5 ml of Buffer QG to the column and again centrifuged. The column was washed by centrifuging with 0.75 ml of Buffer PE. Finally DNA was eluted into a sterile eppendorf tube by centrifuging with 30 µl of elution buffer (10 mM Tris-HCl, pH 8.5). The concentration of DNA was determined by NanoDrop and stored at -20^0C.

2.2.11 Polymerase chain reaction (PCR)

The amplification of the DNA inserts of interest was carried out by using overlap extension PCR for various cloning protocols. The reaction was undergone in a TC-412 Thermal cycler (TECHNE). The preparation of PCR mixture and the reaction cycles was done as shown in Table 2.10.

PCR mixture		
Component	Volume	
	Test	Control
Forward primer (100 µM)	0.5 µl	0.5 µl
Reverse primer (100 µM)	0.5 µl	0.5 µl
dNTPs (10 mM) (Fermentas, UK)	1 µl	1 µl
10x *Pfu* buffer with $MgSO_4$ (Fermentas, UK)	5 µl	5 µl
10x *Pfu* DNA polymerase (Fermentas, UK)	0.5 µl	-
ddH_2O	42.5 µl	43.0 µl
Total	50 µl	50 µl
PCR cycles		
Steps	Conditions	
Initial denaturation	95^0C, 3 mins	
Denaturation (30 cycles)	95^0C, 45 seconds	
Annealing (30 cycles)	2-5^0C below T_m of the primers, 1min/kb	
Extension (30 cycles)	72^0C, 45 seconds	
Final extension	72^0C, 10 mins	

Table 2.10 Components used for PCR reactions and PCR cycles.

2.2.12 Designing a peptide library: α-syn$_{45-54}$ scaffold

The library was designed by incorporating the wild-type sequence while introducing two, three or six residue options at each of the ten amino acid positions at 45-54 region (shown in results: chapter 5). This corresponded to a library size of 209,952 members.

Code letters used to design primers for amino acid randomisation in α-syn$_{45-54}$ region	
Code	**Encoded bases**
A	A
B	CGT
C	C
G	G
H	ACT
R	AG
T	T
V	ACG
W	AT
Primers used to include degenerate codons for residue options	
Primers	**Sequence**
Forward (Invitrogen)	5'- C TGG GCT AGC RAA VAW GBG VTT VTT VAW GBG VTT RHA RCC GGC GCG CCG CTA GAG GCG -3'
Reverse (Invitrogen)	5'- T TTT TTT TTA TAA TAT ATT ATA CGC CTC TAG CGG CGC GCC -3'

Table 2.11 List of code letters encoding amino acids during randomisation and primers used to include degenerate codons for residue options.

2.2.13 Ligation

The vectors and the inserts used for various studies were gel purified for ligation. The fragments were mixed at a molar ratio of 1:3 (vector: insert). The digested, dephosphorylated, purified plasmid DNA vector was added to the required amount of insert in a sterile 0.5 ml eppendorf tube. Digested plasmid alone without insert was plated as negative controls to ensure the success of ligation. Ligation mixture was prepared as shown in Table 2.12 and incubated at 18^0C overnight. The following equation was used to calculate the volume of insert required for ligation reaction.

$$\text{Insert (ng)} = \frac{[\text{Vector(ng) x Insert size(kb)}]}{\text{Vector size (kb)}} \text{x } 3 \qquad \text{(Eq: 2)}$$

Ligation	
Component	**Volume/concentration**
10x ligase buffer (Fermentas)	1 µl
T4 DNA ligase (Fermentas)	1 µl
Plasmid vector	~250 ng
DNA insert	20 ng
ddH_2O	X µl
Total	10 µl

Table 2.12 Components used for ligation reactions.

2.2.14 DNA sequencing

The constructs for correct sequence insert was checked by GATC-Biotech (Germany) initially and Source Bioscience (UK) later. 30 µl of samples containing concentration more than 50-100 ng/µl were sent for sequencing. Samples were analysed using an ABI sequencer and chromatograms

2.3 Protein fragment complementation assay (PCA)

Plasmids: PCA		
Plasmid	**Description**	**Source**
pES300d-α-syn$_{1-140}$-DHFR2	Cloning vector containing target α-syn$_{1-140}$ gene with restriction sites NheI, AscI	Derived from pQE16 (Qiagen, UK)
pES230d-Lib-α-syn$_{45-54}$-DHFR1	Cloning vector containing α-syn$_{45-54}$ library gene with restriction sites NheI, AscI	Derived from pQE16 (Qiagen, UK)
pREP4	For the expression of lac repressor protein	Qiagen, UK

Table 2.13 Plasmids used for PCA.

Media and reagents: PCA protocol	
Medium & Reagents	**Composition**
M9 minimal media (M9) (1 litre)	200 ml 1x M9 salts, 2 ml $MgSO_4.7H_2O$ (1 M), 100 µl $CaCl_2$ (1 M), 20 ml glucose (20 %), made up to 1 litre with ddH_2O.
M9 Salts : 5x (1 litre)	200 mM Na_2HPO_4, 100 mM KH_2PO_4, 100 mM NH_4Cl, 50 mM NaCl
M9 Agar (M9A) (1 litre)	M9 medium + 15 g Bacto agar (0.15 %)
M9A-antibiotics petri plate	M9 agar, autoclaved, cooled to 55^{0}C, then added appropriate antibiotics Amp (100 µg/ml) Cm (100 µg/ml), Kan (50 µg/ml), IPTG (250 µg/ml) and Tmp (1 µg/ml).

Table 2.14 Media and reagents used for PCA.

2.3.1 Single step selection

Once the library was generated, PCA was performed between the target protein and the pooled library members. The target plasmid pES300d-α-syn$_{1-140}$ (Cm^R) encoding mDHFR2 and pREP4 (Qiagen; for the expression of lac repressor protein, Kan^R) were co-transformed (electroporated) into electrocompetent BL21 gold cells and plated on to LB agar plates with the appropriate antibiotics (Kan 50 μg/ml and Cm 25 μg/ml). The transformed BL21 gold cells were made electrocompetent using 10 % DMSO, so that the library plasmids (pES230d-Lib encoding DHFR1, Amp^R) could then be transformed into electrocompetent BL21 gold cells. The transformants were plated on three different conditions:

(a) Positive control: LB media agar plate with three antibiotics (Kan 50 μg/ml, Amp 100 μg/ml, and Cm 25 μg/ml) to demonstrate successful transformation of library plasmid. The colonies were grown in one overnight as LB provides sufficient nutrients.

(b) Negative control: M9 minimal media agar plate with the three appropriate antibiotics as above mentioned along with Tmp 1 μg/ml excluding IPTG upon which no growth was expected. The plates were incubated for 5-10 days along with the large PCA plate as the nutrients in the M9 media is minimal.

(c) PCA plate: A large M9 minimal media agar plate containing Amp, Cm, Kan, Tmp and 1 mM IPTG (to induce expression of the two DHFR fragment fused protein).The plates were Incubated for 5 to 10 days depending on the affinity of interaction between the target and the library members.

2.3.2 Competitive selection

Growth competition experiments were performed to increase the selection stringency of peptides. Colonies that grew from the single step selection M9 plate were pooled and grown in 50 ml of M9 minimal media containing 1 µg/ml Tmp, 1 mM IPTG, 50 µg/ml Kan, 100 µg/ml Amp and 25 µg/ml Cm. Cells were incubated at 37^0C with continuously shaking at 5xg for approximately 3-4 days until it reaches OD_{600}:0.4. When the cell density reached OD_{600}: 0.4, 50 µl was used to inoculate a freshly made 50 ml M9 medium and allowed to grown. The process of serial dilution was carried out over many passages (P1, P2, P3 and so on). At each passage 30 % glycerol stocks (stored at -80^0C) were prepared and sequencing results were obtained for DNA pools as well as individual colonies. The sequencing results showed many background peaks as there were several peptides competing in the early pool passages. Finally a clear, dominant peak with a fewer background noise was obtained and considered it as the strongest affinity binding candidate from the library.

2.4 Peptide synthesis

Among the PCA peptides, only peptide 45-54W was synthesized in the lab as other PCA peptides were commercially bought from Peptide Synthetics, UK. The peptide 45-54W was synthesized using a Liberty Blue™ microwave peptide synthesizer (CEM; Matthews, NC).

Fmoc-l-aminoacids / Reagents	Composition	Source
Alanine	0.16 g in 2.63 ml DMF	AGTC Bioproducts (UK)
Aspargine	0.63 g in 5.25 ml DMF	,,
Aspartate	0.43 g in 5.25 ml DMF	,,
Glycine	0.47 g in 7.88 ml DMF	,,
Isoleucine	0.37 g in 5.25 ml DMF	,,
Lysine	0.98 g in 10.5 ml DMF	,,
Valine	0.71 g in 10.5 ml DMF	,,
Rink amide ChemMatrix™ resin		PCAS Biomatrix, Inc. (Canada)
Acetylation solution	20 % Acetic anhydride in DMF	Thermo Fisher Scientific (UK).
Dimethylformamide (DMF)		,,
Activator solution: 1H-Benzotriazol-1-yloxy)(dimethylamino)-N,N-dimethylmethaniminium hexafluorophosphate (HBTU)	HBTU in DMF	AGTC Bioproducts (UK)
De-protection solution	20 % Piperidine in DMF	Thermo Fisher Scientific (UK).
Cleavage solution (10 ml)	95 % Trifluoroacetic acid, 2.5 % Triisopropylsilane, 2.5 % ddH_2O	,,
Acetonitrile (MeCN)	0.1 % TFA in MeCN used in HPLC	Fisher Scientific (UK)

Table 2.15 Amino acids and reagents used for 45-54W peptide synthesis.

Peptides were synthesized on a 0.1 mmol scale on a PCAS Biomatrix^{TM} Rink amide resin employing Fmoc solid-phase techniques in which the cleavage reactions are less harsh and the use of different protecting group reduces the side chain reactions during cleavage. Coupling reaction was performed with Fmoc amino acid (5 eq), HBTU (4.5 eq) and diisopropylethylamine (10 eq) in 5 ml of DMF for 5 mins with 20 watt microwave irradiation at 90^{0}C. De-protection was carried out by adding 20 % piperidine in DMF for 5 mins with 20 watt microwave irradiation at 80°C. Coupling, de-protection and washing with 5 ml of DMF was repeated four times in between each step. Following synthesis, the peptide was acetylated using 2.63 ml of acetylation solution for 20 min) and then cleaved from the resin with simultaneous removal of side chain-protecting groups by treatment with 10 ml of cleavage solution for 4 hours at room temperature. Triisopropylsilane along with TFA in the cleavage solution acts as scavenger to chemically trap highly reactive species formed during cleavage reaction and thereby preventing the peptide from un-desired side chain reactions. Suspended resin was removed by filtration. The peptide was precipitated using three rounds of crashing in ice-cold diethyl ether, vortexing and centrifugation. The pellet was then dissolved in 50 % Acetonitrile in ddH_2O and freeze-dried. Finally the purification was performed by RP-HPLC using a Phenomenex Jupiter Proteo (C12) reverse phase column (4 µm, 90 Å, 10 mm inner diameter × 250 mm long). The eluents used were solution A (0.1 % TFA in H_2O) and solution B (0.1 % TFA in MeCN). The peptide was eluted by applying a linear gradient (at 3 ml/min) of 20 to 60 % B over 40 min. Fractions collected were examined by electrospray mass spectrometry, and the desired product were pooled, lyophilized and stored at -80^{0}C for future use.

2.5 Characterisation of proteins and peptides; Amyloid fibril study

Biophysical experiments: buffers and reagents	
Buffers and reagents	**Composition**
Potassium phosphate (KPP) buffer (1 litre)	100 mM, pH 7.0 (38.5 ml 1 M KH_2PO_4, 61.5 ml 1 M K_2HPO_4 , 900 ml ddH_2O)
Phosphate buffer 10 mM with salt, pH 7.0 used for aggregation studies	100 ml KPP, 100 ml 1 M Potassium fluoride (KF), 0.05% NaN_3, 800 ml ddH_2O
Hexafluoro-2-propanol (HFIP)	100 % (Sigma aldrich, UK)
Tris (hydroxymethyl)-aminomethane (Tris)	10 mM (0.601 g in 500 ml ddH_2O)
Thioflavin T (ThT)	500 µM (31.9 mg in 200 ml of 10 mM Tris), pH 7.5

Table 2.16 Buffers and reagents used for amyloid fibril studies.

PCA peptides			
Name	**Target**	**Scaffold used for design**	**Sequence**
WTA	wild type α-syn_{1-140}	$_{71}$VTGVTAVAQKTV$_{82}$	Ac-VTGVTANPQRTV-NH_2
WTB	wild type α-syn_{1-140}	,,	Ac-VTGVTADVQETV-NH_2
WTC	wild type α-syn_{1-140}	,,	Ac-VTGVTAPDKGTV-NH_2
A30P W	α-syn$A30P_{1-140}$	,,	Ac-VTGVTAHPQNTV-NH_2
E46K W	α-syn$E46K_{1-140}$	,,	Ac-VTGVTANQNNTV-NH_2
H50Q W	α-syn$H50Q_{1-140}$	,,	Ac-VTGVTANSSDTV-NH_2
A53T W	α-syn$A53T_{1-140}$	,,	Ac-VTGVTADNKETV-NH_2
45-54W	wild type α-syn_{1-140}	$_{45}$KEGVVHGVAT$_{54}$	Ac-KDGIVNGVKA-NH_2

Table 2.17 Winner peptide sequences against each target derived from PCA.

2.5.1 Monomerisation of Protein before aggregation studies

Prior to use, the proteins were monomerised using HFIP (Madine *et al.,* 2008) to ensure that the amyloid growth was initiated from the same monomeric state free from pre-formed aggregated species. Proteins were undergone three rounds of dissolution with HFIP (1 ml to 2 mg of protein), vortexing (2 mins), sonication (2 mins at 25^0C in water bath sonicator), and evaporating completely under a regulated stream of air. Finally the solid sample was dissolved in ddH_2O, concentration was calculated and the samples were aliquoted to appropriate concentrations needed for further experiments and lyophilised using a freeze drier.

2.5.2 Thioflavin T (ThT) assay

ThT inhibition assays were performed with monomerised α-syn or mutants at a concentration of 450 µM; in the presence or absence of peptides, resuspended and incubated with 10 mM Phosphate buffer pH 7.0, at 37^0C for 10 days shaking at 300 rpm. The PCA peptides were resuspended in 10 mM Phosphate buffer, added in (target v/s peptide) molar ratio of 1:0.1 (45 µM), 1:1 (450 µM), 1:2 (900 µM), 1:5 (2250 µM) and 1:10 (4500 µM). An additional sub-stoichiometric ratio of 1:0.01 was also considered in the case of 45-54W peptide (Chapter 5). All the peptide solutions were thoroughly vortexed to ensure complete dissolution. The peptides were aliquoted in Eppendorf tubes as per the desired concentrations and lyophilized using a freeze drier. Finally 500 µl of reaction mixture containing 450 µM target protein added to each Eppendorf tube containing various molar ratios of peptide. The final mixture was vortexed and incubated at 37^0C for 10 days. The working stock ThT solution was prepared from a stock of 500 µM. The stock was aliquoted into 1 ml tubes, covered with aluminium foil and kept frozen until it was needed. The stock

was thawed at room temperature for 10 mins and diluted 25x using 10 mM Tris pH 7.5. A total of 197 µl of ThT solution and 3 µl of each inhibition/ reversal assay sample were mixed thoroughly with pipette and transferred to appropriate well in the 96 well microtitre plate. All the samples were analysed in triplicates (technical replicates) as a part of single experiment. The fluorescence was then measured using Perkin Elmer Luminescence Spectrometer LS55 (FLWin program) set at 450 nm (excitation) and 482 nm (emission). For inhibition assays, fluorescence was measured at the day of reaction set up, then for five consecutive days and the final reading at day 10. For the reversal assays, peptides were added at 10^{th} day to the matured target and incubated together for further 3 days.

2.5.2.1 Continuous growth ThT experiments

The peptide 45-54W (Chapter 5) was characterised by continuous growth ThT experiments. Prior to the experiment, the ThT concentration was optimised as 90 µM which was found to be required for saturating amyloid fibrils formed by 450 µM protein. It was analysed by plotting a graph between ThT fluorescence intensity (mAu) of 450 µM target protein mixed with ThT at seven different concentrations (0, 1, 10, 50, 100, 250, and 500 µM). The ThT signal reached the saturation point at a concentration of approximately 90 µM and was considered as optimum for continuous growth experiments. The 45-54W peptide was lyophilized in the molar concentration ratio as 1:1 with target protein. The reaction mixture containing 450 µM wild type α-syn and peptide was incubated in 90 µM ThT, 10 mM Phosphate buffer (pH:7.0), 100 mM KF and 0.05 % NaN3 at 37^0C with continuously mixing at 10xg using a magnetic flea in a Perkin Elmer Luminescence Spectrometer LS55 for 4500 mins. The same experiment was repeated three times for both peptide free sample (1:0) and for

45-54W (1:1 stoichiometry) containing solutions. The peptide 45-54W was lyophilized in aliquots of various stoichiometries ranging from 1:0.01, to 1:1.

2.5.3 Circular Dichroism (CD) assay

CD analysis was used to investigate the secondary structure formation of proteins with/without PCA peptides. CD measures the differences in absorption of Left-hand circular (LHC) and Right-hand circular (RHC) polarized light. The polarisation transitions is typically observed at a wavelength between 195-200 nm for random coil, 218 nm for β-sheet and between 209-222 nm for α-helix appear as minimum (negative ellipticity) in the CD spectra. The CD experiments were undertaken using aliquots taken from the same samples from which aliquots were taken for ThT experiments. The final protein concentration used for CD scan was 10 µM in Phosphate buffer (pH 7.0). Scans were taken using Applied Photophysics Chirascan CD Spectrometer (UK) in the far UV scanning from wavelength of 190 nm to 300 nm, with a step size of 1 nm, bandwidth of 4 nm, at 20^0C, using 0.1 cm cuvette (Helma). Spectra were recorded as the average of three scans.

CD spectra were analysed using Gaussian distribution approach using the below formula;

$$G = I * e^{\left(-0.5*\left(\frac{X-\mu}{\sigma}\right)^2\right)} \quad \text{(Eq: 3)}$$

Where; I = peak intensity,
X= X value (wavelength in nm),
µ=mean peak,
σ= Standard deviation

Separate distributions were fitted for the two minima at 200 nm (random coil) and 218 nm (β-sheet). Both were then added to get the best fit for the CD scan. Then squared the difference between sum fit value and scan value. Sum of the squared difference was

minimised using Solver tool in Microsoft excel thereby corrected the base line transition in each scan.

2.5.4 Atomic force microscopy (AFM)

Samples were imaged in noncontact mode using a XE- 120 Atomic Force Microscope (Park Systems, South Korea). NSC 15 silicon nitride cantilevers with a spring constant of 40 N/m were used for imaging at a scan rate of 1.0 Hz and a resolution of 256 x 256 pixels. All images were taken at room temperature. 5 µl of samples were taken from each reaction conditions and placed on freshly cleaved mica (thickness 0.3 mm). Following adsorption of the protein aggregates (2 min), the mica was washed with 5 ml of ddH_2O. Excess water was removed and the samples were dried using a stream of nitrogen gas. Samples were immediately analysed by AFM. The image files were flattened before processing (Kad *et al*., 2001 & 2003) and examined for average volume by keeping a threshold value to omit the base level noises using WSxM v5.0 (Nanotec Electronica S.L.).

2.5.5 Cell viability assay

Cell viability (MTT) assay: buffers and reagents	
Buffers and reagents	**Source/Composition**
20 % Dimethylsulphoxide (DMSO)	Sigma aldrich, UK
RPMI 1640 + 2 mM Glutamine	Invitrogen
10 % Horse serum (HS)	Invitrogen
5 % Foetal bovine serum (FBS)	Invitrogen
Gentamicin (20 mg/ml)	Invitrogen
MTT buffer	Invitrogen
10x Phosphate buffer saline (PBS)	80g NaCl, 2g KCl, 14.4g Na_2HPO_4, 2.4g KH_2PO_4. Adjust to pH 7.4 with HCl, made up to 1 liter with ddH_2O and autoclave.

Table 2.18 Buffers and reagents used for MTT assay.

2.5.5.1 Rat phaeochromocytoma (PC12) cells

The PC12 cells were maintained in $4x10^6$ density, 37^0C, 5 % CO_2 grown in medium containing RPMI 1640 + 2 mM Glutamine, supplemented with 10 % HS, 5 % FBS and 20 mg/ml gentamicin (all from Invitrogen). The cells were stored as 1 ml stock (20 % DMSO in FBS) in cryogenic tubes, in liquid nitrogen for long term. Whenever needed, the cells were taken out, immediately thawed using water bath at 37^0C, resuspended in 10 ml of pre-warmed sterile RPMI medium as mentioned above, followed by centrifugation for 5 mins at 2000 rpm. The supernatant was discarded and the cell pellets were resuspended in new 15 ml of medium. Finally the cells were transferred into a culture flask and incubated at 37^0C, 5 % CO_2 until it reached appropriate cell density.

2.5.5.2 MTT [3-(4, 5-dimethylthiazol-2-yl)-2, 5-diphenyltetrazolium bromide] assay

MTT assays were carried out using rat phaeochromocytoma (PC12) cells to access the cellular toxicity of aggregated species formed by the α-syn with/without PCA peptides. The assay is based on the reduction reaction occurring in active live cells in turning yellow coloured MTT into insoluble purple coloured formazan. The assay is based on the amount of formazan which was monitored as absorbance at 570 nm correlates with the number of viable cells. MTT Vybrant® Cell Proliferation Kit (Invitrogen) was used for the assay. The assays were performed with 5 µM target protein without/with peptides at various molar ratios between targets: peptide (1:0.1, 1:1, 1:2, 1:5 and 1: 10) incubated for 10 days under sterile conditions. PC12 cells were transferred into a sterile 96 well microtitre plate with $3x10^4$ cells per well. All the experiments were done in triplicates (technical replicates) as a part of single experiment. A required volume of target-peptide reaction mixture was added to appropriate wells containing PC12. A total of 100 µl was made up using RPMI media in each well. The plates were then incubated for 24 hours at 37^0C and 5 % CO_2. After 24 hours, 10 µl of MTT dye was added to each well and incubated for further 4 hours at 37^0C and 5 % CO_2. A total of 100 µl DMSO was added to each well and incubated for another 10 mins. The absorbance was measured at 570 nm using a Bethold Tristar LB942 plate reader.

Chapter 3: A Protein-fragment Complementation approach using an α-syn$_{71-82}$ template to derive peptide antagonists of α-syn aggregation

3.1 Introduction

In PD, α-syn aggregates are found to deposit as inclusion proteins in the neuronal tissue, eventually leading to neuronal death (Lesage *et al*., 2009). Although fibrillar α-syn is a major component of LBs, recent findings show pre-fibrillar, oligomeric intermediates as the toxic species (Winner *et al*., 2011, Emadi *et al*., 2009, Outeiro *et al*., 2008). α-syn belongs to a family of 'synucleins' along with β-synuclein and ϒ-synuclein expressed primarily in neural tissues (George, 2001). α-syn is expressed in different brain regions and is found to interact with a variety of cellular membranes which is considered critical for at least some of its normal functions. One of its function is found to be as a key factor in determining the complex-I activity of the mitochondrial respiratory chain (Liua *et al*., 2009). Although knowledge about the normal function of α-syn is limited, its association with pre-synaptic vesicles and plasma membranes has been well studied (Snead, and Eliezer, 2014). The protein usually dissociates from the vesicles and re-associates slowly during synaptic activity when there is an electrical stimulation inside the dopaminergic neurons (Fortin *et al*., 2005). Whereas misfolded α-syn is unable to incorporate in the storage of dopamine at pre-synaptic terminal leading to the mis-regulation of dopamine pathway and causes the onset of PD symptoms.

α-syn plays a prominent role in the pathogenesis of several neurodegenerative disorders. The 35 residue long central hydrophobic region known as NAC (Non amyloid component) and its precursor (NACP) were found to show high propensity of β-sheet secondary

structure (Ueda *et al*., 1993; Bodles *et al*., 2001). The lack of these amino acid residues within the hydrophobic region of β-synuclein makes it unable to aggregate even though its structure is homologous to α-syn (Uversky *et al*., 2002; Hashimoto *et al*., 2001). In the NAC region, α-syn$_{71-82}$ reflects an extensive and irreversible self-aggregation property and the majority of the amino acids are involved in the formation of a parallel β-sheet conformation. The deletion of 71-82 in the NAC region of human α-syn was found to prevent protein aggregation. The importance of α-syn$_{71-82}$ for fibril formation was realised when many studies observed a prolonged lag phase for β-synuclein to polymerize into fibrils (Bodles *et al*., 2001; Giasson *et al*., 2001, Bedard *et al*., 2014). To further narrow down the importance of amino acids within this region, shorter deletion mutants (Δ74-82, Δ74-79, Δ76-77) shows a propensity to form spherical oligomers and are unable to assemble into mature fibrils (Waxman *et al*., 2010). A decrease in the aggregation rate was studied after the substitution of Alanine$_{76}$ either with positive Arginine or negative Glutamic acid residue (Giasson *et al*., 2001), and also found to contribute to the structural and assembly behaviour of full length α-syn fibrillisation. The significance of a four residue 'signature motif', Gly-Ala-XX, (where X is an amino acid with an aliphatic side chain) was found to be crucial for the aggregation of amyloidogenic proteins such as β-amyloid, prion protein, islet amyloid polypeptides and α-syn (El Agnaf *et al*., 1998; Uversky *et al*., 2002; Bodles *et al*., 2004; Du *et al*., 2003). The role of this 'signature motif' in α-syn is significant as, the deletion or incorporation of charged residues to ^{68}GAV^{70} prevents β-sheet formation. The lengthy lag phase in fibrillisation of ϒ-synuclein which lacks this signature motif also suggests its importance in the aggregation process. Thus ^{68}GAV^{70} along with ^{71}VTGV^{74} sequence plays an important role in regulating fibrillisation (Du *et al*., 2003). An important therapeutic strategy for preventing amyloid deposition is to identify the agents that can interrupt the fibrillisation process thereby

inhibiting the propagation of fibril growth or accelerating aggregation to non-toxic insoluble deposits or stabilizing the native structure of α-syn (Gilead *et al.*, 2004; Hard *et al.*, 2012). One approach is to synthesize modified short peptides that can bind to the parent protein and prevent its further aggregation. Such modifications include amino acid substitutions, side chain modifications, insertion of Proline or use of D-amino acids into or adjacent to fibrillogenic domains, peptide terminal end modifications, addition of N- and C- terminal blocking groups, peptide cyclization and replacement of amide bonds with ester linkages (Sciarretta *et al*., 2006; Madine *et al.*, 2008). Many groups have considered adding a N-methyl group while designing peptide inhibitors. The concept is; N-methyl group reduces hydrogen bond propensity due to replacement of the amide hydrogen and it leads to the disruption of hydrogen bond network which is essentially required for the formation of a stable β-sheet fibril. A peptide inhibitor based on α-syn$_{68-78}$, N-methylated at Gly73 has been developed with encouraging results (Bodles *et al*., 2004). Madine and colleagues developed a several N-methylated peptides based on α-syn$_{71-82}$ (mVTGVTA, VTGmVTA, VmAQKTV, VAQKTmV and VmAQKTmV). They undertook solid state NMR analysis and identified a peptide VAQKTmV as an effective candidate in preventing the aggregation of full length α-syn to form large insoluble fibrils (Madine *et al.*, 2008). El-Agnaf and co-workers designed another peptide inhibitor (RGAVVTGR) based on α-syn$_{68-72}$ by incorporating one or two hydrophilic residues (R and G) at the N- and/or the C-terminus of ^{68}GAVVT^{72} peptide (El Agnaf *et al*., 2004).

This chapter focuses on characterising new antagonists of α-syn aggregation developed by screening peptide libraries *in vivo* using a protein-fragment complementation assay (PCA) methodology. PCAs have shown promise as a method to screen for specific therapeutic

peptides of numerous protein-protein interactions (PPIs), including amyloid-based systems (Acerra *et al*., 2014; Mason *et al*., 2006; Remy *et al*., 2007; Pelletier *et al*., 1999). In PCA two proteins of interest are fused to incomplete complementary fragments of a third essential protein ('reporter'). The specific protein-protein interaction is dependent on not just proximity but also the peptides must organize precisely in space to allow further folding into the native structure thereby reconstituting its activity. The 'reporter' activity is detectable by the survival of cells expressing the fusion proteins and growth in selective minimal medium. Here murine dihydrofolate reductase (mDHFR) is the enzyme used as 'reporter' in which α-syn$_{1-140}$ is fused to one half and peptide library fused to the other half. The activation of mDHFR is essential for the growth of *E coli* cells on minimal M9 medium in which the bacterial mDHFR has been selectively blocked using trimethoprim. Therefore if a binder from the peptide library interacts with α-syn, it will bring the two halves of mDHFR into close proximity and recombine the enzyme to constitute cell growth under selective conditions. The *E coli* DHFR is selectively inhibited by the antifolate trimethoprim which has 12000 fold more sensitivity than mDHFR (Pelletier *et al*., 1998). The colony growth under selective pressure of trimethoprim along with IPTG is highly restricted only for the cells expressing both mDHFR fragments. PCA has advantageous attributes as it is carried out *in vivo*, meaning that aggregation prone, insoluble, protease sensitive, unstable, and weak binders will be removed at the screening level itself. No assumptions were made during PCA regarding the mechanism of action or the oligomeric state of α-syn that becomes populated. The only pre-requisite for peptide selection was the peptides bind to α-syn such that split reporter enzyme is recombined and expressed. Thus the library members binding to α-syn thought to reduce its toxicity and confer cell survival (Acerra *et al*., 2013). The strategy to design peptide inhibitors was based on α-syn$_{71-82}$ scaffold which should interact specifically

with full length α-syn, interrupt its aggregation or breaking down preformed fibrils to less toxic oligomers. These studies have provided some successful peptide candidates harbour the potential to be further developed into drugs in the future.

3.2 Experimental approach

This chapter describes the purification process of wild type α-syn and characterization of antagonistic peptides generated using semi rational peptide design, combined with PCA.

(1) Purification of α-syn: small ubiquitin related modifier (SUMO) fusion technology was used for enhanced functional α-syn expression in *E coli* cells (Lee *et al*., 2008; Marblestone *et al*., 2006; Butt *et al*., 2005; Malakhov *et al*., 2004; Mossessova *et al*., 2000). SUMO is found to be more effective and productive over other fusion tags in enhancing expression and solubility of recombinant protein. The direct fusion of the target protein to SUMO produces a generation of recombinant protein with native N-terminal sequences. SUMO tag has the ability to associate with SUMO protease enzyme (ULP1) which has the advantage of recognizing the tertiary structure of SUMO (Marblestone *et al*., 2006). Thus SUMO fusion system was found to be ideal for soluble expression of proteins compared to other traditional gene fusion systems. Efficient removal of SUMO tag by ULP1 *in vitro* facilitated the production of pure α-syn. The purified protein was monomerised using hexafluoro-2-propanol (HFIP) treatment (Madine *et al*., 2008- See chapter 2) before using it for any aggregation studies.

(2) Peptide characterisation: The effect of peptides designed using α-syn$_{71-82}$ scaffold against full length α-syn were studied using Thioflavin T (ThT) dye binding experiments

(Wolfe *et al*., 2010; Khurana *et al*., 2005) and circular dichroism (CD) for the quantification of secondary β-sheet structures. Atomic force microscopy (AFM) was used for direct imaging to confirm the ThT and CD data (Kad *et al*., 2001 & 2003). The peptides were analysed for their inhibitory as well as the reversal effects on α-syn aggregation. In this chapter, 450 µM of α-syn (Madine *et al*., 2008) was incubated with 450 µM of each peptide in 500 µL of potassium phosphate buffer (10 mM, pH 7.0), KF (100 mM) and NaN_3 (0.05 %) buffer at 37^0C with continuous shaking in an orbital incubator at 10xg for 10 days in inhibition assay and three more days (post-mix) in reversal assay. Finally, the effect of peptides on the viability of PC12 cells (by reducing α-syn toxicity) was investigated using the MTT cell toxicity assay. MTT assay was performed at 5 µM α-syn with five different molar concentration ratios of peptide (1: 0.1, 1, 2, 5, and 10). Control experiments by incubating peptides alone without α-syn were undertaken to verify the reliability of the peptides. In addition a negative (SGSSGTSSGTSG) and a positive [VAQKTmV (Madine *et al*., 2008)] control at molar ratio 1:1 were also analysed along with peptide winners. The peptide; SGSSGTSSGTSG is the GS linker and is therefore a useful good control peptide in investigating the specificity of PCA derived peptides towards α-syn.

3.3 Results

3.3.1 Purification of α-syn from bacterial culture

The wild type α-syn was synthesized by over expression in *E.coli* (BL21 strain) using SUMO fusion technology. The transformed cells with SUMO fused α-syn were grown in Luria Bertani (LB) broth containing appropriate antibiotics (Amp and Cm; details in chapter 2) at 37^0C and 220 rpm. The cells were induced with 1 mM Isopropyl β-D-thio-galactopyranoside (IPTG) when the cell density reached at OD_{600}: 0.6 after approximately 3 hours. After that the cells were recovered by centrifugation, then sonicated and centrifuged to obtain a supernatant containing expressed SUMO fused α-syn. The fusion protein in the cell lysate was purified by Ni-NTA affinity column and an absorbance peak (A_{280}) obtained using an AKTA prime purifier (GE health care) at an elution volume of approximately 60 ml as shown in Fig 3.1.a. Following Ni-NTA purification, the SUMO conjugated α-syn undergone cleavage reaction to remove SUMO tag using SUMO protease enzyme (ULP1). The cleaved protein was purified using size exclusion chromatography and obtained various fractions as shown in Fig 3.1.b. The un-cleaved protein, purified α-syn and SUMO protein were collected in various fractions. The purity of proteins were analysed by 15 % SDS PAGE gel as shown in Fig 3.1.c, and the actual mass was confirmed by electrospray mass spectrometry as shown in Fig 3.1.d.

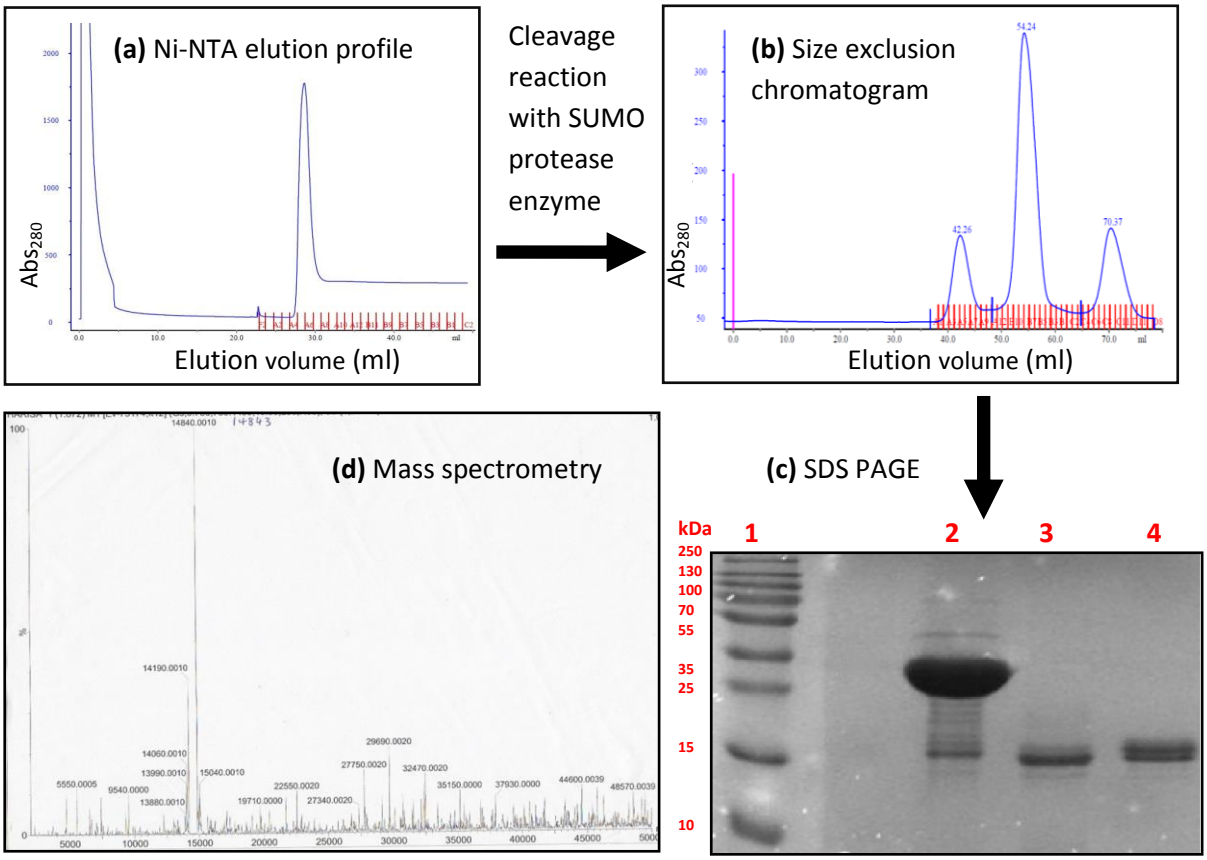

Figure 3.1: ***(a)*** Ni-NTA affinity chromatogram showing the SUMO protein fusion eluted as a peak (Abs_{280}). ***(b)*** The size exclusion (G75) chromatogram showing different peaks (Abs_{280}) of: (1) Uncleaved protein at 42.26 ml, (2) purified α-syn at 54.24 ml and (3) SUMO protein at 70.37 ml as elution fractions. ***(c)*** SDS PAGE gel characterising various elutions from G75 **Lane 1:** Protein ladder, **Lane 2:** Uncleaved protein (27 kDa), **Lane 3:** pure α-syn (14.8 kDa), **Lane 4:** SUMO protein (12.2 kDa). ***(d)*** Mass spectrometry data showing purified protein with mass 14,840 Daltons. (Actual mass expected: 14843 Daltons).

3.3.2 PCA derived peptide characterization

From a semi randomised library designed, three peptide winners were screened using PCA against α-syn$_{1-140}$. The selection approach was based on α-syn$_{71-82}$ which is known to self-aggregate. Among 12 residues, the C-terminal residues $_{77}$VAQK$_{80}$ was fully randomised as studies confirm it to be the most effective residues in forming ordered fibrils (Madine *et al*., 2008). The peptide winners were generated by the project students previously and the characterisation studies were performed by me. The peptides were bought from Peptide Synthetics, Fareham, UK.

Name	Sequence
WTA	Ac-VTGVTANPQRTV-NH_2
WTB	Ac-VTGVTADVQETV-NH_2
WTC	Ac-VTGVTAPDKGTV-NH_2

Table 3.1: PCA derived peptide 'winners' from a screen against full length wild type α-syn. Library was designed by fully randomising four amino acid positions of α-syn at $_{77}$VAQK$_{80}$. Inclusion of N-acetylation and C-amidation was used to provide additional hydrogen bond acceptors and donors.

3.3.2.1 ThT experiments

The fluorescent dye ThT was used to identify the degree of amyloid fibrils formed by α-syn. It was monitored using 10 µM ThT solution (pH: 7.5; buffered using 10 mM Tris HCl). The ThT fluorescence was taken at the same time the peptides were added; this was considered a day 0 reading. The fluorescence was measured consecutively for next five days and the final reading was taken at day 10 (end point sample). The negative (SGSSGTSSGTSG) and positive [VAQKTmV (Madine *et al*., 2008)] control peptides at molar ratio 1:1 were also analysed after 10 days of incubation along with the PCA-selected peptides; WTA, WTB and WTC. The ThT experiments were performed in triplicates (technical replicates) as a part of single experiment using a micro-titre plate and the fluorescence was read with a Perkin Elmer Luminescence Spectrometer LS50B (FLWin program) set at 450 nm (excitation) and 482 nm (emission). During intensity calculation, blank reading was considered and normalised the ThT value to 1:0 (peptide free wild type α-syn) sample.

In the inhibition assay, all the three peptides lead to the reduction of ThT signal (Fig 3.2). It confirms the interaction of PCA peptide with α-syn during the aggregation process. In the case of WTA, the ThT signal was reduced relative to peptide free sample (1:0) until the endpoint sample which marked its inhibitory effect. Peptide WTB was actually facilitating the aggregation process by attaining matured fibrils by second day itself. From the data, WTB was least efficient candidate in inhibiting fibril growth, but it showed a reduction of 33 % in the endpoint sample. This sudden drop in ThT signal was later investigated by using CD and AFM. The peptide WTC showed a delayed inhibition in the initial phase until it regained its inhibition property after four days of incubation. In the inhibition assay, significant

reduction of ThT values in each molar ratio were seen compared to 1:0 which were analysed using 'T' test with the p values; WTA=0.0053, WTB= 0.0041 and WTC=0.0035 (threshold 0.05) in the day 10 samples and WTA=0.0009, WTB=0.347, WTC=0.019 in the reversal approach. The PCA selected peptides were compared with positive control peptide which at a molar ratio of 1:1; demonstrated a moderate reduction of amyloid content and the negative control peptide as expected showed no effect in the aggregation process. In the reversal assay (Fig 3.2), WTA was found to reduce the amyloid load more compared to the other two peptides, while WTB exhibited minimal effect. Collectively the three peptides have minimal effect in reverting or breaking down the matured fibrils. Positive control peptide showed no reversal effect as reported in the literature. Summarising the ThT data, PCA derived peptides have a moderate inhibitory effect on amyloid formation but minimal effect in disintegrating the matured fibrils.

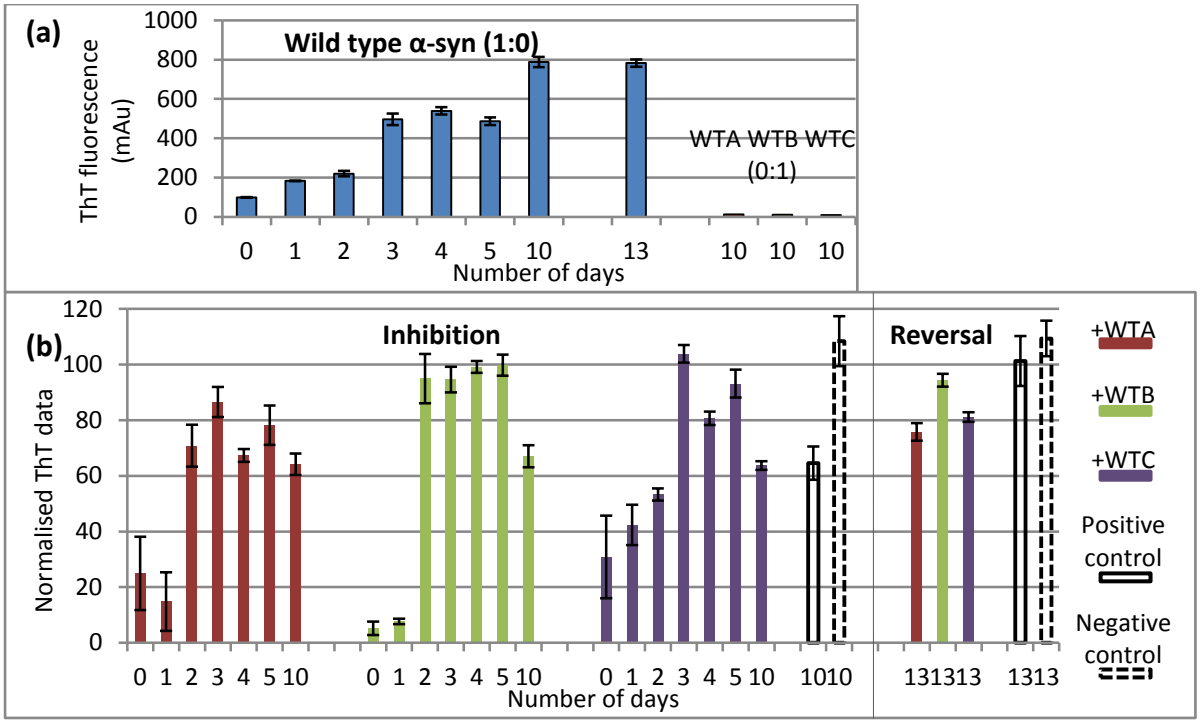

Figure 3.2: ThT fluorescence data: ***(a)*** show the aggregation of wild type α-syn$_{1\text{-}140}$ (1:0) for days 0, 1, 2, 3, 4, 5, 10 (for inhibition) and 13 (for reversal) at a concentration of 450 µM and three peptides alone as control (0:1). ***(b)*** The ThT inhibition and reversal data of wild type α-syn$_{1\text{-}140}$ in the presence of PCA peptides WTA, WTB and WTC (red, green, and purple bar respectively) at a stoichiometry of 1:1 normalised to 1:0. The inhibition assay was performed on days 0, 1, 2, 3, 4, 5, 10 and the reversal assay at day 13 (post mix incubation of 3 days). ThT values were taken in triplicates (technical replicates) as a part of single experiment and the error bars were calculated as the standard deviation of all errors. With WTA, there is consistent reduction in ThT bound aggregates in all data points finally reducing to 36 % at the endpoint sample. While in WTB, the ThT bound from day 2 to 5 show a minimal reduction leading to a sudden drop of 33 % at day 10 sample. A delayed aggregation process until second day can be seen in WTC with 37 % reduction in the end point sample. In the reversal assay, the data show a reduction of 24 % in WTA, 6 % in WTB and 19 % in WTC which appears to be less effective than inhibition assay. Positive and negative (solid and dashed black bars respectively) control peptides were also analysed by both inhibition and reversal approaches.

Positive control peptides showed 36 % reduction at 1:1 stoichiometry at 10^{th} day of incubation but didn't show any effect in reversing matured fibrils.

3.3.2.2 CD assay

The formation of secondary β-sheeted structure during α-syn aggregation was analysed by CD along with ThT experiments. The CD experiments were undertaken using aliquots taken from the same stock samples used for ThT experiments. The final α-syn concentration used for CD analysis was 10 μM. The data (Fig 3.3) shows the spectra with the transition of single negative peak from 200 nm (random coil) to 218 nm (β-sheet). The random coil signal for three peptides in isolation (Fig 3.3.f) confirms the peptides do not self-aggregate.

A 10-30 % reduction found in the final day sample with all three peptides shows a decreased β-structure relative to 1:0. In accordance with ThT data, peptide WTC exhibits a slight delay in the aggregation process as greater random coil signal was retained until second day of incubation but 25 % fibrillar breakdown in reversal assay was in discrepancy with ThT data. WTB showed a greater β-signal compared to other two peptides throughout the process and has least effect in reversing fibril growth. Contradictory to ThT data, WTA appeared to have minimal effect in both aggregation and reversal processes. Approximately 50 % reduction was achieved by positive control peptide, but unexpectedly negative control also inhibited the β-sheet formation. The discrepancy in ThT and CD data regarding negative control was investigated by using AFM imaging. Along with ThT data, CD spectra collectively suggest that peptide WTC possess considerable inhibitory effects and partial reversal effects compared to other two peptides. The reduction of β-signal in the negative control is inconsistent with ThT data. GS linker was used in PCA and is a good negative control as it is not really hydrophobic, Gly and Ser don't interact that strongly during β-formation. Though

there is a possible artefact in PCA that the linkers in peptide and target would bind to each other but is not enough for bringing the peptide closer to the target which shouldn't be binding. The reduction in β-content with the negative peptide was further investigated using AFM.

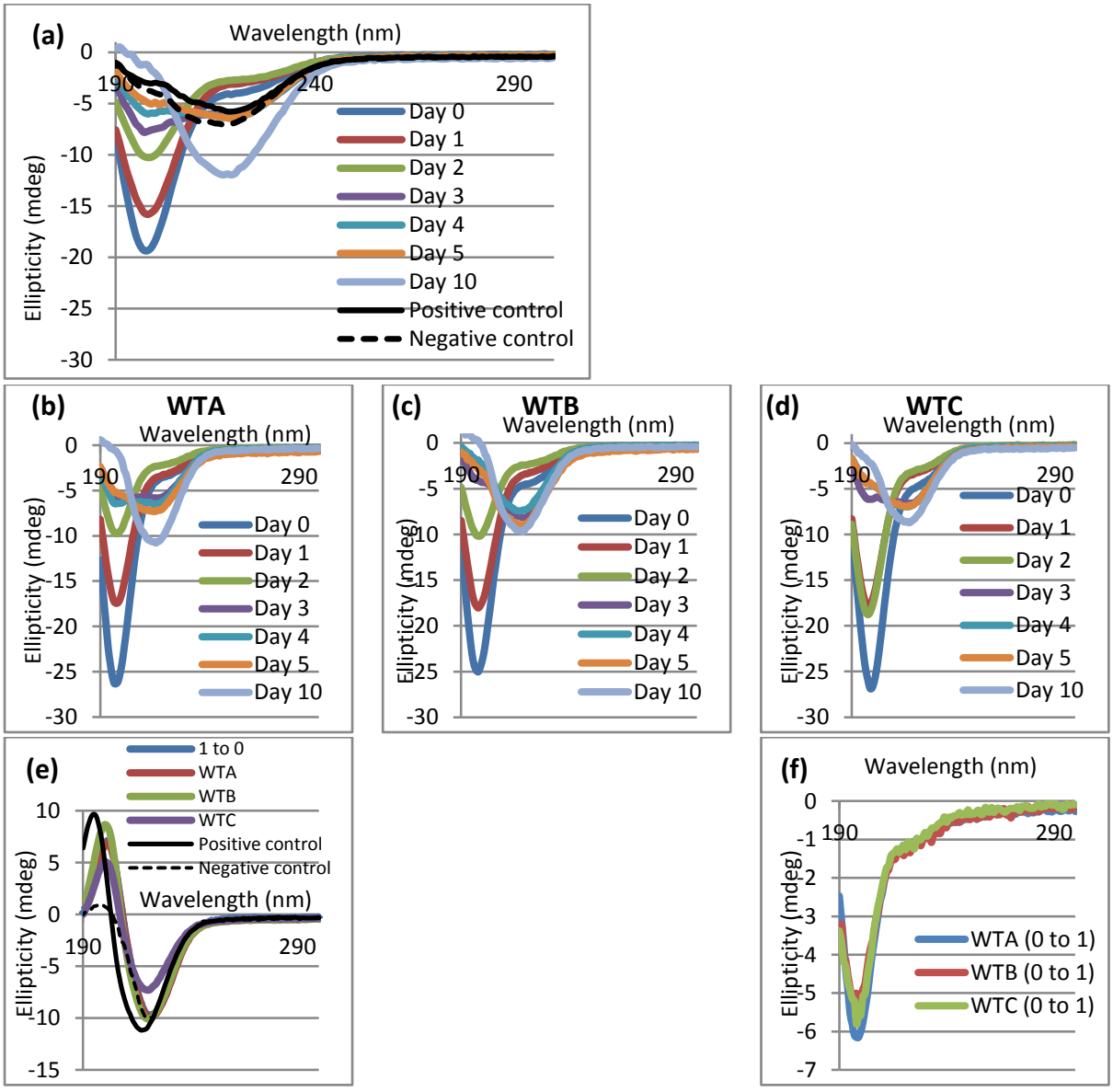

Figure 3.3: CD spectra of: *a)* α-syn$_{1\text{-}140}$ (peptide free sample; 1:0) and with positive/negative control peptides after 10 days of incubation, ***b),c),d)*** Inhibition assay: α-syn$_{1\text{-}140}$ with PCA peptides WTA, WTB, WTC respectively, ***e)*** Reversal assay, and ***f)*** Three peptides alone (0:1) after 10 days of incubation. A single minimum at 200 nm indicates the presence of random coil structure and at 218 nm indicates the amount of β-content. The data shows a gradual transition of random coil to β-sheet in all spectra

in course of time. In support with the ThT data, a reduced amount of β-sheet compared to 1:0 can be found in the endpoint samples with three peptides. In Fig d) the delayed aggregation process in WTC can be seen as the existence of comparatively greater random coil signal until day 2 which is consistent with ThT data. The peptides were compared with positive control which shows approximately 50 % reduction relative to 1:0 but negative control also unexpectedly inhibited secondary structure formation. The reversal data show that WTA and WTB show minimal effect on reducing matured fibrils while a slight decrease of approximately 25-30 % can be seen with WTC which is inconsistent with 19 % in ThT data.

3.3.2.2.1 Gaussian fit analysis of CD spectra

Gaussian fit analysis assumes that there is only the presence of random coil or/and β-structure. Prior to the analysis, the CD spectra of each peptide in isolation were subtracted from that of α-syn in the presence of peptides to identify the real structural changes of α-syn incubated in each condition. Figure 3.4.a shows the range of negative ellipticity values at 200 nm and 218 nm in inhibition assay after Gaussian fit analysis. A gradual decrease of random coil and increase of secondary β-structure can be seen in 1:0. Reduction of 10-30 % at 218 nm signal can be seen in the final sample of all the three peptides compared with 55 % reduction with positive control peptide. In WTC, retention of the random coil signal can be seen stronger even at second day as stated before. In reversal assay (Fig 3.4.b), WTA and WTB followed the profile of 1:0 while approximately 25 % fibril breakdown in WTC. Positive control showed a minimal effect in reverting fibrils.

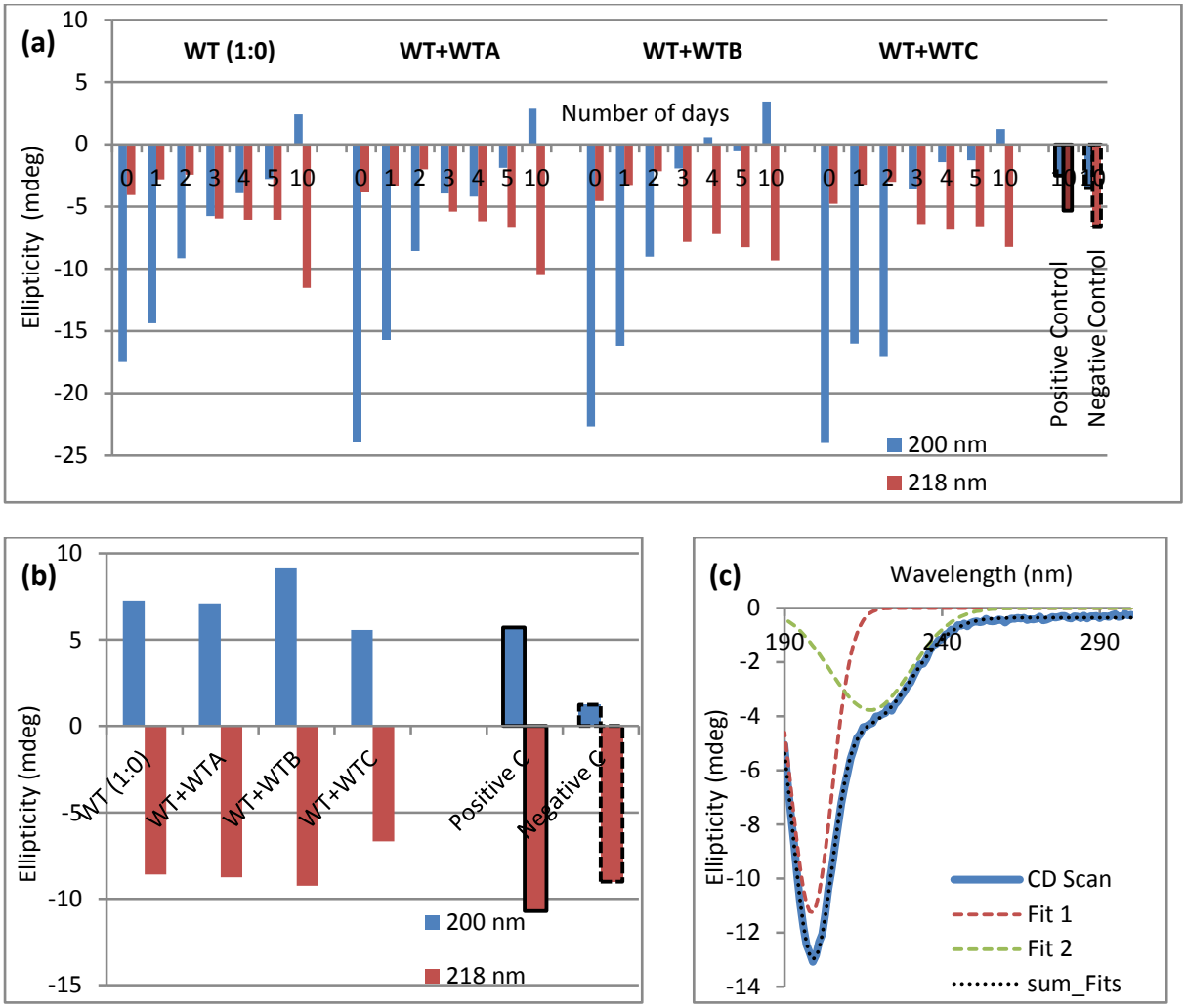

Figure 3.4: The minima at 200/218 nm from all CD spectra after **Gaussian fit analysis;**

(a)* Inhibition assay:** 200/218 nm minima of wild type α-syn with and without WTA, WTB and WTC, positive & negative control peptides. Predominantly the delaying of random coil transition can be seen with WTC supporting the point of delayed aggregation process as seen in ThT assay. Reduction of 10-30 % in the final day sample with each peptide compared with 55 % reduction with positive control peptide can be seen. ***(b)* Reversal assay:** 200/218 nm minima in CD spectra of wild type α-syn with and without peptides, positive & negative control peptides after 3 days (post mix) incubation. 25 % fibril breakdown in WTC can be seen with no effect in WTA and WTB. Positive control showed minimal effect in reverting fibrils. ***(c) A **representative model** of Gaussian distribution analysis displaying the sum of two individual curves (200/218 nm) fits the scan.

3.3.2.3 AFM imaging experiments

AFM was performed on the same samples of wild type α-syn used for ThT and CD experiments for direct visualisation of different aggregated species formed with and without PCA peptides at a molar concentration of 1:1. Samples from both inhibition and reversal assays were imaged using AFM along with controls (peptides alone (0:1), positive and negative control peptides). The aim of imaging was to identify the amount of protein deposited as amyloid. All images were taken at resolution of 256x256 pixels at room temperature. The vertical resolution can be up to 0.1 nm in AFM. Consistent with ThT and CD data the peptides were moderately inhibiting the fibrillisation rather than reversing the process.

3.3.2.3.1 AFM images: Inhibition assay

AFM images were taken for the different species formed during the initial five days and day 10. The images were taken from the first day onwards to show the gradual increase of amyloid content. The absence of any structures at day 0 confirmed the absence of any pre-formed fibrils achieved by monomerisation using HFIP. In the inhibition assay (Fig 3.5), clumps of short fibrils were seen in AFM images of α-syn in the absence and presence of peptides in the day 10 sample. Since it was difficult to visually distinguish the amount of fibril content from the images, they were analysed using histogram of volume average using WSxM v5.0 software.

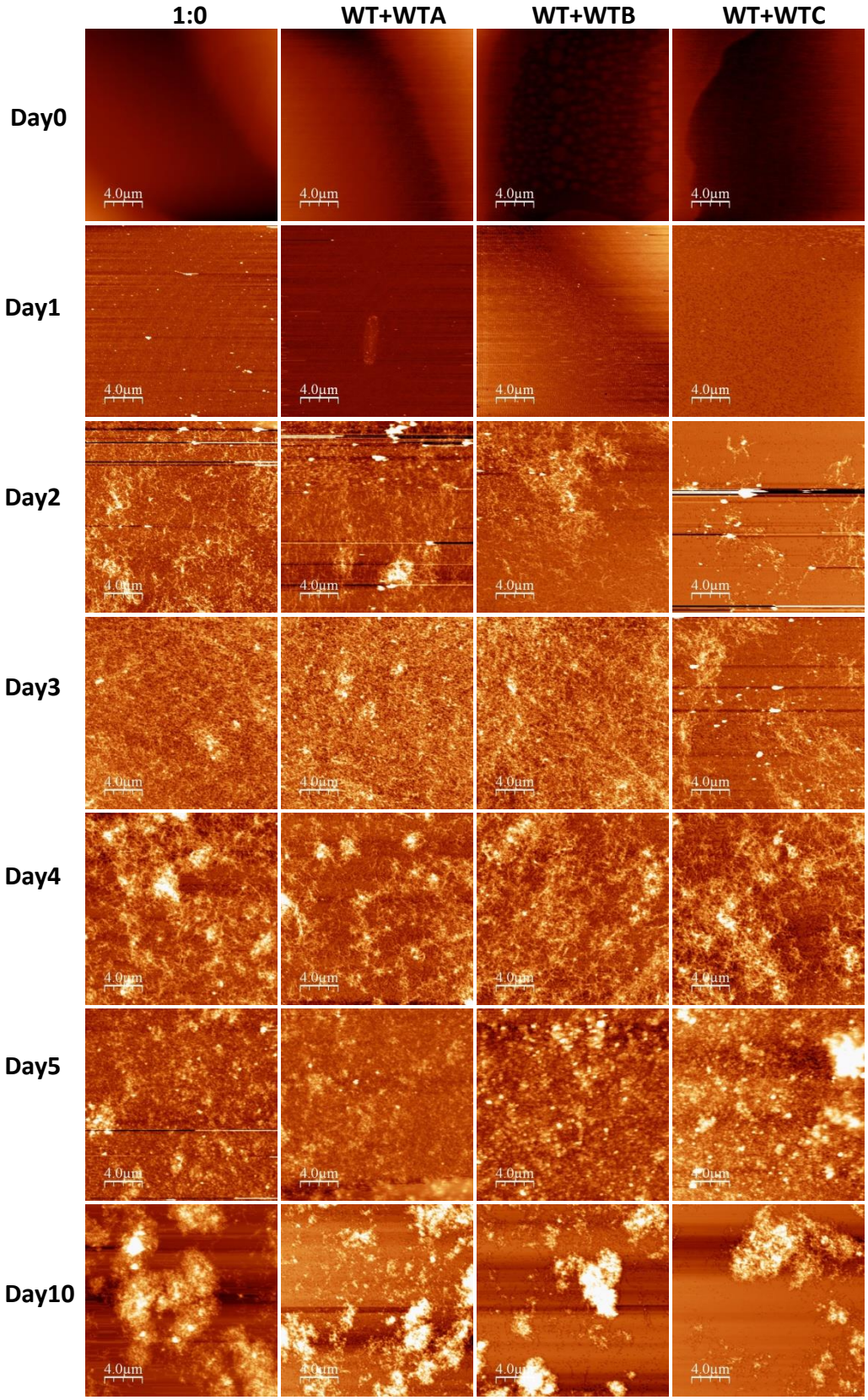

Figure 3.5: AFM images showing α-syn$_{1\text{-}140}$ (1:0) and α-syn with peptides WTA, WTB and WTC. In each condition, a representative image from the images taken in various locations of the mica sheet is shown here. Gradual development of amyloid fibrils was observed in all the conditions.

Comparative reduction of fibril content was observed in WTC on day 2 sample. It confirms the delayed formation of amyloid fibrils as seen in ThT and CD data. In addition, the endpoint samples show a similar pattern of fibril load as 1:0 in all the three peptides. All images were taken at 20 µm scan size. The image files were examined directly using WSxM v5.0 (Nanotec Electronica S.L., www.nanotec.es) and flattened before processing. (Kad *et al*., 2001 & 2003).

3.3.2.3.2 AFM image analysis: Inhibition assay

AFM images were analysed using WSxM v5.0 (Nanotec Electronica S.L., www.nanotec.es). In order to find the volume of aggregated protein covered on the mica surface, the images were flattened before processing (Kad *et al*., 2001 & 2003). The average volume was calculated by maintaining a constant threshold level manually to nullify the background noise, thereby eliminating the non-fibrillated or monomeric α-syn (Fig 3.6). Figure 3.5 showed a representative image in each case from a total of five different areas randomly chosen on the mica sheet. For analysis the average volume of all the five images were considered and the error bars were calculated as the standard deviation of all errors. The analysis demonstrated a reduction of approximately 20-25 % fibril volume, compared to 1:0 can be seen in the final day sample in the presence of three peptides. Consistent with the above assays, WTC distinctively showed a reduced fibril content on samples taken from day 2 and 3 confirming the delayed formation of amyloid fibrils.

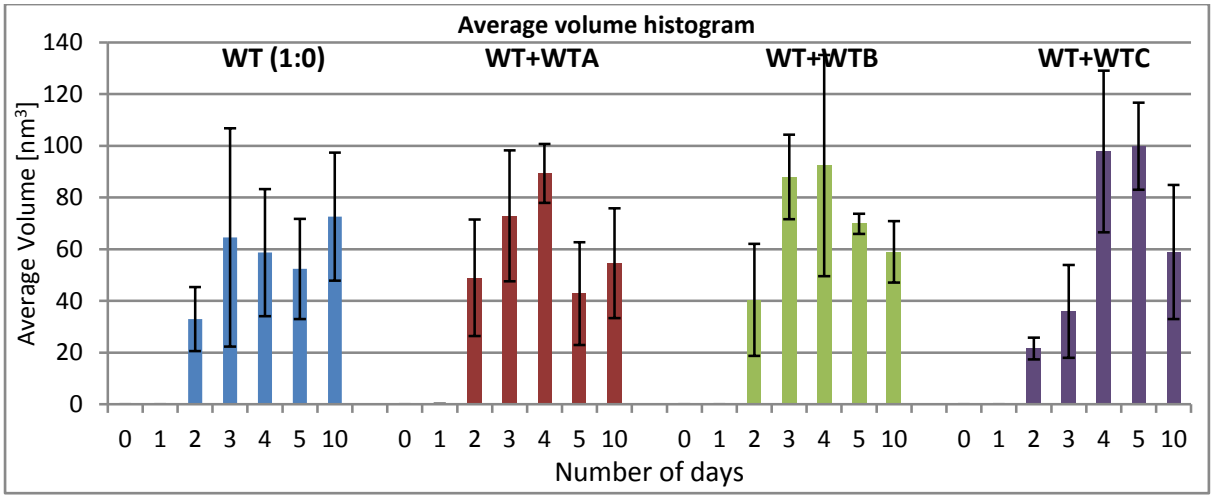

Figure 3.6: Histograms showing average volume of aggregated protein on the mica surface analysed using WSxM v5.0 software. In each condition, the development of fibrils can be seen along with incubation. WTC shows reduced volume at day 2 and 3 samples confirm the delayed amyloid formation. Reduced fibril content of approximately 20-25 % can be seen in the final day sample of three peptides compared to 1:0. Red, green, and purple bar represent WTA, WTB and WTC respectively.

3.3.2.3.3 Control experiments (AFM images of three peptides in isolation (0:1) and positive/negative control peptides): Inhibition assay.

To demonstrate that the peptides do not self-aggregate, AFM imaging was undertaken at molar concentration of 0:1 along with ThT and CD assays. At a concentration of 450 µM each of the three peptides was incubated for 10 days under similar conditions used for α-syn. In Figure 3.7, consistent with ThT and CD data the three peptides show absence of fibril formation after 10 days of incubation. Along with that the positive control peptide (1:1) facilitated the non-fibrillar structure formation and negative control peptide followed the fibril growth to that of 1:0.

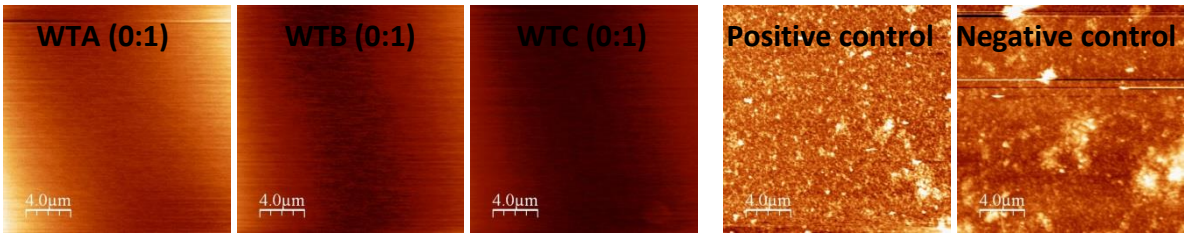

Figure 3.7: AFM images showing the absence of fibril content in the three peptides (WTA, WTB and WTC) in isolation at a molar concentration of 450 µM. The two right side images show positive and negative control peptides. The positive control show non-fibrillar structure while clumps of short fibrils in negative control at stoichiometry of 1:1.

3.3.2.3.4 AFM images: Reversal Assay

In the reversal assay, the peptides were added to α-syn (after 10 days of maturation) at a molar concentration of 1:1 to break down the fully formed fibrils into monomers. The images were taken for all the samples after post mix incubation of three days (Fig 3.8). All the three peptides along with positive control peptide showed no effect in reversing the matured fibrils.

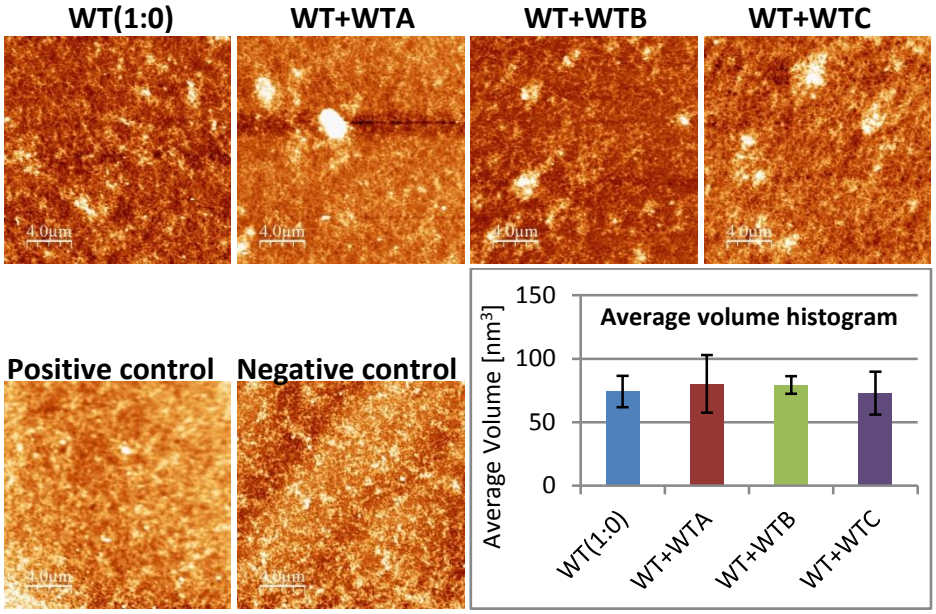

Figure 3.8: AFM images in the top row showing the reversal approach on α-syn$_{1-140}$ (1:0) with peptides WTA, WTB and WTC after a post mix incubation of 3 days. In the bottom row, left two images demonstrates the reversal effect of positive and negative control peptides on α-syn. The histogram at the bottom right showing average volume of aggregated protein in each peptides case analysed using WSxM v5.0 software. Red, green, and purple bar represent WTA, WTB and WTC respectively. The three peptides along with positive control show no effect in breaking down of the fibrils.

3.3.2.4 Cell toxicity: MTT assay

The aim of this study was to evaluate the effect of extracellular α-syn deposits on rat pheochromocytoma (PC12) neuronal-like cells. Though PCA was performed intracellularly in bacteria, MTT was investigating extracellular deposits of α-syn. It was justified by the recent studies which suggest that trivial amounts of α-syn contribute to the progressive spreading of α-syn pathology. Several environmental factors could gain access to the enteric nervous system where they induce α-syn aggregation which would be analogous to the transmission of prion disease (Olanow and Brundin, 2013). Another study suggest that the intragastric administration of the pesticide rotenone resulted in the formation of α-syn aggregates in the enteric nervous system, and the dorsal motor nucleus of the vagus nerve leading to PD symptoms (Montojo *et al*., 2010).

MTT assay determines the cell viability using the reduction of water soluble MTT (3-(4, 5-dimethylthiazol-2-yl)-2, 5-diphenyltetrazolium bromide) into insoluble purple coloured formazan. The concentration of formazan was then determined by the optical density at 570 nm. The amount of formazan is directly proportional to the number of viable cells. All experiments were performed in triplicates (technical replicates) as a part of single experiment and the error bars were calculated as the standard deviation of all errors. First of all, the concentration of α-syn exhibiting PC12 toxicity was optimised. The experiment was performed with three different concentrations of α-syn 0.5, 5 and 45 μM. As a minimum concentration of target required for cellular toxicity, 5 μM was considered for the further peptide studies (Fig 3.9).

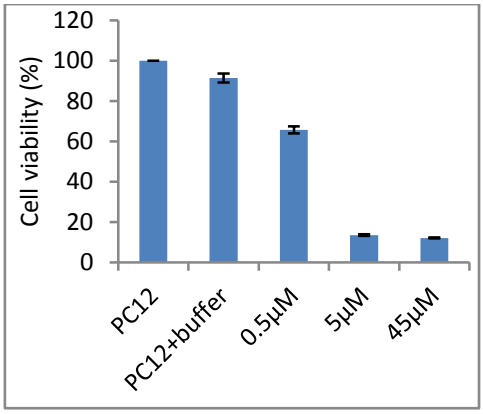

Figure 3.9: MTT assay showing the effect of α-syn at three different concentrations of 0.5, 5 and 45 µM on PC12 cells. 5 and 45 µM show reduced percentage compared to PC12 cells in isolation. PC12 with the buffer (used for aggregation experiments) was used as control which shows minimal effect in cellular toxicity. All the experiments were performed triplicates (technical replicates) as a part of single experiment and the error bars were calculated as the standard deviation of all errors.

In the assay PC12 cells were grown in isolation, with 5 µM α- syn, with α-syn-peptide ratios (1:0.1, 1, 2, 5, and 10), with α-syn-positive/negative control peptides (1:1) and each of the three peptides; WTA, WTB and WTC in isolation (0: 0.1, 1, 2, 5, and 10) all incubated for ten days under aseptic conditions. After that cells were added and incubated for 24 hours followed by 4 hours in MTT dye. Figure 3.10 shows the cell viability across a range of α-syn-peptide ratios relative to PC12 cells in isolation. Apparently the fibril formed by α-syn is toxic to the cells. The aggregated species formed in lower ratios 1:1 and 1:2 in all the three peptides were less toxic compared to higher ratios. In the lower ratios approximately 30-55 % of cell viability was achieved by three peptides whereas super stoichiometric ratios found to be more toxic. Peptides were compared with positive control peptide and surprisingly the species formed found to be toxic to cells. Three peptides in isolation showed negligible effect on cell growth.

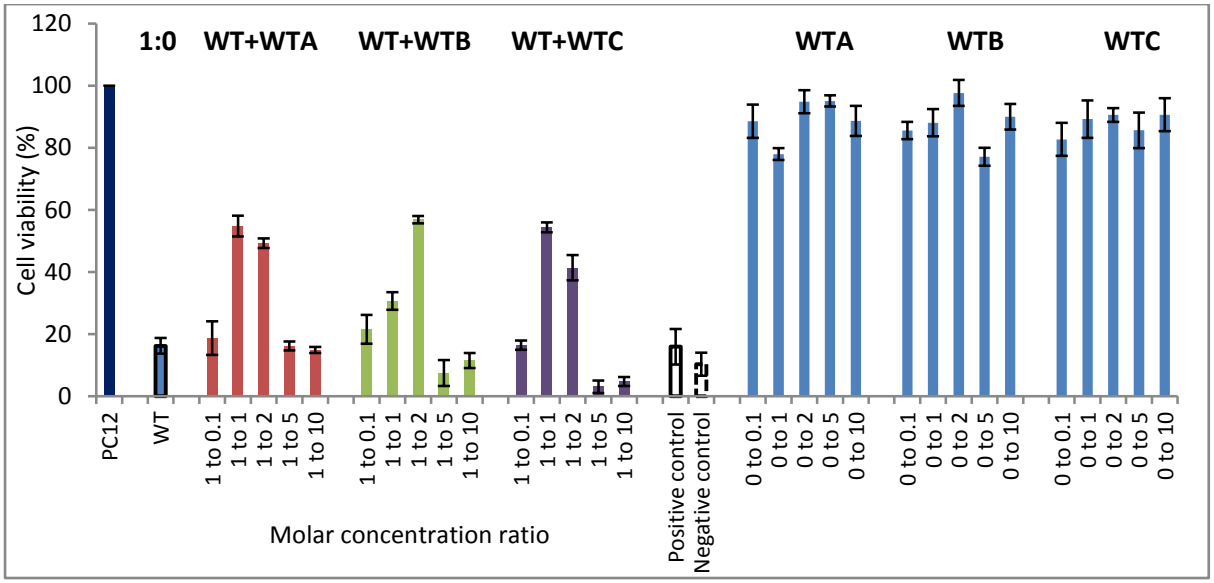

Figure 3.10: MTT toxicity assay showing cell viability with α-syn$_{1\text{-}140}$ (1:0), α-syn with PCA peptides at various molar ratios (red, green and purple bars represent WTA, WTB, WTC respectively), with positive/ negative control peptides and the peptides (WTA, WTB, WTC) in isolation. The assay was performed by incubating PC12 cells and 5 µM α-syn in the presence and absence of peptides at different molar ratios (1: 0.1, 1, 2, 5, and 10) for 24 hours. The endpoint samples incubated for 10 days were used in this assay. The data show that the species formed at molar ratios 1:1 and 1:2 show a cell revival between 40-55 % in WTA and WTC whereas 30-56 % in WTB. The species formed at the higher stoichiometric ratios (1:5, 1:10) in all the three peptides show similar or greater toxicity on PC12 cells. In effect the aggregated species formed with 1:1 and 1:2 of all the three peptides are less toxic compared to 1:0. Positive control peptide showed no effect in cell recovery. The effects of the three peptides in isolation at any molar ratios were minimal on PC12 cells.

3.4 Discussion

In this chapter I have characterised the peptides screened from the semi randomised libraries by intracellular PCA methodology to demonstrate peptide efficacy in binding to α-syn$_{1\text{-}140}$ and thereby lowering its toxicity. The hypothesis was that the α-syn aggregation can be inhibited by the specific binding of the 'β-sheet breaker' peptides to their native (i.e. α-syn$_{71\text{-}82}$ design scaffold) sequence in the α-syn molecule since it is known to self-aggregate. X-ray and electron diffraction studies have previously provided strong evidence for the hydrogen bonded cross β-sheet structure in which the β strands run perpendicular to the long fibre axis (Serpell *et al*., 2000; Eanes *et al*., 1968; Sunde *et al*., 1997). Solid state NMR studies suggest that the major extended β-sheet region is around residues 35-95 (Vilar *et al*., 2008). In this chapter, the peptides were designed on α-syn$_{71\text{-}82}$ scaffold since it is known to aggregate in isolation as well as play a major role in full length α-syn prompting amyloidogenesis. Collectively the data demonstrate that all the three PCA screened peptides lead to moderate levels of fibril reduction. ThT and CD data indicated that the peptides can prevent fibril formation by an average of 35 % reduction in the final day sample at which α-syn was thought to be fully aggregated in isolation, but have minimal effect in reversing it when added to these pre-formed fibrils. As ThT binds to a wide range of different aggregated species (i.e. oligomeric states) and CD measures only an average of overall secondary β-sheet content, direct visualisation using AFM was employed to study the efficacy of peptides. From the AFM data, as it was difficult to determine visually the amount of amyloid load with each peptide condition, average volume was calculated using WSxM v5.0 software and led to identification of an average reduction of 25 % fibril load in all the three peptides compared to peptide free α-syn sample (1:0). All together it is difficult

to declare which of the inhibitors are most effective. However, the delaying property of WTC was prominent in all the assays, providing a promising result for further investigation in derivatives that can further slowdown the progression of α-syn amyloidogenesis.

The reason for the effectiveness of WTC (^{77}PDKG^{80}) is currently unknown; however I speculate that it could be due to the substitution of K80G which might have modified the packing of α-syn fibrils as NMR studies and thermodynamic studies shows that the glycine is a low propensity β-sheet forming residue (Nowick *et al*., 1997; Smith *et al*., 1994). Another point could be the presence of proline residue which facilitates the secondary structure as turns or helices by disfavouring β-strand conformations, as it reduces stability since its side chain can only form one hydrogen bond. The glycine and proline effect together might have made WTC performed comparatively well as β-sheet breaker relative to WTA or WTB. Studies show that Q/N rich sequences self-assemble to form amyloids (Perutz *et al*., 2002). Short peptides like WTA and WTB containing Q residues could have bound to the parent protein making it Q rich and thus favouring aggregation as seen in many prion and polyglutamine diseases. The uncharged polar side chain usually located on the outside of protein could be a protein-protein interaction module. In contrast to that, WTC lacks any Q residue which makes it comparatively a better peptide in slowing down the aggregation process. The hydrophobicity of the residues plays an important role in self aggregation of peptides. Therefore three PCA peptides represent reduced hydrophobicity relative to α-syn$_{71-82}$. The PCA method used here substituted V77 by charged or less hydrophobic residues in all the three peptides. Studies show that the deletion or substitution of V77 prevents the formation of mature amyloid fibrils (Waxman *et al*., 2010). In the MTT assay, reduced toxicity was observed effectively in the lower stoichiometries of all the three peptides. Reduced toxicity supports the ThT, CD and AFM data that the equimolar ratios of

the peptides lead to non-fibrillar species during amyloidosis. Peptides derived in this study compared favourably with previously reported N-methylated VAQKTmV peptide (Madine *et al*., 2008) and a SGSSGTSSGTSG peptide. While designing the negative control peptide, four glycine residues were included so that the lack of side chain facilitates rotational freedom of the backbone conformation of the protein and G/S peptide is a mDHFR-peptide linker and is a good negative control as it shows no binding during the PCA process. Compiling all results; a better inhibitor can be designed by reducing hydrophobicity and introducing charged residues in the 71-82 region which provides a good chance to repel the incoming α-syn monomers on the outward growing face of the fibril. Structural studies reveal that the substitution of the hydrophobic residues in the NAC region with charged ones weaken fibril formation. Particularly the N-terminal half of NAC (61-78) is amyloidogenic region responsible for the aggregation and toxicity of α-syn (Giasson *et al*., 2000; El-Agnaf *et al*., 1998). While selecting peptide residues, PCA ensures a balance between α-syn binding affinity and peptide solubility. In conclusion, I have used an *in vivo* selection approach to derive a range of peptides against α-syn aggregation. Further investigation needed as I have not directly quantified the affinity and specificity of the binding. This is because even though the peptides are reducing the amyloid load, they are not satisfactorily stopping or reversing the fibril growth as anticipated at the PCA level. Notably the delayed amyloid formation seen in WTC peptide shows a positive sign for future investigations and develops as a drug to delay PD progression and its symptoms. Our approach towards an α-syn$_{71-82}$ scaffold was later changed to develop a library based on the wild type α-syn$_{45-54}$ scaffold accommodating the point mutations implicated in the early onset of PD, which will be discussed in chapter 5.

Chapter 4: Use of PCA to derive peptide antagonists of α-syn mutant's aggregation associated with early-onset PD

4.1 Introduction

There are a number of familial point mutations which have been identified in the SNCA gene that are associated with the early onset of PD (Berg *et al*., 2005). Among these, A53T was the most frequently found mutation reported in at least 12 families of Greek and Italian origin (Spira *et al*., 2001) and in a Korean family (Ki *et al*., 2007). The E46K mutation was identified in a Spanish family (Zarrenz *et al*., 2004), and the first brain study of a A30P mutant carrier patient was undertaken by Seidel and colleagues (2010) and reported that increased neuropathology was due to the significant load of insoluble α-syn. The H50Q substitution in α-syn was first identified by two different groups in a caucasian English female (Proukakis *et al*., 2013) and a person from a family of English/Welsh origin (Cresswell *et al*., 2013). Three families have been recently reported to have G51D with early onset ages ranging from 19 to 60 years (Lesage *et al*., 2013; Rutherford *et al*., 2014).

The different mutations exhibit distinct effects on PD progression rate. Many previous studies suggest that; neither the natively unfolded nor the partially folded intermediate conformations are affected by these point mutations. A recent study suggest that these point mutations causes a change from stable tetrameric α-syn structure to monomers, decreases α-syn solubility and thereby induces neurotoxicity and deposition of inclusions in the neurons (Dettmer *et al*., 2015). The α-syn region where the mutations are present and the residues within are clearly important in modulating amyloid formation by increasing α-syn toxicity, decreasing α-helical propensity, increasing β-sheet propensity, and either increasing the rate or the amount of oligomers that are formed during the aggregation

process (Bussell *et al*., 2001; Greenbaum *et al*., 2005; Ghosh *et al*., 2013; and Rutherford *et al*., 2014). The major concern is, how a single point mutation in the natively unfolded α-syn can affect the rate of aggregation and fibrillisation processes. It can be explained in the scenario of 'sequence repeats' found in the N-terminal region of α-syn. Sequence repeats are a main feature of several neurodegenerative disorders that are characterized by protein aggregation. α-syn consist of seven 11-mer imperfect sequences (XKTKEGVXXXX) containing a KTKEGV hexameric motif which is not fully conserved in the sixth and seventh repeats. The repeat sequences in the N-terminal end is identified to decrease the tendency of β-sheet propensity shown by α-syn and favours an α-helix formation in the presence of lipid vesicles and also is likely to be important in maintaining the normal structure and deciding the pathological functions of α-syn (Kesler *et al*., 2003). As a partially folded intermediate of α-syn is needed for amyloid fibril formation, KTKEGV repeats show a significant role in retaining the native unfolded structure of α-syn and thereby preventing aggregation (Sode *et al*., 2006). Mutation in these seven imperfect sequences show effects in the rate of aggregation by decreasing the lag time of fibril formation (Harada *et al*., 2009). All α-syn mutations lie in the imperfect 11 mer sequence except A53T, but it is in close proximity between the fourth and fifth repeats. It suggests that, the mutations inhibit the ability of the repeats to form nonpathogenic species and thereby increases the inherent β-sheet propensity of the repeats. The fibril formation induced by mutation is also found to inhibit the proteasome activity *in vitro* by binding to the 19S subunit in the 26S proteosome (Nonaka, and Hasegawa, 2009).

The A53T and E46K mutants were found to increase the rate of self assembly and fibril formation by adopting β-sheet conformation to form pathological inclusions (Conway *et al*., 2000, Li *et al*., 2001, Choi *et al*., 2004, and Greenbaum *et al*., 2005). A study performed by

Waxman and collegues (2008) on double mutants containing both E46K and A53T suggests that the fibrillisation rate was increased rapidly compared to A53T alone with its amino-terminal region involved in pathological inclusions as detected by conformational specific antibodies . NMR studies suggest that the significant helical propensity shown by N-terminal region of wild type α-syn was changed by A30P mutation to increase the rate of formation of β-sheet protofibrils, while A53T results in modification of a small region around the mutation site providing a preference for extended β-sheet conformations (Bussel *et al*., 2001). Some groups suggest that A30P shows a delayed fibril formation than wild type and decreased maturation of fibrils by enhancing the population of oligomers (Conway *et al*., 2000, Bussel *et al*., 2001). The oligomeric intermediates rather than matured fibrils tend to build up more in A30P carriers and induces pathogenicity. The involvement of residue 30 in β-sheet formation would likely be hindered by the presence of proline mutation (as proline is a very poor ordered β-sheet forming residue: Chou, and Fasman, 1978) reflecting the reduced Ramachandran space available to the preceding residues. In A53T mutation, threonine has higher β-sheet propensity than alanine (Chou, and Fasman, 1978). E46K has been identified in the imperfect repeat sequences present in the N-terminal region leading to decrease in aggregation lag time to fibril formation. Substitution of a Glu for a Lys in the imperfect repeat sequences leads to a rapid conformational change in α-syn to a partially folded intermediate; this then oligomerises which act as a critical nucleus and finally leading to the formation of fibrils (Harada *et al*., 2009). The native, monomeric α-syn is stabilized by long range interactions between N-, C- termini and the NAC region via electrostatic interactions which protects it from oligomerisation and aggregation (Bertoncini *et al*., 2005). Recent findings suggest that the stability is attained by the native tetrameric structure of α-syn (Dettmer *et al*., 2013; 2015; Bartels *et al*., 2011).

The C-terminus has been speculated to act as an aggregation regulator by docking with polycations which destabilizes these interactions and furthermore its truncation enhances aggregation. The high free energy of extended conformations with the solvent exposed NAC region facilitates the nucleation and aggregation processes (Fernandez *et al*., 2004). Though these intramolecular contacts were considered undisturbed in A53T and A30P, altered secondary structure propensity has been speculated to cause fibril formation. In contrast, the E46K mutation causes decreased net negative charge of α-syn, with the increased positive charge of the N-terminal lipid binding domain enhancing such contacts with negatively charged C-terminal domain, thereby accelerating fibril formation (Rospigliosi *et al*., 2009). NMR studies show that residue 46 is not present in β-sheets consisting of the cross-β region located within residues 30-110. Therefore the mutation promotes the formation of new β-sheets without disrupting the endogenous β-structures (Harada *et al*., 2009; Mar *et al*., 2005; Chen *et al*., 2007). NMR studies suggest that, H50Q mutation causes conformational changes on C-terminal and increases the flexibility of this region considerably more than any other previously identified mutants. And also H50Q causes chemical shift perturbations around the mutation site (residues 44-56) thereby modulating the interactions between the NAC region and the C-terminus, thus accelerating α-syn aggregation. Furthermore, His50 is an important residue for Cu(II) binding in α-syn and its replacement may affect the secondary structure of H50Q in the presence of Cu(II) *in vivo* (Rutherford *et al*., 2014). The recently identified G51D causes early onset of PD symptoms and its clinical features show similarities to those with *SNCA* triplications and to A53T cases (Kiely et al., 2013; Lesage *et al*., 2013). Further studies are needed to investigate how H50Q and G51D modulates the pathology of PD. The mutants cause a faster formation rate of fibrils, soluble oligomers, or amorphous aggregates than wild type α-syn (Li *et al.*, 2001).

This chapter focuses on screening libraries and to derive and characterise new peptide inhibitors of α-syn aggregation using mutants associated with early onset PD. These include A30P, E46K, A53T and H50Q and uses ThT, CD, AFM and MTT assays (described in Chapter 3) to characterise the effects of these PCA derived sequences upon α-syn aggregation. The strategy to design peptide inhibitors was based on the α-syn$_{71-82}$ scaffold which is known to aggregate in isolation (Periquet *et al*., 2007; Madine *et al*., 2008) and was therefore hypothesised to interact with full length α-syn mutant. By characterisation of peptides derived from building a library using these sequences as a design template I have aimed to, interrupt α-syn aggregation by preventing amyloid formation or breaking down pre-formed fibrils to less toxic oligomers. G51D has only recently been identified and hence was not investigated in this thesis. These studies would help us to provide some clues about peptide candidates which harness the potential to be further developed into drugs in the future.

4.2 Experimental approach

This chapter describes the characterization of antagonistic peptides of α-syn aggregation for early-onset associated mutants. Peptides were generated using semi rational peptide design, combined with PCA.

(1) Purification of α-syn mutants: Mutants were expressed and purified using SUMO technology as described in Chapters 2 & 3.

(2) Peptide characterisation: The PCA derived peptides were characterised using ThT, CD, AFM and MTT assays as described in Chapter 3. The peptides were analysed for their inhibitory effect as well as the reversal effects on aggregation. In this chapter, 450 µM each of the α-syn mutants were incubated with PCA derived peptides at various molar ratios; 1:0.1, 1:1, 1:2, 1:5 and 1:10 (mutant: peptide), in 500 µL of potassium phosphate buffer (10 mM, pH 7.0), KF (100 mM) and NaN_3 (0.05 %) at 37^0C with continuous shaking in an orbital incubator at 10xg for 10 days (A30P, E46K, A53T) and 20 days (H50Q) for the inhibition assay, and three days (post-mix) for the reversal assay. Finally, the effect of peptides on the viability of PC12 cells was investigated using the MTT cell toxicity assay. The assay was performed at 5 µM α-syn mutant with five different molar ratios as mentioned above. Control experiments by incubating peptides in isolation without target mutants were undertaken to verify the reliability of the peptides. In addition the negative control peptide (SGSSGTSSGTSG) and positive control peptide [$VAQKT_mV$ (Madine *et al*., 2007)] at molar ratio 1:1 were also analysed along with the PCA peptides. The peptide; SGSSGTSSGTSG is the GS linker which is a good control peptide to use to investigate the specificity of PCA derived peptides towards α-syn.

4.3 Results

4.3.1 PCA derived peptide characterization

PCA derived peptides against the aggregation of α-syn mutants were generated using semi-rational peptide design approach using the 71-82 region of α-syn as a design scaffold, as it is known to self-aggregate (Table 4.1). Among those residues, C-terminal residues $_{77}$VAQK$_{80}$ were fully randomised to provide all 20 residue options at these four positions. 77-80 was chosen owing to the fact that solid state NMR studies have provided evidence for these to be the most effective residues in forming ordered fibrils in the 71-82 peptide (Madine *et al*., 2007). The peptide winners were generated by the project students previously and bought from Peptide Synthetics, Fareham, UK for the characterisation studies performed by me.

Name	Sequence based on 71-82 region
A30P	Ac-VTGVTAHPQNTV-NH_2
E46K	Ac-VTGVTANQNNTV-NH_2
A53T	Ac-VTGVTADNKETV-NH_2
H50Q	Ac-VTGVTANSSDTV-NH_2

Table 4.1: PCA derived peptide 'winners' from a screen against full length α-syn mutants. The library was designed by fully randomising four amino acid positions of α-syn mutants at $_{77}$VAQK$_{80}$. The four residues selected between 77-80 region after PCA in each case is highlighted in yellow. Inclusion of N-acetylation and C-amidation was used to provide additional stability to the peptide as well as additional terminal hydrogen bond acceptors and donors.

4.3.2 Inhibition assay

4.3.2.1 ThT fluorescence assay

The ThT experiments for all the mutants were performed in triplicates (technical replicates) as a part of single experiment in a micro titre plate and the error bars were calculated as the standard deviation of all errors (Fig 4.1). The three mutants; A30P, E46K and A53T reached their stationary stable phase from day 10 onwards and is therefore considered as the end point for inhibition assay since no further growth was recorded. H50Q showed a longer lag phase reaching stationary phase at day 20 and is thus considered for taking the inhibition assay readings. In reversal assay, over a period of 3 days after adding peptide to the matured fibrils was considered as there is no further fibrillar modification observed during the stationary phase of mutants.

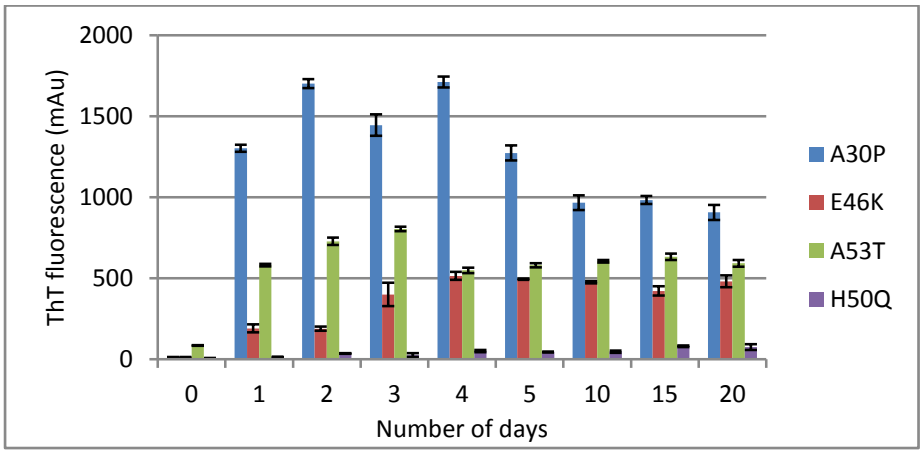

Figure 4.1: Raw ThT fluorescence data: showing comparative growth of four α-syn mutants from day 0 to day 20 at a concentration of 450µM. The amount of fibrils formed is directly proportional to the ThT fluorescence emitted in course of time. A30P exhibits the maximum ThT signal approximately 1700 mAu at day 2 while H50Q showed the smallest fluorescence of approximately 80 mAu at day 15. A53T reached a maximum of 805 mAu at day 3 while E46K showed 514 mAu at day 4.

In the case of all the mutants, blank reading was considered and normalised the ThT value at each time point to 1:0 (peptide free sample) during intensity calculation. ThT values were taken in triplicates (technical replicates) as a part of single experiment and the error bars were calculated as the standard deviation of all errors. According to the ThT data, in A30P mutant (Fig 4.2); an increased ThT signal was observed at day 0 when the PCA derived peptide was added. Though there was slight reduction of ThT signal in the following days of incubation until day 4, the effect of peptide is found to be minimal in inhibiting the fibril formation relative to 1:0. The PCA peptide was clearly unable to maintain reduced amyloid level beyond day 4 at any of the stoichiometries. Later MTT assay was performed assuming that it could explain whether the species formed are toxic or not.

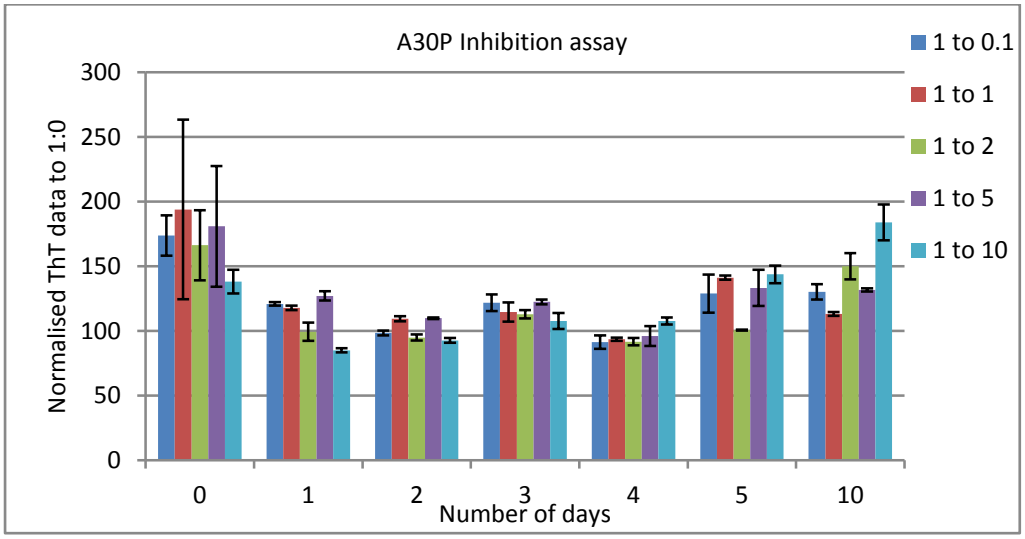

Figure 4.2: ThT fluorescence data showing inhibition assay of A30P using PCA peptide at five different molar stoichiometries (1:0.1, 1:1, 1:2, 1:5, and 1:10) in days 0,1,2,3,4,5 and 10. The 'y' axis values are relative to the peptide free (1:0) sample in %. The data shows an increase in ThT fluorescence at day 0 at the moment of adding PCA peptides. Gradually a tendency to lower the amyloid content can be seen in the following days of incubation, but the peptide failed to retain the decreased amyloid load further day 4. Increased ThT at the final day samples shows the inability of the PCA peptide to inhibit fibril formation in A30P.

In E46K mutant (Fig 4.3), similar to A30P; the PCA selected peptide at any molar ratios was unable to inhibit the aggregation process at any point during 10 days of incubation. Instead it was facilitating the amyloid load to a greater extent that at higher concentration it showed 7 times more signal relative to 1:0. A gradual increase of ThT signal was observed until day 2 in all stoichiometries. Then the ThT signal was seen to decrease towards the later phases of incubation. Overall, PCA peptide was identified to facilitate amyloid formation rather than inhibiting the process.

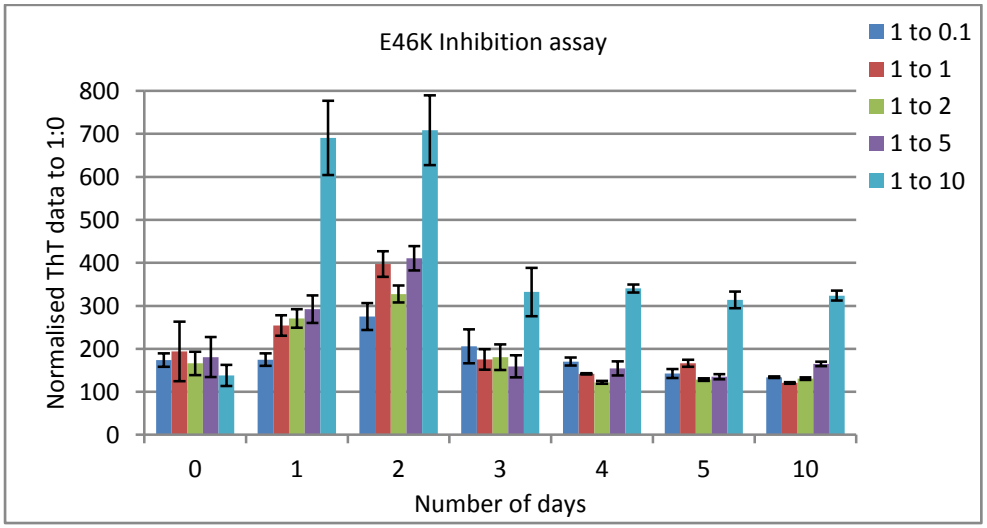

Figure 4.3: ThT fluorescence data showing Inhibition assay of E46K using PCA derived peptide at five molar stoichiometries (1:0.1, 1:1, 1:2, 1:5, and 1:10) in days 0,1,2,3,4,5 and 10. The data shows the peptide is not identified to inhibit in any of the molar ratio, despite it increases the fibril load. An increase of ThT value towards day 2, which then gradually diminished near the later phase of incubation can be seen in all stoichiometries. At the highest ratio (1:10) the peptide showed an enhancement of amyloid load for about 7 times during day 1 and 2 and later it diminished to 3 times compared to 1:0.

In A53T mutant (Fig 4.4), 1:0.1, 1:1, 1:2 and 1:5 showed reduction in ThT fluorescence, but the peptide was seen to lose its inhibitory property in the later phases of incubation. The higher ratio of 1:10 possessed a gradual decrease in fluorescent intensity reaching a maximum of 34 % reduction in the day 10 sample. According to the ThT data, the PCA peptide appeared to be effective in higher stoichiometry to inhibit the fibril progression. CD and AFM assays were undertaken to confirm the efficacy of peptide at higher concentration.

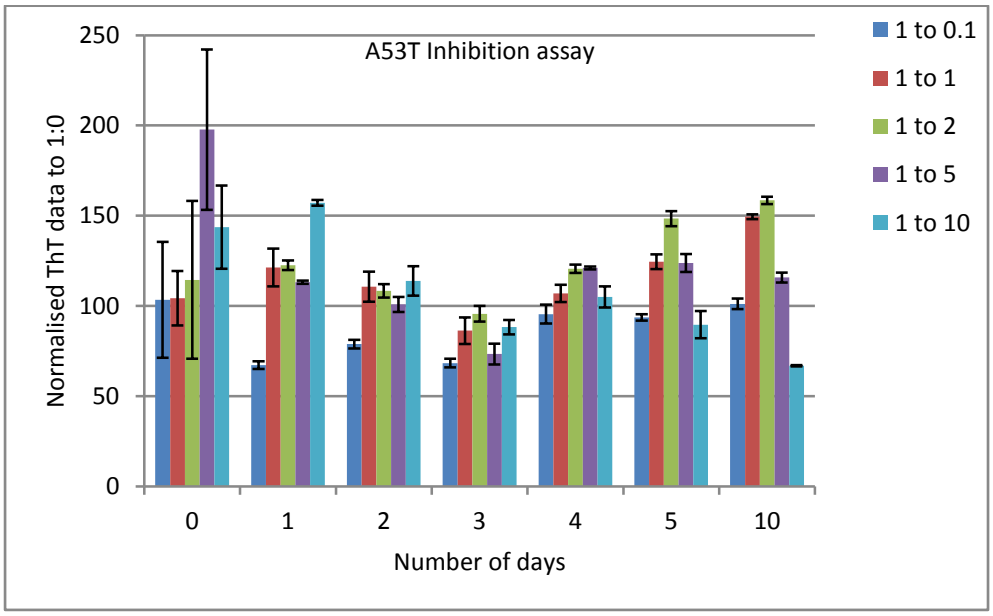

Figure 4.4: ThT fluorescence data showing Inhibition assay of A53T using PCA derived peptide at five molar stoichiometries (1:0.1, 1:1, 1:2, 1:5, and 1:10) in days 0,1,2,3,4,5 and 10. The data shows that there is a 20-30 % reduction in ThT fluorescence in the initial days with 1:0.1 which was unable to retain its inhibitor property towards the final phase. 4-15 % reduction was seen in other ratios (1:1, 1:2, and 1:5) at day 3 sample which were found to be ineffective inhibitor ratio in the later phase. Contrast to all these ratios, 1:10 possessed an increased ThT signal initially which subsided with a reduction of 34 % in the final day sample.

In the case of H50Q (Fig 4.5), an increase of ThT fluorescence was identified with an increase in peptide concentration. The only reduction of 6 % was seen in early stages of equimolar ratio. Other lower stoichiometries showed an increase in fluorescence at various time points. A massive increase of amyloid load was seen in the higher stoichiometries of 1:5 and 1:10. The PCA peptide was found to facilitate the aggregation of H50Q as it formed high ThT signals compared to 1:0. The samples were later studied using CD, AFM and MTT assays.

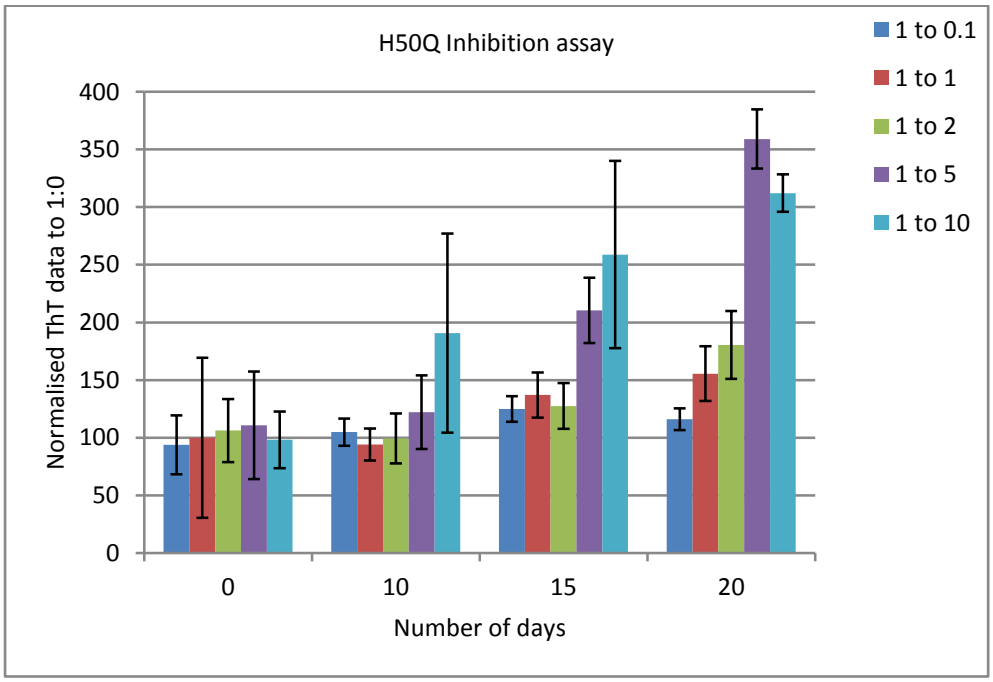

Figure 4.5: ThT fluorescence data showing Inhibition assay of H50Q using PCA derived peptide at five molar stoichiometries (1:0.1, 1:1, 1:2, 1:5, and 1:10) in days 0,1,2,3,4,5 and 10. The data shows an increase in ThT fluorescence in a dose dependency manner. 10-15 % increase in fluorescence was found in 1:0.1 ratio. In 1:1, there was a reduction of 6 % in fluorescence but later increased by 30-50 %. In 1:2, an increase of 30-80 % fluorescence was seen. A massive increase of 2-3 times in fluorescence was identified in the higher molar ratios depicting the amount of amyloid fibrils increases with increase in peptide concentration. Increased ThT at day 20 samples shows that the peptide was unable to inhibit but enhances the H50Q amyloid load.

4.3.2.2 CD assay

The CD experiments of mutants were undertaken using aliquots taken from the same stock samples used for ThT experiments at a final concentration of 10 µM. The CD spectra show the transition of single negative peak from 200 nm (random coil) to 218 nm (β-sheet) (Fig 4.6). CD spectra were analysed using Gaussian distribution analysis (Fig 4.6.c). Prior to the analysis, the CD spectra of the peptide in isolation were subtracted from that of target with peptide to identify the structural changes of mutant when incubated in each condition.

In A30P (Fig 4.6.b), greater β-signal at 218 nm for all molar ratios can be seen in the final day sample. The slight decrease of amyloid content in ThT data during the mid-phase of incubation is not supported by CD data as it exhibits an increased 218 nm signal in all stoichiometries relative to the peptide free (1:0) sample. The CD data confirms the PCA derived peptide appeared to facilitate the formation of secondary β-structure in all molar ratios and failed to inhibit the fibril formation. This could be assumed at this level as the peptide might have served as nucleus to facilitate aggregation. To confirm this discrepancy in data, the samples were analysed using AFM and MTT assays later.

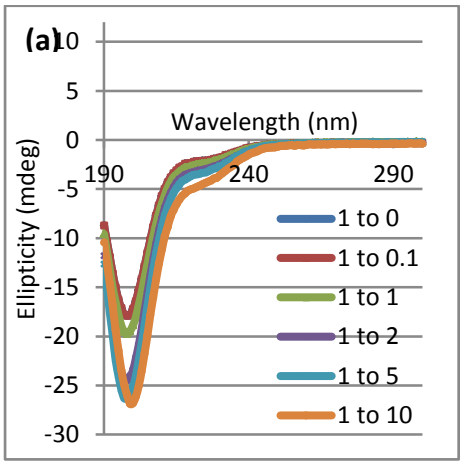

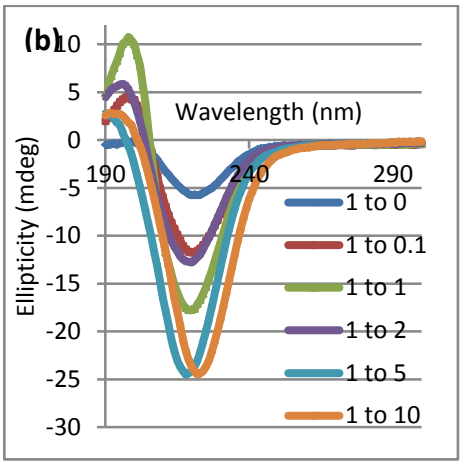

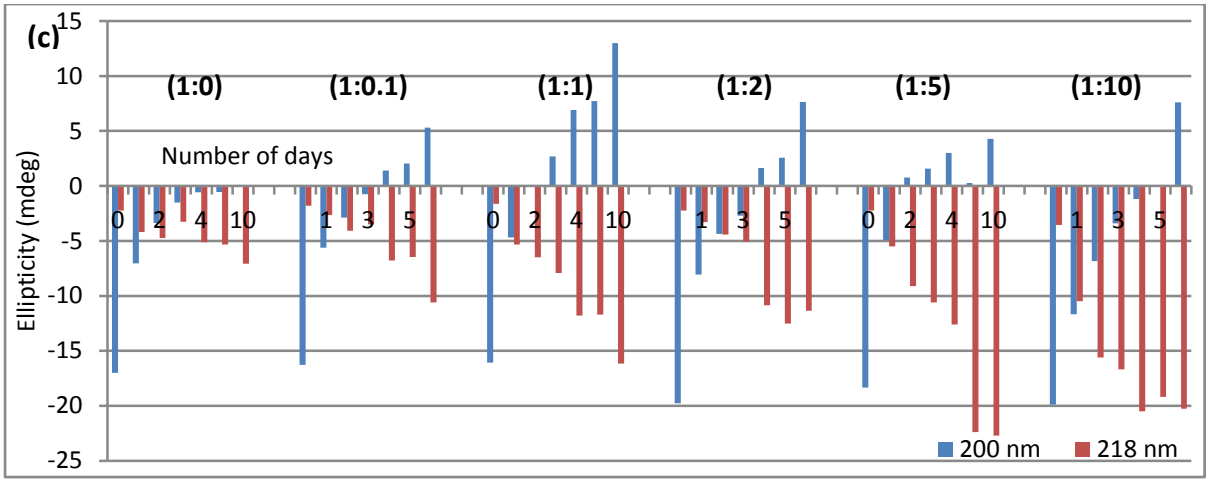

Figure 4.6: Raw CD spectra of: ***(a)*** day 0 samples, ***(b)*** day 10 samples of **A30P** with PCA derived peptide at molar stoichiometries; 1:0.1, 1:1, 1:2, 1:5, and 1:10 relative to the peptide free (1:0) sample and ***(c)*** Gaussian fit analysis data showing 200/218 nm minima of A30P with and without peptides at day 0 to 5 and day 10. In the figs a) and b), it shows a gradual transition of random coil to β-sheet in all molar ratio in course of time. Consistent with the ThT data, the day 10 samples show a greater 218 nm signal indicating an increased amyloid content in the presence of peptide at all molar ratios compared to 1:0. 2-3 times more β-sheet secondary structure can be seen in all ratios. Contrary to ThT, amyloid load relative to 1:0 at day 4 is seen increased in all the samples. The greater 218 nm minima at 1:5 and 1:10 suggest that, the more peptide present; the more it facilitates β-sheet formation.

In E46K (Fig 4.7), a gradual increase of greater β-signal at 218 nm confirms the increased amyloid content in all molar ratios during 10 days of incubation. The increase of β-signal was in a dose dependence manner. The greater the peptide content, the more β-sheeted structure formed. Inconsistent with the ThT data, the higher ratio 1:10 exhibited a gradual increase in the amyloid content rather than an increased secondary structure during day 1 and 2 as seen in ThT data (Fig 4.7 b and c). The peptide appeared to facilitate the formation of secondary β-structure in all molar ratios instead of inhibiting the process.

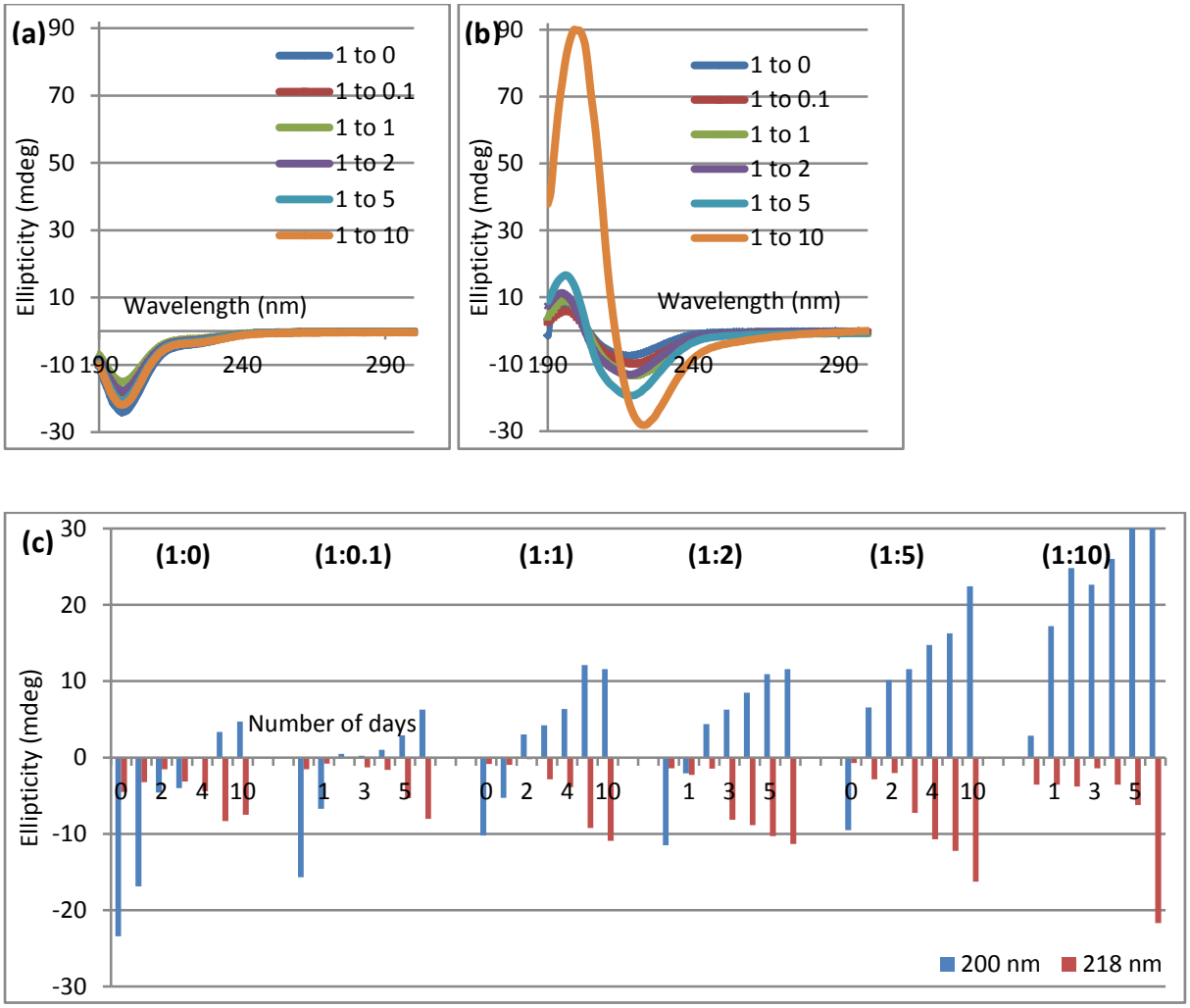

Figure 4.7: Raw CD spectra of: ***(a)*** day 0 samples, ***(b)*** day 10 samples of **E46K** with PCA derived peptide at molar stoichiometries; 1:0.1, 1:1, 1:2, 1:5, and 1:10 relative to the peptide free (1:0) sample and ***(c)*** Gaussian fit analysis data showing 200/218 nm minima of E46K with and without peptides at day 0 to 5 and day 10. The data shows a gradual transition of random coil to β-sheet in all spectra in course of time. In Fig (b), the 1:10 ratio possesses the highest β-content among all stoichiometries. In consistent with the ThT data, day 10 samples in all stoichiometries show a gradual increase of 218 nm signal in a dose dependant manner confirms the peptide facilitating amyloid formation.

In A53T (Fig 4.8), the peptide in all molar ratios exhibited an increased β-signal relative to peptide free sample (1:0) in the day 10 sample. Even though the day 3 samples showed a slight reduction in 218 nm signal as seen in ThT data which confirms the delayed aggregation process in lower stoichiometries, the signal is much greater compared to that of 1:0. In contrast to the ThT data, 1:10 showed a greater β-signal suggesting an accumulation of the secondary species which were unable to bind ThT dye. The peptide appeared to facilitate the formation of secondary β-structure in all molar ratios inconsistent with the reduced ThT value at higher peptide concentration. Further structural analysis was undertaken on the same samples using AFM imaging.

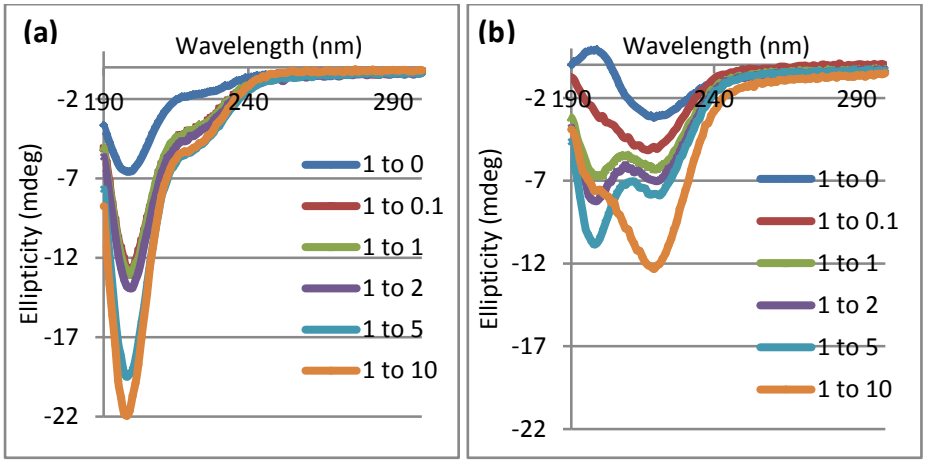

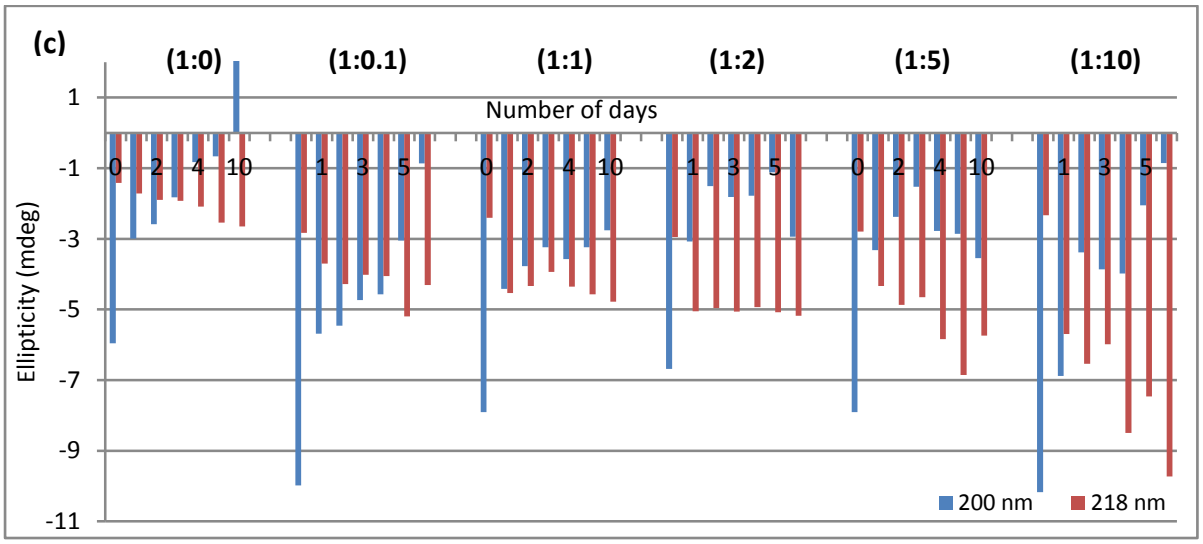

Figure 4.8: Raw CD spectra of: ***(a)*** day 0 samples, ***(b)*** day 10 samples of **A53T** with PCA derived peptide at molar stoichiometries; 1:0.1, 1:1, 1:2, 1:5, and 1:10 relative to the peptide free (1:0) sample and ***(c)*** Gaussian fit analysis data showing 200/218 nm minima of A53T with and without peptides at day 0 to 5 and day 10. The PCA peptide in all molar ratios has enhanced β-sheet secondary structure (2-4 times) formation relative to peptide free (1:0) sample. Contrary to ThT data, 1:10 showed highest β-signal at the end of the incubation. Consistency with ThT data, slight reduction in the 218 nm signals at day 3 (Fig: c) portrays the delay in amyloid formation, but it is much greater value compared to that of 1:0. The peptide was found to induce amyloid formation. Gradual increase of 218 nm signal is found in 1:5 and 1:10. The peptide at highest concentration (1:10) showed the highest β-signal compared to other ratios in all day samples.

In H50Q (Fig 4.9), CD spectra were undertaken on days 0, 10, 15 and 20. As a representation only day 0 and day 20 are shown here. The data confirms the increase of secondary β-sheet with an increase of peptide concentration. There was a fast transition of random coil to β-sheet seen in higher molar ratios. The β-signal in the last day of incubation confirms that the peptide is facilitating secondary β-structure formation rather than inhibiting it. Compared to other mutants the 218 nm CD signal is found to be very low indicating a reduced amyloid load in H50Q aggregation process. Further analysis of the nature of secondary structure formed was undertaken on the same samples using AFM imaging.

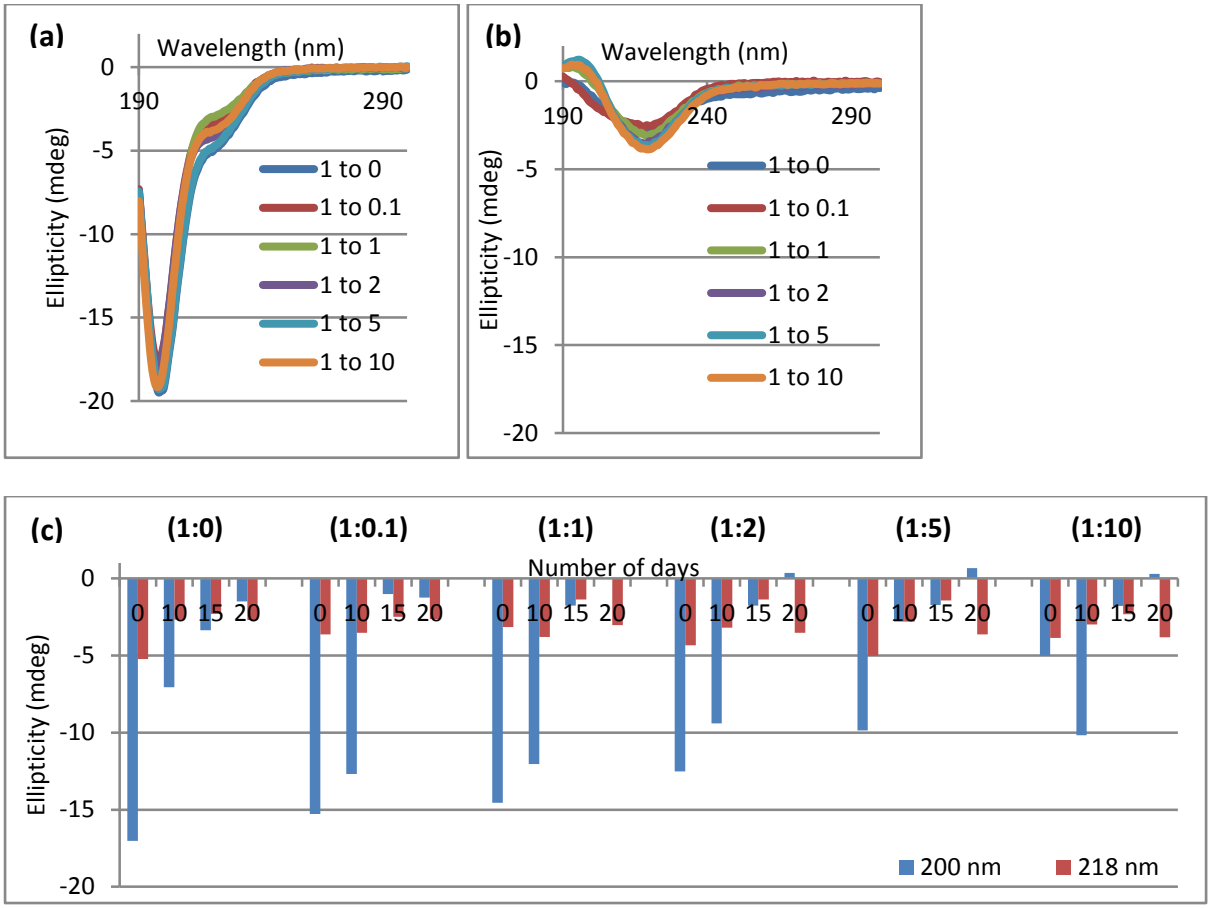

Figure 4.9: Raw CD spectra of: ***(a)*** day 0 samples, ***(b)*** day 20 samples of **H50Q** with PCA derived peptide at molar stoichiometries; 1:0.1, 1:1, 1:2, 1:5, and 1:10 relative to the peptide free (1:0) sample and ***(c)*** Gaussian fit analysis data showing 200/218 nm minima of H50Q with and without peptides at day 0, 10, 15 and 20. According to CD all molar ratio exhibits a 218 nm β-signal relative to 1:0 at day 20 samples. The reduced random coil signal at 1:5 and 1:10 compared to other ratios at day 10 confirms a fast transition to β-sheet in the presence of more peptide. Consistent with ThT data, slight increase in β-signal at 218 nm can be seen increasing with the peptide concentration at day 20 samples. Thereby confirming the peptide is facilitating amyloid fibril formation rather than inhibiting it.

4.3.2.3 AFM experiments

The aim of AFM imaging was to identify the amount and nature of amyloid fibrils formed during aggregation process. Since each assay is measuring a different output, AFM is very useful as it is a much more direct assay than ThT or CD. AFM was performed to identify the amount of aggregated mutant with or without PCA derived peptides. Aliquots of same samples used for ThT and CD experiments were used for direct visualisation of different aggregated species formed at various molar ratios. Inhibition samples were imaged using AFM along with controls (Peptides alone, positive and negative control peptides). All images were taken at 20 µm scan size. The image files were examined directly using WSxM v5.0 (Nanotec Electronica S.L., www.nanotec.es) and flattened before processing. (Kad *et al*., 2001 & 2003). The length and volume of the fibrils were measured.

In A30P, the AFM images (Fig 4.10) and average volume analysis (Fig 4.11) showed a gradual increase in amyloid load as the incubation progresses. Long, distinct amyloid fibrils were seen in lower molar concentration ratios. At higher ratios of 1:5 and 1:10, the aggregates were appeared as clumps of protein showing their abundance across the entire mica sheet surface. It was clear that the peptide was enhancing the formation of aggregates at higher concentrations while long fibrils were formed in the lower ratios. The peptide appears to enhance nucleation stage to initiate the aggregation process in a dose dependant manner. This can be justified by the appearance of oligomeric structures at comparatively early stage (day 3) in 1:5 and 1:10. Consistent with the ThT and the CD data, AFM image of day 10 samples showed enormous amount of fibrils confirms the inability of peptide in inhibiting the fibrillisation process.

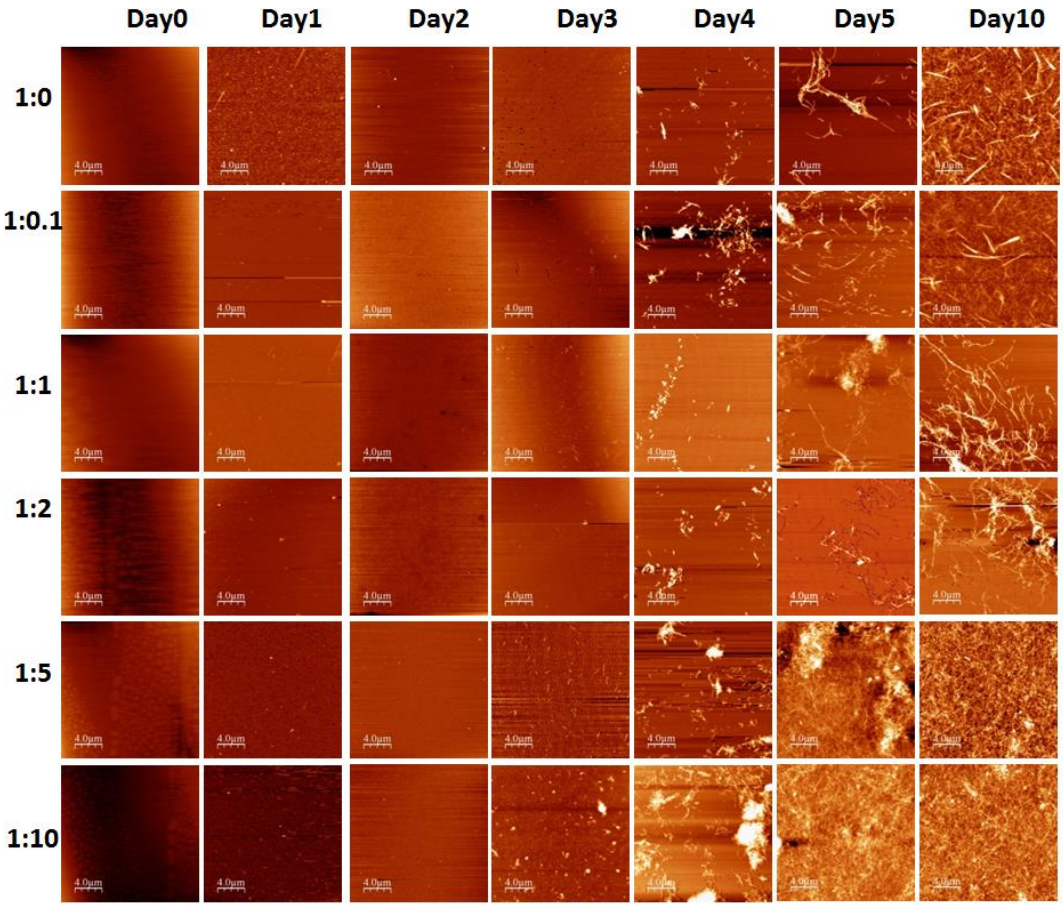

Figure 4.10: AFM images showing **A30P** alone (1:0) and A30P with PCA derived peptide at different molar concentrations 1:0.1, 1:1, 1:2, 1:5, and 1:10. At each molar ratio and time point, a representative image from the images taken in various locations of the mica sheet is shown here. On the final day sample, long amyloid fibrils of approximately 4-8 µm can be seen in 1:0, 1:0.1, 1:1, and 1:2. The peptide at higher concentrations (1:5 and 1:10) directed to the formation of clumps of aggregates which was entirely covering the mica sheet. This confirms the stronger secondary structure signal produced by final day CD data. At the higher concentrations, the peptide appears to facilitate more aggregates and at lower concentrations didn't show any sign of preventing its formation.

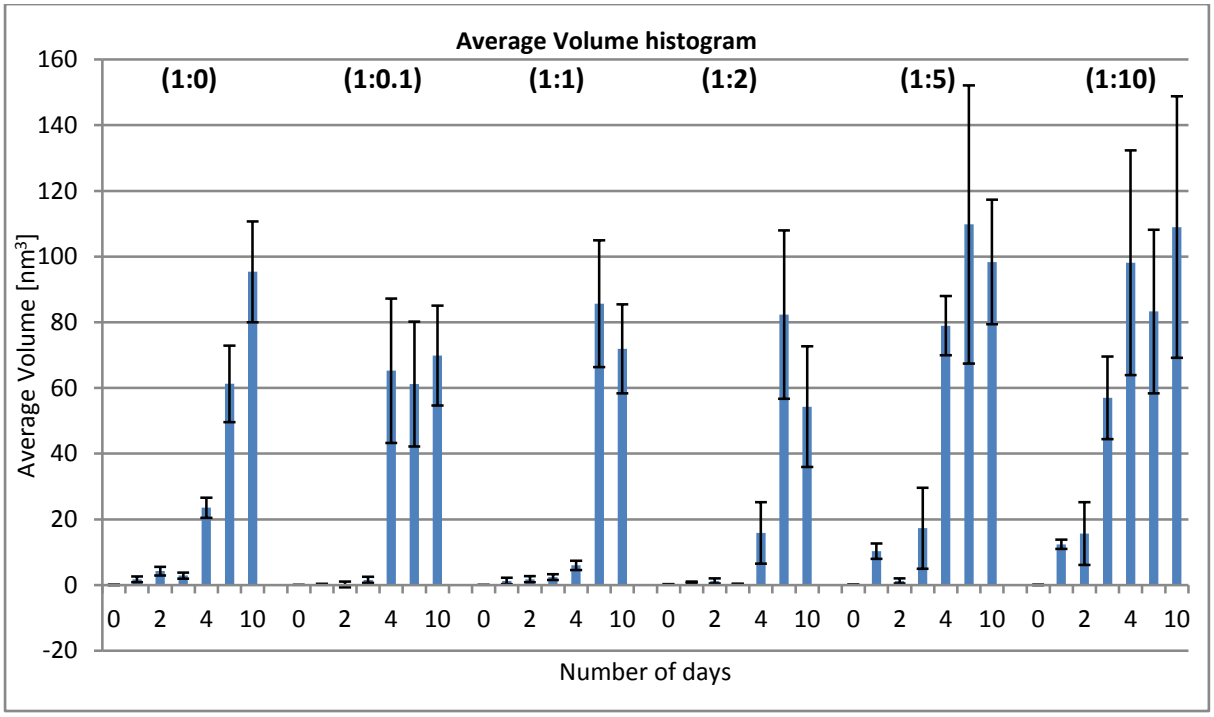

Figure 4.11: Histograms showing average volume of aggregated **A30P** on the mica surface. A gradual increase of fibril load can be seen in all stoichiometries. The higher ratios were seen to enhance amyloid load by decreasing the lag phase and increasing the nucleation phase.

In E46K (Fig 4.12 and 4.13), the AFM images show that amyloid fibrils of approximately 4-8 µm in length were formed during 10 days of aggregation process. In the presence of peptide, morphologically different oligomeric structures of 1-2 µm in length were formed at molar ratios 1:0.1, 1:1, 1:2 and 1:5 despite long fibrils seen in 1:0. Those were identified as protein clumps co-existing along with <4 µm long fibrils abundantly on the mica sheet at day 10. Short fibrils inter-twisted to form thick bundles of fibres were seen in higher molar ratio of 1:10. Structural changes and its contribution in fibril elongation attributed with the PCA peptide were identified in all molar ratios. Consistent with ThT data and CD data, AFM image confirmed the inability of the peptide in inhibiting the fibrillisation process at all five stoichiometries.

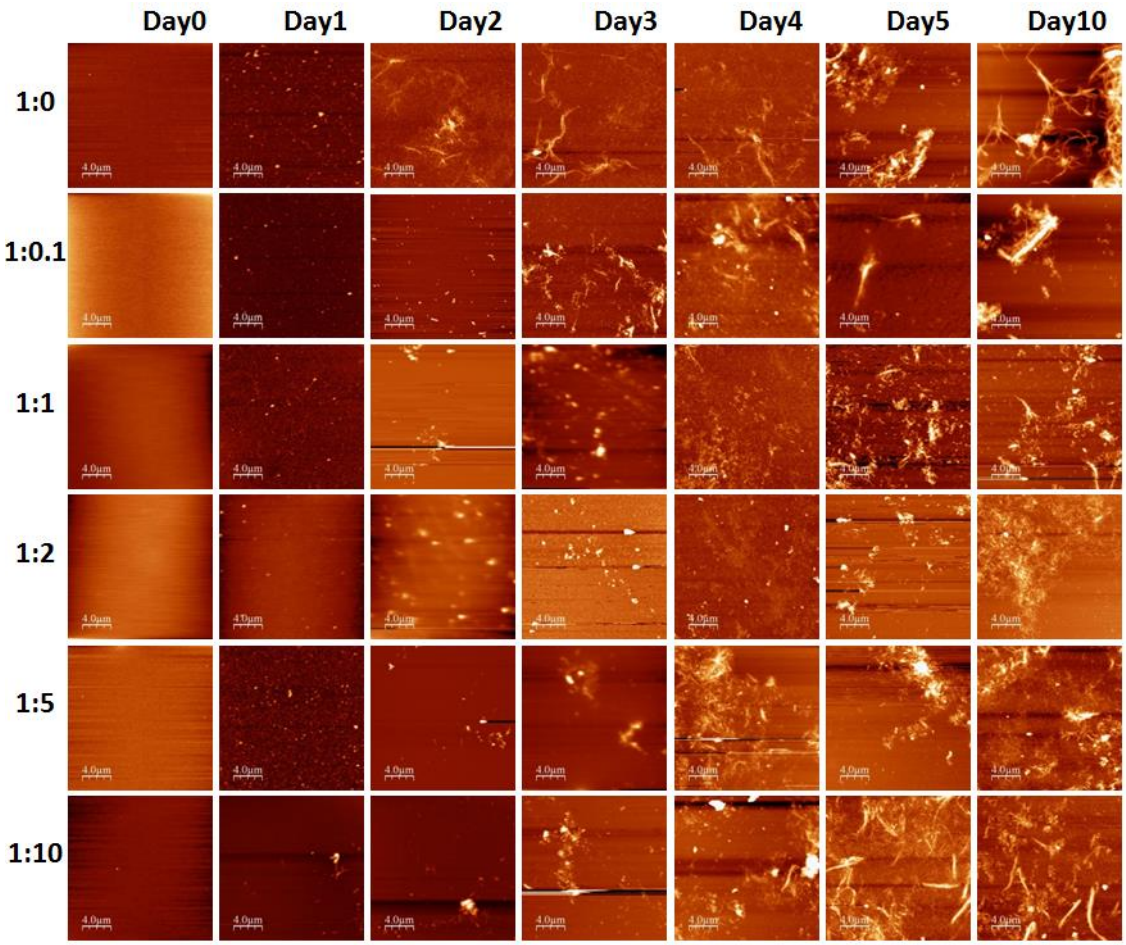

Figure 4.12: AFM images showing **E46K** (1:0) and E46K with PCA peptide at molar concentrations 1:0.1, 1:1, 1:2, 1:5, and 1:10. At each molar ratio and time point, a representative image from the images taken in various locations of the mica sheet is shown here. At the final day sample, long amyloid fibrils of approximately 4-8 µm can be seen in 1:0. The aggregates formed in the presence of peptide at various concentrations vary in their appearance. At the ratios 1:0.1, 1:1, 1:2 and 1:5, small oligomers of 1-2 µm were formed instead of long fibrils found in 1:0. Especially in 1:1, 1:2 and 1:5, the aggregates were found associated with each other and formed clumps of proteins scattered all over the mica sheet in the final day of incubation. There were a few small fibrils of <4 µm were seen in those ratios. In 1:10, short fibrils were found inter-twisted to form relatively thicker fibril bundles abundantly on the mica sheet.

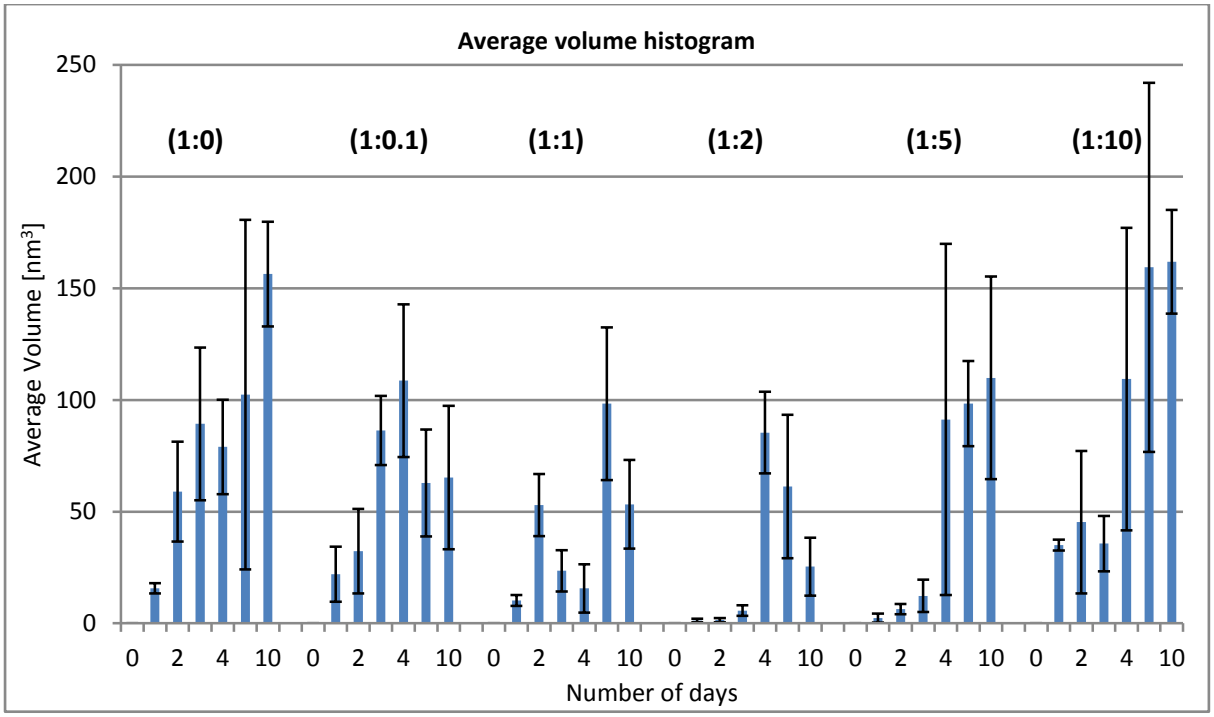

Figure 4.13: Histograms showing average volume of aggregated **E46K** on the mica surface. A gradual increase of fibril load can be seen in 1:0. Considerable increase in the amyloid load found in 1:10 relative to 1:0. This might be due to the increase in the volume caused by association of fibrils in the higher ratios. Comparatively the ratios 1:1 and 1:2 appear to show slight inhibitory properties, but it is inconsistent with CD and ThT data.

In A53T (Fig 4.14 and 4.15), a gradual increase of amyloid load can be seen as the incubation progresses. Amyloid fibrils of approximately 1-2 µm were formed in 1:0. In 1:0.1, the fibrils were less abundant when compared to 1:0 in the initial days of incubation. There was a delay in fibril formation seen in lower stoichiometries until day 3 which exhibited shorter fibrils of 1 µm accumulated as protein clumps later. Various morphological structures where seen in 1:5 concentration. Instead of distinct long fibrils, small oligomeric structures can be seen. In consistent with low ThT value, 1:10 showed an increase in fibril load with long fibres of 3 µm associated together to form thicker bundles covering all over the surface. In

summary, the peptide showed a slight inhibitory property in lower concentrations especially in 1:2, by delaying the process and preventing the formation of long fibrils.

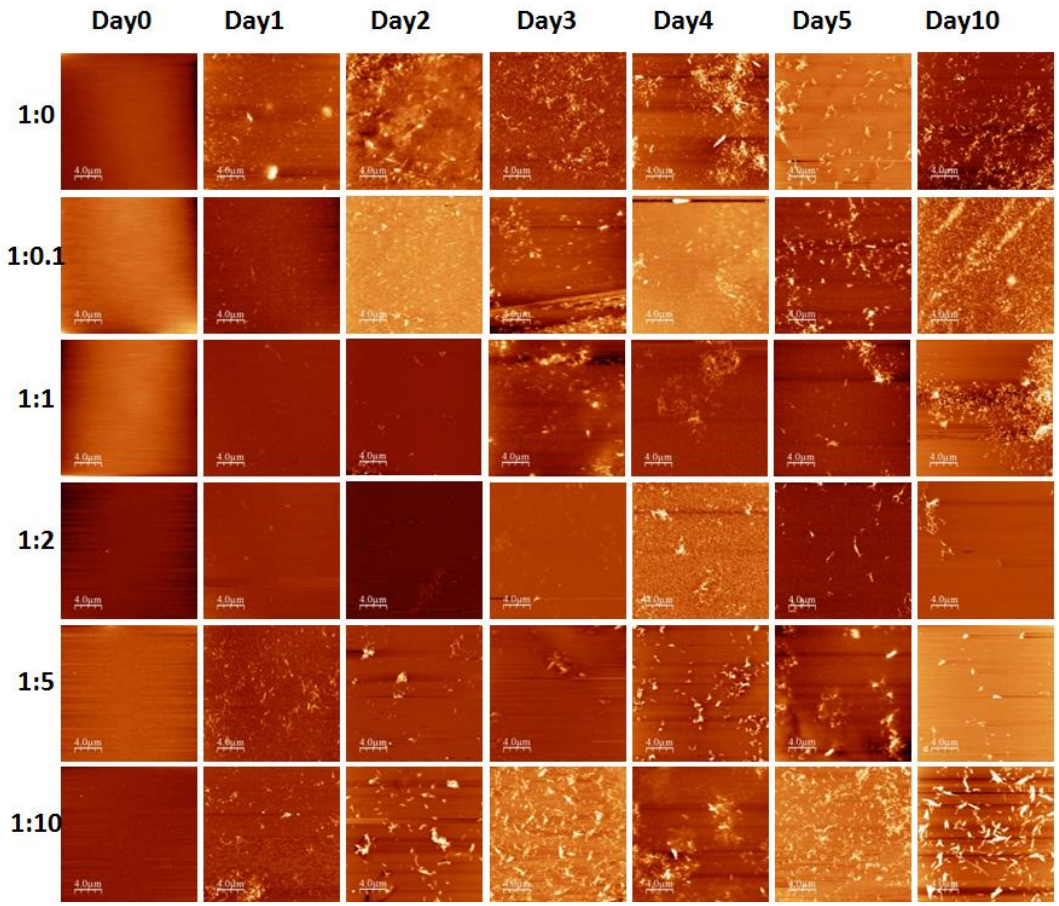

Figure 4.14: AFM images showing A53T (1:0) and **A53T** with PCA peptide at molar concentrations 1:0.1, 1:1, 1:2, 1:5, and 1:10. At each molar ratio and time point, a representative image from the images taken in various locations of the mica sheet is shown here. The data shows a gradual development of amyloid fibrils of approximately 1-2 µm in A53T alone (1:0) during 10 days of incubation. At 1:0.1, initially the amount of fibrils visible was less relative to 1:0. 1:1 found to delay the fibril formation until day3 and consistent with CD data, 1:2 show comparatively less fibril load than 1:0. In 1:5, various morphological structures of protein aggregates were seen during the aggregation process. On day 2, short fibrils of average 1 µm can be seen which gradually changed to protein clumps entirely covering the mica sheet. The peptide appeared to enhance fibril formation

at 1:10. The abundance of long fibrils was greater than that of 1:0. The final day sample shows long (~3 µm), abundant and thick bundles of amyloid fibrils.

The average volume analysis was performed by considering five random images in each molar ratio. The localised differences in the deposition of aggregated species on the surface of mica sheet could have reflected a reduced amyloid volume in 1:10 at day 3 which was inconsistent with that of AFM image. And also the height of the deposited aggregates also matters as a threshold value was introduced inorder to nullify the background noise of small oligomers or non-aggregated species.

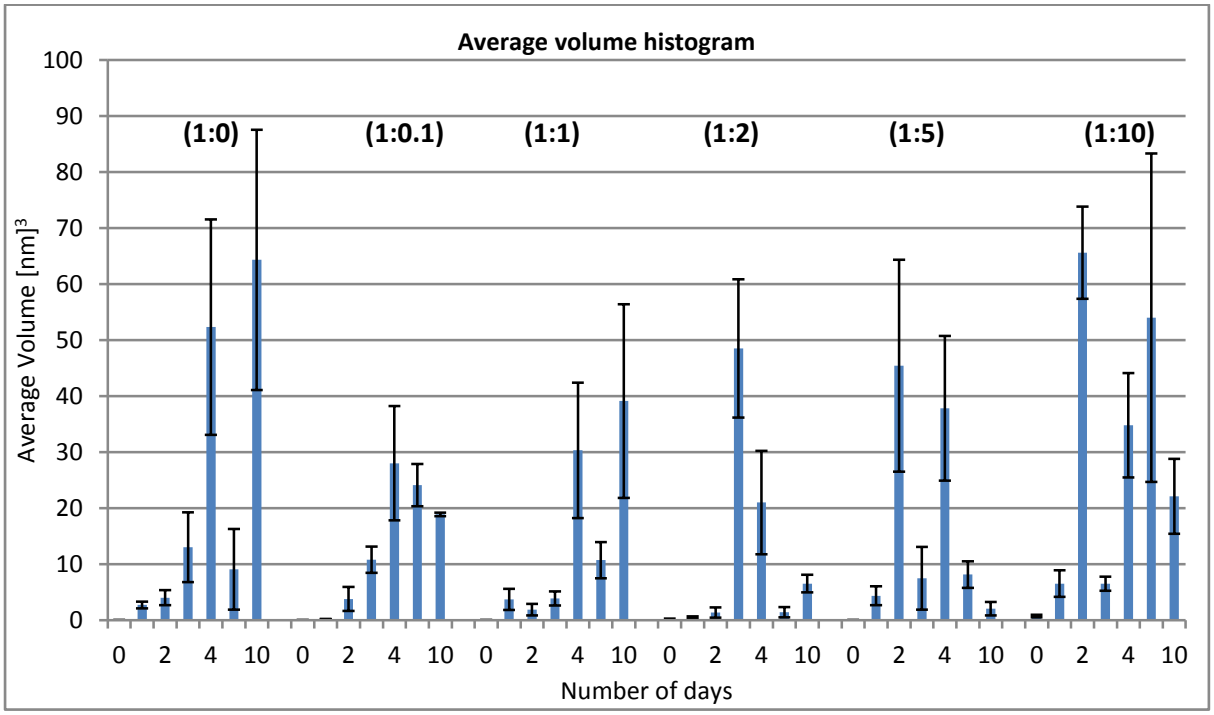

Figure 4.15: Histograms showing average volume of aggregated **A53T** on the mica surface. A gradual increase of fibril load can be seen in 1:0 with an exception in day 5 which could be due to the differences in the distribution over the mica sheet. Notably day 4 samples in the presence of peptide in all ratios show a decrease relative to 1:0. The final day sample indicates a reduction in the lower stoichiometries.

In H50Q (Fig 4.16 and 4.17), AFM images confirm the aggregation of H50Q forming fibrils of length approximately 1-2 µm. No fibrils, instead small oligomeric structures were seen initially in the course of incubation time. A delayed amyloid formation was seen in H50Q mutant compared to wild type α-syn and other mutants. Lower peptide stoichiometries showed a similar pattern of fibril formation as that of 1:0 while clumps of proteins appeared in higher molar ratio samples. The peptide appeared to mediate the association of fibrils rather than increasing the length or thickness of individual fibrils. The peptide enhances fibril formation rather than inhibiting in all stoichiometries.

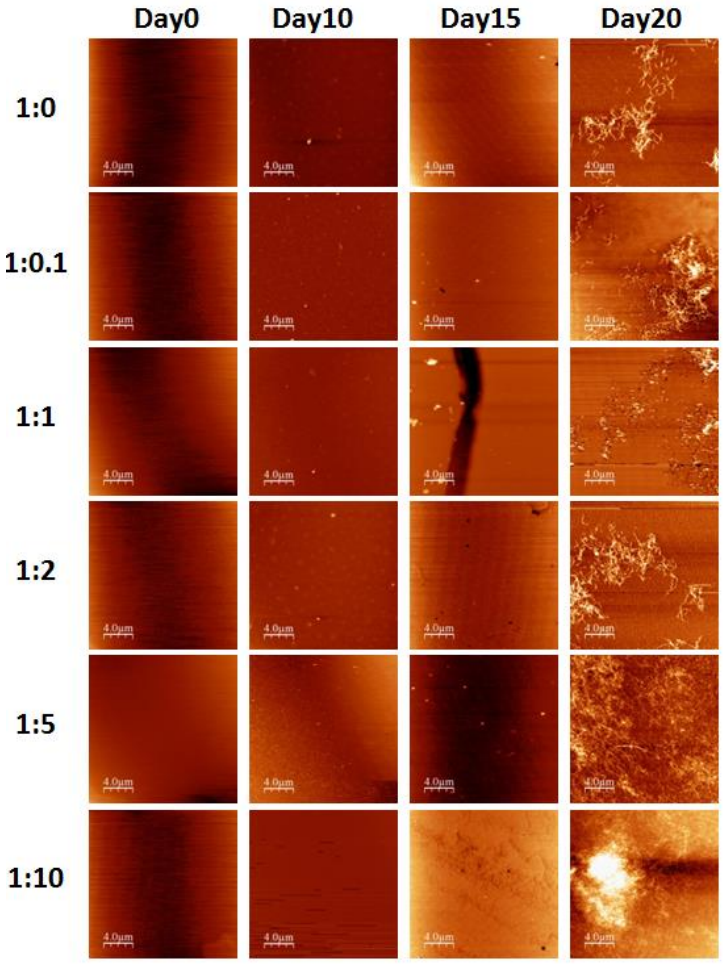

Figure 4.16: AFM images showing **H50Q** alone (1:0) and H50Q with PCA peptide at molar concentrations 1:0.1, 1:1, 1:2, 1:5, and 1:10. At each molar ratio and time point, a representative image from the images taken in various locations of the mica sheet is shown here. The data shows

the development of amyloid fibrils of approximately 1-2 µm in H50Q alone (1:0) during 20 days of incubation. A very few oligomeric structures and no fibrils were seen in the samples at day 10 and 15. A delayed amyloid formation was seen in H50Q compared to wild type α-syn and other mutants. At the lower stoichiometries, similar fibrils to that of 1:0 were found at the day 20 samples. In the higher stoichiometries of 1:5 and 1:10, association of small fibrils to form clumps of protein which were scattered abundantly on mica sheet were found. The peptide appears to involve in mutual association of fibrils in higher stoichiometries rather than increase in length or thickness of individual fibrils which causes the increased ThT and CD signal.

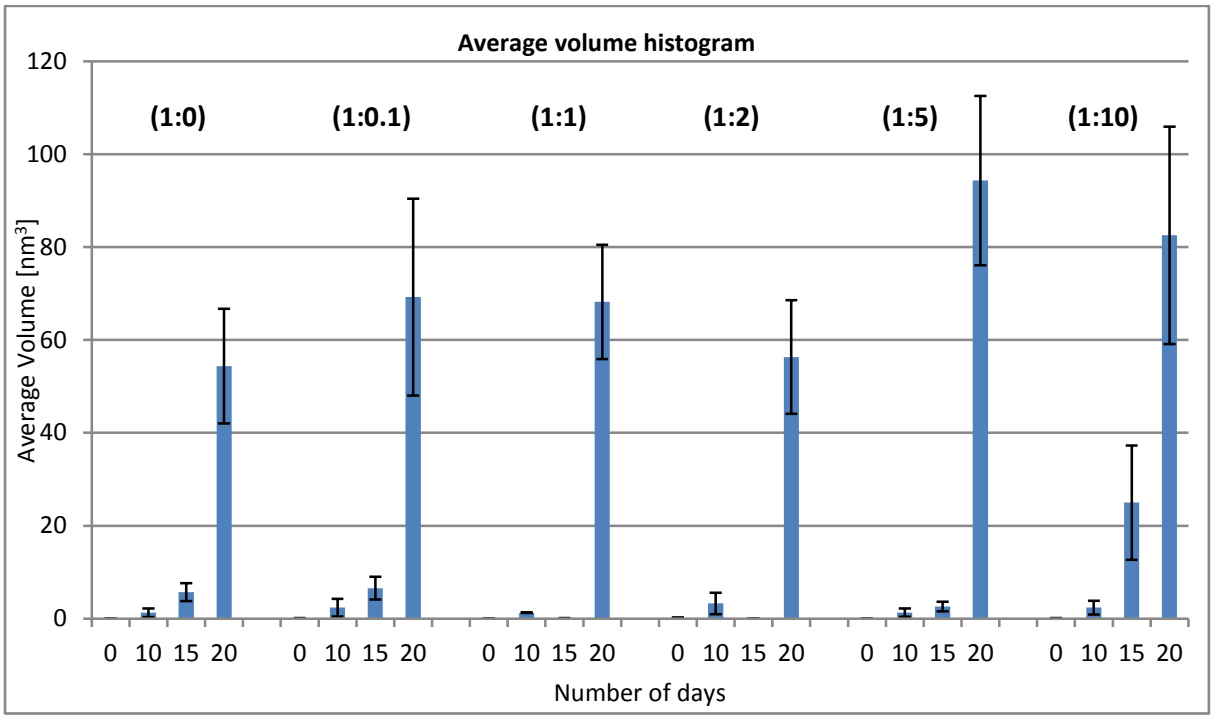

Figure 4.17: Histograms showing average volume of aggregated **H50Q** on the mica surface. The lengthy lag phase in forming fully matured fibrils is confirmed by the massive amyloid signal at day 20. The fibril load is more in higher stoichiometries compared to that at lower ratios. The presence of peptide enhances the fibril formation relative to 1:0.

4.3.3 Reversal assay

The effect of PCA winners on breaking down the matured fibrils was also studied using reversal experiments. The peptides were added in molar ratios of 1:0.1, 1:1, 1:2, 1:5 and 1:10 (mutant: peptide) to the fully grown matured fibrils. The amount of fibrils were characterised using ThT, CD, and AFM studies after 3 days of post mix incubation.

4.3.3.1 ThT fluorescence assay

According to Figure 4.18; with A30P, it shows that the fluorescence was seen to be reduced at certain molar ratios. At a ratio of 1:1 the peptide was found to be comparatively effective, with a 40 % reduction in signal relative to peptide free (1:0) sample. However, inconsistency in concentration dependence was identified at 1:2. In E46K, the peptide was able to break down fibrils as a reduced ThT signal of 5-15 % relative to 1:0 was observed in all molar ratios except in 1:10. The peptide at 1:10 ratio, interacted with matured fibrils and exhibited a greater increase in the fluorescence intensity. According to ThT data, the PCA peptide at any molar ratio was unable to breakdown or reverse the aggregation process in A53T. An increase of 8-25 % in the lower stoichiometries and 40 % in higher molar ratio was observed in reversal approach. In H50Q, 20 day old matured fibrils were used for this assay and the ThT data shows a slight reduction of 5 % in 1:5 molar ratio.

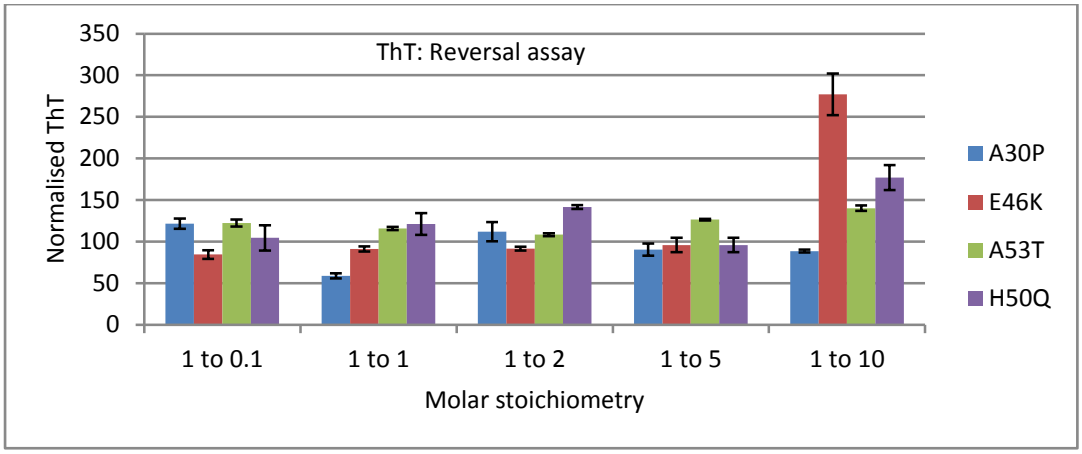

Figure 4.18: ThT fluorescence data(Reversal): In A30P (blue bar), 40 % fibril breakdown at 1:1, 10-12 % breakdown at 1:5 and 1:10, but an increase found in 1:2. This discrepancy confirms the presence of a secondary structure unable to bind ThT which is later confirmed by CD and AFM. In E46K (red bar), 5-15 % reduction in the ThT signal was found in smaller ratios of 1:0.1, 1:1, 1:2, and 1:5. But the ThT signal increased by 177 % in 1:10 might be showing an interaction of peptide at higher concentration with matured fibrils. In A53T (green bar), the peptide at any molar ratio is unable to breakdown matured fibrils. But an increase of 8-25 % in 1:0.1, 1:1, 1:2, 1:5 and 40 % in 1:10. In H50Q (violet bar), the peptide at 1:5 shows a slight reduction of 5 % in the amyloid content relative to 1:0. All the other ratios show an increased amyloid secondary structure.

4.3.3.2 CD assay

In the case of A30P (Fig 4.19.a), the inconsistency with concentration dependence was analysed using CD. CD data confirmed the presence of increased secondary β-structure in all molar ratios relative to peptide free (1:0) sample. The inconsistency with ThT data might be due to the presence of some species which are unable to bind ThT. In E46K (Fig 4.19.b), the spectra showed the retention of 218 nm signal similar to that of 1:0. In A53T (Fig 4.19.c), the increase in ThT signals at all molar ratios is confirmed by CD showing more β-signal compared to 1:0. In H50Q (Fig 4.19.d), the CD spectra is inconsistent with ThT signal

identified in 1:5 and 1:0.1.AFM imaging was undertaken to visually identify the nature and amount of fibrils formed in each mutant during the reversal approach.

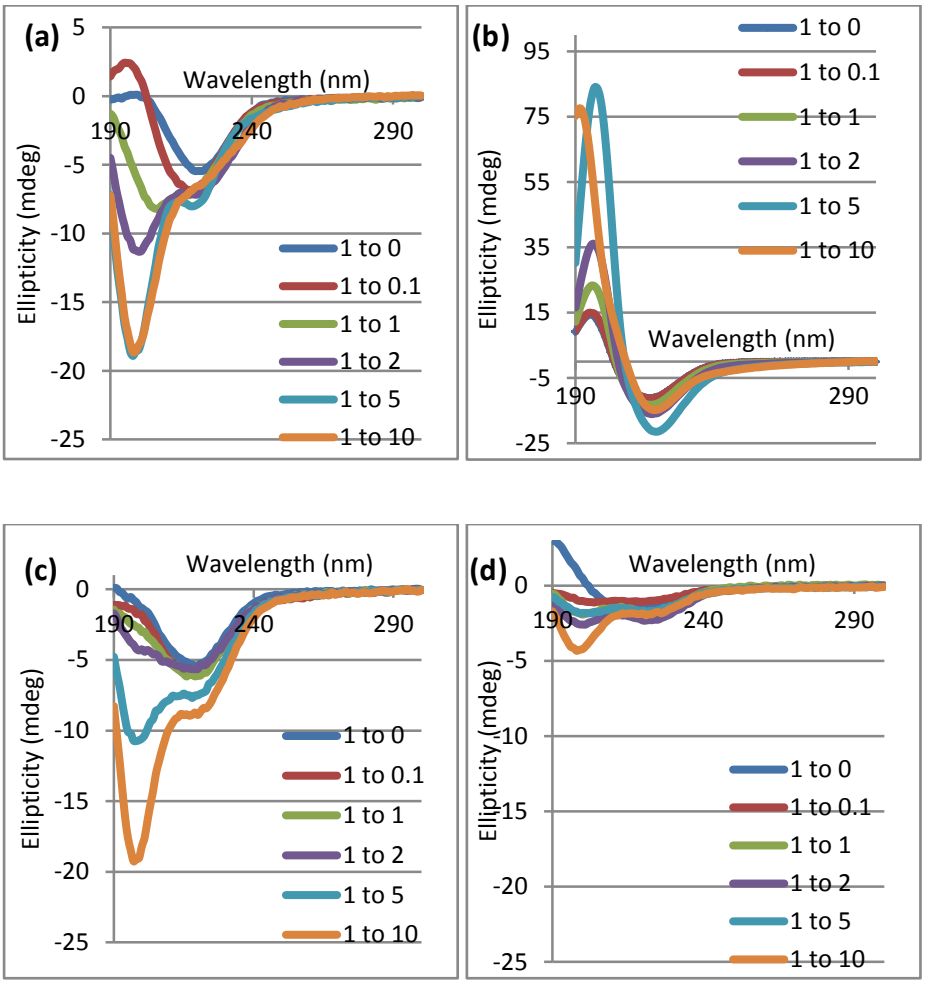

Figure 4.19: CD Spectra (Reversal) of ***(a)*** A30P ***(b)*** E46K ***(c)*** A53T and ***(d)*** H50Q**:** In A30P, the CD data (Fig a) shows an increase in the secondary structure (218 nm signal) at all molar concentration and the discrepancy with ThT data confirms the presence of a secondary structure unable to bind ThT. In E46K, the CD data inconsistently shows an increased β-signal relative to peptide free (1:0) sample in all molar ratios (Fig b). Consistent with ThT data, CD (Fig c) confirms an increase in the secondary signal (218 nm) at all molar concentrations in A53T. In H50Q, 1:0.1 ratio shows a reduced 218 nm signal but in contrast no reduction was seen in the ThT signal (Fig d).

4.3.3.3 AFM studies

AFM imaging (Fig 4.20) and analysis (Fig 4.21) were undertaken for the aliquots taken from the same samples used for ThT and CD studies. In A30P and E46K, long fibrils were seen entirely covering the mica sheet surface in all samples. AFM images confirm the presence of fibrils consistent with CD data. In E46K, 1:0.1 exhibited a similar pattern of fibrils to that of 1:0 with slightly less abundance. In 1:10, the mica sheet was entirely covered with bundles of matured fibrils. In A53T, there was no much difference in the amyloid load compared to 1:0 in the lower stoichiometries. At higher ratios, abundant protein clumps were seen as if the peptide involved in association of fibrils to form clumps. In H50Q, abundant protein clumps were seen in all samples with no reduction in the amyloid load compared to 1:0 at any of the molar ratios. In summary, the PCA derived peptides has minimal effect in breaking down the fibrils or reversing the mutant's aggregation process.

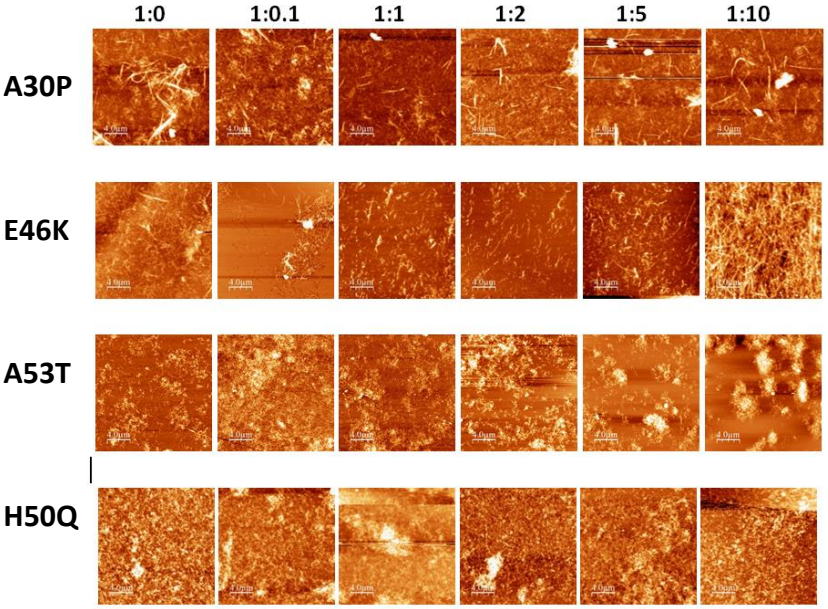

Figure 4.20: AFM images (Reversal): showing the presence of amyloid fibrils in the reversal approach. The images were taken for 1:0, 1:0.1, 1:1, 1:2, 1:5 and 1:10 after 3 days of post mix incubation. In A30P, long fibrils of 4-8 µm can be seen in 1:0. Addition of peptide at various molar concentrations show negligible reduction in the amyloid load. In E46K, inconsistent with the ThT

signal, bundles of matured fibrils covering up the entire mica surface can be seen in 1:10. 1:0.1 sample showed both long fibrils of 4 µm and clumps of aggregated species. Varied lengths of fibrils; approximately 1-4 µm were found in other molar ratios. In A53T, 1:0.1 to 1:2 resembles that of 1:0. Consistent with higher signals in ThT and CD, the rich clumps of protein fibrils can be seen initiated in 1:5 where as it is abundant in 1:10 . Addition of peptides at various molar concentrations show negligible effect in reducing the amyloid load.

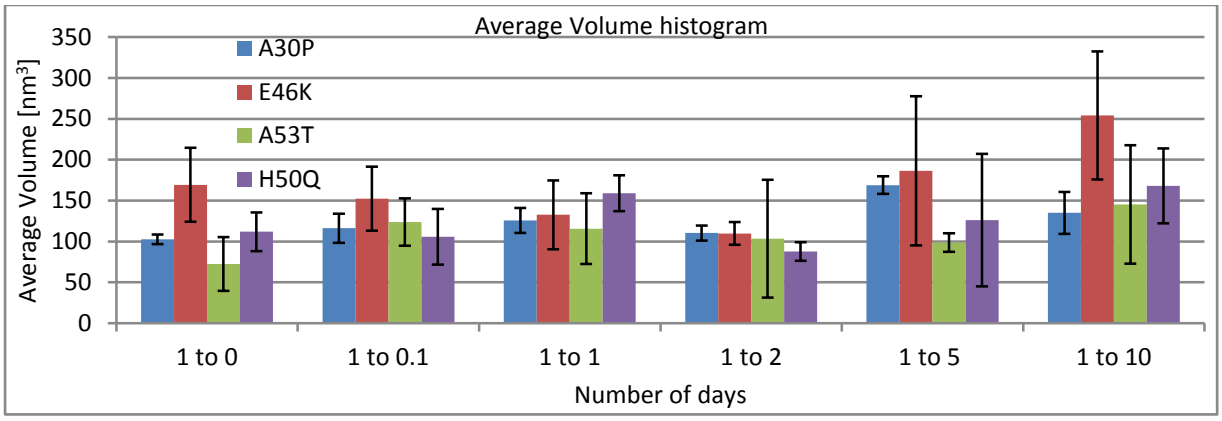

Figure 4.21: Histograms showing average volume: of mutants in the presence or absence of PCA peptide on the mica surface. In **A30P**, increased amount of matured fibrils unaltered by peptide at all molar concentration confirms the inability of A30P winner to reduce amyloid content in reversal approach. In **E46K**, reduced amount of fibrils were seen in lower stoichiometries shows the absence of larger amyloid species compared to increased amyloid content in the higher stoichiometries. The peptide is comparatively effective in breaking down the matured fibrils at 1:1 and 1:2 ratios. In **A53T**, increased amyloid volume relative to 1:0 can be seen in all molar ratios confirming the presence of large amyloid structure not broken down by peptide at any concentrations. In **H50Q**, molar ratio 1:2 shows a slight reduction relative to 1 to 0. Increased amyloid load were seen in all the other molar ratios.

4.3.4 Cell toxicity: MTT assay

MTT cell viability assay was performed to verify the effect of extracellular mutant α-syn deposits on rat pheochromocytoma (PC12) neuronal-like cells. The assay determines the cell viability using the reduction of water soluble MTT (3-(4, 5-dimethylthiazol-2-yl)-2, 5-diphenyltetrazolium bromide) into insoluble purple coloured formazan which was then determined by OD at 570 nm. The formazan concentration determines the number of viable cells. All experiments were performed in triplicates (technical replicates) as a part of single experiment and the error bars were calculated as the standard deviation of all errors. Mutant concentration of 5 μM was used for the MTT assay. In the assay PC12 cells were grown in isolation, with 5 μM mutant α-syn, with mutant: peptide ratios (1:0.1, 1, 2, 5, and 10), and with peptides in isolation (0: 0.1, 1, 2, 5, and 10). A30P, E46K and A53T were incubated for ten days under aseptic conditions while H50Q incubated for 20 days. Then the PC12 cells were added and incubated for 24 hrs followed by 4 hrs in MTT dye. Figure (4.22) shows that the cell viability across a range of mutants-peptide ratios relative to PC12 cells. It appeared that the matured fibrils formed by each mutant after their incubation period were toxic to the cells. The A30P peptide and E46K peptide showed moderate cell revival in 1:1 ratio. A maximum efficiency of 50 % was shown by A53T peptide in three molar stoichiometries. H50Q fibrils found to be less toxic compared to other mutants. The aggregated species in the presence of H50Q winner showed approximately 37 % cell survival.

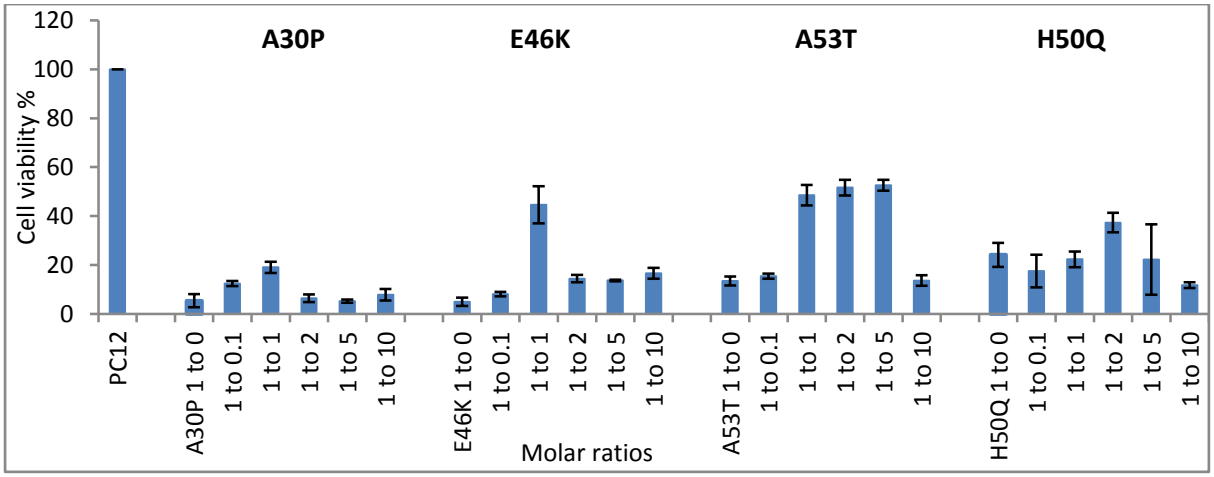

Figure 4.22: MTT assay: showing cell viability with α-syn mutants alone (1:0) and with PCA peptides at various molar ratios. In **A30P**, only 1:1 showed a slight revival of 19 % PC 12 cells. In **E46K**, again the molar ratio 1:1 showed a reasonable cell revival of 45 %. In **A53T**, 1:1, 1:2 and 1:5 showed 50 % cell survival. Compared to all other mutants **H50Q** was less toxic to the PC12 cells, 25 % of cells were viable in 1:0. Among all ratios of H50Q peptide, 1:2 showed a 37 % cell survival. The aggregated species in all the other ratios of four mutants were considerably toxic to the PC12 cells.

Following the (target: peptide) study, the effect of PCA peptides in isolation on PC12 was studied using MTT assay. Though the peptides in isolation showed minimal tendency of self-aggregation in the ThT, CD and AFM assays, it causes considerable loss in PC12 cells (Fig 4.23). The 10 day old A30P, E46K, A53T peptide winners and 20 day old H50Q peptide winner were used in this assay. A30P winner peptide unexpectedly induced PC12 cell death in various molar ratios. Approximately 50 % cells died with E46K peptide winner at higher concentrations. A53T peptide and H50Q peptide were showing minimal effect on PC12 cells in various ratios.

.

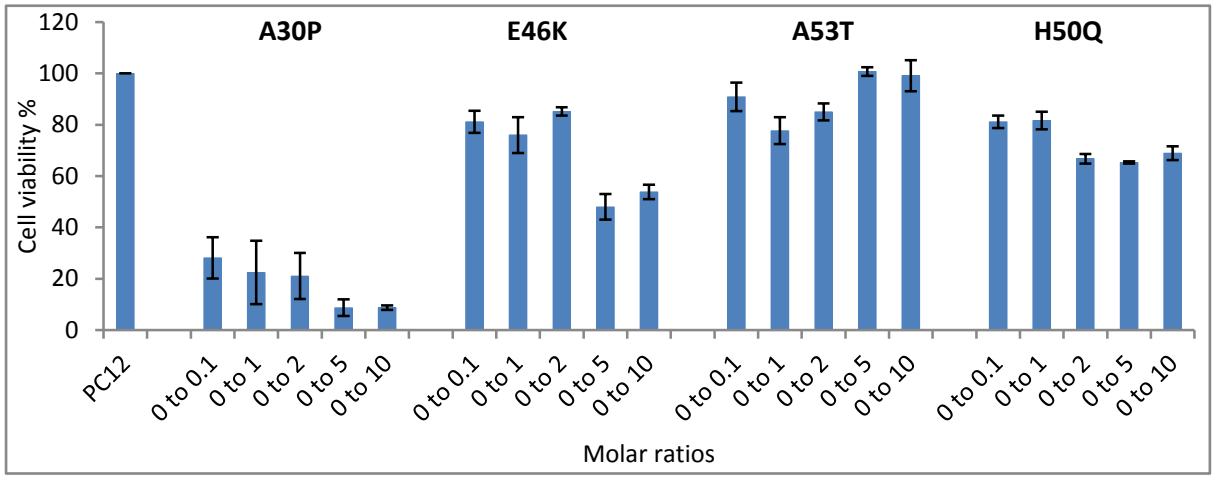

Figure 4.23: MTT assay with PCA peptides in isolation at various molar ratios (0:0.1, 0:1, 0:2, 0:5 and 0:10). The assay was performed by incubating PC12 cells for 24 hours; with peptides alone allowed to aggregate along with main characterisation experiment. The A30P winner showed 75-90 % toxicity to PC 12 cells in various stoichiometries range. Cell loss of 15-25 % in the lower ratios and 50 % at the higher concentrations were seen in E46K winner peptide. In A53T, 25 % reduction in PC 12 cells was seen in lower stoichiometries. H50Q showed a cell death of 20-35 %.

4.3.5 Control experiments

4.3.5.1 PCA derived peptide in isolation

As a control experiment, the PCA derived peptides were studied in isolation using ThT, CD and AFM considering the same molar ratios used for the characterisation studies. The peptides at molar ratios; 0:0.1, 0:1, 0:2, 0:5 and 0:10 were incubated at same conditions used for mutant: peptide characterisation experiments. The ThT signal in each case was considerably smaller compared to peptide free (1:0) sample confirms the lack of self-aggregating property of PCA peptides (Fig 4.24). The retention of 200 nm signal in the CD spectra for all the peptides in all molar ratios (Fig 4.25) confirms the random coil structure exhibited by peptide even after its full tenure of incubation. The absence of any oligomeric or fibril structure in AFM data (Fig 4.26) also supports the above points.

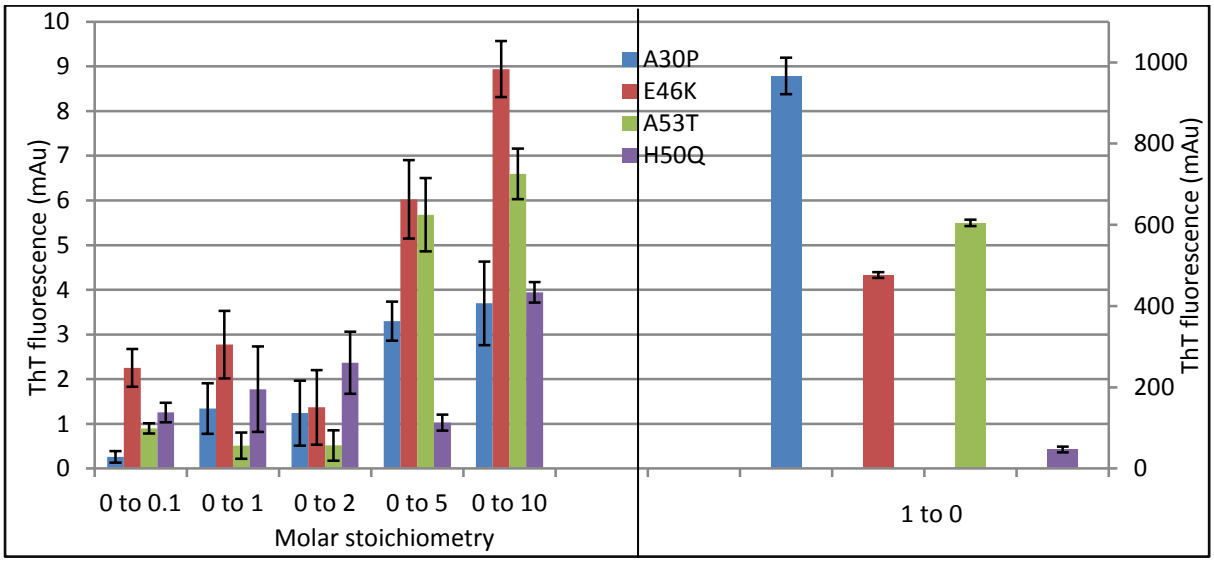

Figure 4.24: ThT fluorescence data: of PCA peptides in isolation at concentrations of 0:0.1, 0:1, 0:2, 0:5 and 0:10 (mutant: peptide) represented on the left side of the figure. The ThT signals of end point samples are considerably small compared to that of the peptide free (1:0) sample shown on the right side of the figure; plotted on a secondary 'y' axis (ThT fluorescence (1:0): A30P= 966.7 mAu, E46K= 476.4 mAu, A53T= 604.9 mAu and H50Q= 46.78 mAu).

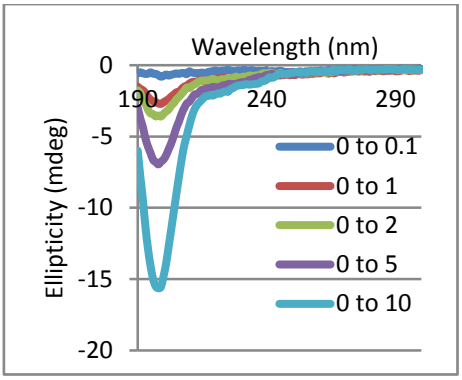

Figure 4.25: CD spectra: showing retention of random coil for the peptides at different ratios. This is a representative image as all the PCA derived peptides of each mutant exhibited similar pattern. The data confirms the lack of self aggregating properties of peptides at the end of incubation period.

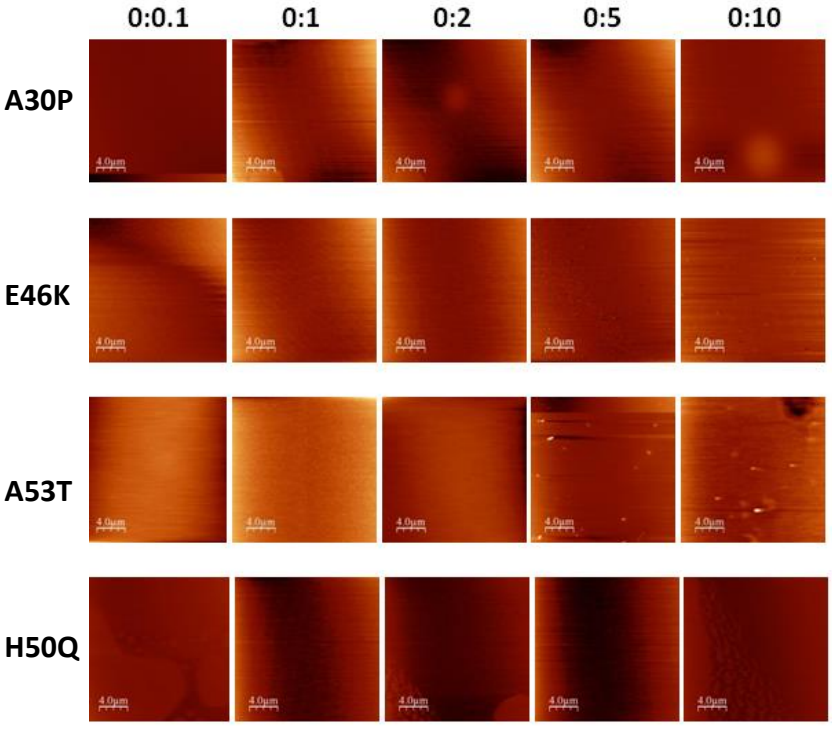

Figure 4.26: AFM images: of PCA peptides at concentrations 0:0.1, 0:1, 0:2, 0:5 and 0:10. The images show that the peptide do not self-aggregate to form oligomers or fibrils in isolation even after 10 days of incubation as consistent with ThT and CD data. In A53T peptide, small oligomeric structures were visible at 0:5 and 0:10 which could be anticipated as precipitation of peptide at high concentrations (2250 and 4500 µM respectively).

4.3.5.2 Positive and negative control experiments

To confirm the reliability of mutants and PCA derived peptides, control experiments with negative control peptide (SGSSGTSSGTSG) and positive control peptide [VAQKT$_m$V (Madine *et al.*, 2007)] were performed along with the peptide characterisation studies against all four mutants. The negative control (SGSSGTSSGTSG) peptide is a GS linker used in PCA. The N-methylated α-syn$_{77-82}$ (VAQKTV) peptide was used as positive control to disrupt α-syn aggregation. ThT, CD and AFM assays were performed to analyse its effect on the aggregation of mutants. The mutants were allowed to fibrillise with each of the two control peptides at molar ratio 1:1 until it reached maturation. All the readings were taken at the final day of incubation i.e., day 10 for A30P, E46K, A53T and day 20 for H50Q. According to the ThT data (Fig 4.27), the positive control peptide showed approximately 5-25 % reduction in total amyloid load formed by various α-syn mutants. As expected the negative control peptide did not prevent the aggregation.

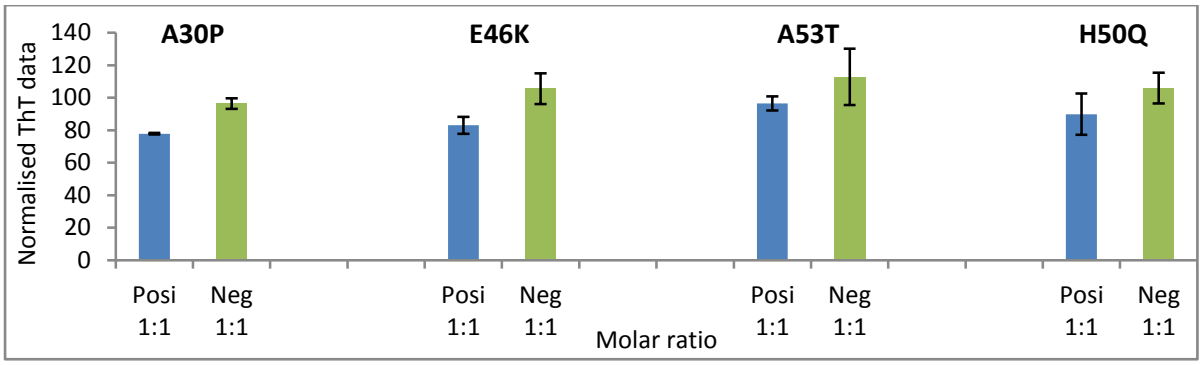

Figure 4.27: ThT fluorescence data: shows the effect of positive control and negative control peptides on mutants at molar ratio 1:1 relative to peptide free (1:0) sample. The positive control peptide (blue solid bar) showed 23 % reduction in A30P, 17 % in E46K, 4 % in A53T and 11 % in H50Q in total amyloid content after 10 days of incubation. The negative control peptide (green solid bar) showed minimal effect on A30P, E46K and H50Q amyloid load relative to 1:0. It showed a 12 % increase in A53T.

CD experiments were undertaken using aliquots taken from the same stock samples used for ThT experiments. In the Fig 4.28, β-sheet structure was shown by four mutants at the end of incubation period. Consistent with ThT data, reduced β-signal was seen in A30P, E46K and H50Q mutants. There was co-existence of β-sheet with random coil seen in A53T in the presence of positive control peptide. The negative control peptide showed an increased 218 nm signal in A53T. Following CD, AFM imaging was also performed to confirm the presence of fibrils in each condition (Fig 4.29).

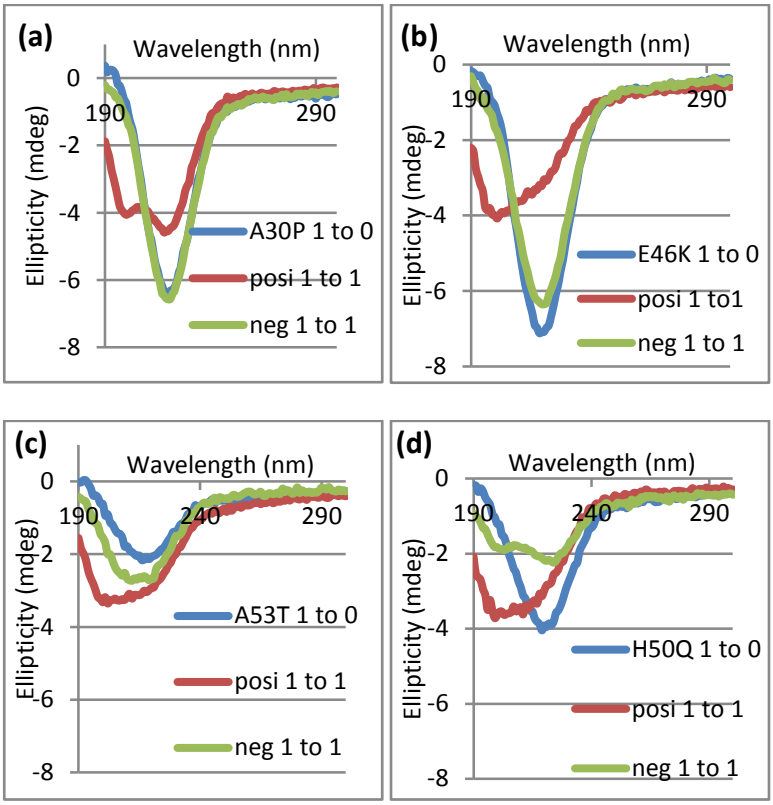

Figure 4.28: CD spectra: showing the effect of positive control and negative control peptides on ***(a)*** A30P, ***(b)*** E46K, ***(c)*** A53T and ***(d)*** H50Q at molar ratio 1:1. All peptide free mutant samples (1 to 0) showed β-sheet structure at the end of incubation period. In A30P the positive peptide showed a reduced β-content along with a random coil signal and unaltered by negative control peptide. The effect of positive peptide in E46K and H50Q exhibited a dominant random coil signal. Consistent with ThT data, A53T showed an increased 218 nm β-signal co-existing with the random coil

structure. Increased β-signal is visible in A53T with the negative peptide as of in ThT. In contrast to ThT, H50Q showed a reduced β-signal with negative control peptide.

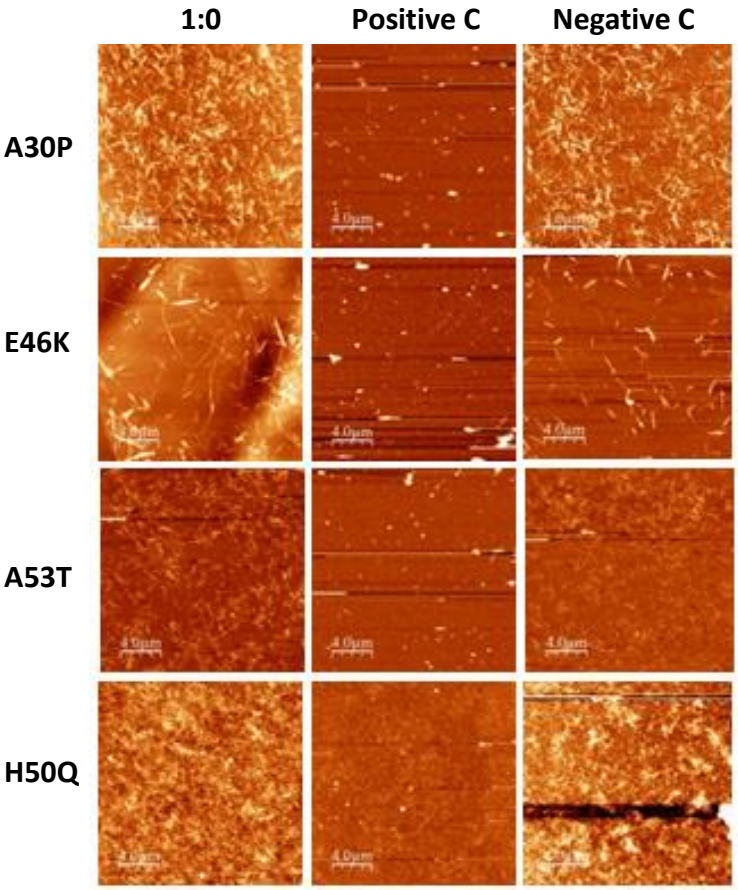

Figure 4.29: AFM images showing the effect of positive and negative control peptide on aggregation of α-syn mutants. All mutants (1:0) formed fibrils or aggregates after the incubation period. The increased ThT and CD signal shown in A53T with positive control peptide was not visible as fibrils in AFM image. There were oligomeric structures found abundantly in mica sheet. Reduction of fibrils was seen in A30P and E46K with positive peptide. The fibrils found in H50Q in the presence of positive control peptide were not prominent compared to 1:0. Negative peptide replicated 1:0 images in all mutants.

4.4 Discussion

In this chapter the peptides screened from the semi-randomised libraries by PCA were characterised to identify the peptide efficacy in lowering the toxicity of full length mutant α-syn$_{1\text{-}140}$. As seen in the previous chapter the peptides were designed on scaffold of 71-82 region and anticipated the inhibition by specifically binding to full length α-syn mutant. The ThT, CD and AFM data of endpoint samples in the Fig 4.30 shows the effect of peptides on each mutant during its aggregation in the presence of PCA derived peptides.

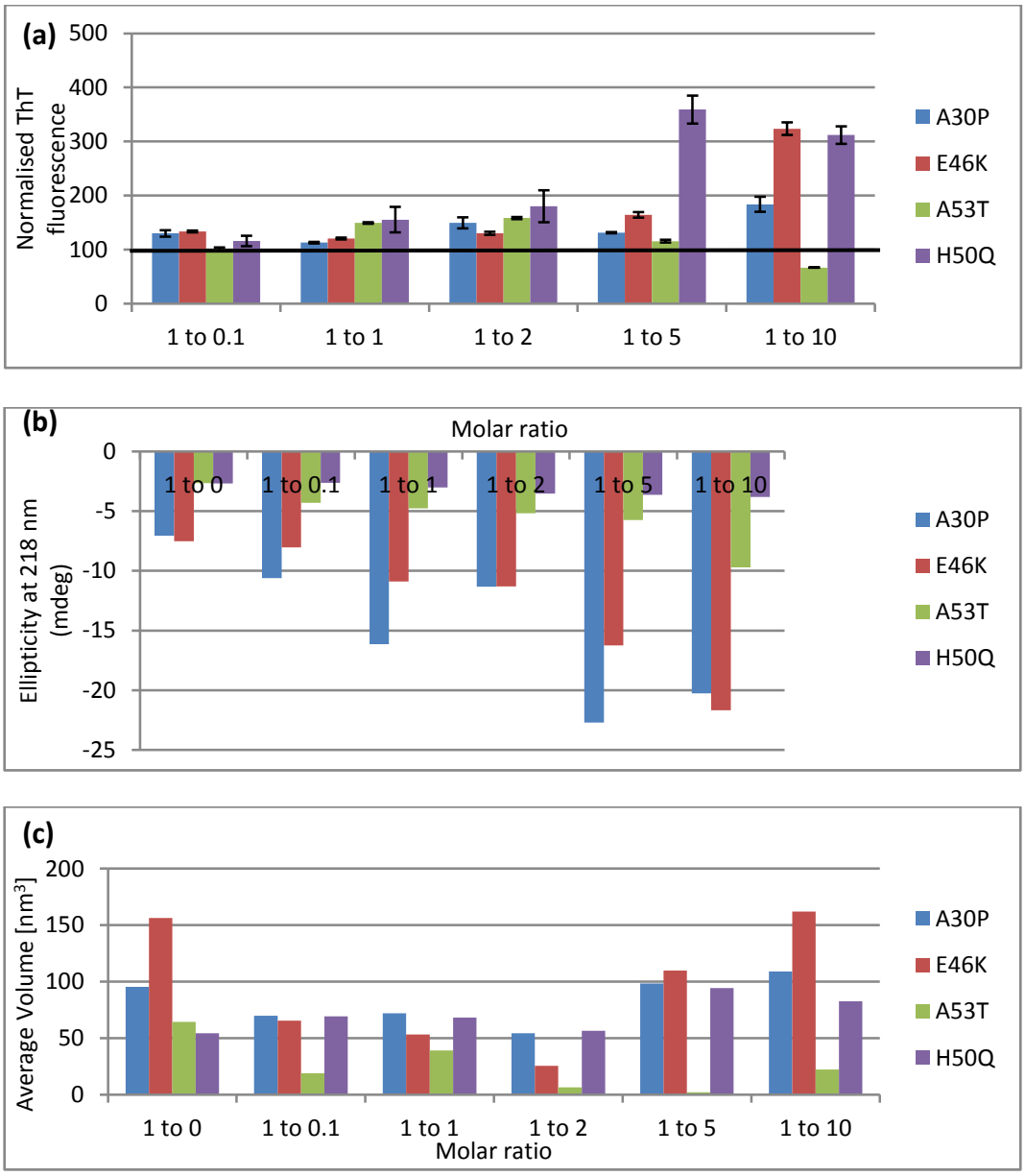

Figure 4.30: ***(a)*** **ThT data** relative to peptide free sample (1:0, represented by black bold line) in %, ***(b)*** **Ellipticity (mdeg)** at 218 nm representing β-sheet formed during aggregation and ***(c)*** **Average volume** of fibrils seen in the AFM images. All these data represent the end point samples at different molar ratios of four mutants. As seen in (Fig a), none of the peptides at any molar ratio inhibited the aggregation except 1:10 ratio of A53T. Among all the PCA peptides, ThT data shows that the A53T peptide is comparatively effective on A53T aggrgegation as the fibril growth is seen deteriorating . In consistent with the ThT data, CD data confirmed the development of β-sheet structure at higher stoichiometry showing the formation of fibril species that are unable to fix ThT dye (Fig b). The moderate inhibition or delaying property of A53T peptide can be seen reflected in AFM images (Fig c).

Collectively the data confirms that the PCA screened peptides lead to moderate levels of antagonistic property against A53T aggregation, while low efficacy against A30P, E46K and H50Q. MTT assay also assured a 50 % cell survival with A53T peptide at lower stoichiometries.

In the case of A30P, even though a small reduction was observed in ThT signal during the mid-phase of incubation, it was inconsistently denied by CD results which confirmed the development of increased β-signal as the incubation progresses. A slight delay in the aggregation process was seen in ThT data confirmed later by AFM images especially in the lower stoichiometries while higher ratios were identified to enhance fibril formation. The proline residue in A30P peptide winner ($_{77}$**HPQN**$_{80}$**)** was anticipated to facilitate the secondary structure into turns or helices and thus disfavouring β-strand due to its conformational rigidity of cyclic pyrrolidine side chain and inability to participate as hydrogen bond donor. There might have an overruling of 'proline effect' by adjacent residues in the later phases as they are polar and may have participated in hydrogen bond formation. The peptide failed to inhibit the aggregation process as the residues 71-82 might

not be an appropriate target to design a peptide library against A30P. The MTT data also confirms the toxicity of aggregated species formed in all stoichiometries which are non-viable to the cells. Further studies needed so that the residues in a different target region can be considered for developing potent peptide inhibitors against A30P aggregation.

In E46K, the peptide in all ratios caused enormous increase in ThT and CD signal confirming the formation of considerable load of amyloid fibrils. Notably small fibres were identified in all stoichiometries compared to that formed in 1:0. The higher ratio 1:10, showed a distinguishable association of fibrils into bundles. A small reduction was seen in ThT during reversal approach in lower stoichiometries but was not supported by CD. The volume histogram analysis of AFM data showed a slight decrease of fibril content in lower stoichiometries supports ThT data. MTT assay showed the aggregated species in all stoichiometries induce cell toxicity. The E46K peptide has randomised residues; $_{77}$**NQNN**$_{80}$ which are polar and favours β-confirmation by hydrogen bond formation. N and Q have opposite effects on amyloid formation. I assumed that the N richness would promote the formation of benign, self-ordered amyloids. Although short peptides like A30P and E46K winners contain glutamine which could bind to the target protein, making it Q rich. Q residue is known to produce toxic, non-amyloid disordered conformations. The uncharged polar side chain usually locates on the outside of protein could be a protein-protein interaction module (Halfmann *et al*., 2011). In summary, E46K peptide failed to inhibit amyloid formation and as suggested previously the target region 71-82 might not be suitable for designing peptide inhibitors.

The inhibitory effect shown by A53T winner peptide was moderate. The peptide has randomised residues $_{77}$**DNKE**$_{80}$, shows a reduced hydrophobicity relative to α-syn$_{71-82}$. The substitution of hydrophobic residues may pass the threshold required to prevent

fibrillisation. The peptide was identified to reduce the ThT signal in the mid-phase after a larger fluorescence exhibited during initial phase in the lower stoichiometries. And also prominent cell recovery was identified in MTT assay suggests a less toxic species formed in the lower stoichiometries. A higher proportion of polar/charged residues being selected were assumed to show anti-amyloid property. A reduced ThT signal of 34 % was identified in the higher ratio of 1:10. Though it wasn't supported by CD data or AFM images, as if there was an accumulation of distinct β-sheet structure which is unable to bind ThT dye. A few physical differences in the generation of fibrils can cause fluorescence differences. ThT binding would be less efficient on thick, large clumps of fibrils as the dye may not penetrate thick clumps as isolated fibrils (Petkova *et al*., 2009). More structural studies like labelling fibril samples and solid-state NMR spectroscopy can give a clue to define the effect of PCA peptides on the possible ThT binding sites (involving the benzyl group) on amyloid fibrils (Ye *et al*., 2008). The peptide was found to enhance the formation of thick bundles of fibrils at higher stoichiometries. As the peptide contains aspartate as well as glutamate which are frequently involved in protein active or binding sites (Betts and Russell, 2003), the peptide was found to have interacted with the target protein.

The PCA peptide against H50Q aggregation with randomised sequence $_{77}$**NSSD**$_{80}$, is found to enhance rather than inhibit fibrillisation. I speculate that the PCA peptides initiated the aggregation process as the ThT signals were comparable with that of other mutants in the inhibition assay as the signals were low in the sample without peptide (1:0). The presence of serine with its primary hydroxyl group participates extensively in hydrogen bond formation. The higher stoichiometries provided more serine residues to form abundant β-amyloid species as per ThT and CD data. Discrepancy was found in ThT and CD data in reversal assay suggesting the inability of H50Q peptide to function as a β-breaker. In contrast to all the

available studies about H50Q aggregation, there was a long lag phase observed, delaying the aggregation process. It is unclear that the H50Q mutant showed a small ThT value compared to the other mutants (section 4.3.2.1). All the PCA peptides in isolation did not exhibit any self-aggregating property and thus confirmed the signals are truly from the fibrils formed by mutants in various conditions. A moderate level of efficacy was identified in the reversal approach in breaking down the matured fibrils among A30P and E46K but no reversal effect seen in A53T or H50Q. In conclusion, *in vivo* selection approach was used to derive a range of peptides against mutant's aggregation. Though the peptides are not satisfactorily terminating the aggregation process as anticipated at the PCA level, we can conclude that the 71-82 region is inappropriate for the development of an antagonistic peptide. Later the study leads to focus on a different target region to develop inhibitor peptide against α-syn aggregation.

Chapter 5: Semi-rational design combined with PCA approach using an α-syn$_{45-54}$ template to derive peptide antagonists of α-syn aggregation

5.1 Introduction

Many researchers have focused on the 71-82 region of α-syn during design of inhibitors as it is responsible for the aggregation of the full length protein. As I discussed in the earlier chapters, the previous peptide libraries were designed based on this scaffold. In the literature; non-modified peptides (El Agnaf *et al*., 2004; Sciarretta *et al*., 2006) and N-methylated peptides (Bodles *et al*., 2004, Madine *et al.*, 2008) were also designed based on this region. However, many of the known point mutations in the α-syn gene associated with early onset PD are located between 45-54 region with A30P located in close proximity. This chapter thus focuses on designing a new library based on the fact that this region and its residues play a vital role in modulating the structure of α-syn and thereby influencing amyloid formation. These mutations lead to structural changes such as decreased α-helicity, increased β-sheet propensity, and an increase in either the rate or number of oligomers formed during α-syn aggregation (Conway *et al*., 2000, Li *et al*., 2001, Bussell et al., 2001, Choi *et al*., 2004, Greenbaum *et al*., 2005, Ghosh *et al*., 2013, Rutherford *et al*., 2014). A peptide library containing 209,952 members was consequently created using α-syn$_{45-54}$ as the template. The amino acids options corresponding to E46K, H50Q and A53T were also included while designing the library. This chapter utilises an approach which successfully produced a peptide sequence that could antagonise α-syn aggregation. This could provide a basis for future drug development against PD.

5.2 Experimental approach

(1) Expression and purification of α-syn: The protein was expressed and purified according to the methodology in chapter 2 and 3.

(2) PCA: The library was screened using PCA to derive a peptide capable of interacting with full length wild type α-syn.

(3) Peptide 45-54W synthesis: The peptide was synthesized using a Liberty Blue™ microwave peptide synthesizer [CEM; Matthews, NC] according to the methods outlined in chapter 2.

(4) Peptide characterisation: Continuous amyloid growth was monitored by ThT fluorescence to provide real-time information on the formation of amyloid. Structural studies were additionally monitored by CD and, AFM, while SDS-PAGE analysis was also performed. Collectively these approaches were used in order to assess the fibril load reduction and the changes in the fibril morphology. Along with that the toxicity of the amyloid fibrils was studied by MTT assay on PC12 cells.

5.3 Results

A peptide library was generated based on the α-syn$_{45-54}$ region and PCA used to screen for an interaction with the full length α-syn$_{1-140}$ target. The library incorporated the wild-type sequence along with two, three or six residue options (at positions 46, 50 and 53) at each of the positions including three of the known point mutation residues associated with the early onset of PD (Fig 5.1). Unlike 71-82, the 45-54 region is not known to aggregate into toxic amyloid fibrils in isolation and has not been previously considered in the design of α-syn aggregation inhibitors. PCA was next undertaken to identify the most effective peptide antagonist of wild type α-syn aggregation from the library based on 45-54 region. Single step selection and competition selection was undertaken, resulting in one clean dominant sequence; KDGIVNGVKA from a library size containing 209,952 members (Fig 5.1 and 5.2).

Wild type α-syn	**^{45}K**	**^{46}E**	**^{47}G**	**^{48}V**	**^{49}V**	**^{50}H**	**^{51}G**	**^{52}V**	**^{53}A**	**^{54}T**
Degenerate codons used for library construction	RAA	VAW	GBG	VTT	VTT	VAW	GBG	VTT	RHA	RCC
Amino acid options encoded by each codon.	**K** **E**	**E** **Q** **N** **K** **D** **H**	**G** **A** **V**	**V** **I** **L**	**V** **I** **L**	**H** **Q** **N** **K** **D** **E**	**G** **A** **V**	**V** **I** **L**	**A** **V** **T** **I** **K** **E**	**T** **A**
45-54W peptide	**K**	**D**	**G**	**I**	**V**	**N**	**G**	**V**	**K**	**A**

Figure 5.1: The residues of wild type α-syn$_{45-54}$ are shown in the top row with yellow highlight showing the three well studied point mutation sites (46, 50 and 53). The second row shows degenerate codons used for library construction (R=A/G, V=A/C/G, W=A/T, B=C/G/T and H=A/C/T). The amino acid options at each position to generate a 209,952 (2*6*3*3*3*6*3*3*6*2) member peptide library are shown in the third row. The wild type options and alternative options including

point mutations associated with early onset PD (underlined) are also considered in the library design. The PCA selected winner peptide 45-54W (KDGIVNGVKA) is shown in the bottom row.

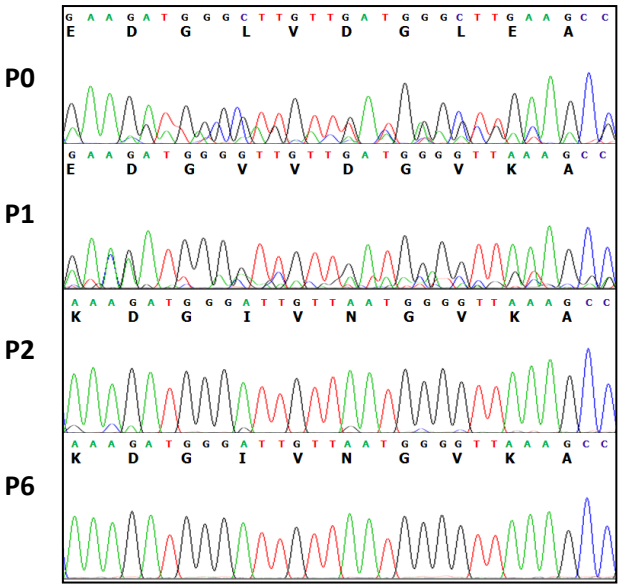

Figure 5.2: **DNA sequencing results** showing single-step selection (*P0*) and competition selection (*P1, P2, and P6*) steps involved in PCA. It shows the emergence of clear dominant peptide sequence KDGIVNGVKA from passage 2 until passage 6.

The PCA derived peptide; KDGIVNGVKA (45-54W) was next synthesized using a Liberty Blue™ microwave peptide synthesizer (CEM; Matthews, NC) (methodology detailed in chapter 2). The efficacy of peptide to inhibit fibril formation was characterised using ThT, CD, AFM, MTT and SDS-PAGE assays. The peptide was also studied in isolation along with the characterisation experiments.

5.3.1. ThT continuous growth experiments

ThT binding assay was used to quantitatively determine the amount of wild type α-syn fibrils formed in the absence or presence of the 45-54W peptide. Prior to the experiment, α-syn was monomerised to confirm the absence of any pre-formed fibrils and the ThT concentration was optimised as 90 µM (Fig 5.3) (details in chapter 2). Monomerised α-syn was incubated at a concentration of 450 µM and 37^{0}C with peptide at four different stoichiometries; 1:0.01, 1:0.1, 1:0.5, and 1:1. The peptide was added at time zero to a solution containing 90 µM ThT and a fluorescence reading was measured at every five minutes over a 4500 minute period. The experiment was performed by continuous mixing using a magnetic flea in an LS55 fluorescence spectrophotometer (Perkin Elmer). According to the data, the ThT signal was significantly reduced at a 1:1 molar ratio indicating the peptide can bind to α-syn and reduce its aggregation propensity. The molar ratio 1:0.5 slows down the aggregation rate, but does not prevent aggregation. Dose dependency was observed as reduced ThT signals were exhibited by lower stoichiometry ratios. The reference peptide; 71-82W (WT-B; shown in chapter 3) and the control peptide; wild type 45-54 fragment (45-54wt) at 1:1 molar ratios had minimal effect upon α-syn, demonstrating sequence specificity for the 45-54W peptide.

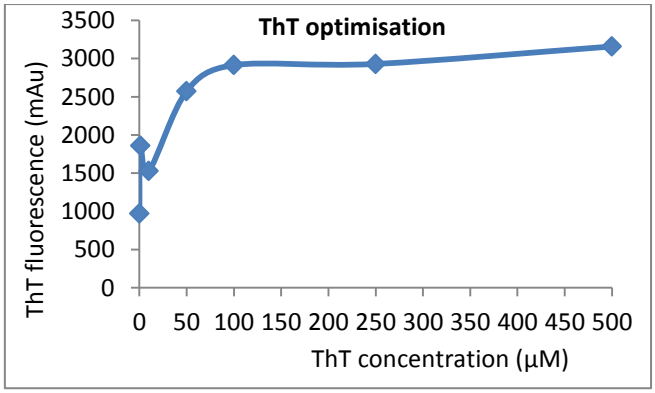

Figure 5.3: ThT optimisation data showing ThT signal of 450 µM target protein mixed with various concentrations of ThT ranging from 0, 1, 10, 50, 100, 250, and 500 µM. The ThT signal was found to be flattened at approximately 90 µM and it was considered optimum for the continuous growth experiments.

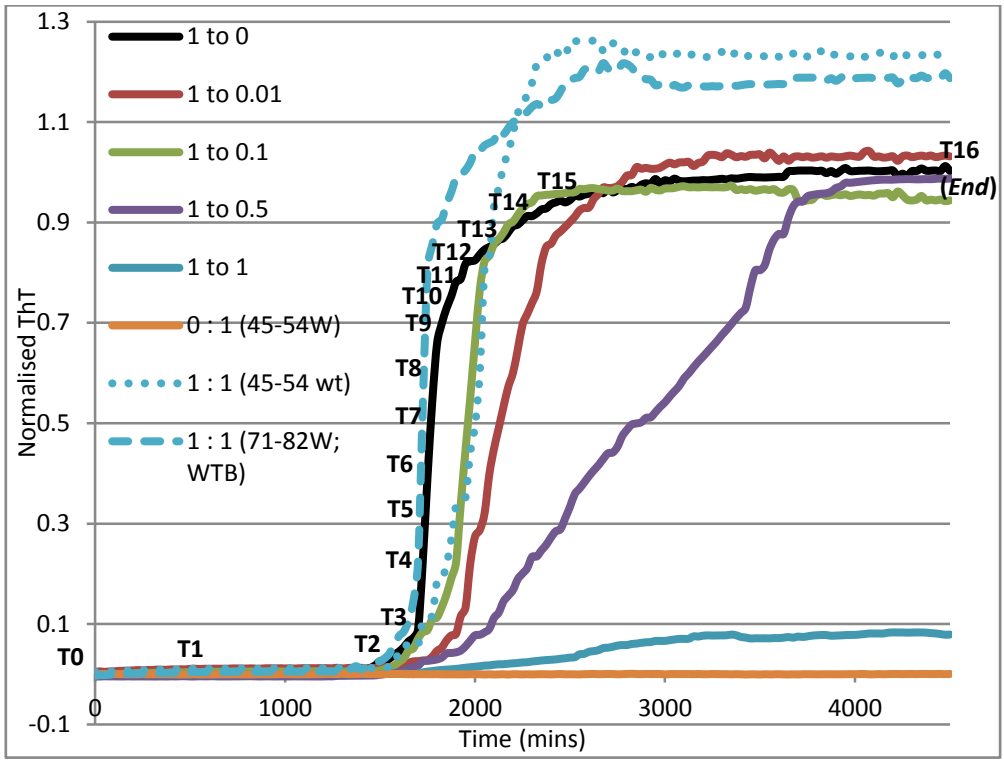

Figure 5.4: **Continuous ThT growth.** The data show a considerable reduction of ~92 % in ThT signal at 1:1 stoichiometry with 45-54W peptide. The ThT signal at stoichiometry 1:0.5 shows a reduction in aggregation compared to that of wild type. At increasingly sub stoichiometric ratios, the greater ThT signal indicates a reduced peptide activity in an expected dose-dependent manner. The 0:1 sample (peptide 45-54W alone) showed no ThT binding, indicating that it does not have self-aggregating property. The control peptides 71-82W (WTB) and wild type 45-54 fragment (45-54wt) at stoichiometry 1:1 has no effect upon α-syn, demonstrating sequence specificity for the 45-54W peptide. Aliquots of samples at 17 different time points from lag phase, exponential phase and stationary phase for inhibitor free; 1:0 sample (black line) were collected for further analysis by CD and AFM. The time points were T0= 0 min , T1= 600 mins , T2=1525 mins , T3= 1625 mins , T4= 1700 mins, T5= 1725 mins, T6= 1735 mins , T7= 1745 mins , T8= 1750 mins , T9= 1825 mins , T10= 1875

mins, T11= 1900 mins , T12= 1950 mins, T13= 2100 mins , T14= 2225 mins , T15= 2400 mins ,and T16= 4500 mins (*End*). Aliquots of three time points for the 1:1 sample (T0, T1 and *End*) were also collected for CD and AFM analysis.

5.3.2 CD assay

The structural characterisation of ThT continuous growth samples were performed by CD spectroscopy. According to the data, a single negative peak at 218 nm corresponding to β-sheet structure developed. This, along with the loss of minima at ~200 nm corresponding to the loss of a random coil structure was identified in 1:0 across the time course (Fig 5.5.a). Consistent with the ThT data, α-syn in the presence of 45-54W peptide at 1:1 stoichiometry did not progress to a β-sheet structure, but rather retained the random coil signal at 200 nm (Fig 5.5.b). The 45-54W peptide showed a similar random coil structure indicating the peptide lacks self-aggregating property in isolation (0:1 stoichiometry) after 4500 minutes of incubation. The absence of 218 nm signal for α-syn with 45-54W peptide could be recognised as increasingly aggregating or precipitating out of the solution. However, AFM experiments were undertaken for the same samples as the morphology of species formed can be clearly observed in imaging experiments. In these experiments, 45-54W in isolation showed no oligomers or fibrils. In addition, the control peptides; WTB or 45-54wt showed no effect upon the formation of β-sheet structure, again demonstrating the sequence specificity of the 45-54W peptide towards α-syn (Fig 5.5.c-d).

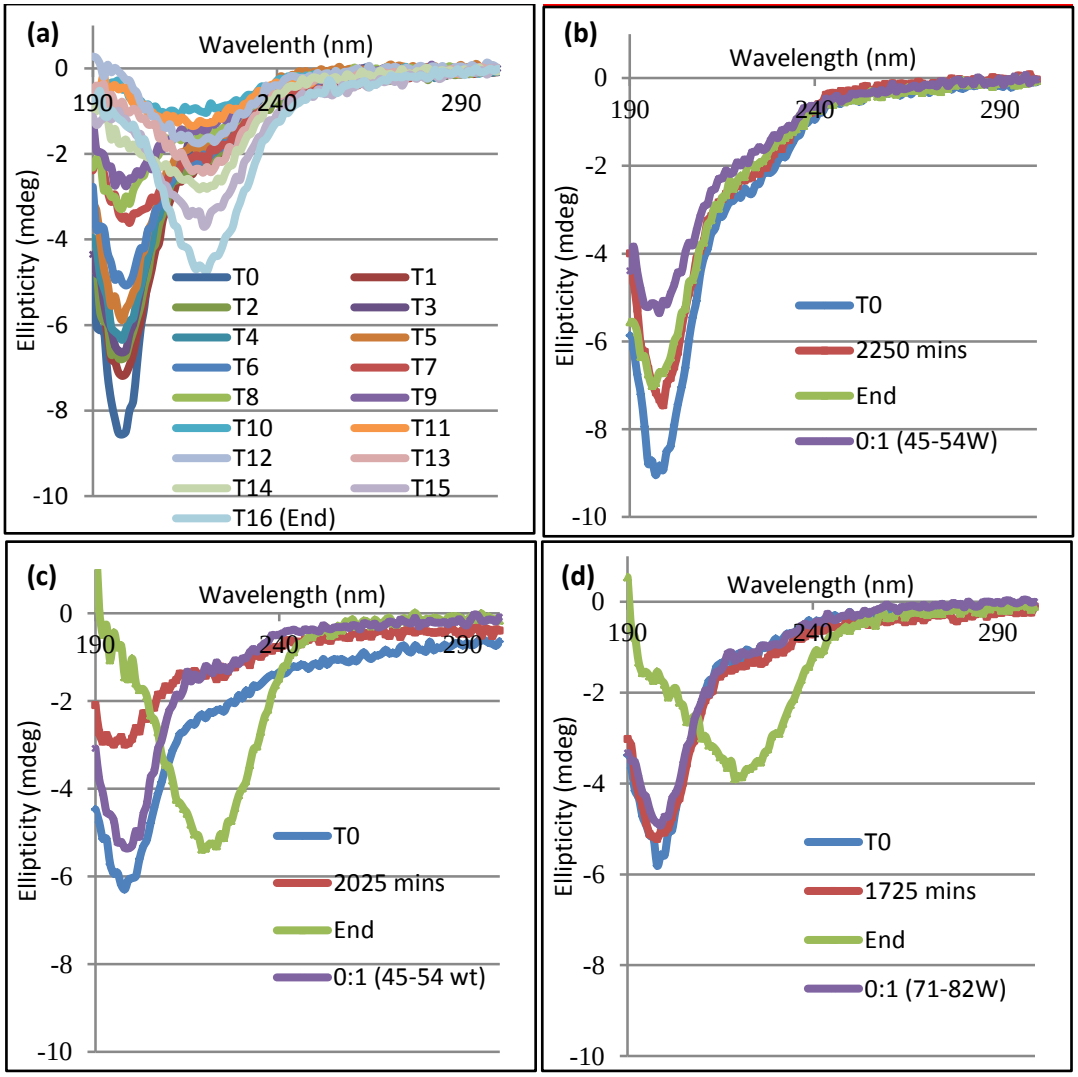

Figure 5.5: **CD spectra *(a)*** showing the gradual development of a minimum at 218 nm (β-sheet structure) across the time course along with loss of a minimum at 200 nm (random coil structure) in 1:0. ***(b)*** The data shows the efficacy of peptide (45-54W) at 1:1 stoichiometry in retaining the random coil structure (~200 nm minimum) even after incubation for 4500 mins with no development of β-sheet structure. The peptide alone (0:1) showed a similar spectra indicating that it does not form β-sheet structure in isolation. ***(c)*** The data shows the wild type α-syn 45-54 sequence at stoichiometry 1:1 had no effect upon transition of random coil to the β-sheet structure. It also did not adopt β-sheet structure in isolation. ***(d)*** Similarly, the previously studied peptide; WTB based on α-syn$_{71\text{-}82}$ considered here as a negative control which showed no effect upon conversion to the β-sheet structure and loss of random coil at stoichiometry 1:1. And also the peptide in isolation did not adopt a β-sheet structure.

5.3.3 AFM imaging

The samples used in ThT continuous growth experiments and CD assays were used for imaging. 5 µl of endpoint samples of all stoichiometries along with peptide in isolation (0:1) were imaged (Fig 5.6.a). Aliquots were taken and imaged in detail at different time points for 1:0 (Fig 5.6.b) and 1:1 since it was found to be the most effective in ThT experiments (Fig 5.6.c). At this stoichiometry, a significant reduction in the fibril content was observed relative to inhibitor free; 1:0 control. No fibrils were observed in 45-54W (0:1) in isolation. Gradual increase of fibril content was identified in 1:0 across 17 time points. The control peptides; WTB and 45-54wt had no effect upon fibril formation (Fig 5.6.d-e) confirming the specificity of α-syn towards 45-54W peptide. All images were taken at 20 µm scan size at room temperature. The image files were examined directly using WSxM v5.0 (Nanotec Electronica S.L., www.nanotec.es) and flattened before processing. (Kad *et al*., 2001 & 2003).

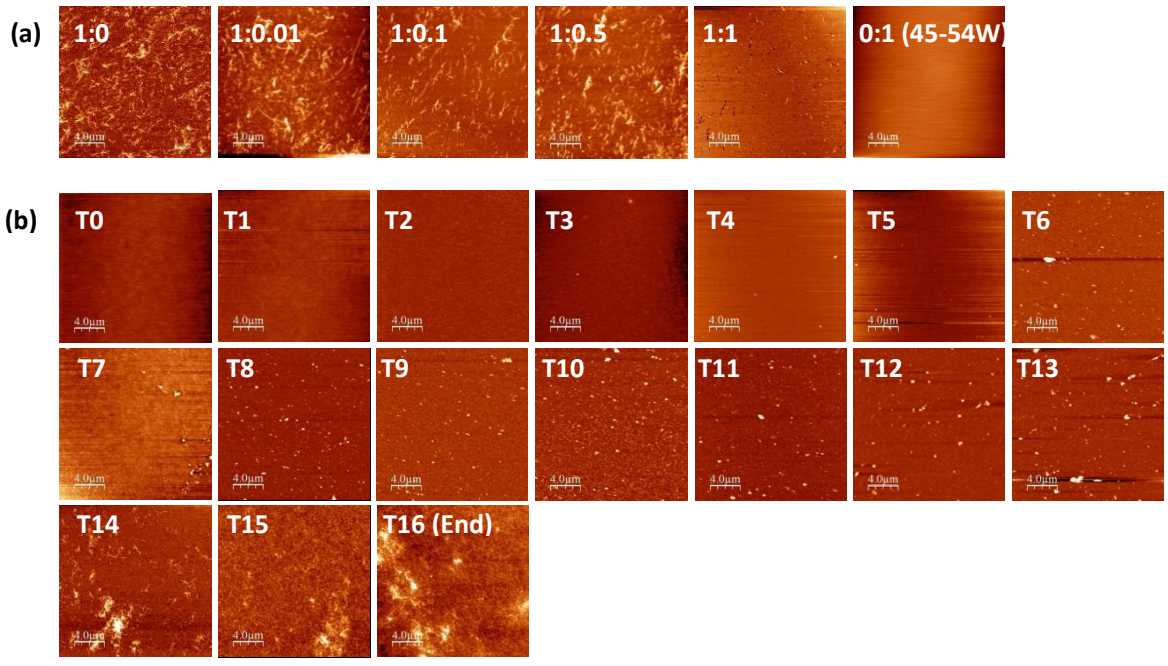

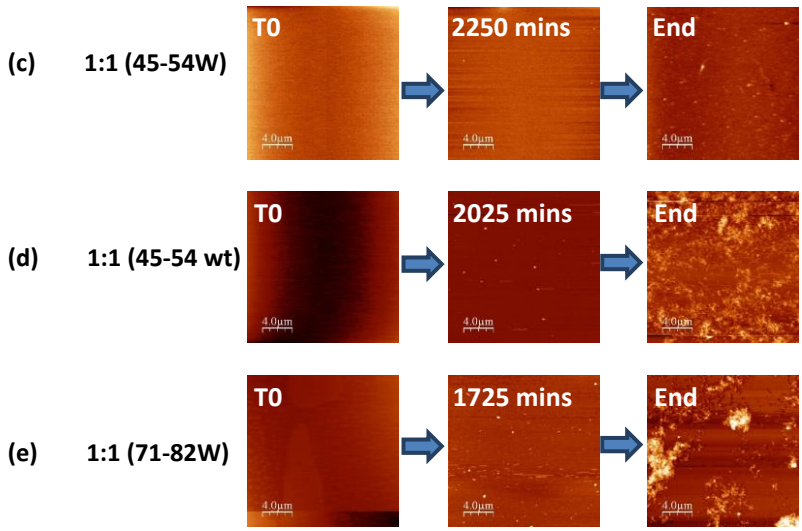

Figure 5.6: **AFM images *(a)*** showing the endpoint samples (4500 mins) for all molar ratios used in continuous ThT experiments. A considerable reduction in fibril load is observed at 1:1 stoichiometry. All other molar ratios showed no reduction of fibril load compared to 1:0. The 45-54W peptide (0:1) showed no aggregation in isolation. ***(b)*** Images showing gradual fibril growth along various time points (T0 to T16) for 1:0 as mentioned in ThT continuous growth experiments. ***(c)*** A considerable reduction of amyloid content along three time points (T0= 0 min, T1=2250 mins, and T2=4500 mins) was observed with 45-54W at 1:1 ratio. ***(d)*** Images showing no fibril reduction with wild type α-syn$_{45-54}$ fragment at 1:1 stoichiometry along three time points (T0=0 min, T1= 2025 mins, and T2=4500 mins). ***(e)*** No amyloid reduction observed with negative control peptide (71-82W; WTB) at 1:1 ratio along three time points (T0=0 min, T1= 1725 mins, and T2= 4500 mins).

5.3.4 MTT cell toxicity assay

To assess the effect of 45-54W peptide on cell viability as well as the ability of this peptide to prevent α-syn toxicity, MTT assays were performed using PC12 neuronal cells. Control experiments were performed to establish that neither ThT and/or buffer have any effect on the cell viability (Fig 5.7.a). Next, α-syn at a concentration of 5 μM with buffer and ThT leading to a large reduction in cell viability was performed. The experiments were next repeated using 45-54W at various sub- and super-stoichiometric ratios. The most efficient peptide ratio of 1:1 improved cell viability by 65-85 % relative to α-syn in isolation (Fig 5.7.b). Consistent with ThT and AFM data, the sub-stoichiometric ratios showed no effect of peptide on α-syn toxicity. A partial cell recovery in cell viability was observed at a molar ratio (α-syn: 45-54W) of 1:0.5, with the effect maximised at a ratio of 1:1. This effect was not improved at increasingly higher molar ratios was identified (Fig 5.7.b). In addition, MTT experiments using different time point samples taken during continuous growth assay demonstrated that the toxicity of α-syn increases progressively with time. The most toxic species was found within the stationary phase of fibril growth (Fig 5.7.c). MTT experiments using control peptides; WTB and 45-54wt demonstrate that the peptides have minimal effect upon α-syn toxicity, but are not toxic in isolation (Fig 5.7.d). Finally, increasing concentrations of 45-54W in isolation also demonstrated that the peptide is not toxic to the cells.

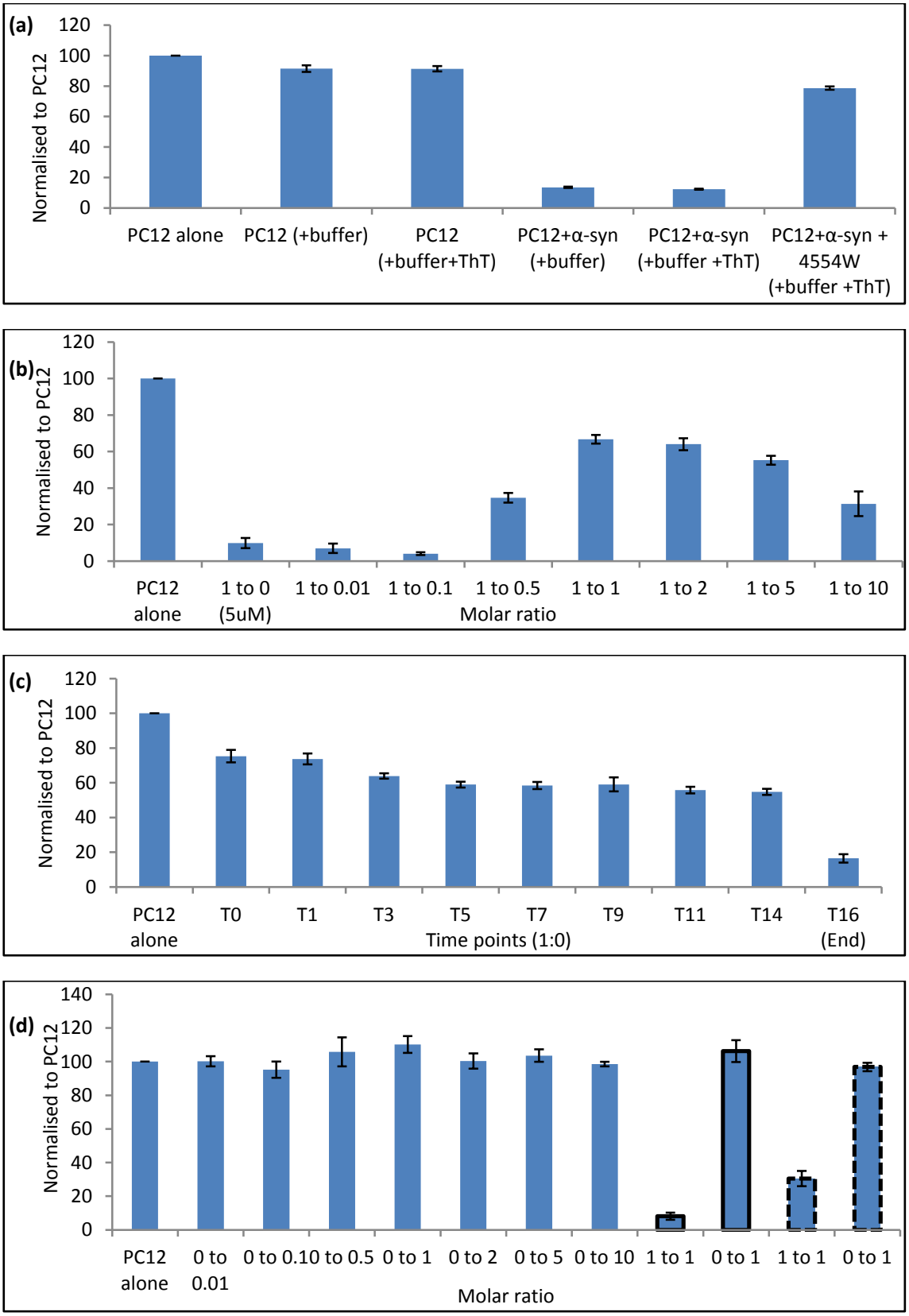

Figure 5.7: **MTT cell viability assays** showing inhibitory effect of 45-54W peptide on α-syn aggregation relative to PC12 cells alone. ***(a)*** Shown are i) PC12 cells alone, ii) PC12 cells in potassium phosphate buffer, iii) PC12 cells in buffer and ThT, iv) PC12 cells plus α-syn (5 µM) in buffer, v) PC12

cells with α-syn (5 μM) in buffer and ThT, and vi) PC12 cells with α-syn and 45-54W at 1:1 molar ratio. α-syn with 45-54W showed a cell revival of ~85 %. ***(b)*** Increasing stoichiometries of α-syn: 45-54W showed dose dependency. No effect of cell revival observed in 1:0.01 or 1:0.1. A partial cell recovery of ~28 % can be observed in 1:0.5 which increases at 1:1 to ~65 % and becomes progressively less effective at increasingly higher stoichiometries. All the samples were endpoint samples taken from continuous growth experiments after 4500 mins under sterile conditions. ***(c)*** Data demonstrates that cyto-toxicity increases as the sample ages and reaches its maximum within the stationary phase of continuous growth experiment. ***(d)*** Control MTT experiments: Increase in concentrations of 45-54W in isolation and as a result, an unaltered MTT signal demonstrates that the peptide is not toxic to PC12 cells on its own. MTT experiments using 45-54wt (bold surround) or 71-82W; WTB (hashed surround) peptides show that both had no effect on toxicity reduction at 1:1 and also not toxic in isolation.

5.3.5 SDS PAGE analysis

The endpoint samples from continuous growth experiments were used for the SDS PAGE analysis. In the Figure 5.8, two clear bands at ~40 kDa and ~60 kDa suggesting the presence of α-syn trimers (40/14.7 = 2.72) and tetramers (60/14.7 = 4.08) were found in 1:0, 1:0.01, 1:0.1 and 1:0.5 samples. At stoichiometries of 1:1 or higher these bands disappeared and were replaced by three lower molecular weight bands. The α-syn: 45-54W complex may have appeared as a band at ~15 kDa and the others two are below the resolution limit of the gel but could be representing monomeric α-syn (14.7 kDa) and inhibitor alone (1 kDa). The molecular weight was determined by graph analysis of log MW vs. relative migration distance. SDS analysis demonstrates that the peptide is able to interact with α-syn and lower oligomeric state possibly to the monomer. Since these species are observed on a denaturing gel, the precise oligomeric states observed must be treated with some caution.

However, the results provide further evidence that the 45-54W peptide is able to interact with α-syn and that the major effect is to reduce the size of oligomers that are populated within the sample.

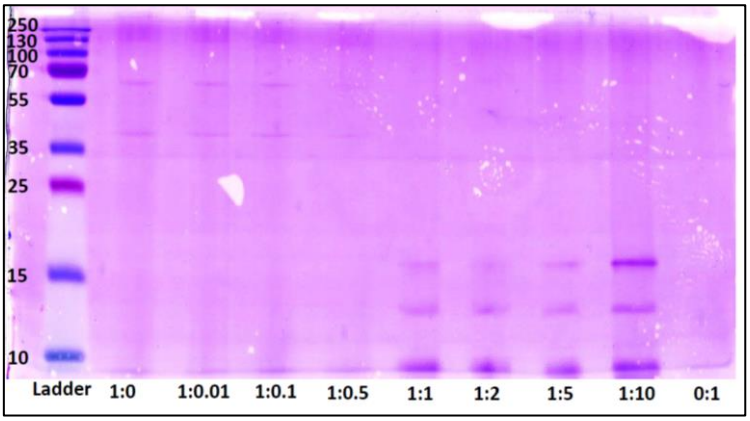

Figure 5.8: **SDS PAGE analysis** showing the endpoint samples of continuous growth experiments after 4500 mins. At 1:0, 1:0.01, 1:0.1, and 1: 0.5, two clear bands at ~40 kDa and ~60 kDa can be seen suggesting the presence of α-syn trimers and tetramers. At stoichiometries 1:1 or higher, these bands are absent and are replaced by three bands with lower molecular weight. The band at ~15 kDa may represent α-syn: 45-54W complex. The second and third bands are below the resolution limit of the gel but are likely to represent monomeric α-syn (14.7 kDa) and the inhibitor alone (1 kDa).

5.4 Discussion

To develop a peptide-based inhibitor the approach taken in this chapter was to create a peptide library scaffold on 45-54 region of wild type α-syn in which the known familial mutants in the early onset of PD are found. All the mutants were reported to increase the aggregation rate of α-syn, increased numbers of oligomers and its associated toxicity. All the residues in the 45-54 region were replaced by two, three or six residue options, which includes wild type options as well as the mutations, giving rise to a library containing 209,952 members. In the PCA selected winner, the wild type residues were re-selected (at 45K, 47G, 49V, 51G, 52V) in half of the ten positions while the remaining five resulted in new selections (E46D, V48I, H50N, A53K and T54A). As per the thermodynamic and NMR studies, these newly selected residues can be ordered according to their β-sheet propensity as D<A<K<N (Smith *et al*., 1994; Nowick *et al*., 1997). Among ten residues of the peptide, two are Gly which is expected to have low β-sheet propensity (Nowick *et al*., 1997; Smith *et al*., 1994; Minor *et al*., 1994). Asp residue in the 45-54W might have played a significant role in maintaining the stability of native α-syn. Studies suggest that the age-related chemical modifications of aspartyl residues to the form of succinimide or isoaspartyl methyl ester can initiate nucleation events in amyloidogenesis of many neurodegenerative disorders (Orpiszewski *et al*., 1999). However, the propensity for β-sheet depends on many factors such as the position of residues whether exposed or buried conformation, the folding properties such as the twist of a β-strand or association between two β- sheets (Fujiwara *et al*., 2012).

According to the results, in the continuous amyloid inhibition growth at stoichiometry 1:1, ThT signal is held at ~8 % relative to the inhibitor free (1:0) sample. At molar ratio 1:0.5,

fibrillisation is considerably delayed, taking approximately twice the time to reach the fluorescent intensity of the 1:0 sample. An expected dose dependency is observed in 1:0.1 or lower stoichiometries as the inhibitory property is lost and followed the sigmoidal curve similar to that of inhibitor free sample; 1:0. The peptide efficacy shown in continuous ThT growth experiments is supported by CD data which showed the retention of random coil signal at 1:1 sample. Moreover, the absence of fibrils is observed directly by AFM imaging. The MTT data showed that the toxicity associated with α-syn aggregation is almost reduced and showed a cell survival of ~65-85 % in the presence of 45-54W peptide. Finally, the data is verified by SDS-PAGE analysis that shows a shift from higher to lower molecular weight species, in the presence of 45-54W at 1:1 stoichiometry or higher.

In conclusion, I have combined semi-rational design with intracellular PCA to validate this as an effective approach for the development of α-syn antagonists. Based on 45-54 region, I have designed a library and have created a potent peptide inhibitor against α-syn aggregation. In the future it may be possible to derive more potent inhibitors based on this region or this point to a new target for designing new inhibitors which can be modified into drugs to slow or even prevent the onset of PD.

Chapter 6: General Discussion and Conclusion

This thesis focuses on semi-rational design combined with intracellular PCA to screen for peptide antagonists of wild type and mutant α-syn aggregation. Specifically, I sought to identify peptides capable of preventing or reversing the formation of toxic oligomers. Structural studies on α-syn have revealed a crucial region which is responsible for the aggregation of α-syn (Waxman *et al*., 2010; Madine *et al*., 2008; Giasson *et al*., 2000; El-Agnaf *et al*., 1998). Therefore peptides were screened using library templates based on amino acids 71-82 initially and later on the 45-54 region of α-syn in which many key mutations associated with early onset PD are found. In both cases I targeted the peptide-based libraries at the wild type protein or again by using mutated versions associated with early onset PD. In our work, PCA was preferred over other library screening strategies for several reasons. The most prominent being that, as it is carried out *in vivo*; aggregation prone, insoluble, bacterial protease sensitive, unstable, and weak binders will be removed at the screening level itself. Thus, the first phase of this thesis (Chapter 3) successfully employed PCA to screen three peptides against full length wild type α-syn. The ability of the PCA peptides to prevent or revert the aggregation were analysed using ThT, CD, and AFM assays while the ability to reduce α-syn toxicity was verified by MTT assay using Rat phaeochromocytoma (PC12) neuronal like cells. According to the data, the peptide WTC functioned moderately by delaying the formation of α-syn. As discussed in Chapter 3, these effects of WTC are speculated to be of different amino acid substitutions in the peptide compared to the target sequence. For instance, V77P and K80G; the two substitutions of residues in the peptide sequence might have reduced the fibril propensity of the parent protein (Nowick *et al*., 1997; Smith *et al*., 1994; Waxman *et al*., 2010). Reduced toxicity was

observed during MTT assay effectively in the lower stoichiometries (1:1 and 1:2) in all the three peptides as it showed 30-55 % of cell survival. The three peptides were confirmed to have minimal effect during the reversal assay. However, from the initial phase; the main objectives achieved were: PCA was successfully used to screen three peptides, one peptide showed a positive result in delaying the aggregation, and finally the peptides showed moderate signs of reducing α-syn toxicity during MTT assay. Following this work, Chapter 4 dealt with the characterisation of the PCA peptides against aggregation of α-syn mutants. Peptides were screened against full length A30P, E46K, A53T and H50Q. The A53T peptide only showed a moderate level of antagonistic property against A53T aggregation, while minimal efficacy was exhibited by A30P, E46K and H50Q peptides. MTT assay also assured a 50 % cell survival only with A53T peptide at different stoichiometries (1:1, 1:2, and 1:5). A moderate level of efficacy was identified in the reversal approach in breaking down the mature fibrils among A30P and E46K but no reversal was seen in A53T or H50Q. The peptides did not satisfactorily prevent the aggregation process as anticipated at the PCA level; we concluded that the 71-82 region is inappropriate for the development of an antagonistic peptide. Later Chapter 5 solved this issue by using a new library based on a different target α-syn$_{45-54}$. This sequence was considered as it accommodates many of the known point mutations associated with early onset PD. It was based on the fact that this region plays an important role in modulating the structure of α-syn and thereby influencing the rate of amyloid formation. At the PCA level all the residues in the 45-54 region were replaced by different options that included wild type and mutations, to create a library of almost 210,000 members. The derived peptide KDGIVNGVKA (45-54W) and its effect on aggregation of full length α-syn was characterised by continuous ThT growth experiments, CD, AFM, MTT and SDS-PAGE assays. The peptide was confirmed to have efficient inhibitory

property at 1:1 stoichiometry. In the presence of peptide, the ThT data showed 92 % reduction in the amyloid growth relative to the inhibitor free (1:0) sample, which was later confirmed by the retention of random coil signal shown by CD and the absence of fibrils seen in AFM images, using the same sample as that in the ThT experiments. The molar ratio 1:0.5 showed a significant delay in the aggregation process and an expected loss of inhibitory effect in a dose dependency manner was observed in the lower stoichiometries. The MTT data showed a cell survival of ~65-85 % in the presence of peptide and found the peptide to be non-toxic in isolation. Moreover, SDS-PAGE analysis, again taken from the same sample, showed a shift from higher to lower molecular weight species in the presence of peptide at 1:1 stoichiometry or higher. As described in Chapter 5, the inhibitory effect of 45-54W can be attributed to the nature of residues selected and their β-sheet propensities. I have therefore demonstrated that the PCA derived peptide is effective in reducing the α-syn aggregation toxicity *in vitro* and *in vivo*.

In summary, several α-syn targeted peptides based on two different targets within α-syn were selected using PCA. At the PCA level, no assumptions were made regarding the mechanism of action for the selected binders or oligomeric state of α-syn that becomes populated. The characterisation assays showed that, some of those selected peptides had the effect of delaying or even preventing the aggregation process, with others providing more subtle effects in reversing the fully formed amyloid fibrils, while some peptides enhancing the fibrillisation process. In the case of mutants, I speculate that the conflicting information regarding α-syn toxicity in PCA and MTT studies could be attributable to different factors such as interaction with other proteins, cofactors, protease, and structural rearrangements *in vivo*. Further investigation needed as I have not directly quantified the

affinity and specificity of the peptide binding. Structural studies such as solid state NMR and analysing the effectiveness in different model systems (for example, fruit flies or assays using primary neurons) may demonstrate the specificity, structural rearrangement and efficacy further. It would also provide insights into the binding sites of the target protein and affinity of the peptides towards it. The peptide-protein interaction also depends on the residues, whether they are conserved in the binding sites or exposed and later decides the structural stability on folding (Ma *et al*., 2003). In the future, when attempting to translate these peptides as drugs; the major concerns would be bioavailability issues, pharmacokinetics, protease degradation susceptibility, effect of oxidants, immune responses, poor metabolic stability, limited permeability across the blood-brain barrier or cell membranes, rapid clearance and high production costs. Despite the limitations, these peptide-based drugs have many advantages such as high potency, high selectivity, broad range of targets, potentially less toxicity, low tissue accumulation and chemical/biological diversity (Craik *et al*., 2013). Most of the research to develop α-syn targeted PD drugs focuses on preventing the protein from aggregating in the first place, to break up aggregated species, or to halt the toxic effects of the aggregates. The peptides derived mostly interfere with the β-sheet formation by preventing propagation of hydrogen bonds along the long axes of β-sheets. Stabilising the native structure of protein is another strategy that can be used in developing PD drugs as recent studies suggested that, α-syn forms a stable helically folded tetrameric structure able to resist aggregation (Wang *et al*., 2011; Bartels *et al*., 2011). Due to ambiguity in the native structure and normal biological function of α-syn, wide spread research is needed for developing new therapeutic interventions against PD. As the formation of amyloid fibrils characterizes the PD pathology, another approach is anti-amyloid therapies based around the concept of inhibiting protein-protein

interactions. Though, a group of researchers from the Stanford University showed that amyloid fibrils composed of hexapeptides act as active biological agent that can lessen the neuroinflammation in multiple sclerosis and autoimmune encephalomyelitis (Kurnellas *et al*., 2013 and 2014). These studies begin to suggest the new idea that full length, amyloid forming proteins produced by the body may have in fact protective behaviour rather than destructive. In conclusion, I have demonstrated that the PCA strategy can be used as a basic, generalised method for deriving peptide inhibitors against α-syn aggregation. In the future, it may be possible to derive more potent inhibitors of the mutagenic versions of α-syn using scaffold of 45-54 region. As per the encouraging results in Chapter 5, it may be possible to derive more α-syn antagonists or use this new target; 45-54 region for designing more effective new inhibitors that can be modified into drugs to slow or even prevent the onset of PD.

References

Abe, K., Kobayashi, N., Sode, K., and Ikebukuro, K. (2007) Peptide ligand screening of α-synuclein aggregation modulators by *in silico* panning. *BMC Bioinformatics* 8 (451), 1-7.

Acerra, N., Kad, N.M., Griffith, D.A., Ott, S., Crowther, D.C., and Mason, J.M. (2014) Retro-inversal of Intracellular selected β-amyloid-interacting peptides: Implications for a novel Alzheimer's disease treatment. *Biochemistry* 53, 2101-2111.

Acerra, N., Kad, N.M., and Mason, J.M. (2013) Combining intracellular selection with protein-fragment complementation to derive Aβ interacting peptides. *Protein Engineering, Design & Selection* 26 (7), 463-470.

Ahmad, B., and Lapidus, L.J. (2012) Curcumin prevents aggregation in α-synuclein by increasing reconfiguration rate. *The Journal of Biological Chemistry* 287, 9193-9199.

Ahsan, N., Mishra, S., Jain, M.K., Surolia, A., and Gupta, S. (2015) Curcumin Pyrazole and its derivative (N-(3-Nitrophenylpyrazole) Curcumin inhibit aggregation, disrupt fibrils and modulate toxicity of wild type and mutant α-synuclein. *Scientific Reports* 5 (9862), 1-16.

Am, O.B., Amit, T., and Youdim, M.B.H. (2004) Contrasting neuroprotective and neurotoxic actions of respective metabolites of anti-Parkinson drugs rasagiline and selegiline. *Neuroscience Letters* 355, 169-172.

Ariesandi, W., Chang, C., Chen, T., and Chen, Y. (2013) Temperature-dependent structural changes of Parkinson's alpha-synuclein reveal the role of pre-existing oligomers in alpha-synuclein fibrillization. *PLoS ONE* 8(1), 1-10.

Baba, M., Nakejo, S., Tu, P.H., Tomita, T., Nakaya, K., Lee, V.M., Trojanowski, J.Q., and Iwatsubo, T. (1998) Aggregation of α-synuclein in Lewy Bodies of Sporadic Parkinson's disease and Dementia with Lewy Bodies. *American Journal of Pathology* 152, 879-884.

Bartels, T., Choi, J.G., and Selkoe, D.J. (2011) α-synuclein occurs physiologically as a helically folded tetramer that resists aggregation. *Nature* 477, 107-111.

Bartl, J., Muller, T., and Grunblatt, E. (2014) Chronic monoamine oxidase-B inhibitor treatment blocks monoamine oxidase-A enzyme activity. *Journal of Neural Transmission*. 121, 379-383.

Bedard, L., Lefevre, T., Michaud, E.M., and Auger, M. (2014) Besides fibrillization: putative role of the peptide fragment 71−82 on the structural and assembly behavior of α-synuclein. *Biochemistry* 53, 6463-6472.

Berg, D., Niwar, M., Maass, S., Zimprich, A., Moller, J.C., Wuellner, U., Hubsch, T.S., Klein, C., Tan, E.K., Schols, L., Marsh, L., Dawson, T.M., Janetzky, B., Muler, T., Woitalla, D., Kostic, V., Pramstaller, P.P., Oertel, W.H., Bauer, P., Krueger, R., Gasser, T., and Riess, O. (2005) Alpha-Synuclein and Parkinson's Disease: Implications from the screening of more than 1,900 patients. *Movement Disorders* 20 (9), 1191-1194.

Bertoncini, C.W., Jung, Y.S., Fernandez, C.O., Hoyer, W., Griesinger, C., Jovin, T.M., and Zweckstetter, M. (2005) Release of long-range tertiary interactions potentiates aggregation of natively unstructured α-synuclein. *PNAS* 102, 1430-1435.

Betts, M.J., and Russell, R.B. (2003) Amino acid properties and consequences of substitutions. *Bioinformatics for Geneticists*. 289-316.

Bodles, A.M., El-Agnafb, O.M.A., Greer, B., Gutheriea, D.J.S., and Irvine, G.B. (2004) Inhibition of fibril formation and toxicity of a fragment of α-synuclein by an N-methylated peptide analogue. *Neuroscience Letters* 359, 89–93.

Bodles, A.M., Gutheriea, D.J.S., Greer, B., and Irvine, G.B. (2001) Identification of the region of non-Aβ component (NAC) of Alzheimer's disease amyloid responsible for its aggregation and toxicity. *The Journal of Neurochemistry* 78, 384-395.

Bonifati, V. (2014) Genetics of Parkinson's disease. *Parkinsonism and Related Disorders: Elsevier*, S23-S28.

Breydo, L., Morgan, D., and Uversky, V.N. (2015) Pseudocatalytic anti-aggregation activity of antibodies: Immunoglobulins can influence α-synuclein aggregation at substoichiometric concentrations. *Molecular Neurobiology*, 1-10.

Bussell, R., and Eliezer, D. (2001) Residual structure and dynamics in Parkinson's Disease-associated mutants of α-synuclein. *The Journal of Biological Chemistry* 276, 45996-46003.

Butt, T.R., Edavettal, S.C., Hall, J.P., and Mattern, M.R. (2005) Sumo fusion technology for difficult to express proteins. *Protein expression & purification, Elsevier* 43, 1-9.

Caruana, M., Hogen, T., Levin, J., Hillmer, A., Giese, A., and Vassallo, N. (2011) Inhibition and disaggregation of α-synuclein oligomers by natural polyphenolic compounds. *FEBS Letters* 585, 1113-1120.

Chan, H.F., Kukkle, P.L., Merello, M., Lim, S.Y., Poon, Y.Y., and Moro, E. (2013) Amantadine improves gait in PD patients with STN stimulation. *Parkinsonism and Related Disorders* 19, 316-319.

Chen, M., Margittai, M., Chen, J., and Langen, R. (2007) Investigation of α-synuclein fibril structure by Site-directed Spin Labeling. *The Journal of Biological Chemistry* 282, 24970-24979.

Chen, S., Gao, S., Cheng, D., and Huang, J. (2014) The characterization and comparison of amyloidogenic segments and non-amyloidogenic segments shed light on amyloid formation. *Biochemical and Biophysical Research Communications* 447, 255-262.

Chen, X., Wales, P., Quinti, L., Zuo, F., Moniot, S., Herisson, F., Rauf, N.A., Wang, H., Silverman, R.B., Ayata, C., Maxwell, M., Steegborn, C., Schwarzschild, M.A., Outeiro, T.F., and Kazantsev, A.G. (2015) The Sirtuin-2 Inhibitor AK7 Is Neuroprotective in Models of Parkinson's Disease but Not Amyotrophic Lateral Sclerosis and Cerebral Ischemia. *PLoS ONE*, 1-15.

Cheruvara, H., Allen-Baume, V.L., Kad, N.M., and Mason, J.M. (2015) Intracellular screening of a peptide library to derive a potent inhibitor of α-synuclein aggregation. *The Journal of Biochemistry* 290 (12), 7426-7435.

Chiti, F., and Dobson, C.M. (2006) Protein misfolding, functional amyloid, and human disease. *Annu.Rev.Biochem*. 75, 333-366.

Choi, W., Zibaee, S., Jakes, R., Serpell, L.C., Devletov, B., Crowther, R.A., and Goedert, M. (2004) Mutation E46K increases phospholipid binding and assembly into filaments of human α-synuclein. *FEBS Letters* 576, 363-368.

Chou, P.Y., and Fasman, G.D. (1978) Empirical predictions of protein conformation. *Ann. Rev. Biochem*. 47, 251-276.

Conway, K., Harper, J.D., and Lansbury, P.T. (2000) Fibrils formed *in vitro* from α-synuclein and two mutant forms linked to Parkinson's Disease are typical Amyloid. *Biochemistry* 39, 2552-2563.

Cresswell, S.A., Guell, C.V., Encarnacion, M., Sherman, H., Yu, I., Shah, B., Weir, D., Thompson, C., Szu-Tu, C., Trinh, J., Aasly, J.O., Rajput, A., Rajput, A.H., Stoessl, J., and Farrer, M.J. (2013) Alpha-synuclein p.H50Q, a novel pathogenic mutation for Parkinson's disease. *Movement Disorders* 28(6), 811-813.

Damier, P., Hirsch, E.C., Agid, Y., and Graybiel, A.M. (1999) The substantia nigra of the human brain I. Nigrosomes and the nigral matrix, a compartmental organization based on calbindin D_{28K} immunohistochemistry. *Brain* 122, 1421-1436.

Dettmer, U., Newman, A.J., Luth,E.S., Bartels, T., and Selkoe, D. (2013) *In vivo* Cross-linking Reveals Principally Oligomeric Forms of α-synuclein and β-synuclein in Neurons and Non-neural Cells. *The Journal of Biological Chemistry* 288 (9), 6371-6385.

Dettmer, U., Newman, A.J., Soldner, F., Luth, E.S., Kim, N.C., Saucken, V.E., Sanderson, J.B., Jaenisch, R., Bartels, T., and Selkoe, D. (2015) Parkinson-causing α-synuclein missense mutations shift native tetramers to monomers as a mechanism for disease initiation. *Nature*, 1-15.

Du, H.N., Tang, L., Luo, X.Y., Li, H.T., Hu, J., Zhou, J.W., and Hu, H.J. (2003) A Peptide Motif consisting of Glycine, Alanine, and Valine is required for the fibrillization and cytotoxicity of Human α-synuclein. *Biochemistry* 42, 8870-8878.

Eanes, E.D., and Glenner, G.G., (1968) X-ray diffraction studies on amyloid filaments. *The Journal of Histochemistry and Cytochemistry* 16, 673-677.

El-Agnaf, O.M.A., Bodles, A.M., Guthrie, D.J.S., Harriott, P., and Irvine, B.G. (1998) The N-terminal region of non-A β component of Alzheimer's Disease amyloid is responsible for its tendency to assume β-sheet and aggregate to form fibrils. *European Journal of Biochemistry* 258, 157-163.

El-Agnaf, O.M.A., Paleologou, K.E., Greer, B., Abrogrein, A.M., King, J.E., Salem, S.A., Fullwood, N.J., Benson, F.E., Hewitt, R., Ford, K.J., Martin, F.L., Harriott, P., Cookson, M.R., and Allsop, D. (2004) A strategy for designing inhibitors of α-synuclein aggregation and toxicity as a novel treatment for Parkinson's disease and related disorders. *The FASEB Journal* 10, 1-34.

Eliezer, D., Kutluay, E., Bussell, R., and Browne, G. (2001) Conformational properties of α-synuclein in its free and lipid-associated states. *Journal of Molecular Biology* 307, 1061-1073.

Emadi, S., Barkhordarian, H., Wang, M.S., Schulz, P., and Sierks, M.R. (2007) Isolation of a Human Single Chain Antibody Fragment against oligomeric α-synuclein that inhibits aggregation and prevents α-synuclein-induced toxicity. *Journal of Molecular Biology* 368, 1132-1144.

Emadi, S., Kasturirangan, S., Wang, M.S., Schulz, P., and Sierks, M.R. (2009) Detecting morphologically distinct Oligomeric forms of α-synuclein. *The Journal of Biological Chemistry* 284, 11048-11058.

Emadi, S., Liu, R., Yuan, B., Schulz, P., McAllister, C., Lyubchenko, Y., Messer, A., and Sierks, M.R. (2004) Inhibiting aggregation of α-synuclein with Human Single Chain Antibody Fragments. *Biochemistry* 43, 2871-2878.

Emre, M., Aarsland, D., and Albanese, A. (2004) Rivastigmine for Dementia Associated with Parkinson's Disease. *The New England Journal of Medicine* 351, 2509-2518.

Fandrich, M., Meinhardt, J., and Grigorieff, N. (2009) Structural polymorphism of Alzheimer Aβ and other amyloid fibrils. *Prion* 3(2), 89-93.

Fernandez, C.O., Hoyer, W., Zweckstetter, M., Jares-Erijman, E.A., Subramaniam, V., Griesinger, C., and Jovin, T.M., (2004) NMR of α-synuclein–polyamine complexes elucidates the mechanism and kinetics of induced aggregation. *The EMBO Journal* 23, 2039-2046.

Fortin, D.L., Nemani, V.M., Voglmaier, S.M., Anthony, M.D., Ryan, T.A., and Edwards, R.H. (2005) Neural activity controls the synaptic accumulation of α-synuclein. *The Journal of Neuroscience* 25(47), 10913–10921.

Fujiwara, K., Toda, H., and Ikeguchi, M. (2012) Dependence of α-helical and β-sheet amino acid propensities on the overall protein fold type. *BMC Structural Biology* 12, 1-15.

Gallea, J.I., and Celej, M.S. (2014) Structural insights into amyloid oligomers of the Parkinson disease- related protein α-synuclein. *The Journal of Biological Chemistry* 289 (39), 26733-26742.

George, J.M. (2001) The synucleins. *Genome Biology* 3 (1), 1-6.

Ghosh, D., Mondal, M., Mohite, G.M., Singh, P.K., Ranjan, P., Anoop, A., Ghosh, S., Jha, N.N., Kumar, A., and Maji, S.K. (2013) The Parkinson's disease associated H50Q mutation accelerates α-synuclein aggregation *in vitro*. *Biochemistry* 52, 6925-6927.

Giasson, B.I., Murray, I.V.J., Trojanowski, J.Q., and Lee, V.M.Y. (2000) A hydrophobic stretch of 12 aminoacid residues in the middle of α-synuclein is essential for filament assembly. *The Journal of Biological Chemistry* 276, 2380-2386.

Gilead, S., and Gazit, E. (2004) Inhibition of amyloid fibril formation by peptide analogues modified with α-aminoisobutyric acid. *Angew.Chem.Int.Ed*. 43, 4041-4044.

Giovanni, S.D., Eleuteri, S., Paleologou, K.E., Yin, G., Zweckstetter, M., Carrupt, P.A., and Lashuel, H.A. (2010) Entacapone and Tolcapone, two Catechol-*O*-Methyltransferase inhibitors, block fibril formation of α-synuclein & β-amyloid and protect against Amyloid-induced toxicity. *The Journal of Biological Chemistry* 285, 14941-14954.

Glaser, C.B., Yamin, G., Uversky, V.N., and Fink, A.L. (2005) Methionine oxidation, α-synuclein and Parkinson's disease. *Biochimica et Biophysica Acta* 1703, 157-169.

Greenbaum, E.A., Graves, C.L., Eberz, A.J.M., Lupoli, M.A., Lynch, D.R., Englander, S.W., Axelsen, P.H., and Giasson, B.I. (2005) The E46K mutation in α-synuclein increases amyloid fibril formation. *The Journal of Biological Chemistry* 280, 7800-7807.

Hald, A., and Lotharius, J. (2005) Oxidative stress and inflammation in Parkinson's disease: Is there a causal link?. *Experimental Neurology* 193, 279-290.

Halfmann, R., Alberti, S., Krishnan, R., Lyle, N., O'Donnell, C.W., King, O.D., Berger, B., Pappu, R.V., and Lindquist, S. (2011) Opposing effects of Glutamine and Asparagine govern Prion formation by intrinsically disordered proteins. *Molecular Cell* 43, 72-78.

Harada, R., Kobayashi, N., Kim, J., Nakamura, C., Han, S.W., Ikebukuro, K., and Sode, K. (2009) The effect of amino acid substitution in the imperfect repeat sequences of α-synuclein on fibrillation. *Biochimica et Biophysica Acta* 1792, 998-1003.

Hard, T., and Lendel, C. (2012) Inhibition of amyloid formation. *Journal of Molecular Biology* 421, 441-465.

Hardy, J., Cai, H., Cookson, M.R., Hardy, K.G., and Singleton, A. (2006) Genetics of Parkinson's Disease and Parkinsonism. *Annals of Neurology* 60, 389-398.

Hashimoto, M., Rockenstein, E., Mante, M., Mallory, M., and Masliah, E. (2001) β-synuclein inhibits α-synuclein aggregation: A possible role as an anti- Parkinsonian factor. *Neuron* 32, 213-223.

Huang, C., Cheng, H., Hao, S., Zhou, H., Zhang, X., Gao, J., Sun, Q.H., Hu, H., and Wang, C. (2006) Heat Shock Protein 70 inhibits α-synuclein fibril formation via interactions with diverse intermediates. *Journal of Molecular Biology* 364, 323–336.

Huleatt, P.B., Khoo, M.L., Chua, Y.Y., Tan, T.W., Liew, R.S., Balogh, B., Deme, R., Goloncser, F., Magyar, K., Sheela, D.P., Ho, H.K., Sperlagh, B., Matyus, P., and Chai, C.L.L. (2015) Novel Arylalkenylpropargylamines as neuroprotective, potent, and selective Monoamine Oxidase B inhibitors for the treatment of Parkinson's Disease. *Journal of Medicinal Chemistry* 58, 1400-1419.

Iannuzzi, C., Irace, G., and Sirangelo, I. (2015) The effect of Glycosaminoglycans (GAGs) on Amyloid aggregation and toxicity. *Molecules* 20, 2510-2528.

Jo, E., McLaurin, J., Yip, C.M., Hyslop, P.G., and Fraser, P.E. (2000) α-synuclein membrane interactions and lipid specificity. *The Journal of Biological Chemistry* 44, 34328-34334.

Kad, M.N., Myers, S.L., Smith, D.P., Smith, D.A., Radford, S.E., and Thomson, N.H. (2003) Hierarchical assembly of β_2-microglobulin amyloid *in vitro* revealed by atomic force microscopy. *Journal of Molecular Biology* 330, 785-797.

Kad, M.N., Thomson, N.H., Smith, D.P., Smith, D.A., and Radford, S.E. (2001) β_2-microglobulin and its deamidated variant N17D form amyloid fibrils with a range of morphologies *in vitro*. *Journal of Molecular Biology* 313, 559-571.

Kalia, L.V., Kalia, S.K., McLean, P.J., Lozano, A.M., and Lang, A.E. (2013) α-Synuclein Oligomers and Clinical Implications for Parkinson Disease. *Ann Neurol.* 73, 155-169.

Kanazawa, T., Uchihara, T., Takahashi, A., Nakamura, A., Orimo, S., and Mizusawa, H. (2008) Three-layered structure shared between Lewy Bodies and Lewy Neurites—Three-Dimensional reconstruction of Triple-Labeled sections. *Brain Pathology* 18, 415-422.

Karyo, R.S., Pinter, M.F., Matia, N.E., Marom, A.F., Shalev, D.E., Segal, D., and Gazit, E. (2010) Inhibiting α-synuclein Oligomerization by Stable Cell-penetrating β-synuclein fragments recovers phenotype of Parkinson's Disease model flies. *PLoS ONE* 5, 1-13.

Kessler, J.C., Rochet, J.C., and Lansbury, P.T. (2003) The N-Terminal repeat domain of α-synuclein inhibits β-sheet and amyloid fibril formation. *Biochemistry* 42, 672-678.

Khan, N.L., Jain, S., Lynch, J.M., Pavese, N., Abou, P., Holton, J.L., Healy, D.G., Gilks, W.P., Sweeney, M.G., Ganguly, M., Gibbons, V., Gandhi, S., Vaughan, J., Eunson, L.H., Katzenschlager, R., Gayton, J., Lennox, G., Revesz, T., Nicholl, D., Bhatia, K.P., Quinn, N., Brooks, D., Lees, A.J., Davis, M.B., Piccini, P., Singleton, A.B., and Wood, N.W. (2005) Mutations in the gene LRRK2 encoding dardarin (PARK8) cause familial Parkinson's disease: clinical, pathological, olfactory and functional imaging and genetic data. *Brain* 128, 2786-2796.

Khurana, R., Zanetti, C.I., Pope, M., Li, J., Nielson, L., Alvarado, M.R., Regan, L., Fink, A.L., and Carter, S. (2003) A general model for Amyloid Fibril Assembly based on morphological studies using Atomic Force Microscopy. *Biophysical Journal* 85, 1135-1144.

Ki, C.S., Stavrou, E.F., Davanos, N., Lee, W.Y., Chung, E.J., Kim, J.Y., and Athanassiadou, A. (2007) The Ala53Thr mutation in the α-synuclein gene in a Korean family with Parkinson disease. *Clin.Genet.* 71, 471-473.

Kiely, A.P., Asi, Y.T., Kara, E., Limousin, P., Ling, H., Lewis, P., Proukakis, C., Quinn, N., Lees, A.J., Hardy, J., Revesz, T., Houlden, H., and Holten, J.L. (2013) α-Synucleinopathy associated with G51D SNCA mutation: a link between Parkinson's disease and multiple system atrophy?. *Acta Neuropathol.* 125, 753-769.

Knowles, T.P.J., Vendruscolo, M., and Dobson, C.M. (2014) The amyloid state and its association with protein misfolding diseases. *Nature,* 384-396.

Kosten, J., Binolfi, A., Stuiver, M., Verzini, S., Theillet, F.X., Bekei, B., Rossum, M., and Selenko, P. (2014) Efficient modification of α-synuclein Serine 129 by protein kinase CK1 requires phosphorylation of Tyrosine 125 as a priming event. *ACS Chemical Neuroscience* 5, 1203-1208.

Kurnellas, M.P., Adams, C.M., Sobel, R.A., Steinman, L., and Rothbard, J.B. (2013) Amyloid fibrils composed of hexameric peptides attenuate neuroinflammation. *Science Translational Medicine* 179, 1-20.

Kurnellas, M.P., Schartner, J.M., Fathman, C.G., Jagger, A., Steinman, L., and Rothbard, J.B. (2014) Mechanisms of action of therapeutic amyloidogenic hexapeptides in amelioration of inflammatory brain disease. *The Journal of Experimental Medicine* 211, 1847-1856.

Kuroda, Y., Maeda, Y., Hanaoka, H., Miyamoto, K., Nakagawa, T.(2004) Oligopeptide-mediated acceleration of amyloid fibril formation of amyloid β (Aβ) and *α*-synuclein fragment peptide (NAC). *Journal of Peptide Science* 10, 8-17.

Lamberto, G.R., Monserrat, V.T., Bertoncini, C.W., Salvatella, X., Zweckstetter, M., Griesingar, C., and Fernandez, C.O. (2011) Towards the discovery of effective polycyclic inhibitors of α-synuclein amyloid assembly. *The Journal of Biological Chemistry* 286, 1-16.

Lee, C.D., Sun, H.C., Hu, S.M., Chiu, C.F., Homhuan, A., Liang, S.M., Leng, C.H., and Wang, T.F. (2008) An improved SUMO fusion protein system for effective production of native proteins. *Protein Science* 17, 1241-1248.

Lee, H.J., Choi, C., and Lee, S.J. (2002) Membrane bound α-synuclein has a high aggregation propensity and the ability to seed the aggregation of the cytosolic form. *The Journal of Biological Chemistry* 277, 671-678.

Lesage, S., Anheim, M., Letournel, F., Bousset, L., Honore, A., Rozas, N., Pieri, L., Madiona, K., Durr, A., Melki, R., Verny, C., and Brice, A. (2013) G51D α-synuclein mutation causes a novel Parkinsonian-Pyramidal syndrome. *Ann Neurology* 73, 459-471.

Lesage, S., and Brice, A. (2009) Parkinson's disease: from monogenic forms to genetic susceptibility factors. *Human Molecular Genetics* 18, 48–59.

Li, J., Englund, E., Holton, J.L., Soulet, D., Hagell, P., Lees, A.J., Lashley, T., Quinn, N.P., Rehncrona, S., Bjorklund, A., Widner, H., Revesz, T., Lindvall, O., and Brundin, P. (2008) Lewy bodies in grafted neurons in subjects with Parkinson's disease suggest host-to-graft disease propagation. *Nature medicine* 14 (5), 501-503.

Li, J., Uversky, V.N., and Fink, A.L. (2001) Effect of Familial Parkinson's Disease Point Mutations A30P and A53T on the structural properties, aggregation, and fibrillation of Human α-Synuclein. *Biochemistry* 40, 11604-11613.

Li, J.Y., Englund, E., Holton, J., Soulet, D., Hagell, P., Lees, A.J., Lashley, T., Quinn, N.O., Rehncrona, S., Bjorklund, A., Widner, H., Revesz, T., Lindvall, O., and Brundin, P. (2008) Lewy bodies in grafted neurons in subjects with Parkinson's disease suggest host-to-graft disease propagation. *Nature Medicine* 14, 501-503.

Liua, G., Zhangb, C., Yina, J., Ji, X., Chenga, F., Li, Y., Yang, H., Uedaa, K., Chana, P., and Yu, S. (2009) α-synuclein is differentially expressed in mitochondria from different rat brain

regions and dose-dependently down-regulates complex I activity. *Neuroscience Letters* 454 , 187–192.

Lucking, C.B., Durr, A., Bonifati, V., Vaughan, J., Michele, G.D., Gasser, T., Harhangi, B.S., Meco, G., Denefle, P., Wood, N.W., Agid, Y., and Brice, A. (2000) Association between early-onset Parkinson's disease and mutations in the Parkin gene. *The New England Journal of Medicine* 342, 1560-1567.

Lundvig, D., Lindersson, E., and Jensen, P.H. (2005) Pathogenic effects of α-synuclein. *Molecular Brain Research* 134, 3-17.

Ma, B., Elkayam, T., Wolfson, H., and Nussinov, R. (2003) Protein-protein interactions: Structurally conserved residues distinguish between binding sites and exposed protein surfaces. *PNAS* 100 (10), 5772-5777.

Madine, J., Doig, A.J., and Middleton, D.A. (2008) Design of an N-Methylated peptide inhibitor of α-synuclein aggregation guided by solid state NMR. *Journal of American Chemical Society* 130, 7873-7881.

Malakhov, M.P., Mattern, M.R., Malakhova, O.A., Drinker, M., Weeks, S.D., and Butt, T.R. (2004) Sumo fusions and SUMO specific protease for efficient expression and purification of proteins. *Journal of structural and functional genomics* 5, 75-86.

Mar, C.D., Greenbaum, E.A., Mayne, L., Englander, S.W., and Woods, V.L. (2005) Structure and properties of α-synuclein and other amyloids determined at the amino acid level. *PNAS* 102 (43), 15477-15482.

Marblestone, J.G., Edavettal, S.C., Lim, Y., Lim, P., Zuo, X., and Butt, T.R. (2006) Comparison of SUMO fusion technology with traditional gene fusion systems: Enhanced expression and solubility with SUMO. *Protein Science* 15, 182-189.

Mason, J.M., Schmitz, M.A., Muller, K.M., and Arndt, K.M. (2006) Semirational design of Jun-Fos coiled coils with increased affinity: Universal implications for leucine zipper prediction and design. *PNAS* 103, 8989-8994.

Masso, J.F.M., Martinez, J.R., Ruiz, C.P., Gorostidi, A., Bergareche, A., Munain, A.L., Alzualde, A., and Tur, J.P. (2015) Parkin and LRRK2/Dardarin mutations in early onset Parkinson's Disease in the Basque Country (Spain). *Journal of Behavioural and Brain Science* 5, 101-108.

Masuda, M., Suzuki, N., Taniguchi, S., Oikawa, T., Nonaka, T., Iwatsubo, T., Hisanaga, S., and Goedert, M. (2006) Small Molecule inhibitors of α-synuclein filament assembly. *Biochemistry* 45*,* 6085-6094.

Mata, I.F., Wedemeyer, W.J., Farrer, M.J., Taylor, J.P., and Gallo, K.A. (2006) LRRK2 in Parkinson's disease: protein domains and functional insights. *TRENDS in Neurosciences* 29, 286- 293.

Mattson, M.P.(2012) Parkinson's disease: don't mess with calcium. *The Journal of Clinical Investigation* 122(4), 1195-1198.

Maturana, M.G.V., Pinheiro, A.S., Souza, T.L.F., and Follmer, C. (2015) Unveiling the role of the pesticides paraquat and rotenone on α-synuclein fibrillation *in vitro*. *NeuroToxicology* 46, 35-43.

Mazzulli, J.R., Mishizen, A.J., Giasson, B., Lynch, D.R., Thomas, S.A., Nakashima, A., Nagatsu, T., Ota, A., and Ischiropoulos, H. (2006) Cytosolic catechols inhibit α-synuclein aggregation and facilitate the formation of intracellular soluble oligomeric intermediates. *The Journal of Neuroscience* 26(39), 10068 –10078.

McCann, H., Stevens, C.H., Cartwright, H., and Halliday, G.M. (2014) α-synucleinopathy phenotypes. *Parkinsonism and Related Disorders*, S62-S67.

Minor, D.L., and Kim, P.S. (1994) Measurement of the β-sheet forming propensities if amino acids. *Nature* 367, 660-663.

Mirzaei, H., Schieler, J.L., Rochet, J.C., and Regnier, F. (2006) Identification of Rotenone-induced modifications in α-synuclein using affinity pull-down and Tandem Mass Spectrometry. *Analytical Chemistry* 78, 2422-2431.

Mizuno, Y., Hattori, N., Kubo, S., Sato, S., Nishioka, K., Hatano, T., Tomiyama, H., Funayama, M., Machida, Y., and Mochizuki, H. (2008), Progress in the pathogenesis and genetics of

Parkinson's disease. *Philosophical Transactions of The Royal Society Biological sciences* 363, 2215-2227.

Montojo, F.P., Anichtchik, O., Dening, Y., Knels, L., Pursche, S., Jung, R., Jackson, S., Gille, G., Spillantini, M.G., Reichmann, H., and Funk, R.H.W. (2010) Progression of Parkinson's Disease pathology is reproduced by intragastric administration of rotenone in mice. PLoS ONE 5, 8762-8772.

Mossessova, E., and Lima, C.D. (2000) Ulp1-SUMO crystal structure and genetic analysis reveal conserved interactions and a regulatory element essential for cell growth in Yeast. *Molecular Cell* 5, 865-876.

Murata, M., Horiuchi, E., and Kanazawa, I. (2001) Zonisamide has beneficial effects on Parkinson's disease patients. *Neuroscience* 41, 397-399.

Myohanen, T.T., Hannula, M.J., Elzen, R.V., Gerard, M., Veken, P.V.D., Garcia-Horseman, J.A., Baekelandt, V., Mannisto, P.T., and Lambeir, A.M. (2012) A prolyl oligopeptidase inhibitor, KYP-2047, reduces α-synuclein protein levels and aggregates in cellular and animal models of Parkinson's disease. *British Journal of Pharmacology* 166, 1097-1113.

Neumann, M., Kahle, P.J., Giasson, B.I., Ozmen, L., Borroni, E., Spooren, W., Muller, V., Odoy, S., Fujiwara, H., Hasegawa, M., Iwatsubo, T., Trojanowski, J.Q., Kretzschmar, H.A., and Haass, C. (2002) Misfolded proteinase K-resistant hyperphosphorylated α-synuclein aged transgenic mice with locomotor deterioration and in human α-synucleinopathies. *The Journal of Clinical Investigation* 110, 1429-1439.

Nonaka, T., and Hasegawa, M. (2009) A cellular model to monitor proteasome dysfunction by α-synuclein. *Biochemistry* 48, 8014-8022.

Nowick, J.S. (1999) Chemical models of protein β-sheets. *Acc.Chem.Res* 32, 287-296.

Olanow, C.W., and Brundin, P. (2013) Parkinson's disease and alpha synuclein: Is Parkinson's Disease a Prion-Like disorder? *Movement disorders* 28, 31-40.

Orpiszewski, J., and Benson, M. (1999) Induction of β-sheet structure in amyloidogenic peptides by neutralization of Aspartate: A model for amyloid nucleation. *Journal of Molecular Biology* 289, 413-428.

Outeiro, T.F., Kontopoulos, E., Altmann, S.M., Kufareva, I., Strathearn, K.E., Amore, A.M., Volk, C.B., Maxwell, M.M., Rochet, J.C., McLean, P.J., Young, A.B., Abagyan, R., Feany, M.B., Hyman, B.T., and Kazantsev, A.G. (2007) Sirtuin 2 inhibitors rescue α-synuclein mediated toxicity in models of Parkinson's Disease. *Science* 317, 516-519.

Outeiro, T.F., Putcha, P., Tetzlaff, J.E., Spoelgen, R., Koker, M., Carvalho, F., Hyman, B.T., and McLean, P.J. (2008) Formation of Toxic Oligomeric α-Synuclein Species in Living Cells. *PLoS ONE* 3(4), 1-9.

Parkinson's UK (2015) About Parkinson's [online]. Available at: http://www.parkinsons.org.uk/content/about-parkinsons [Accessed 10 March 2015].

Pasternak, B., Svanstrom, H., Nielson, N.M., Fugger, L., Melbye, M., and Hviid, A. (2012) Use of Calcium channel blockers and Parkinson's Disease. *American Journal of Epidemiology* 175(7), 627-635.

Paytona, J.E., Perrinb, R.J., Claytona, D.F., and George, J.M. (2001) Protein–protein interactions of alpha-synuclein in brain homogenates and transfected cells. *Molecular Brain Research* 95, 138–145.

Pelletier, J.N., Arndt, K.M., Pluckthun, A., and Michnick, S.W. (1999) An in vivo library-versus-library selection of optimized protein-protein interactions. *Nature Biotechnology*, 683-690.

Pelletier, J.N., Valois, C.F.X., and Michnick, S.W. (1998) Oligomerisation domain-directed reassembly of active dihydrofolate reductase from rationally designed fragments. *Biochemistry*, 12141-12146.

Periquet, M., Fulga, T., Myllykangas, L., Schlossmacher, M.G., and Feany, M.B. (2007) Aggregated α-synuclein mediates dopaminergic neurotoxicity *in vivo. The Journal of Neuroscience* 27(12), 3338 –3346.

Perutz, M.F., Pope, B.J., Owen, D., Wanker, E.E., and Scherzinger, E. (2002) Aggregation of proteins with expanded glutamine and alanine repeats of the glutamine-rich and asparagine-rich domains of Sup35 and of the amyloid β-peptide of amyloid plaques. *PNAS* 99(8), 5596-5600.

Pirkkala, L., Alastalo, T.P., Zuo, X., Benjamin, I.J., and Sistonen, L. (2000) Disruption of Heat Shock Factor 1 reveals an essential role in the Ubiquitin Proteolytic Pathway. *Molecular and cellular biology* 20, 2670-2675.

Porat, Y., Abramowitz, A., and Gazit, E. (2006) Inhibition of amyloid fibril formation by polyphenols: structural similarity and aromatic interactions as a common inhibition mechanism. *Chem. Biol. Drug Des.* 67, 27-37.

Proukakis, C., Dudzik, C.G., Brier, T., MacKay, D.S., Cooper, J.M., Millhauser, G.L., Houlden, H., and Schapira, A.H. (2013) A novel α-synuclein missense mutation in Parkinson's disease. *Neurology* 80, 1062-1064.

Rascol, O., Brooks, D.J., Korczyn, A.D., De Deyn, P.P., Clarke, C.E., and Lang, A.E. (2000) A five year study of the incidence of Dyskinesia in patients with early Parkinson's disease who were treated with Ropinirole or Levodopa. *The New England Journal of Medicine* 342, 1484-1491.

Remy, I., Valois, F.X.C., and Michnick, S.W. (2007) Detection of protein-protein interactions using a simple survival protein fragment complementation assay based on the enzyme dihydrofolate reductase. *Nature protocols* 2, 2120-2125.

Roberts, R.F., Martins, R.W., and Abarrategui, J.A. (2015) Direct visualization of alpha-synuclein oligomers reveals previously undetected pathology in Parkinson's disease brain. *Brain*, 1-16.

Rospigliosi, C.C., McClendon, S., Schmid, A.W., Ramlall, T.F., Barre, P., Lashuel, H.A., and Eliezer, D. (2009) E46K Parkinson's- linked mutation enhances C-terminal to N-terminal contacts in α-synuclein. *Journal of Molecular Biology* 388, 1022-1032.

Rutherford, N.J., Moore, B.D., Golde, T.E., and Giasson, B.I. (2014) Divergent effects of the H50Q and G51D SNCA mutations on the aggregation of α-synuclein. *Journal of Neurochemistry* 131, 859-867.

Savolainen, M.H., Richie, C.T., Harvey, B.K., Mannisto, P.T., Maguire-Zeiss, K.A., and Myohanen, T.T. (2014) The beneficial effect of a prolyl oligopeptidase inhibitor, KYP-2047, on alpha-synuclein clearance and autophagy in A30P transgenic mouse. *Neurobiology of Disease* 68, 1-15.

Schapira, A.H.V., Olanow, C.W., Greenmyre, J.T., and Bezard, E. (2014) Slowing of neurodegeneration in Parkinson's disease and Huntington's disease: future therapeutic perspectives. *The Lancet* 384, 545-555.

Sciarretta, K., Gordon, D.J., and Meredith, S.C., (2006) Peptide based inhibitors of amyloid assembly. *Methods in Ezymology* 413, 273-311.

Scira, O.W., Dunn, A., Aloglu, A.K., Sakallioglu, I.T., and Coskuner, O. (2013) Structures of the E46K mutant-type α-synuclein protein and impact of E46K mutation on the structures of the wild-type α-synuclein protein. *ACS Chem. Neuroscience* 4, 498-508.

Seidel, K., Schols, L., Parwez, E.P., Gierga, K., Wszolek, Z., Dickson, D., Gai, W.P., Bornemann, A., Riess, O., Rami, A., Dunnen, W.F.A., Deller, T., Rub, U., and Kruger, R. (2010) First appraisal of brain pathology owing to A30P mutant alpha-synuclein. *Ann. Neurology* 67, 684-689.

Serpell, L.C., Berriman, J., Jakes, R., Goedert, M., and Crowther, R.A. (2000) Fiber diffraction of synthetic α-synuclein filaments shows amyloid- like cross- β conformation. *PNAS* 97 (9), 4897-4902.

Smith, C., Withka, J.M., and Regan, L. (1994) A thermodynamic scale for the β-Sheet forming tendencies of the amino acids. *Biochemistry* 33, 5510-5517.

Sode, K., Ochiai, S., Kobayashi, N., and Usuzaka, E. (2007) Effect of reparation of repeat sequences in the human α-synuclein on fibrillation ability. *Int.J.Biol.Sci* 3, 1-7.

Spillantini, M.G., Crowther, R.A., Jakes, R., Hasegawa, M., and Goedert, M. (1998) α-Synuclein in filamentous inclusions of Lewy bodies from Parkinson's disease and dementia with Lewy bodies. *Neurobiology PNAS*, 6469-6473.

Spillantini, M.G., Schmidt, M.L., Lee, V.M.Y., and Trojanowski, J.Q. (1997) α-synuclein in Lewy bodies. *Nature* 388, 839-840.

Spira, P.J., Sharpe, D.M., Halliday, G., Cavanagh, J., and Nicholson, G.A. (2001) Clinical and pathological features of a Parkinsonian Syndrome in a family with an Ala53Thr α-synuclein mutation. *Ann. Neurology* 49, 313-319.

Snead, D., and Eliezer, D. (2014) Alpha-synuclein function and dysfunction on cellular membranes. *Experimental Neurobiology*, 292-313.

Sunde, M., Serpell, L.C., Bartlam, M., Fraser, P.E., Pepys, M.B., and Blake, C.C.F. (1997) Common core structure of Amyloid fibrils by Synchrotron X-ray Diffraction. *Journal of Molecular Biology* 273, 729-739.

Takeda, A., Mallory, M., Sundsmo, M., Honer, W., Hansen, L., and Masliah, E. (1998) Abnormal accumulation of NACP/α--synuclein in neurodegenerative disorders. *American Journal of Pathology* 152, 367-372.

Tofaris, G.K. (2012) Lysosome-dependent pathways as a unifying theme in Parkinson's Disease. *Movement Disorders* 27 (11), 1364-1369.

Tofaris, G.K., Razzaq, A., Ghetti, B., Lilley, K.S., and Spillantini, M.G. (2003) Ubiquitination of α-synuclein in Lewy bodies is a pathological event not associated with impairment of proteosome function. *The Journal of Biological Chemistry* 45, 44405-44411.

Ueda, K., Fukushima, H., Masliah, E., Xia, Y., Iwai, A., Yoshimoto, M., Otero, D.A.C., Kundo, J., Ihara, Y., and Saitoh, T. (1993) Molecular cloning of cDNA encoding an unrecognized component of amyloid in Alzheimer disease. *Proc.Natl.Acad.Sci.USA* 90, 11282-11286.

Uversky, V.N., Gillespie, J.R., and Fink, A.L. (2000) Why are “Natively Unfolded” proteins unstructured under physiologic conditions?. *PROTEINS* 41, 415-427.

Uversky, V.N., Li, J., and Fink, A.L. (2001) Metal-triggered structural transformations, aggregation, and fibrillation of human α-Synuclein. *The Journal of Biological Chemistry* 276 (47), 44284-44296.

Uversky, V.N., Yamin, G., Souillac, P.O., Goers, J., Glaser, C.B., and Fink, A.L. (2002) Methionine oxidation inhibits fibrillation of human α-synuclein *in vitro*. *FEBS Letters* 517, 239-244.

Vilar, M., Chou, H., Luhrs, T., Maji, S.K., Loher, D.R., Verel, R., Manning, G., Stahlberg, H., and Riek, R. (2008) .The fold of α-synuclein fibrils. *PNAS* 105, 8637-8642.

Wang, W., Perovicc, I., Chittulurud, J., Kaganoviche, A., Nguyena, L.T.T., Liaoa, J., Auclairc, J.R., Johnsona, D., Landerua, A., Simorellisf, A.K., Juf, S., Cooksone, M.R., Asturiasd, F.J., Agarc, J.N., Webbg, B.N., Kangg, C., Ringef, D., Petskof, G.A., Pochapskyf, T.C., and Hoang, Q. (2011) A soluble α-synuclein construct forms a dynamic tetramer. *PNAS*, 1- 6.

Waxman, E.A., Emmer, K.L., and Giasson, B.I. (2010) Residue Glu83 plays a major role in negatively regulating α-synuclein amyloid formation. *Biochemical and Biophysical Research Communications* 391, 1415-1420.

Waxman, E.A., and Giasson, B.I. (2008) Characterization of antibodies that selectively detect α-synuclein in pathological inclusions. *Acta Neuropathology* 116 (1), 37-46.

Waxman, E.A., and Giasson, B.I. (2009) Molecular mechanisms of α-synuclein neurodegeneration. *Biochimica et Biophysica Acta* 1792, 616-624.

Winner, B., Jappelli, R., Maji, S.K., Desplats, P.A., Boyer, L., Aigner, S., Hetzer, C., Loher, T., Vilar, M., Campioni, S., Tzitzilonis, C., Soragni, A., Jessberger, S., Mira, H., Consiglio, A., Pham, E., Masliah, E., Gage, F.H., and Riek, R. (2011) In vivo demonstration that α-synuclein oligomers are toxic. *PNAS* 108, 4194-4199.

Wolfe, L.S., Calabrese, M.F., Nath, A., Blaho, D.V., Miranker, A.D., and Xiong Yong (2010) Protein-induced photophysical changes to the amyloid indicator dye thioflavin T. *PNAS* 107(39), 16863-16868.

Yagi, H., Kusaka, E., Hongo, K., Mizobata, T., and Kawata, Y. (2005) Amyloid Fibril Formation of α-Synuclein Is Accelerated by Preformed Amyloid Seeds of Other Proteins. *The Journal of Biological Chemistry* 280, 38609-38616.

Ye, L., Velasco, A., Fraser, G., Beach, T.G., Sue, L., Osredkar, T., Libri, V., Spillantini, M.G., Goedert, M., and Lockhart, A. (2008) *In vitro* high affinity α-synuclein binding sites for the amyloid imaging agent PIB are not matched by binding to Lewy bodies in postmortem human brain. *Journal of Neurochemistry* 105, 1428-1437.

Yoshida, W., Kobayashi, N., Sasaki, Y., Ikebukuro, K., and Sode, K. (2013) Partial peptide of α-synuclein modified with small-molecule inhibitors specifically inhibits Amyloid Fibrillation of α-synuclein. *International Journal of Molecular Sciences* 14, 2590-2600.

Youdim, M.B.H., Gross,A., and Finberg, J.P.M. (2001) Rasagiline [N-propargyl-1R(+)-aminoindan], a selective and potent inhibitor of mitochondrial monoamine oxidase B. *British Journal of Pharmacology* 132, 500-506.

Yu, S., Li, X., Liu, G., Han, J., Zhang, C., Li, Y., Xu, S., Liu, C., Gao, Y., Yang, H., Ueda, K., and Chan, P. (2007) Extensive nuclear localization of α-synuclein in normal rat brain neurons revealed by a novel monoclonal antibody. *Neuroscience* 145, 539–555.

Zarranz, J.J., Alegre, J., Gomez-Esteban, J.C., Lezcano, E., Ros, R., Ampuero, I., Vidal, L., Hoenicka, J., Rodriguez, O., Atares, B., Llorens, V., Tortosa, E.G., Ser, T., Munoz, D.G., and Yebenes, J.G (2004) The new mutation, E46K of α-synuclein causes Parkinson and Lewy Body Dementia. *Ann Neurology* 55, 164-173.

Appendix

THE JOURNAL OF BIOLOGICAL CHEMISTRY VOL. 290, NO. 12, pp. 7426–7435, March 20, 2015

Intracellular Screening of a Peptide Library to Derive a Potent Peptide Inhibitor of α-Synuclein Aggregation*

Received for publication, October 21, 2014, and in revised form, January 12, 2015 Published, JBC Papers in Press, January 23, 2015, DOI 10.1074/jbc.M114.620484

Harish Cheruvara[‡], Victoria L. Allen-Baume[‡], Neil M. Kad[§1], and Jody M. Mason[¶1,2]

From the [‡]School of Biological Sciences, University of Essex, Wivenhoe Park, Colchester, Essex CO4 3SQ, the [§]School of Biosciences, University of Kent, Canterbury, Kent CT2 7NJ, and the [¶]Department of Biology and Biochemistry, University of Bath, Claverton Down, Bath BA2 7AY, United Kingdom

Background: Deposition of α-synuclein into Lewy bodies is considered the primary event in Parkinson disease.
Results: A peptide selected via PCA library screening functions by inhibiting fibril formation.
Conclusion: A semirational design combined with intracellular PCA is an effective methodology to develop α-synuclein aggregation antagonists.
Significance: The technique can be applied to a number of diseases from Parkinson to Alzheimer.

Aggregation of α-synuclein (α-syn) into toxic fibrils is a pathogenic hallmark of Parkinson disease (PD). Studies have focused largely on residues 71–82, yet most early-onset mutations are located between residues 46 and 53. A semirationally designed 209,952-member library based entirely on this region was constructed, containing all wild-type residues and changes associated with early-onset PD. Intracellular cell survival screening and growth competition isolated a 10-residue peptide antagonist that potently inhibits α-syn aggregation and associated toxicity at a 1:1 stoichiometry. This was verified using continuous growth measurements and 3-(4,5-dimethylthiazol-2-yl)-2,5-diphenyltetrazolium bromide cytotoxicity studies. Atomic force microscopy and circular dichroism on the same samples showed a random-coil structure and no oligomers. A new region of α-syn for inhibitor targeting has been highlighted, together with the approach of using a semirational design and intracellular screening. The peptides can then be used as candidates for modification in drugs capable of slowing or even preventing the onset of PD.

Deposition of α-synuclein (α-syn)[3] into neuronal inclusions known as Lewy bodies is considered the causative agent in the pathogenesis of Parkinson disease (PD), a debilitating disease that results principally in rigidity, tremor, and slowness of movement and that accounts for ~15% of all dementias (1, 2). The accumulation of toxic Lewy bodies in the cytoplasmic space of dopaminergic neurons in the substantia nigra pars compacta region of the brain leads to cell death, decreased dopamine levels, and ultimately the symptoms of the disease. There is a substantial and growing body of evidence implicating α-syn in PD (3), including (i) synthetic α-syn rapidly aggregates into β-sheet-rich fibrils similar to those found in Lewy bodies; (ii) rare familial mutations that increase fibril aggregation rates and toxicity lead to early-onset PD; (iii) α-syn gene duplications lead to increased protein expression and therefore accelerate disease onset; and (iv) α-syn oligomers are toxic to therapeutically relevant cells in culture. To intervene in PD, we utilized a novel intracellular screen to identify peptides capable of binding to and reducing the associated toxicity of a-syn aggregation. Our approach has the potential to address recent findings that suggest that prefibrillar oligomers are the toxic species (4).

There is a wealth of experimental data demonstrating that region 71–82 is responsible for aggregation of the full-length 140-amino acid protein (5–7). Indeed, numerous groups have used this region as a starting point for the design of inhibitors. This has included unmodified peptides (8) and *N*-methylated peptides (9). Given the interest in this region and its requirement for aggregation of the full-length protein, many groups have focused their efforts on producing libraries based on this scaffold. However, of the known point mutations in the α-syn gene associated with early-onset PD, three (E46K, H50Q, A53T) are located between residues 46 and 53, with the fourth (A30P) located in close proximity. More recently, a fifth mutation (G51D) was identified (10). This region and the residues within are clearly important in modulating amyloid formation such that toxicity associated with the α-syn protein increases, with the changes leading to decreased α-helicity, increased β-sheet propensity, and an increase in either the rate or number of oligomers that are formed (11–14).

In this study, we generated peptide inhibitors using a multiplexed intracellular protein-fragment complementation assay (PCA) library screening system (15, 16), followed by direct imaging of the samples. Successfully selected peptides must bind α-syn to reduce amyloid cytotoxicity and confer bacterial cell survival. During PCA, no assumptions are therefore made regarding the mechanism of action or the oligomeric state of α-syn that becomes populated. The only prerequisites for peptide selection are that (i) peptides bind to α-syn such that the split reporter enzyme is recombined and (ii) the result is lower

* This work was supported by Parkinson's UK Ph.D. Studentship H-1001 (to H. C., N. M. K., and J. M. M.) and by Cancer Research UK Career Establishment Award A11738 (to J. M. M.).
[1] Both authors contributed equally to this work.
[2] To whom correspondence should be addressed. E-mail: j.mason@bath.ac.uk.
[3] The abbreviations used are: α-syn, α-synuclein; PD, Parkinson disease; PCA, protein-fragment complementation assay; ThT, thioflavin T; AFM, atomic force microscopy; MTT, 3-(4,5-dimethylthiazol-2-yl)-2,5-diphenyltetrazolium bromide; SUMO, small ubiquitin-like modifier; Fmoc, *N*-(9-fluorenyl)methoxycarbonyl.

toxicity such that cell survival is facilitated. In addition, the PCA approach is predicted to select peptides that are resistant to degradation by bacterial proteases, soluble, nontoxic, and target-specific in the presence of other cytoplasmic proteins.

Using α-syn(45–54) as a template for our library design, we created a 209,952-member peptide library 10 amino acids in length that spans residues 45–54, containing the wild-type 45–54 sequence, including residue options corresponding to E46K, H50Q, and A53T, which, when mutated, give rise to early-onset PD. PCA was used to screen the peptide library for an interaction with wild-type α-syn. The effectiveness of an amyloid/PCA-selected peptide (45–54W) was subsequently tested by performing four key experiments upon the same sample: a continuous amyloid growth assay, monitored using thioflavin T (ThT) fluorescence; CD, to report on changes in β-sheet content; and atomic force microscopy (AFM) and SDS-PAGE analysis, to directly image any reduction in fibril load and changes in the fibril morphology. We found the peptide derived using this approach to be capable of binding to the disease-relevant wild-type α-syn and reducing associated amyloid formation by >90%. In this study, we both successfully verified the methodology for producing anti-α-syn aggregation peptide inhibitors using the amyloid/PCA approach and produced a lead peptide sequence that is expected to provide a scaffold for future drug candidates.

Our data collectively indicate that the PCA-derived winner sequence (45–54W) is able to prevent the aggregation of wild-type α-syn at a stoichiometry of 1:1. The ThT fluorescence signal associated with amyloid formation did not progress beyond ~8% of the original 1:0 sample. AFM experiments showed that in the same continuous growth samples, there was a striking decrease in the number of fibrils relative to the 1:0 samples. 3-(4,5-Dimethylthiazol-2-yl)-2,5-diphenyltetrazolium bromide (MTT) cytotoxicity studies using the same samples showed a reduction in cell death of 65–85% compared with α-syn in isolation. Finally, CD experiments using samples taken from the same continuous growth experiment once again showed that the conversion from a random-coil structure to a β-sheet-rich structure was almost completely abolished in the 1:1 sample. At a molar ratio of 1:0.5, the formation of the mature amyloid fibrils found in the 1:0 sample was slowed but ultimately not prevented (see Fig. 3*a*). At stoichiometries of 1:0.1 and 1:0.01, the rate of amyloidosis was not significantly lowered relative to the 1:0 sample.

EXPERIMENTAL PROCEDURES

Primers and Library Cloning—Primers were designed such that the desired library could be generated using overlap-extension PCR. Bases overlapped in a non-randomized region of the primers to give an approximate annealing temperature of 66 °C. Correct amplification was enabled via an elongated reverse primer and verified by agarose gel electrophoresis. The correct PCR product was then digested using NheI and AscI restriction enzymes for subcloning the library into the pES230d vector (restriction enzyme recognition sites shown). Primer sequences used were 5′-C TGG GCT AGC RAA VAW GBG VTT VTT VAW GBG VTT RHA RCC GGC GCG CCG CTA GAG GCG-3′ (forward) and 5′-T TTT TTT TTA TAA TAT ATT ATA CGC CTC TAG CGG CGC GCC-3′ (reverse). An additional 30 residues on the 5′-end of the reverse primer were used to observe the correct PCR product prior to restriction digestion.

Single-step Selection PCA—Escherichia coli XL-1 cells were used for construction and cloning of libraries as described previously (16–18). First, pES300d-α-syn target and pREP4 (for expression of the Lac repressor protein; Qiagen) were cotransformed into BL21-Gold cells (Stratagene) and plated onto LB agar with the appropriate antibiotics (kanamycin and chloramphenicol). These cells were next made electrocompetent before transformation with the pES230d-45–54 library plasmid. Transformed cells were plated onto three different media. One-twentieth of the cells were plated onto LB agar with three antibiotics (kanamycin, ampicillin, and chloramphenicol) as a positive control of transformation efficiency. Another one-twentieth of the solution was plated onto M9 minimal agar containing 1 μg/ml trimethoprim and the same three antibiotics as a negative control. Finally, the remaining 90% of the transformed cells were plated onto M9 minimal agar in the presence of the three antibiotics, 1 μg/ml trimethoprim, and 1 mM isopropyl β-D-thiogalactopyranoside to induce expression of the two dihydrofolate reductase fragment-fused peptides. This single-step selection PCA led to ~200 colonies from the initial library of 209,952, meaning that >99.9% of all library members were removed at this stage.

Competition Selection PCA—To increase selection stringency, growth competition experiments were undertaken. Selected colonies were pooled from the plate, grown in M9 minimal agar under selective conditions (containing kanamycin, ampicillin, chloramphenicol, trimethoprim, and isopropyl β-D-thiogalactopyranoside), and serially diluted over five passages. Using these sequential rounds of competition selection, subtle differences in growth rate can become amplified, increasing the stringency of selection relative to the single-step method. Competition selection therefore allows the most effective one or two sequences to be isolated from the ~200 α-syn binders initially identified during single-step selection. At each passage, glycerol stocks were prepared, and sequencing results were obtained (Source Bioscience, Nottingham, United Kingdom) for DNA pools and individual colonies. For each passage, 50 μl of liquid culture was added to 50 ml of fresh M9 minimal agar, resulting in an A_{600} of ~0.01. Cells were incubated at 37 °C until an A_{600} of ~0.4 was reached (typically 2–3 days) before moving to the next passage.

Protein Expression and Purification—Wild-type α-syn was synthesized by overexpression in the *E. coli* BL21 strain using a small ubiquitin-like modifier (SUMO) fusion protein (19). SUMO modulates protein structure and function by covalently binding to the lysine side chains of the target protein to enhance expression and solubility of the α-syn protein. *E. coli* BL21 competent cells were transformed with the pET21b plasmid construct, grown on LB agar plates containing ampicillin and chloramphenicol, and grown overnight. Single colonies were next picked, inoculated in LB broth containing ampicillin and chloramphenicol, and shaken at 37 °C. These cultures were then used to inoculate 2 liters of liquid LB broth containing ampicillin and chloramphenicol and grown to mid-log phase (A_{600} = 0.6–0.8) before being further induced by 1 mM isopro-

pyl β-D-thiogalactopyranoside for 3 h at 37 °C. Cells were obtained by centrifugation at 4000 rpm for 20 min at 4 °C in a Sorvall RC Superspeed centrifuge. Cell pellets were then resuspended in binding buffer (50 mM NaH_2PO_4, 300 mM NaCl, and 10 mM imidazole (pH 8)) and homogenized using a magnetic stirrer for 15 min on ice, followed by sonication (40% amplification). Lysed cells were next centrifuged at 18,500 rpm for 20 min at 4 °C using an SS-34 rotor (Sorvall RC Superspeed centrifuge). The supernatant containing the protein was stored at −20 °C.

The fusion protein was purified by applying the supernatant from the cell lysate to a nickel-nitrilotriacetic acid affinity column three times at a flow rate of 3 ml/min to allow the protein to bind. The column was next washed with 40 ml of wash buffer (50 mM NaH_2PO_4, 300 mM NaCl, and 30 mM imidazole (pH 8)), and the protein was eluted using elution buffer (50 mM NaH_2PO_4, 300 mM NaCl, and 500 mM imidazole (pH 8)). The protein sample was then exchanged to cleavage buffer (20 mM Tris and 0.5 mM DTT (pH 8)) using a PD-10 desalting column. The His_6-SUMO tag was removed using the SUMO protease-specific UlP1 enzyme (1 mg/ml for 10 mg/ml target protein) at 30 °C for 16 h.

His_6-SUMO was finally removed using a size-exclusion column. A Sephadex G-75 column was washed three times with 10 mM MES and 150 mM NaCl (pH 8.0). The protein was concentrated to 2 ml and injected onto the column, and fractions were eluted according to their molecular mass. Finally, SDS-PAGE was used to determine the purity of the α-syn and to verify the expected molecular mass of different fractions containing α-syn (14.5 kDa), SUMO protein (12.2 kDa), and SUMO protease (27 kDa). The correct mass of α-syn was further confirmed by electrospray mass spectrometry. The protein concentration was determined in a Varian Cary 50 spectrophotometer. The purified protein was lyophilized using a freeze drier and stored at −80 °C.

Monomerization of Protein for Aggregation Studies—To monomerize the protein prior to aggregation experiments, 1 ml of hexafluoro-2-propanol was added to 2 mg of lyophilized peptide. This was next vortexed for ~2 min to fully dissolve the peptide, followed by sonication at 25 °C for 5 min in a water bath sonicator. Hexafluoro-2-propanol was allowed to evaporate completely under a regulated stream of air. The process was repeated three times, followed by dissolution of the peptide sample in double-distilled water, vortexing for 3 min, and lyophilization for further use (9).

Peptide Synthesis—Rink amide ChemMatrix resin was obtained from PCAS BioMatrix Inc. (Saint-Jean-sur-Richelieu, Quebec, Canada). Fmoc-L-amino acids and (1*H*-benzotriazol-1-yloxy)-(dimethylamino)-*N*,*N*-dimethylmethaniminium hexafluorophosphate were obtained from AGTC Bioproducts (Hessle, United Kingdom). All other reagents were of peptide synthesis grade and obtained from Thermo Fisher Scientific (Loughborough, United Kingdom). Peptide 45–54W was synthesized on a 0.1-mmol scale on PCAS BioMatrix Rink amide resin using a Liberty Blue microwave peptide synthesizer (CEM Corp., Matthews, NC) employing Fmoc solid-phase techniques (for review, see Ref. 20) with repeated steps of coupling, deprotection, and washing (4× 5 ml of dimethylformamide). Coupling was performed as follows: Fmoc-L-amino acids (5 eq), (1*H*-benzotriazol-1-yloxy)(dimethylamino)-*N*,*N*-dimethylmethaniminium hexafluorophosphate (4.5 eq), and diisopropylethylamine (10 eq) in dimethylformamide (5 ml) for 5 min with 20-watt microwave irradiation at 90 °C. Deprotection was performed as follows: 20% piperidine in dimethylformamide for 5 min with 20-watt microwave irradiation at 80 °C. Following synthesis, the peptide was acetylated (acetic anhydride (3 eq) and diisopropylethylamine (4.5 eq) in dimethylformamide (2.63 ml) for 20 min) and then cleaved from the resin with concomitant removal of side chain-protecting groups by treatment with a cleavage mixture (10 ml) consisting of TFA (95%), triisopropylsilane (2.5%), and H_2O (2.5%) for 4 h at room temperature. Suspended resin was removed by filtration, and the peptide was washed by three rounds of crashing in ice-cold diethyl ether, vortexing, and centrifugation. The pellet was then dissolved in 1:1 MeCN/H_2O and freeze-dried. Purification was performed by reverse-phase HPLC using a Phenomenex Jupiter Proteo (C12) reverse-phase column (4 μm, 90 Å, 10 mm, inner diameter × 250 mm long). Eluents used were as follows: 0.1% TFA in H_2O (eluent A) and 0.1% TFA in MeCN (eluent B). The peptide was eluted by applying a linear gradient (at 3 ml/min) of 20–60% eluent B over 40 min. Fractions collected were examined by electrospray mass spectrometry, and those found to contain the desired product exclusively were pooled and lyophilized. Analysis of the purified final product by reverse-phase HPLC indicated a purity of >95%.

Peptide Preparation—Stock solutions of 1 mM inhibitor and control peptides were dissolved in ultrapure water. At this concentration (a 2–200-fold excess of that used in experiments), no aggregation or precipitation was observed. In addition, bioinformatics tools (*e.g.* Waltz (21), AmylPred (22), PASTA (23), Zyggregator (24), and TANGO (25)) did not predict the peptide to contain amyloidogenic sequences or to aggregate in isolation. Finally, dye-binding experiments demonstrated that this sequence did not bind ThT or aggregate and form random coil-like species in isolation by CD (see Figs. 3 and 4).

Continuous Growth ThT Experiments—Peptides were lyophilized at the molar concentration of the target protein and inhibitory peptide (1:1). The reaction mixture containing 450 μM wild-type α-syn and inhibitory peptide was incubated in 90 μM ThT, 10 mM phosphate buffer (pH 7.0), 100 mM KF, and 0.05% NaN_3 at 37 °C with continuous mixing using a magnetic stir bar in an LS 55 fluorescence spectrophotometer (Perkin-Elmer Life Sciences) for 4500 min (75 h). The same experiment was repeated three times for both the 1:0 sample- and peptide 45–54W-containing solutions at a variety of stoichiometries, as well as at 1:1 molar ratios with the wild-type 45–54 and 71–82W (Ac-VTGVTADVQETV-NH2) control peptides. The PCA winner peptide, 45–54W, was lyophilized in aliquots of different molar concentrations of target protein and inhibitory peptide ranging from 1:0.01 to 1:1.

CD Experiments—Far-UV CD spectra were recorded using an Applied Photophysics Chirascan spectrometer at 20 °C using the same samples from the continuous growth ThT experiments. Spectra were recorded over the 190–300-nm range at a scan rate of 10 nm/min with step size of 1 nm. Spectra were recorded as the average of three scans. Peptide (10 μM in 10 mM potassium phosphate buffer (pH 7.4)) was added to a

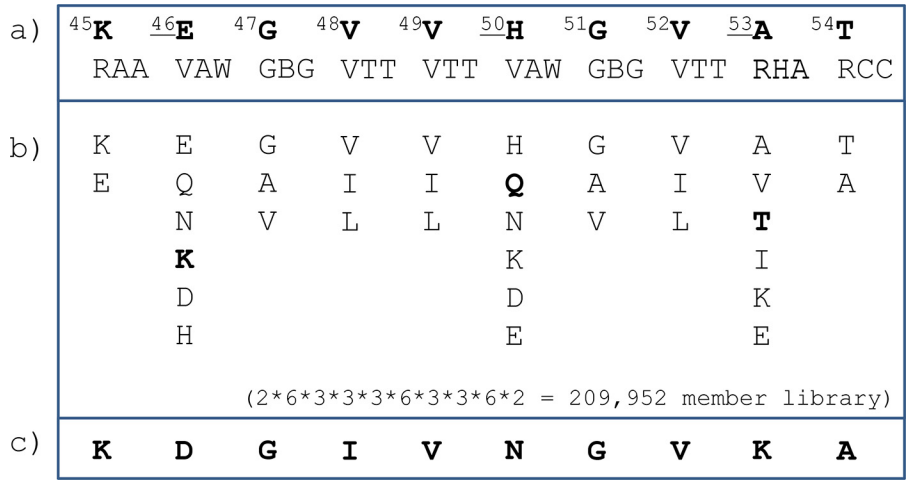

FIGURE 1. *a*, shown are residues 45–54 of wild-type α-syn (KEGVVHGVAT), as well as the three well studied point mutation sites (positions 46, 50, and 53). Degenerate codons for library construction are shown below (*R* = A/G, *V* = A/C/G, *W* = A/T, *B* = C/G/T, and *H* = A/C/T). *b*, shown are amino acid options at each position to generate a 209,952-member peptide library. The wild-type residue options (top line) and alternative options, including those point mutations associated with early-onset PD (shown in *boldface*), were also considered in the library design. *c*, the PCA winner peptide (KDGIVNGVKA) emerged from single-step selection, followed by two rounds of competition selection PCA.

0.1-cm cuvette (Hellma Analytics). Spectra were recorded as raw ellipticity.

AFM Experiments—Samples were imaged in noncontact mode using an XE-120 atomic force microscope (Park Systems, Suwon, South Korea). NSC15 silicon nitride cantilevers with a spring constant of 40 newtons/m were used for imaging at a scan rate of 1.0 Hz and a resolution of 256 × 256 pixels. All images were obtained at room temperature. The AFM data were taken from continuous growth experiments. A 5-μl sample was taken from the 450 μM α-syn continuous growth experiment and placed on freshly cleaved mica (0.3-mm thickness). Following adsorption of the protein aggregates (2 min), the mica was washed with 5 ml of double-distilled water. Excess water was removed, and the samples were dried using a stream of nitrogen gas. Samples were immediately analyzed by AFM. The image files were examined using WSxM 5.0 (Nanotec Electronica S.L.) and flattened before processing (26).

MTT Cell Toxicity Assay—MTT experiments were undertaken using rat pheochromocytoma (PC12) cells to assess the cytotoxicity effect of α-syn. PC12 cells are known to be particularly sensitive, and their use in this assay is well established (27). A Vybrant MTT cell proliferation assay kit (Invitrogen) was used to measure conversion of the water-soluble MTT dye to formazan, which was then solubilized, and the concentration was determined by a purple color change monitored via absorbance measurement at 570 nm. The change in absorbance can be used as an indicator of PC12 cell health in this assay. The assay was performed with a 5 μM α-syn and peptide stoichiometry corresponding to 1:1. PC12 cells were maintained in RPMI 1640 medium and 2 mM glutamine mixed with 10% horse serum and 5% fetal bovine serum and supplemented with 20 mg/ml gentamycin. Cells were transferred to a sterile 96-well plate with 30,000 cells/well, and experiments were performed in triplicate. The required volume of peptide and target solutions was added to PC12 cells. A total of 100 μl of PC12/RPMI 1640 medium combined with an appropriate volume of peptide/α-syn target mixture (5 μM peptide + 5 μM α-syn target) was transferred to a 96-well microtiter plate. Because the samples contained 90 μM ThT, control experiments with PC12 cells and α-syn alone both with and without ThT were undertaken. These samples were incubated for 24 h at 37 °C and 5% CO_2 prior to the addition of the MTT dye. A total of 10 μl of the dye was added to each well and incubated for an additional 4 h at 37 °C and 5% CO_2. A total of 100 μl of dimethyl sulfoxide was then added to each well and allowed to stand for 10 min. The absorbance was measured at 570 nm using a Berthold TriStar LB 942 plate reader.

SDS-PAGE—Gel analysis was carried out using 15% Tris bisacrylamide gels operated at a constant voltage of 150 V. The running buffer was 25 mM Tris-HCl, 193 mM glycine, and 0.1% SDS (pH 8.3). 3 μl of 450 μM α-syn and peptides at different stoichiometries was mixed with 7 μl of loading buffer containing 50 mM Tris-HCl (pH 6.8), 1% SDS, 5% glycerol, and 25% bromphenol blue. 10 μl of each sample was then loaded in each well. The gel was stained with 0.1% Coomassie Blue R-250.

RESULTS

α-syn(45–54) Library Generation—PCA was undertaken with the full-length α-syn(1–140) target using a library based on the α-syn(45–54) region, in which three of the four α-syn mutations associated with early-onset PD are located (KEGVVHGVAT, wild-type 45–54). Unlike α-syn(71–82), this is not a region of the molecule known to aggregate into toxic fibrils in isolation (28–30) and therefore has not been exploited as a starting point for deriving α-syn binders capable of inhibiting aggregation. The library incorporated the wild-type sequence while introducing two-, three-, or six-residue options at each of the 10 amino acid positions (Fig. 1). This corresponded to a library size of 209,952. Single-step selection on M9 plates was undertaken, followed by competition selection in liquid M9 medium, resulting in one clean sequencing result by passage 6: KDGIVNGVKA (Fig. 2).

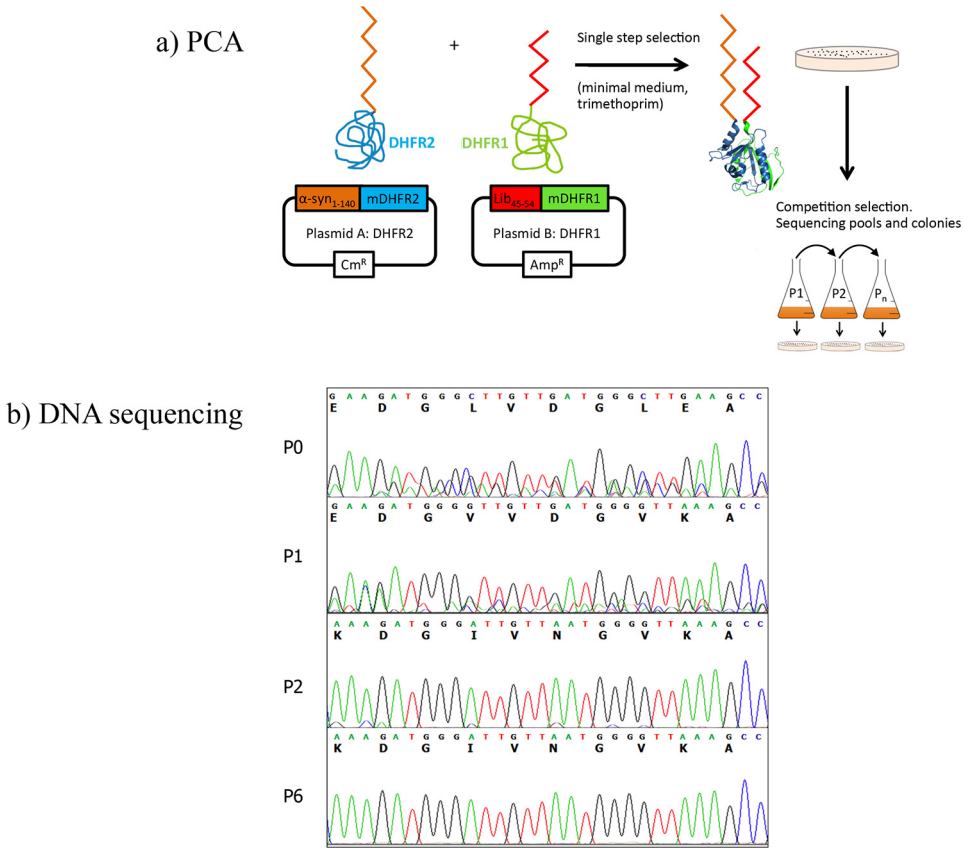

FIGURE 2. *a*, PCA. Peptide library members that bind to wild-type α-syn(1–140) recombine murine dihydrofolate reductase (*mDHFR*) and lead to colonies under selective conditions (bacterial dihydrofolate reductase is specifically inhibited using trimethoprim). Those peptides that bind with the highest affinity to the α-syn target are able to confer cell growth by (i) reconstituting murine dihydrofolate reductase to restore activity and (ii) reducing the toxicity associated with any given oligomeric amyloid state. In competition selection, subsequent passages in liquid medium isolate potential PCA winners with the highest efficacy. Because PCA is performed in the cytoplasm of *E. coli*, the nonspecific, unstable, aggregation-prone (insoluble), protease-susceptible members are removed. *b*, DNA sequencing results of library pools for passages 0–6. Both single-step selection (*P0*) and competition selection (*P1*, *P2*, and *P6*) are shown. The peptide sequence KDGIVNGVKA was seen to dominate from passage 2 onwards. Cm^R, chloramphenicol resistance; Amp^R, ampicillin resistance.

Peptide Characterization—PCA-derived peptide sequences (Fig. 1) were synthesized and characterized using a number of experiments, including ThT dye binding, CD, AFM, and MTT cytotoxicity experiments, to verify that the peptides do not aggregate in isolation and to determine whether they are able to reduce aggregation and/or breakdown preformed fibrils to a nontoxic species.

Continuous Growth ThT Experiments Demonstrate a Significant Reduction in Fibril Load—To determine the ability of PCA-derived peptides to reduce fibril assembly (inhibition) and/or to breakdown preformed fibrils (reversal), ThT binding was used to quantify amyloid species. First, α-syn was rendered monomeric (9) and aggregated into amyloid by resuspending and incubating at 37 °C. For the continuous growth assay, peptides were added at time 0, and a reading was taken every 5 min over a 75 h period. The ThT signal was significantly reduced at a 1:1 molar ratio, indicating that the peptides were able to bind α-syn and reduce aggregation levels. At increasingly lower substoichiometric ratios, we observed progressively reduced activity consistent with a general dose dependence. The control peptide 71–82W and the wild-type 45–54 sequence at 1:1 molar rations had no effect on aggregation, demonstrating α-syn specificity for peptide 45–54W.

AFM Indicates a Large Reduction in Amyloid Levels—As a second direct qualitative measure of fibril formation, samples used in continuous growth experiments were imaged using AFM (Fig. 3, *b–f*). A stoichiometry of 1:1 (450 μM) was chosen for AFM experiments, as this was found to be the most effective in ThT experiments (Fig. 3*b*). At this stoichiometry, a major reduction in the amount of amyloid was observed relative to the α-syn control across several time points (Fig. 3*d*). No fibrils were observed for peptide 45–54W in the absence of α-syn. The control peptide 71–82W and the wild-type 45–54 sequence had no effect upon fibril formation (Fig. 3, *e* and *f*), supporting α-syn specificity for peptide 45–54W.

CD Demonstrates a Large Reduction in β-Sheet Content—Because amyloid fibrils are predominately β-sheet, we also used CD spectroscopy for structural characterization of the aggregates in the continuous growth ThT experiments. The data presented in Fig. 4*a* show spectra over 17 time points of the continuous growth assay. A single negative peak at 218 nm develops across the time course, along with the loss of the minimum at ~200 nm, consistent with the gain of β-sheet structure and the loss of a random coil. As predicted from the ThT data above, the β-structure did not form for α-syn incubated with peptide 45–54W at a 1:1 stoichiometry (Fig. 4*b*). In addition, the minimum at ~200 nm did not significantly diminish. A similar spectrum was observed for peptide 45–54W alone (*i.e.* 0:1 stoichiometry) after 75 h of incubation, indicating that this peptide does not aggregate in isolation. The lack of CD signal

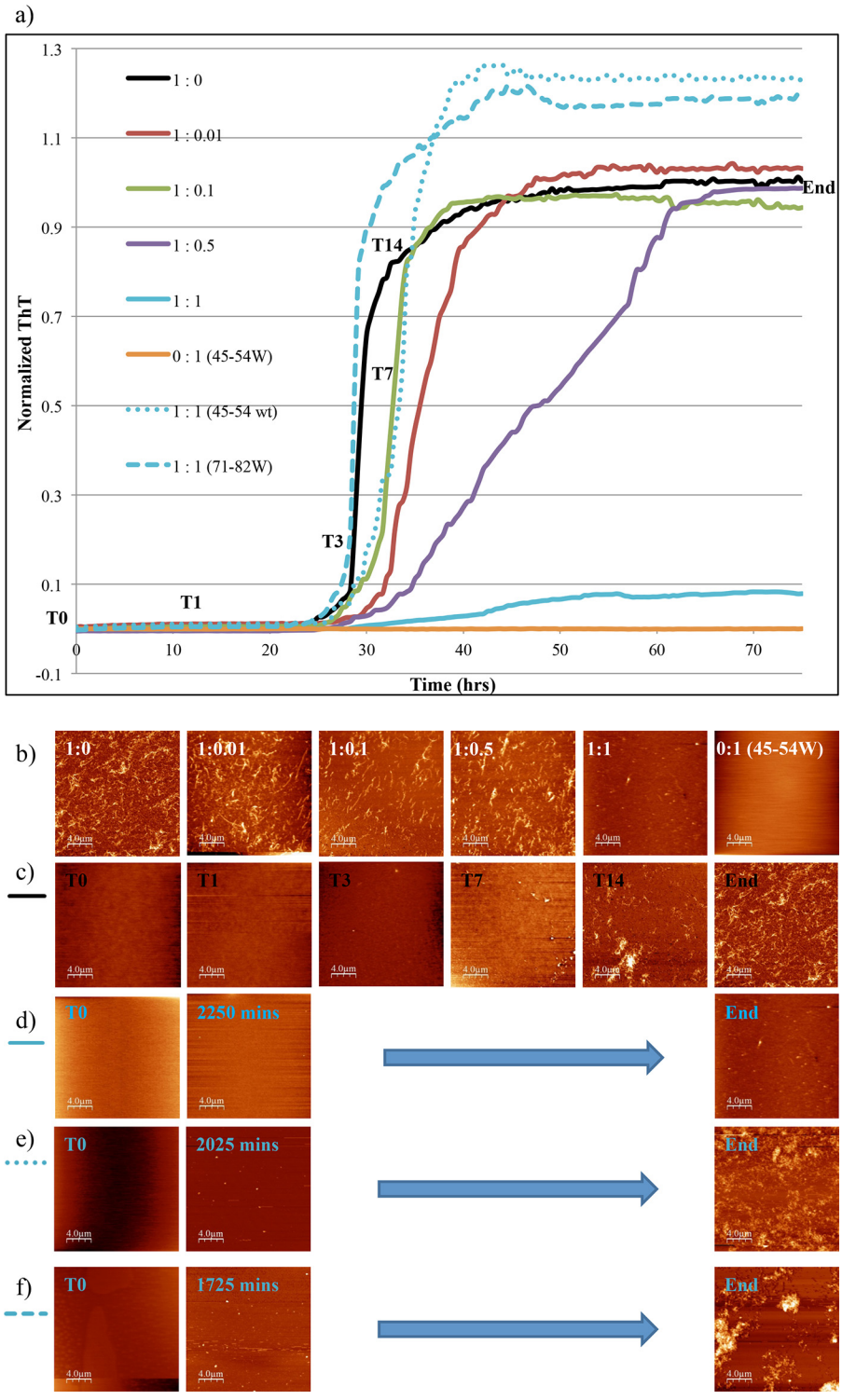

FIGURE 3. *a*, continuous ThT growth. The data show a significant reduction in ThT signal (~92%) at a 1:1 stoichiometry. The ThT signal at a molar ratio of 1:0.5 shows that the amyloid growth rate was significantly reduced compared with the wild type. At increasingly substoichiometric ratios, the ThT fluorescence indicates reduced peptide activity in an expected dose-dependent manner. Peptide 45–54W alone (0:1 sample) showed no ThT binding, indicating that it does not aggregate in isolation. Aliquots of samples were collected at 17 different time points for the 1:0 sample (lag phase (*T0* and *T1*), exponential phase (*T3*, *T7*, and *T14*), and stationary phase (*End*) are shown) and three time points for the 1:1 sample (*T0*, *T1*, and *End*) for further analysis by AFM and CD. *b*, AFM images showing the end point samples (75 h) for all stoichiometries used in continuous growth ThT experiments. A considerable reduction in fibril load was observed at a molar ratio of 1:1. All other stoichiometries showed no major reduction in amyloid content relative to the 1:0 sample. Peptide 45–54W (0:1 sample) did not aggregate in isolation. *c*, AFM images showing the gradual increase in amyloid content along various time points for the 1:0 sample. Shown are six samples (*T0*, *T1*, *T3*, *T7*, *T14*, and *End*) taken from the lag, exponential, and stationary phases. The time points for these were 0, 10, 33.3, 37.5, 49, and 75 h, respectively. *d*, a large reduction in amyloid content was observed for the 1:1 sample with peptide 45–54W. For these images, $T0 = 0$ h, $T1 = 37.5$ h, and $T2 = 75$ h. *e*, no reduction in amyloid content was observed for the 1:1 sample with the wild-type 45–54 sequence. For these images, $T0 = 0$ h, $T1 = 33.75$ h, and $T2 = 75$ h. *f*, no reduction in amyloid content was observed for the 1:1 sample with peptide 71–82W. For these images, $T0 = 0$ h, $T1 = 28.75$ h, and $T2 = 75$ h. For all samples, many images were taken at each time point to confirm the morphology and number of fibrils present in each image.

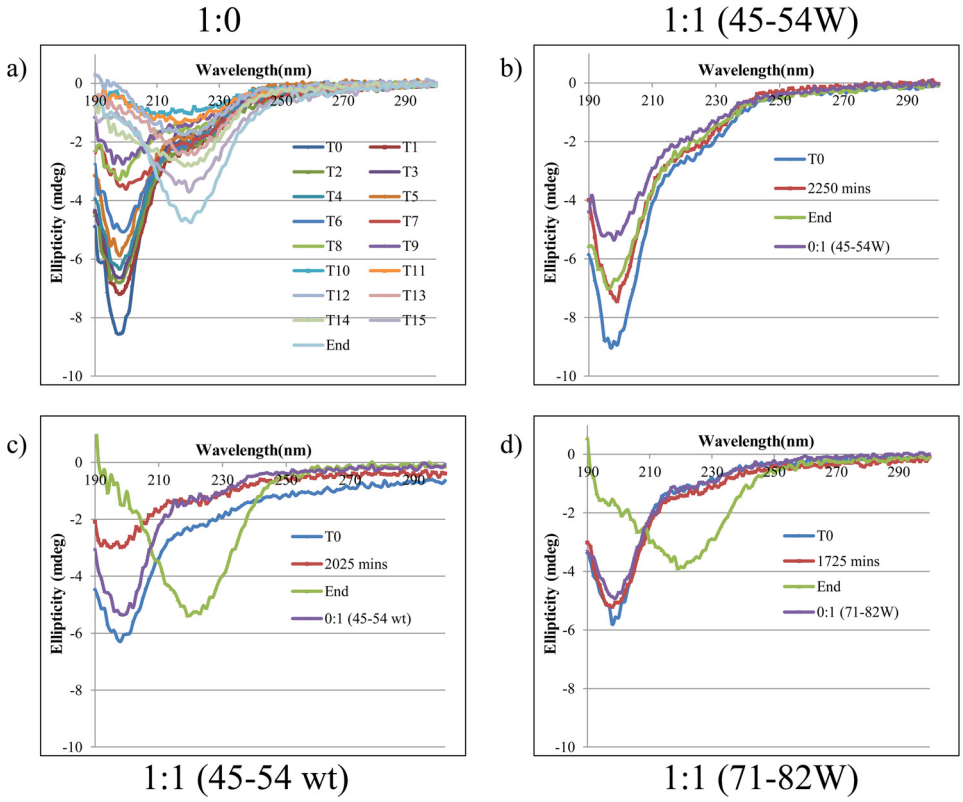

FIGURE 4. *a*, CD spectra of the same samples used in the ThT and AFM experiments. Shown is the gradual development of a minimum at 218 nm across the time course along with the loss of a minimum at 200 nm, consistent with the gain of β-sheet structure and the loss of a random coil in the 1:0 sample. *b*, in the 1:1 samples, the minimum at ~200 nm was prominent even after 75 h of incubation, with no development of a 218 nm signal, confirming the efficacy of peptide 45–54W in preventing the formation of β-sheet structure. A similar spectrum was obtained for peptide 45–54W (0:1 samples), confirming that the peptide does not adopt a β-sheet structure in isolation. *c*, a 1:1 sample with the wild-type 45–54 sequence had no effect upon conversion to the β-sheet structure and loss of a random coil. The wild-type 45–54 sequence in isolation (0:1 samples) did not adopt a β-sheet structure in isolation. *d*, similarly, a PCA-derived peptide based on region 71–82 of α-syn had no effect upon conversion to β-sheet structure and loss of a random coil. Again peptide 71–82W in isolation (0:1 samples) did not adopt a β-sheet structure in isolation. *mdeg*, millidegrees.

intensity at 218 nm for α-syn incubated with peptide 45–54W is unlikely to be attributed to increased aggregation or precipitation. This is because any peptides causing increased precipitation would also generate large increases in ThT binding and would be clearly observed in AFM imaging experiments. Neither wild-type α-syn(45–54) nor peptide 71–82W had any effect upon conversion to the β-structure (Fig. 4, *c* and *d*), again demonstrating α-syn specificity for peptide 45–54W.

MTT Studies Demonstrate Reduced Amyloid Toxicity of Cells—MTT cell toxicity experiments were performed using rat pheochromocytoma (PC12) neuron-like cells to assess the toxicity of α-syn and the preventative effects of peptide 45–54W generated in this study. MTT assays were performed at a α-syn/peptide 45–54W ratio of 1:1 and are presented as raw A_{570} signal (Fig. 5*a*). At this stoichiometry, peptide 45–54W improved cell viability by 65–85% relative to α-syn in isolation. Dose dependence experiments demonstrated that at molar ratios of 1:0.01 and 1:0.1, there was no effect on toxicity. At 1:0.5, the recovery was improved, maximizing at 1:1 and becoming less pronounced at increasingly higher molar ratios (Fig. 5*b*). In addition, MTT experiments using samples taken throughout the continuous growth experiment demonstrated that α-syn became progressively more toxic with time and was most toxic within the stationary phase of fibril growth (Fig. 5*c*). As predicted from ThT, CD, and AFM experiments, MTT experiments using the wild-type 45–54 sequence or peptide 71–82W demonstrated that although these peptides were not toxic in isolation, they had very little effect on α-syn toxicity (Fig. 5*d*). Finally, increasing the concentrations of peptide 45–54W in isolation demonstrated that it was not toxic.

SDS-PAGE Analysis Demonstrates that Peptide 45–54W Is Able to Interact with α-syn and Lower the Oligomeric State—A range of samples were taken from the end point (75 h) of the continuous growth experiments and subjected to SDS-PAGE analysis (Fig. 6). Two clear bands at ~40 and ~60 kDa (as determined by graph analysis of log molecular mass *versus* relative migration distance; data not shown) were found to be present in the 1:0 sample, as well as in the 1:0.01, 1:0.1, and 1:2 samples and, to a lesser extent, the 1:5 sample, suggesting the presence of α-syn trimers (40/14.5 = 2.8) and tetramers (60/14.5 = 4.1). No bands corresponding to dimers or 5–8-mers were observed. At a molar ratio of 1:1 or higher, these bands were found to absent and were replaced with three low molecular mass bands. One band at ~15 kDa may represent the α-syn·peptide 45–54W complex. The second and third bands are below the resolution limit of the gel but are likely to represent monomeric α-syn (14.5 kDa) and the inhibitor alone (1 kDa). Although under denaturing conditions (therefore precluding more detailed interpretation), this experiment demonstrated that

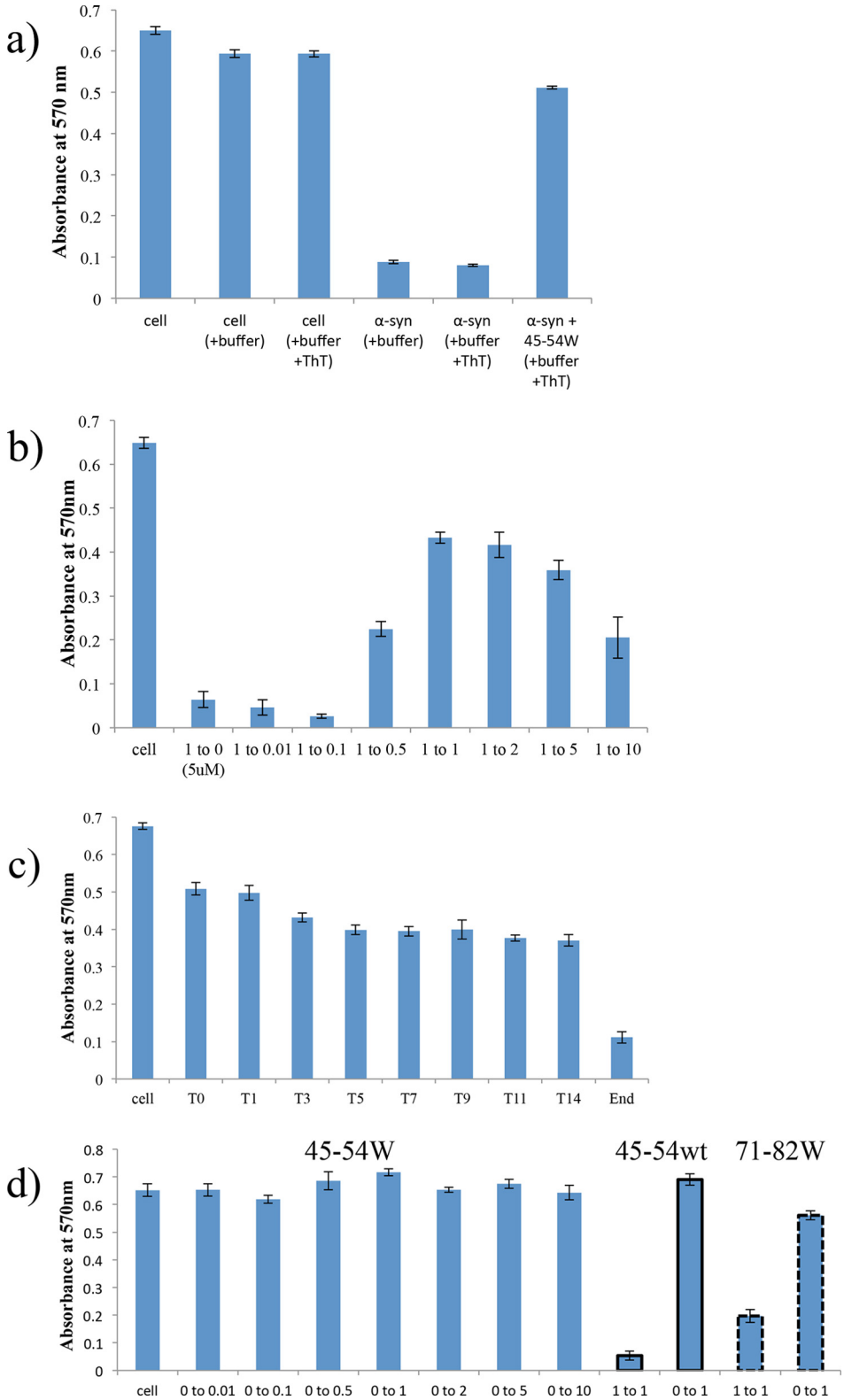

FIGURE 5. **MTT cytotoxicity assays using rat pheochromocytoma (PC12) cells and α-syn and the inhibitory effect of peptide 45–54W on α-syn aggregation.** *a*, shown from left to right are PC12 cells only, PC12 cells plus buffer, PC12 cells plus buffer and ThT, PC12 cells plus α-syn (5 μM) in buffer, PC12 cells plus α-syn (5 μM) in buffer plus ThT, and α-syn with peptide 45–54W at a 1:1 stoichiometry. The latter led to a large restoration of activity (~85%). *b*, increasing α-syn/peptide 45–54W molar ratios demonstrates a dose dependence. Samples were taken from the end point of the continuous growth experiment (75 h) and show that no effect on toxicity was observed at 1:0.01 or 1:0.1 and that a molar ratio of 1:0.5 was needed to partially rescue the cells (~28% recovery) from the cytotoxic effect of α-syn. This increased at 1:1 (~63%) and became progressively less pronounced at increasingly higher molar ratios. *c*, effect of incubation time on toxicity using samples taken directly from the continuous growth experiment. Results demonstrate that toxicity progressively increased as the sample aged and was at its maximum in the stationary phase of continuous growth. *d*, increasing concentrations of peptide 45–54W demonstrate that the peptide in isolation was not toxic to PC12 cells. MTT experiments using wild-type 45–54 sequence or peptide 71–82W demonstrate that the peptide was not toxic in isolation but at a ratio of 1:1 with α-syn had almost no effect upon toxicity. All experiments were undertaken in triplicate, and errors are shown as S.D.

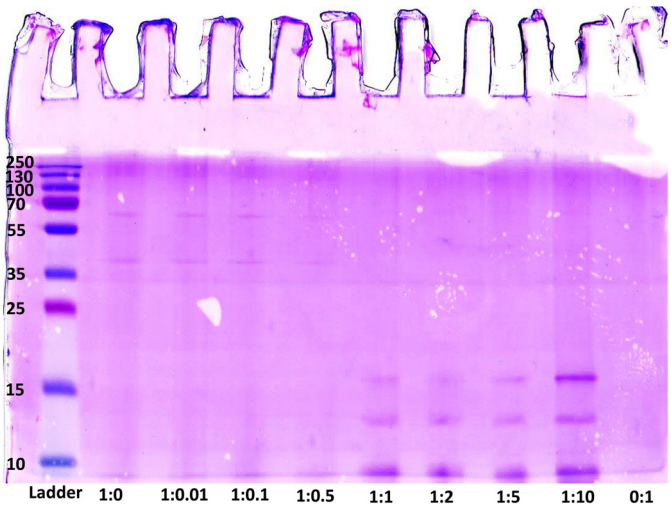

FIGURE 6. **SDS-PAGE analysis shows a range of samples taken from the end point (75 h) of continuous growth experiments.** Two clear bands at ~40 and ~60 kDa (as determined by graph analysis of log molecular mass *versus* relative migration distance) are present in the 1:0 sample, as well as in the 1:0.01, 1:0.1, 1:2, and 1:5 samples, suggesting the presence of α-syn trimers (40/14.5 = 2.8) and tetramers (60/14.5 = 4.1). At molar ratios of 1:1 or higher, these bands were absent and were replaced with three low molecular mass bands. One band at ~15 kDa may represent the α-syn·peptide 45–54W complex. The second and third bands are below the resolution limit of the gel but are likely to represent monomeric α-syn (14.5 kDa) and the inhibitor alone (1 kDa).

peptide 45–54W was able to interact with α-syn and lower the oligomeric state, possibly to the monomer.

DISCUSSION

In conclusion, we employed a semirational design combined with intracellular PCA to demonstrate this as an effective methodology for developing α-syn aggregation antagonists. To date, the majority of β-sheet breaker compounds either are designed to target or are based specifically on region 71–82 of the protein because it is known to aggregate in isolation and therefore thought to be responsible for instigating amyloidosis of the parent protein. Inhibitors include *N*-methylated derivatives of the same sequence (9), single-chain antibodies (31), and small-molecule compounds such as curcumin (32) and epigallocatechin gallate (33).

In contrast, our approach has focused on the development of a library centered on sequence 45–54, in which four of the five known α-syn familial mutants implicated in early-onset PD are found. All of the known mutations in this region result in either increased α-syn aggregation rates or increased numbers of oligomers and therefore increased levels of toxicity. All residues in sequence 45–54 were therefore scrambled to give two, three, or six options, giving rise to a library of 209,952 members (Fig. 1). This was constructed to include all wild-type options and the mutations found in E46K, A53T, and H50Q, respectively. Half of the 10 positions reselected the wild-type residues, whereas the remaining five resulted in new selections. These were E46D, V48I, H50N, A53K, and T54A. In amyloid inhibition experiments (*i.e.* inhibitor and monomeric α-syn mixed at time 0 and amyloid growth continuously monitored) and at a stoichiometry of 1:1, we observed that the classical sigmoidal amyloid growth for an inhibitor-free (1:0) sample was abolished. Instead, the signal was held at ~8% of the signal observed in the stationary phase of the 1:0 sample. At a stoichiometry of 1:0.5, amyloid growth was significantly slower, taking approximately twice as long for the fluorescence intensity to match that of the 1:0 sample. In accordance with an expected dose dependence, at a 1:0.1 stoichiometry or lower, the inhibitory effect was lost. The impressive efficacy of the 1:1 sample in continuous growth ThT experiments is supported by both CD data, which show that the conversion from a random coil-like structure consistent with native α-syn to a classical amyloid β-sheet signal did not occur in the 1:1 sample, and MTT data, which show that toxicity associated with α-syn aggregation was almost completely reversed in the presence of peptide 45–54W. Moreover, a clear reduction to almost no fibrils was observed by direct AFM imaging. This was corroborated by SDS-PAGE experiments showing the loss of low molecular mass oligomers in the presence of peptide 45–54W at a 1:1 stoichiometry or higher.

We have designed a library based on sequence 45–54 of wild-type α-syn and have created a potent peptide inhibitor of aggregation. In the future, it may be possible to derive more potent inhibitors of the mutagenic versions of α-syn that are in turn more effective with the wild-type protein. Not only does this point toward a new target for the design of new inhibitors, the peptide derived here using PCA has the potential itself to be modified into drugs to slow or even prevent the onset of PD.

Acknowledgments—We acknowledge use of the Park Systems XE-120 atomic force microscope, which was on loan from the Engineering and Physical Sciences Research Council Engineering Instrument Pool. We thank Dr. Miao Yu for excellent technical support.

REFERENCES

1. Fink, A. L. (2006) The aggregation and fibrillation of α-synuclein. *Acc. Chem. Res.* **39,** 628–634
2. Cookson, M. R. (2009) α-Synuclein and neuronal cell death. *Mol. Neurodegener.* **4,** 9
3. Irvine, G. B., El-Agnaf, O. M., Shankar, G. M., and Walsh, D. M. (2008) Protein aggregation in the brain: the molecular basis for Alzheimer's and Parkinson's diseases. *Mol. Med.* **14,** 451–464
4. Outeiro, T. F., Putcha, P., Tetzlaff, J. E., Spoelgen, R., Koker, M., Carvalho, F., Hyman, B. T., and McLean, P. J. (2008) Formation of toxic oligomeric α-synuclein species in living cells. *PLoS ONE* **3,** e1867
5. Giasson, B. I., Murray, I. V., Trojanowski, J. Q., and Lee, V. M. (2001) A hydrophobic stretch of 12 amino acid residues in the middle of α-synuclein is essential for filament assembly. *J. Biol. Chem.* **276,** 2380–2386
6. Madine, J., Doig, A. J., Kitmitto, A., and Middleton, D. A. (2005) Studies of the aggregation of an amyloidogenic α-synuclein peptide fragment. *Biochem. Soc. Trans.* **33,** 1113–1115
7. Periquet, M., Fulga, T., Myllykangas, L., Schlossmacher, M. G., and Feany, M. B. (2007) Aggregated α-synuclein mediates dopaminergic neurotoxicity *in vivo*. *J. Neurosci.* **27,** 3338–3346
8. El-Agnaf, O. M., Paleologou, K. E., Greer, B., Abogrein, A. M., King, J. E., Salem, S. A., Fullwood, N. J., Benson, F. E., Hewitt, R., Ford, K. J., Martin, F. L., Harriott, P., Cookson, M. R., and Allsop, D. (2004) A strategy for designing inhibitors of α-synuclein aggregation and toxicity as a novel treatment for Parkinson's disease and related disorders. *FASEB J.* **18,** 1315–1317
9. Madine, J., Doig, A. J., and Middleton, D. A. (2008) Design of an *N*-methylated peptide inhibitor of α-synuclein aggregation guided by solid-state NMR. *J. Am. Chem. Soc.* **130,** 7873–7881
10. Lesage, S., Anheim, M., Letournel, F., Bousset, L., Honoré, A., Rozas, N., Pieri, L., Madiona, K., Dürr, A., Melki, R., Verny, C., Brice, A., and French

Parkinson's Disease Genetics Study Group (2013) G51D α-synuclein mutation causes a novel parkinsonian-pyramidal syndrome. *Ann. Neurol.* **73,** 459–471
11. Bussell, R., Jr., and Eliezer, D. (2001) Residual structure and dynamics in Parkinson's disease-associated mutants of α-synuclein. *J. Biol. Chem.* **276,** 45996–46003
12. Greenbaum, E. A., Graves, C. L., Mishizen-Eberz, A. J., Lupoli, M. A., Lynch, D. R., Englander, S. W., Axelsen, P. H., and Giasson, B. I. (2005) The E46K mutation in α-synuclein increases amyloid fibril formation. *J. Biol. Chem.* **280,** 7800–7807
13. Ghosh, D., Mondal, M., Mohite, G. M., Singh, P. K., Ranjan, P., Anoop, A., Ghosh, S., Jha, N. N., Kumar, A., and Maji, S. K. (2013) The Parkinson's disease-associated H50Q mutation accelerates α-synuclein aggregation *in vitro*. *Biochemistry* **52,** 6925–6927
14. Rutherford, N. J., Moore, B. D., Golde, T. E., and Giasson, B. I. (2014) Divergent effects of the H50Q and G51D SNCA mutations on the aggregation of α-synuclein. *J. Neurochem.* **131,** 859–867
15. Pelletier, J. N., Campbell-Valois, F. X., and Michnick, S. W. (1998) Oligomerization domain-directed reassembly of active dihydrofolate reductase from rationally designed fragments. *Proc. Natl. Acad. Sci. U.S.A.* **95,** 12141–12146
16. Mason, J. M., Schmitz, M. A., Müller, K. M., and Arndt, K. M. (2006) Semirational design of Jun-Fos coiled coils with increased affinity: universal implications for leucine zipper prediction and design. *Proc. Natl. Acad. Sci. U.S.A.* **103,** 8989–8994
17. Acerra, N., Kad, N. M., Cheruvara, H., and Mason, J. M. (2014) Intracellular selection of peptide inhibitors that target disulphide-bridged Aβ42 oligomers. *Protein Sci.* **23,** 1262–1274
18. Acerra, N., Kad, N. M., and Mason, J. M. (2013) Combining intracellular selection with protein-fragment complementation to derive Aβ interacting peptides. *Protein Eng. Des. Sel.* **26,** 463–470
19. Butt, T. R., Edavettal, S. C., Hall, J. P., and Mattern, M. R. (2005) SUMO fusion technology for difficult-to-express proteins. *Protein Expr. Purif.* **43,** 1–9
20. Fields, G. B., and Noble, R. L. (1990) Solid-phase peptide synthesis utilizing 9-fluorenylmethoxycarbonyl amino acids. *Int. J. Pept. Protein Res.* **35,** 161–214
21. Maurer-Stroh, S., Debulpaep, M., Kuemmerer, N., Lopez de la Paz, M., Martins, I. C., Reumers, J., Morris, K. L., Copland, A., Serpell, L., Serrano, L., Schymkowitz, J. W., and Rousseau, F. (2010) Exploring the sequence determinants of amyloid structure using position-specific scoring matrices. *Nat. Methods* **7,** 237–242
22. Frousios, K. K., Iconomidou, V. A., Karletidi, C. M., and Hamodrakas, S. J. (2009) Amyloidogenic determinants are usually not buried. *BMC Struct. Biol.* **9,** 44
23. Trovato, A., Seno, F., and Tosatto, S. C. (2007) The PASTA server for protein aggregation prediction. *Protein Eng. Des. Sel.* **20,** 521–523
24. Tartaglia, G. G., and Vendruscolo, M. (2008) The Zyggregator method for predicting protein aggregation propensities. *Chem. Soc. Rev.* **37,** 1395–1401
25. Fernandez-Escamilla, A. M., Rousseau, F., Schymkowitz, J., and Serrano, L. (2004) Prediction of sequence-dependent and mutational effects on the aggregation of peptides and proteins. *Nat. Biotechnol.* **22,** 1302–1306
26. Kad, N. M., Myers, S. L., Smith, D. P., Smith, D. A., Radford, S. E., and Thomson, N. H. (2003) Hierarchical assembly of β_2-microglobulin amyloid *in vitro* revealed by atomic force microscopy. *J. Mol. Biol.* **330,** 785–797
27. Shearman, M. S., Ragan, C. I., and Iversen, L. L. (1994) Inhibition of PC12 cell redox activity is a specific, early indicator of the mechanism of β-amyloid-mediated cell death. *Proc. Natl. Acad. Sci. U.S.A.* **91,** 1470–1474
28. Hughes, E., Burke, R. M., and Doig, A. J. (2000) Inhibition of toxicity in the β-amyloid peptide fragment β-(25–35) using *N*-methylated derivatives: a general strategy to prevent amyloid formation. *J. Biol. Chem.* **275,** 25109–25115
29. Pike, C. J., Walencewicz-Wasserman, A. J., Kosmoski, J., Cribbs, D. H., Glabe, C. G., and Cotman, C. W. (1995) Structure-activity analyses of β-amyloid peptides: contributions of the β25–35 region to aggregation and neurotoxicity. *J. Neurochem.* **64,** 253–265
30. Hung, L. W., Ciccotosto, G. D., Giannakis, E., Tew, D. J., Perez, K., Masters, C. L., Cappai, R., Wade, J. D., and Barnham, K. J. (2008) Amyloid-β peptide (Aβ) neurotoxicity is modulated by the rate of peptide aggregation: Aβ dimers and trimers correlate with neurotoxicity. *J. Neurosci.* **28,** 11950–11958
31. Emadi, S., Liu, R., Yuan, B., Schulz, P., McAllister, C., Lyubchenko, Y., Messer, A., and Sierks, M. R. (2004) Inhibiting aggregation of α-synuclein with human single chain antibody fragments. *Biochemistry* **43,** 2871–2878
32. Singh, P. K., Kotia, V., Ghosh, D., Mohite, G. M., Kumar, A., and Maji, S. K. (2013) Curcumin modulates α-synuclein aggregation and toxicity. *ACS Chem. Neurosci.* **4,** 393–407
33. Bieschke, J., Russ, J., Friedrich, R. P., Ehrnhoefer, D. E., Wobst, H., Neugebauer, K., and Wanker, E. E. (2010) EGCG remodels mature α-synuclein and amyloid-β fibrils and reduces cellular toxicity. *Proc. Natl. Acad. Sci. U.S.A.* **107,** 7710–7715

Protein Structure and Folding:

Intracellular Screening of a Peptide Library to Derive a Potent Peptide Inhibitor of α-Synuclein Aggregation

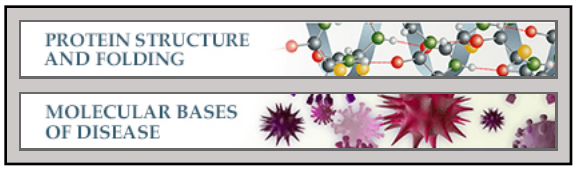

Harish Cheruvara, Victoria L. Allen-Baume, Neil M. Kad and Jody M. Mason

J. Biol. Chem. 2015, 290:7426-7435.
doi: 10.1074/jbc.M114.620484 originally published online January 23, 2015

THE PROTEIN SOCIETY

Intracellular selection of peptide inhibitors that target disulphide-bridged $A\beta_{42}$ oligomers

Nicola Acerra, Neil. M. Kad, Harish Cheruvara, and Jody M. Mason*

School of Biological Sciences, University of Essex, Wivenhoe Park, Colchester, Essex CO4 3SQ, United Kingdom

Received 1 May 2014; Accepted 18 June 2014
DOI: 10.1002/pro.2509
Published online 20 June 2014 proteinscience.org

Abstract: The β-amyloid (Aβ) peptide aggregates into a number of soluble and insoluble forms, with soluble oligomers thought to be the primary factor implicated in Alzheimer's disease pathology. As a result, a wide range of potential aggregation inhibitors have been developed. However, in addition to problems with solubility and protease susceptibility, many have inadvertently raised the concentration of these soluble neurotoxic species. Sandberg *et al*. previously reported a β-hairpin stabilized variant of $A\beta_{42}$ that results from an intramolecular disulphide bridge (A21C/A31C; $A\beta_{42cc}$), which generates highly toxic oligomeric species incapable of converting into mature fibrils. Using an intracellular protein-fragment complementation (PCA) approach, we have screened peptide libraries using *E. coli* that harbor an oxidizing environment to permit cytoplasmic disulphide bond formation. Peptides designed to target either the first or second β-strand have been demonstrated to bind to $A\beta_{42cc}$, lower amyloid cytotoxicity, and confer bacterial cell survival. Peptides have consequently been tested using wild-type $A\beta_{42}$ via ThT binding assays, circular dichroism, MTT cytotoxicity assays, fluorescence microscopy, and atomic force microscopy. Results demonstrate that amyloid-PCA selected peptides function by both removing amyloid oligomers as well as inhibiting their formation. These data further support the use of semirational design combined with intracellular PCA methodology to develop Aβ antagonists as candidates for modification into drugs capable of slowing or even preventing the onset of AD.

Keywords: amyloid; protein misfolding; protein–protein interactions; library screening; protein-fragment complementation assay; Alzheimer's disease

Introduction

It has been widely speculated that small soluble oligomers of Aβ play a major role in the pathology of Alzheimer's disease (AD).[1–4] However, developing drugs that prevent the accumulation of these species has proven difficult. Initial studies that sought to

Abbreviations: Aβ42, β-amyloid 1–42 variant; CD, circular dichroism; HFIP, hexafluoroisopropanol; MTT, (3-(4,5-Dimethylthiazol-2-yl)−2,5-diphenyltetrazolium bromide; PCA, protein-fragment complementation assay; PPI, protein–protein interaction; TEM, transmission electron microscopy; TFA, trifluoroacetic acid; ThT, Thioflavin-T; OAF, oblique angle fluorescence; AFM, atomic force microscopy

Additional Supporting Information may be found in the online version of this article.

Grant sponsor: Pilot project (Alzheimer's Research UK; J.M.M.); Grant number: ART/PPG2008B/2. Grant sponsor: AgeUK [New Investigator Award (#304)]. Grant sponsor: Cancer Research UK Career Establishment Award (J.M.M.); Grant number: C29788/A11738. Grant sponsor: Wellcome Trust Project; Grant number: WT090184MA. Grant sponsor: BBSRC (New Investigator Award N.M.K.); Grant number: BB/I003460/1. Grant sponsor: University of Essex Departmental Studentship (N.A.). Grant sponsor: Parkinson's UK PhD Studentship (H-1001; J.M.M and N.M.K).

*Correspondence to: Jody M. Mason; School of Biological Sciences, University of Essex, Wivenhoe Park, Colchester, CO4 3SQ, United Kingdom. E-mail: jmason@essex.ac.uk

breakdown large insoluble oligomers have in some instances led to an accumulation of small toxic species,[5] while more recent work has shown that even dimers or trimers of Aβ are toxic and able to impair synaptic function.[6] In screening libraries to identify peptides capable of modifying aggregation, an elegant approach would be to lock $A\beta_{42}$ into a toxic conformation. This would ensure population of an oligomeric state that is pathogenically relevant to the disease. Sandberg *et al*. previously studied the effect of an intramolecular disulphide-bridged double mutant of $A\beta_{42}$ (A21C/A31C; $A\beta_{42cc}$).[7] In this approach, conservative mutations were used to create a disulphide bridge and force an otherwise unstructured and monomeric $A\beta_{42}$ into the β-hairpin conformation found in mature fibrils. The conformation, therefore, provides the structural basis for subsequent amyloidogenesis.[8] Disulphide tethering was found to stabilize highly toxic Aβ oligomers that retained the conformational and biological properties of wild-type Aβ. Moreover, these molecules did not go on to convert into mature fibrils and were shown to contain SDS-stable dimeric and trimeric species. Experiments using SH-SY5Y human neuroblastoma cells demonstrated that $A\beta_{42cc}$ oligomers or protofibrillar species formed by these oligomers were 50 times more potent inducers of neuronal apoptosis than amyloid fibrils or samples of monomeric wild-type $A\beta_{42}$, in which toxic aggregates were only transiently formed.

A wide variety of approaches have been used to create amyloid inhibitors, including small molecule, antibody, and peptide-based inhibitors. These have ranged from those that stabilize the native state, sequester monomers, inhibit amyloid growth, as well as those that initiate clearance via chaperones and proteases (see Ref. 9 for an overview). In our own studies, we previously presented a novel variation of the intracellular protein-fragment complementation assay (PCA) selection system whereby bacteria were used to screen peptide libraries and generate Aβ aggregation antagonists[10] and subsequently their retroinversed analogues.[11] During PCA a "core recognition element" $A\beta_{25–35}$, was used as the target since, along with $A\beta_{15–21}$, it is known to form amyloid fibrils in isolation and instigate amyloid formation in the parental protein. $A\beta_{25–35}$ was fused to one half of murine dihydrofolate reductase (mDHFR) with a peptide library fused to the second half. Library members that bound $A\beta_{25–35}$ resulted in a colony under selective conditions. The most effective binders were then further enriched by growth competition to isolate from binders that led to lower growth rates. Reduced bacterial growth rates are due to the inherent propensity for Aβ to aggregate and lead to increased cytotoxic effects.[12,13] Three outcomes are possible for any given library member:

A. Library members bind Aβ, reduce its toxicity and recombine mDHFR to confer cell survival.
B. Library members bind Aβ and recombine mDHFR but either populate or do not prevent population of a toxic species. These result in reduced cell growth relative to 1, or cell death.
C. Library members with no affinity for Aβ and, therefore, no effect on amyloid formation will not recombine mDHFR, resulting in cell death.

Intracellular selection means no assumptions are made regarding the mechanism of antagonist action or which amyloid state becomes populated during selection, aiding the removal of molecules with undesirable properties from the library such as those that are too hydrophobic hence insoluble, those tagged for degradation, those susceptible to protease action, and those that are nonspecific.

To further strengthen this approach, we report on the use of full length $A\beta_{42cc}$ as the target molecule rather than $A\beta_{15–21}$ or the $A\beta_{25–35}$ amyloidogenic regions of the molecule used previously.[10] In this experiment, PCA is undertaken using $A\beta_{42cc}$ under oxidizing conditions to ensure that:

1. During selection the Aβ42cc target is constrained into the β-hairpin structure associated with the pathology of the disease
2. The "core recognition elements" of Aβ42cc associated with instigation of amyloid formation remain exposed, largely unmodified, and in the correct conformation.
3. Aβ42cc is able to form soluble oligomeric structures that are highly toxic and associated with AD pathology, thus ensuring that a larger number of structurally relevant epitopes are presented relative to larger and/or insoluble fibrils populated in the absence of the bridge.
4. Expressing the increased toxicity variant Aβ42cc raises the sensitivity of the PCA relative to Aβ42. This is because cells in scenario B above are predicted to die more readily or grow at reduced rates.

We find the peptides derived using this approach to be capable of binding to the disease relevant wild-type $A\beta_{42}$ and reducing associated amyloid formation. To understand the mechanism of peptide action we have studied the effectiveness of peptides and found them to be capable of removing preformed fibrils as well as preventing amyloid from forming. These studies have successfully produced a number of lead peptide sequences that are expected to provide a scaffold for future drug candidates.

Results

We have combined semirational design with intracellular selection using amyloid-PCA to screen peptide

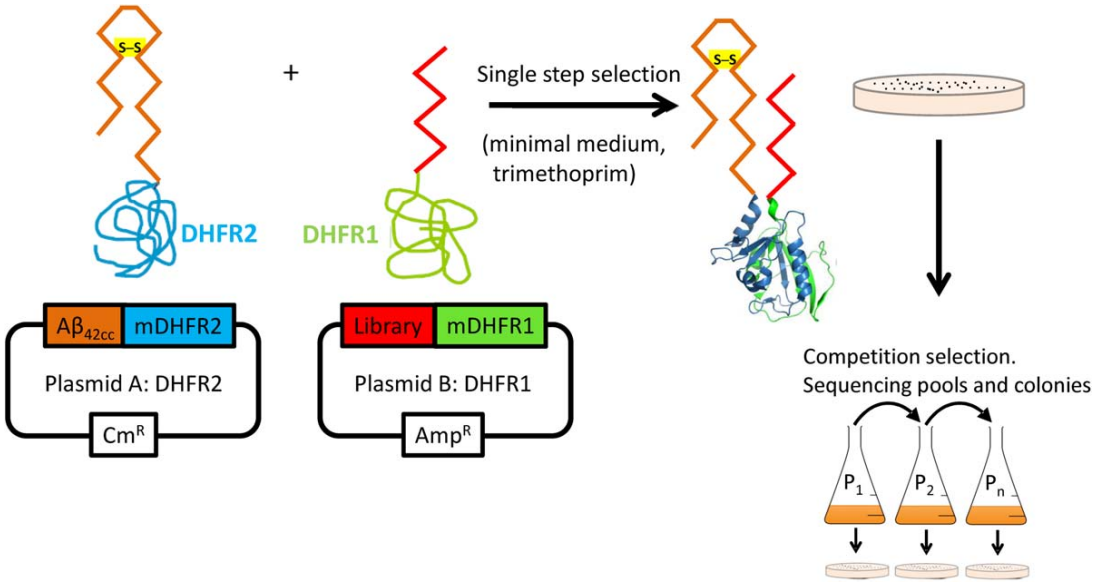

Figure 1. The PCA for amyloid systems. Selection is undertaken using SHuffle cells that harbor an oxidizing cytoplasmic environment to promote disulphide bond formation. Library members that bind to $A\beta_{42cc}$ lead to the recombination of murine DHFR and lead to a colony under selective conditions (bacterial DHFR is specifically inhibited using trimethoprim). Subsequent competition selection in liquid media isolates winners of highest efficacy. Those library members that bind the target and are able to confer faster growth rates by reducing the toxic effects of the amyloid protein most effectively will be selected. As the assay is performed in the cytoplasm of *E.coli*, any nonspecific, unstable, aggregation prone (insoluble), protease susceptible members are removed.

libraries and select $A\beta_{42}$ aggregation antagonists.[10,14,15] A disulphide-bridged variant of $A\beta_{42}$, known as $A\beta_{42cc}$, has been used as the target for library screening since it constrains the protein into the β-hairpin structure found in amyloid structures that form oligomers associated with AD toxicity (Fig. 1). PCA libraries were initially screened and selected on M9 minimal agar plates. Following this initial single-step selection, colonies underwent competition selection where they were pooled and grown before dilution into liquid M9 minimal media. This process was repeated multiple times as passages to select for the most effective binding sequence. In this process, 1–2 high affinity binders that inhibit amyloid formation and reduce bacterial toxicity were found to display the fastest growth and dominate the bacterial pool. The selection process indicated that only a very limited subset of library members were able to bind $A\beta_{42cc}$ (<1%) and that these can be further separated during competition selection PCA to isolate the most effective binders. DNA sequencing continued throughout passaging until selection arrived at one discrete peptide. All subsequent aggregation studies were undertaken using $A\beta_{42}$ as $A\beta_{42cc}$ is not found naturally, with ThT binding and TEM data demonstrating that fibrils do not form when the intramolecular disulphide bridge is intact.[7] We demonstrate that the sequences identified using the $A\beta_{42cc}$ target can be transferred to the biologically relevant $A\beta_{42}$.

Library generation

PCA was undertaken using an $A\beta_{42cc}$ target with sequences corresponding to $A\beta_{15-21}$ (QKLVFFA) $A\beta_{29-35}$ (GAIIGLM), and $A\beta_{36-42}$ (VGGVVIA) as library templates. The first of these two regions are known to aggregate into toxic fibrils in isolation[16–18] and therefore provided a strong starting point for deriving peptides known to bind to $A\beta_{42cc}$ and potentially capable of inhibiting aggregation. The third sequence incorporates the two additional C-terminal amino acids (Ile-Ala) that renders $A\beta_{42}$ much more toxic than $A\beta_{40}$. The first library incorporated four fully randomized residues at positions 17–20 of $A\beta_{15-21}$, generating a library size of 160,000 (^{15}QKxxxxA^{21}), and resulted in one winner (cys_{1521}; Table I). Interestingly, this library had previously resulted in no colonies when using either $A\beta_{42}$ or $A\beta_{15-21}$ as target, suggesting an improved epitope for binding on introduction of the cysteine-bridge. Moreover, the selected sequence, QKVLLFA, bared remarkable similarity to the $A\beta_{15-21}$ (QKLVFFA) parental sequence on which it was based, having been enriched during PCA from four fully randomized residues at positions 17–20. The $A\beta_{15-21}$ peptide has been previously shown to form amyloid in isolation and found to be toxic in MTT experiments.[19,20] The second library incorporated four fully randomized positions at 29–30 and 34–35 of $A\beta_{29-35}$, with residues 31–33 fixed from a previous selection,[10] generating a 160,000 member library (^{29}xxKATxx^{35}),

Table I. *PCA Derived Sequences*

Name	Sequence
cys_{1521}	Ac-QK**VLLF**A-NH_2
cys_{2935a}	Ac-**AG**KAT**GL**-NH_2
cys_{2935b}	Ac-**GA**KAT**AN**-NH_2
cys_{3642}	Ac-**RW**GVV**WG**-NH_2
iAβ5	Ac-LPFFD-NH_2

Four libraries consisting of 160,000 members each and based around residues 15–21, 29–35, and 36–42 of the $Aβ_{1–42}$ were fully randomised at positions shown underlined to allow options for all amino acids. A second library consisting of 160,000 members was fully randomised at positions 29–30 and 34–35 with the KAT sequence from the first selection fixed. $Cys_{2935a/b}$ is based on a previously selected sequence that targeted $Aβ_{29–35}$.[10] Acetylation and amidation of the protein was added to mimic the polypeptide backbone and provide additional potential hydrogen-bond acceptors and donors. The positive control sequence, iAβ5, is also shown.

and resulted in two amyloid-PCA winners (cys_{2935a} and cys_{2935b}; Table I) with no sequence homology to the amyloid template on which they were based. The last library fixed residues 38–40 of $Aβ_{36–42}$ as "GVV" as is found in wild-type $Aβ_{40}$ and $Aβ_{42}$, but was fully randomized at residues 36–37 and importantly at residues 41–42 associated with the increased toxicity of $Aβ_{42}$, generating a 160,000 member library (^{36}xxGVVxx^{42}), and resulting in one winner (cys_{3642}; Table I).

Peptide characterization

PCA derived peptide sequences (Table I) were synthesized and characterized using a number of experiments that included thioflavin-T (ThT) dye binding, circular dichroism (CD), oblique angle fluorescence (OAF), and atomic force microscopy (AFM). The results demonstrate that the peptides do not aggregate in isolation, and are able to prevent $Aβ_{42}$ aggregation and/or remove preformed fibrils. In addition, growth competition assays using *E.coli* under PCA conditions in M9 media and an MTT assay using PC12 cells, both using the $Aβ_{42}$ parent peptide, were undertaken to establish cytotoxicity to bacterial and mammalian cells. The growth competition experiments simultaneously demonstrate that peptides bind to $Aβ_{42}$ and reduce its associated toxicity during bacterial selection. MTT experiments were used to establish that the toxicity associated with extracellular $Aβ_{42}$ to mammalian cells could be reduced when incubated in the presence of PCA selected peptides.

Cell growth experiments

The effect of inhibitors on the growth of *E.coli* harboring pES300d-$Aβ_{42cc}$-DHFR2 target and pES230d-antagonist-DHFR1 fusion plasmids as present in the final PCA selection round were tested (Fig. 2). In this experiment, cells were grown in a shaking incubator from a starting OD_{600} of 0.02 under PCA conditions in M9 minimal media containing Cm, Amp, and Kan to retain target and antagonist expressing plasmids as well as pREP4 for expression of the lac repressor. In addition Tmp was included for inhibition of bacterial DHFR and IPTG to induce high levels of target and antagonist expression. This experiment monitors both mDHFR reassembly, and, therefore, binding of antagonist to the $Aβ_{42cc}$ target, as well as the toxicity of the oligomeric state that is populated. As expected, expression of the toxic $Aβ_{42cc}$ did not result in significant levels of growth even though the protein is well documented to self-associate (Fig. 2). In addition, western blots (Supporting Information Fig. S5) show that $Aβ_{42cc}$ is expressed in the soluble fraction, suggesting that the protein is both soluble and toxic and is, therefore, populating toxic protofibrillar structures. All four antagonists in this study, along with the positive control cJun-FosW, were clearly able to restore bacterial growth thereby providing strong evidence for direct binding and reduced toxicity in the context of this bacterial selection system.

ThT experiments demonstrate a reduction in amyloid content

To determine the ability of PCA derived peptides to prevent fibril assembly (inhibition) or to breakdown preformed fibrils (reversal), ThT fluorescence was used as an indicator of the degree to which $Aβ_{42}$ aggregates into amyloid fibrils. In these assays, $Aβ_{42}$

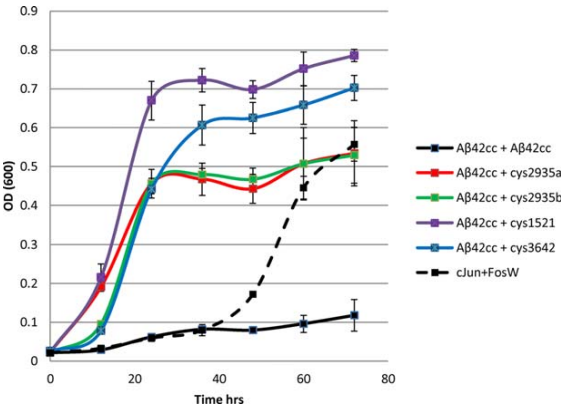

Figure 2. To confirm that expression of $Aβ_{42cc}$-DHFR1 / $Aβ_{42cc}$-DHFR2 fusions impedes the growth rate of *E. coli*, and to ascertain substitution with antagonist-DHFR1 fusions are able to reverse this effect, growth competition experiments were undertaken in M9 liquid media in an identical manner to that during the PCA selection process. In these experiments, cells expressed either i) $Aβ_{42cc}$ + $Aβ_{42cc}$, ii) $Aβ_{42cc}$ + antagonist, or iii) nontoxic cJun+FosW. In this experiment, only scenarios ii) and iii) led to significant growth rates in *E. coli*, providing evidence that a high affinity interaction is formed and that toxicity associated with expression of $Aβ_{42cc}$ has been lowered, leading to significant growth rates relative to i).

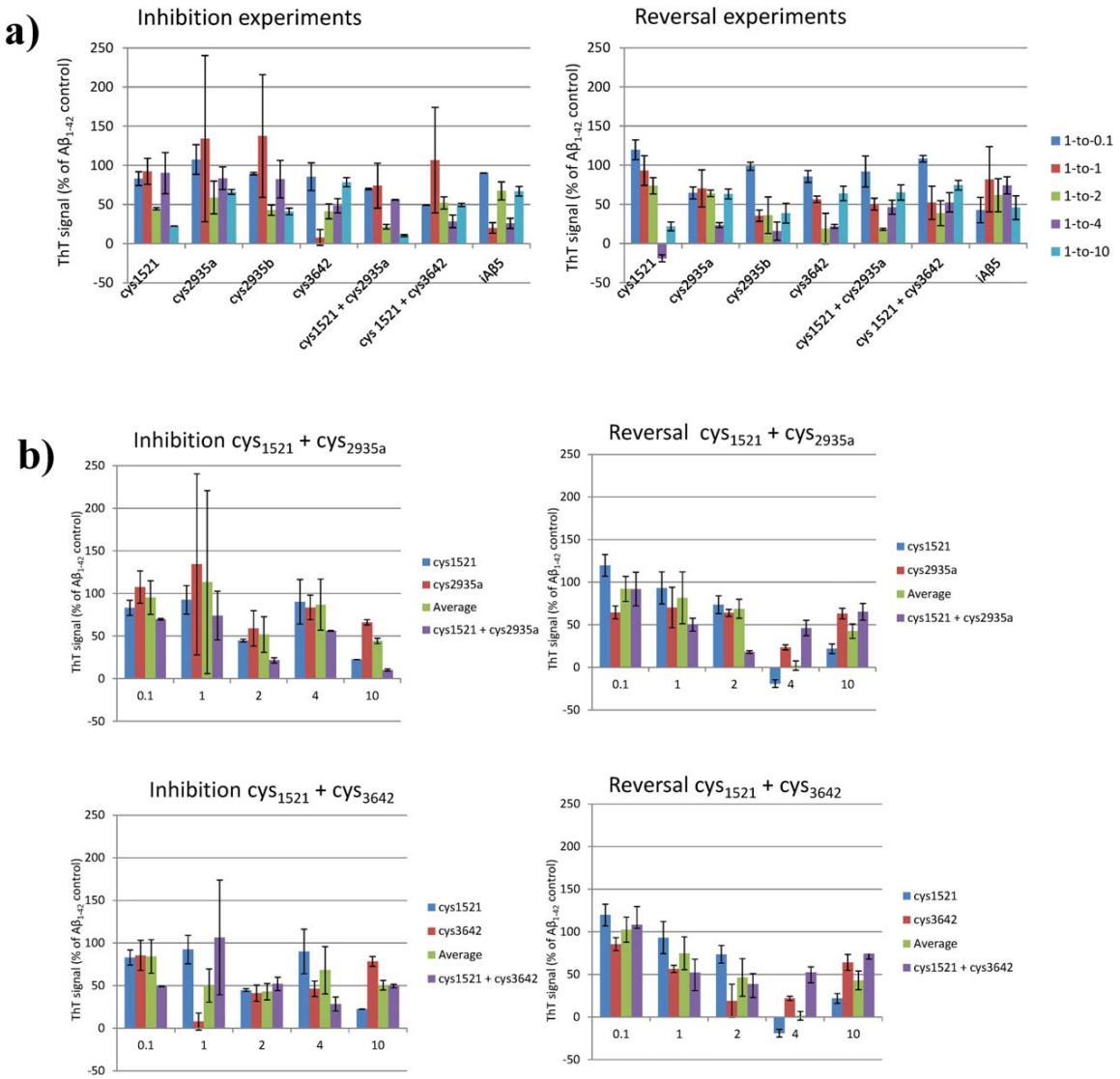

Figure 3. ThT Inhibition and Reversal data for a) individual peptides and b) peptides used in combination. The data show the effects of different stoichiometries of the inhibitors cys_{1521}, cys_{2935a}, cys_{2935b}, cys_{3642}, $cys_{1521} + cys_{2935a}$, $cys_{1521} + cys_{3642}$, and iAβ5 on the aggregation of 50 μ*M* $A\beta_{42}$. The assay was undertaken at 3 days for the inhibition assay. For the reversal assay, $A\beta_{42}$ was incubated in isolation before addition of peptides on Day 3 with the assay undertaken on Day 6. The assay was performed at 10 μ*M* $A\beta_{42}$ concentrations. All errors are expressed as the standard error of the mean.

was rendered monomeric[21] and freeze-dried before being resuspended and incubated at 37°C, leading to formation of amyloid aggregates. For the inhibition assay, PCA-selected peptides were added on Day 0 and their ability to prevent amyloid formation was assessed after 3 days. For the reversal assay $A\beta_{42}$ was incubated in isolation for three days to allow amyloid formation before addition of peptide, followed by incubation for a further 3 days to monitor the ability of peptides to breakdown amyloid aggregates. In all cases, a positive control peptide from the literature (iAβ5[22,23]) known to perform well in ThT assays was used. Figure 3 shows the results of inhibition and reversal experiments for the four single PCA-selected peptides and two examples of peptides administered in combination. Both inhibition and reversal experiments have been undertaken at five different $A\beta_{42}$:peptide ratios ranging from 10-fold substoichiometric to 10-fold superstoichiometric. For every peptide, and at the majority of stoichiometries, the ThT-bound signal was reduced for both inhibition and reversal experiments, indicating that peptides are able to bind $A\beta_{42}$ and lower the amount of ThT-bound amyloid in solution. Consistent with previous studies, changes in $A\beta_{42}$:inhibitor stoichiometry altered binding although it was not clear if this was dependent on dose.[10,24] However, on average the effects observed at ratios of 1:0.1 are small

while ratios of 1:1 are lower than 1:2 or 1:4 (see Supporting Information Fig. S4). These ratios were required to consistently elicit an effect in both inhibition and reversal experiments. Increasing the ratio to 1:10 led to poorer levels of inhibition for several peptides (and consequently increased ThT fluorescence). What is also clear from these experiments is that ThT-bound amyloid can be frequently reduced to less than 50% of the signal found in the $A\beta_{42}$ positive control, with peptides performing well in both inhibition and reversal experiments. Reassuringly, the positive control iAβ5 peptide was also able to reduce the ThT signal by >40%.

In addition, we have conducted experiments where amyloid-PCA derived peptides predicted to target different regions of the disulphide tethered $A\beta_{42cc}$ have been combined [Supporting Information Fig. 3(b)]. These combinations were (a) cys_{1521}/cys_{2935a} and (b) cys_{1521}/cys_{3642}. In both instances, these peptides were derived from libraries based on (and, therefore, predicted to independently target) the first and second strands within the tethered β-hairpin structure of $A\beta_{42cc}$. Indeed, cys_{2935a} is based on a sequence that was selected using the $A\beta_{25-35}$ target,[10] with the same library unable to yield any binding sequences when using the wild-type $A\beta_{42}$ or $A\beta_{15-21}$ as a target. In addition, the library used to generate cys_{1521} was also unable generate any hits against wild-type $A\beta_{42}$. This is significant since it suggests that $A\beta_{42cc}$ represents a far more accessible target for intracellular library screening and antagonist selection. Despite this, ThT experiments in which these peptides were combined generated only one instance where two peptides assayed together were, within error, consistently more effective across the stoichiometries than the average of the individual component peptides [Fig. 3(b)]. This was observed for inhibition experiments that combined cys_{1521} and cys_{2935a}. In this case, an additional 25–35% reduction in ThT fluorescence was observed over the average of the individual peptides at 1:0.1, 1:2, 1:4, and 1:10 stoichiometries, indicating a benefit in combining them [Fig. 3(b), green vs. purple]. At 1:1, large cumulative errors precluded any interpretation. In contrast, combinations of cys_{1521} and cys_{3642} gave no consistent benefit in inhibition experiments. For peptides tested in combination during reversal experiments, no consistent benefit was observed over either peptide assayed alone. Rather, combinations of cys_{1521} and cys_{2935a} displayed signs of synergy at 1:1 to 1:2 molar ratios with the trend reversing for 1:4 and 1:10, indicating that higher concentrations of peptide can lead to increased ThT fluorescence. As increasing the molar ratio did not lead to improvements in the reversal of amyloid in most cases, this indicated that a two-fold excess of peptide:Aβ may be sufficient to reverse fibril formation. A similar trend was true of combining cys_{1521} and cys_{3642} in reversal experiments. However, in both cases the trend was not observed in inhibition assays, perhaps reflecting the fact that more binding sites are available in monomerized $A\beta_{42}$ to which inhibitor can bind and, therefore, remain soluble relative to aged and aggregated samples. Lastly, it cannot be ruled out that the combined peptides do not interact with each other; however, mixing peptides does not result in any gain in amyloid formation as increased ThT signals are not observed.

CD experiments demonstrate a reduction in β-sheet content

As amyloid fibrils are predominately β-sheet, we used CD spectroscopy to provide an end-point characterization of the aggregates formed once ThT experiments were complete. Consistent with a β-sheet structure, spectra show a negative peak at 218 nm. At higher molar ratios (1:2 or greater for inhibition and 1:4 or greater for reversal) an additional large minima of up to −11 millidegrees was observed at 200 nm for the majority of peptides, indicating the adoption of a mixture of β-sheet ($A\beta_{42}$) and random coil-like structures (peptides). This minima was noticeably less pronounced for the cys_{3642} peptide and was not observed for iAβ5, which adopted a spectrum consistent with a β-sheet structure at all concentrations. During CD experiments, we observed a decrease in β-sheet content in the majority of samples, supporting the ThT data by demonstrating that peptides reduce the global β-sheet content relative to the $A\beta_{42}$ sample and, therefore, the amyloid content. These experiments therefore suggest that peptides can bind $A\beta_{42}$ and exert their effect by reducing the amount of protein in the amyloid form. Lastly, ThT and CD spectroscopy experiments undertaken on peptides in isolation that have been incubated at 50 μ*M* for 3 days under conditions identical to those used in aggregation assays using $A\beta_{42}$ demonstrate that peptides do not bind significant amounts of ThT, and that the CD signal for all peptides (at 0:1) is consistent with that of a random coil or weakly helical conformation.

OAF microscopy

Samples used in ThT and CD experiments were also imaged using OAF microscopy for both inhibition and reversal experiments. To prevent bias toward any one sample the experiment was carried out blind.[25] This technique allows for surface associated and stacked aggregates of amyloid fibers to be directly imaged. It was possible to assess the amount of protein deposited as amyloid and its morphology. OAF experiments were undertaken for both inhibition and reversal at all of the molar ratios assayed in ThT experiments (Fig. 4). In almost every case, for both inhibition and reversal experiments, a reduction in the amount of amyloid was observed relative to $A\beta_{42}$ incubated in isolation under

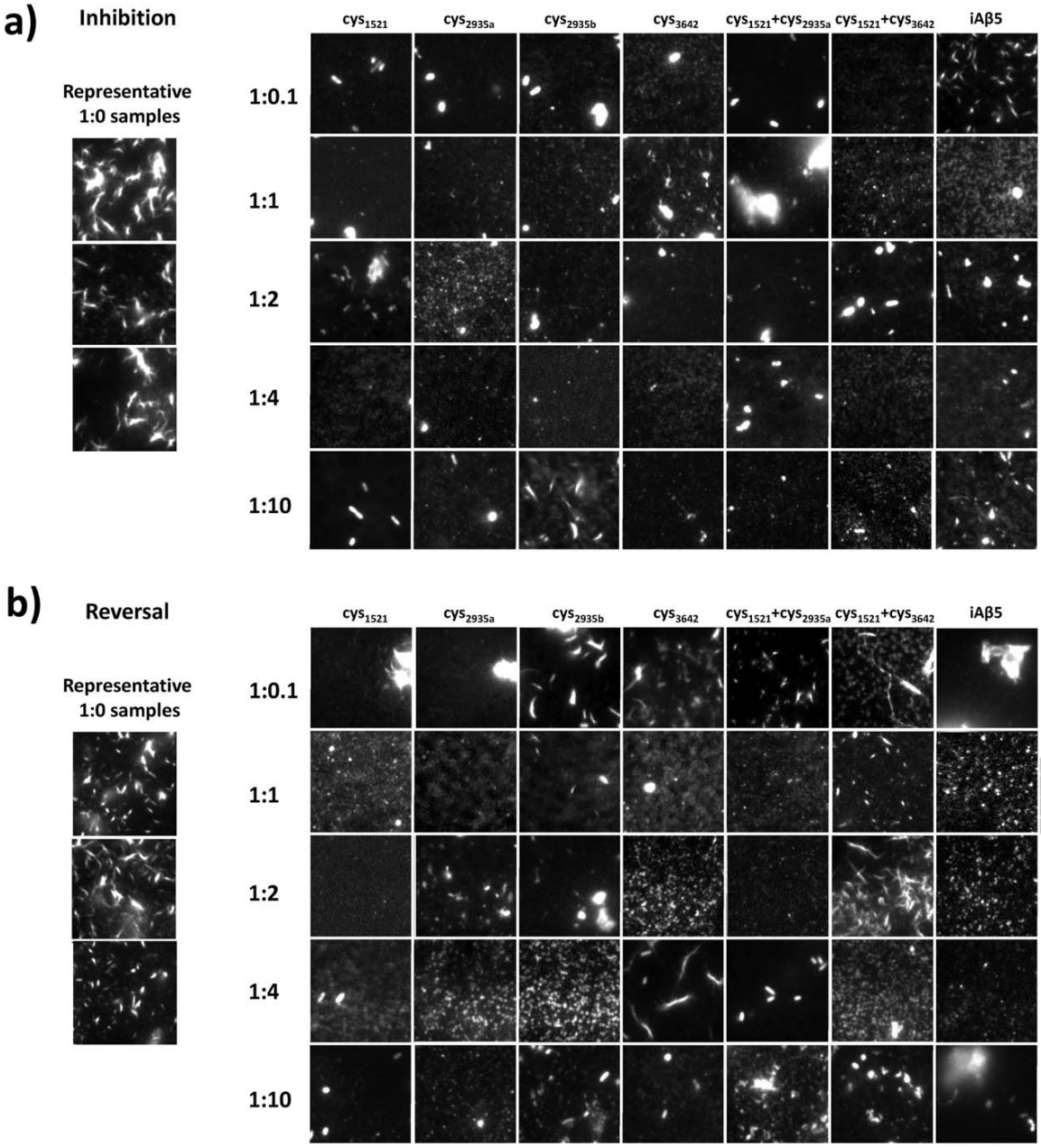

Figure 4. OAF Microscopy data for all inhibitors at all stoichiometries. During inhibition experiments, $A\beta_{42}$ was grown with inhibitor for 3 days and assayed for peptide induced inhibition of amyloid formation. During reversal experiments, $A\beta_{42}$ was grown without inhibitor for 3 days, after which inhibitor was added at a stoichiometry of 1:1 and followed by a further 3 days incubation to assay for peptide induced reversal of amyloid deposition. Each sample was then imaged by fluorescence microscopy and panels showing representative images obtained. To quantify amyloid deposition the mean grey value over a 160 px × 160 px (13 μm × 13 μm) area randomly chosen for five separate images is plotted as fluorescence intensity. Each data point is scaled to overcome the "background noise" by taking Aβ (1:0) as the maximum and iAβ5 as the minimum [i.e., (signal-iAβ5)/($A\beta_{42}$-iAβ5)]. This defines the range over the positive and negative controls.

identical conditions. In a number of cases amyloid deposits much smaller in size were observed.

Atomic force microscopy

Again samples used in ThT and CD experiments were imaged using AFM as a second direct qualitative measure of fibril formation (Fig. 5). A stoichiometry of 1:2 (50 μ*M*:100 μ*M*) was chosen for AFM experiments as this was the concentration at which peptide inhibitors were on average deemed to be most effective in ThT experiments. AFM was undertaken for both inhibition and reversal experiments on

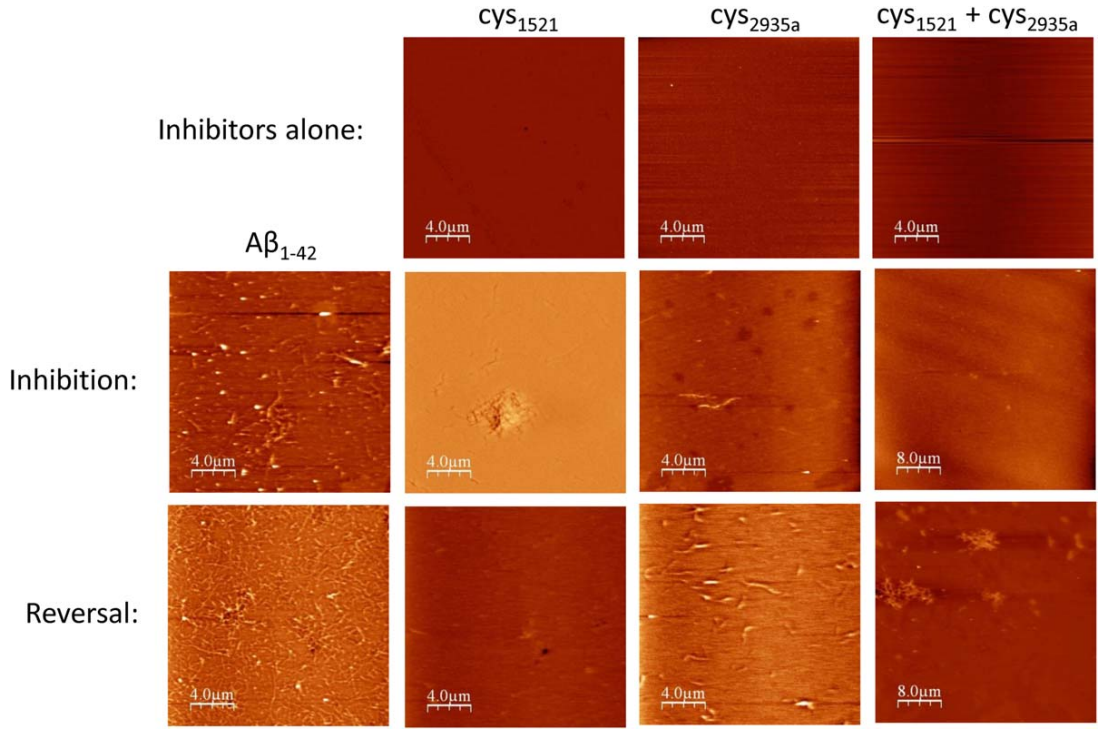

Figure 5. AFM data. To demonstrate that inhibitors cys_{1521}, cys_{2935a}, and $cys_{2935a} + cys_{1521}$ do not aggregate in isolation, they were grown alone for 3 days at a concentration of 100 μ*M* (i.e., 0:2 molar ratio) under the same conditions as inhibition experiments. In all cases, no fibril formation was observed. Inhibition experiments were undertaken at an $A\beta_{42}$:inhibitor stoichiometry of 1:2 (row two). In this experiment, the same sample was used as for ThT experiments, in which $A\beta_{42}$ was grown with inhibitor for 3 days at 37°C. All of the peptides are inhibitory, in particular the combination of $cys_{2935} + cys_{1521}$. For reversal experiments, $A\beta_{42}$ was grown alone for 3 days, after which inhibitor was added at a stoichiometry of 1:2 and followed by a further 3 days incubation to assay for peptide induced reversal of amyloid deposition. Each of the samples were imaged by AFM and panels showing representative images obtained. Also in reversal experiments, it can be clearly observed that for all of inhibitors there is a reduction of fibril, although this is less pronounced than for inhibition experiments. Scale bars are shown.

cys_{1521}, cys_{2935a}, and cys_{1521}+cys_{2935a} as an additional measure of the extent to which these peptides are effective when mixed. A major reduction in the amount of amyloid was observed for all samples relative to the $A\beta_{42}$ control. No fibrils were observed for peptides in the absence of $A\beta_{42,}$ either alone or when mixed. For inhibition experiments in the case of $cys_{1521} + cys_{2935a}$ no fibrils were observed; with mixing appearing to remove fibrils present for the cys_{1521} sample. For reversal experiments, the residual fibrils observed in the cys_{2935a} were also largely removed on mixing with cys_{1521}.

Cell-toxicity experiments

MTT ((3-(4,5-Dimethylthiazol-2-yl)-2,5-diphenyltetrazolium bromide)) cell toxicity experiments were performed using Rat phaeochromocytoma (PC12) neuronal-like cells to reflect the nature of toxicity in the disease via the reduction of a redox dye (Fig. 6). We assessed the toxicity of extracellular $A\beta_{42}$ deposits on PC12 cell integrity and its amelioration by preincubation of $A\beta_{42}$ with peptides. Cells incubated with buffer alone resulted in a reduction of the redox dye MTT, leading to a color change from yellow to purple that can be measured by a change at A_{540}. In contrast, incubation of cells with $A\beta_{42}$ resulted in a large decrease in cell viability and consequently the ability to reduce MTT, leading to a smaller signal change. To study, the ability of inhibitors to reverse the effect on cell viability MTT assays were performed with a range of molar ratios relative to $A\beta_{42}$ and normalized relative to cells in isolation (normalized as 0% death) and cells incubated with $A\beta_{42}$ alone (normalized as 100% death). Although the changes are small and the cumulative errors resulting from comparatively small changes can be large, we were nonetheless able to draw some general conclusions from this assay. In particular, we observed that effective peptides were able to generate modest reductions in toxicity of 5–20% in the majority of cases. Neither cys_{2935a} or cys_{2935b} appeared effective in this assay, displaying almost no improvement across all stoichiometries. Cys_{1521} was able to elicit a small decrease of 5–15% in a nondose dependent manner. Cys_{3642} demonstrated a decrease across all molar ratios of 10–20%. A combination of $cys_{1521} + cys_{2935a}$ or $cys_{1521} + cys_{3642}$ did not conclusively lead to additional lowering of

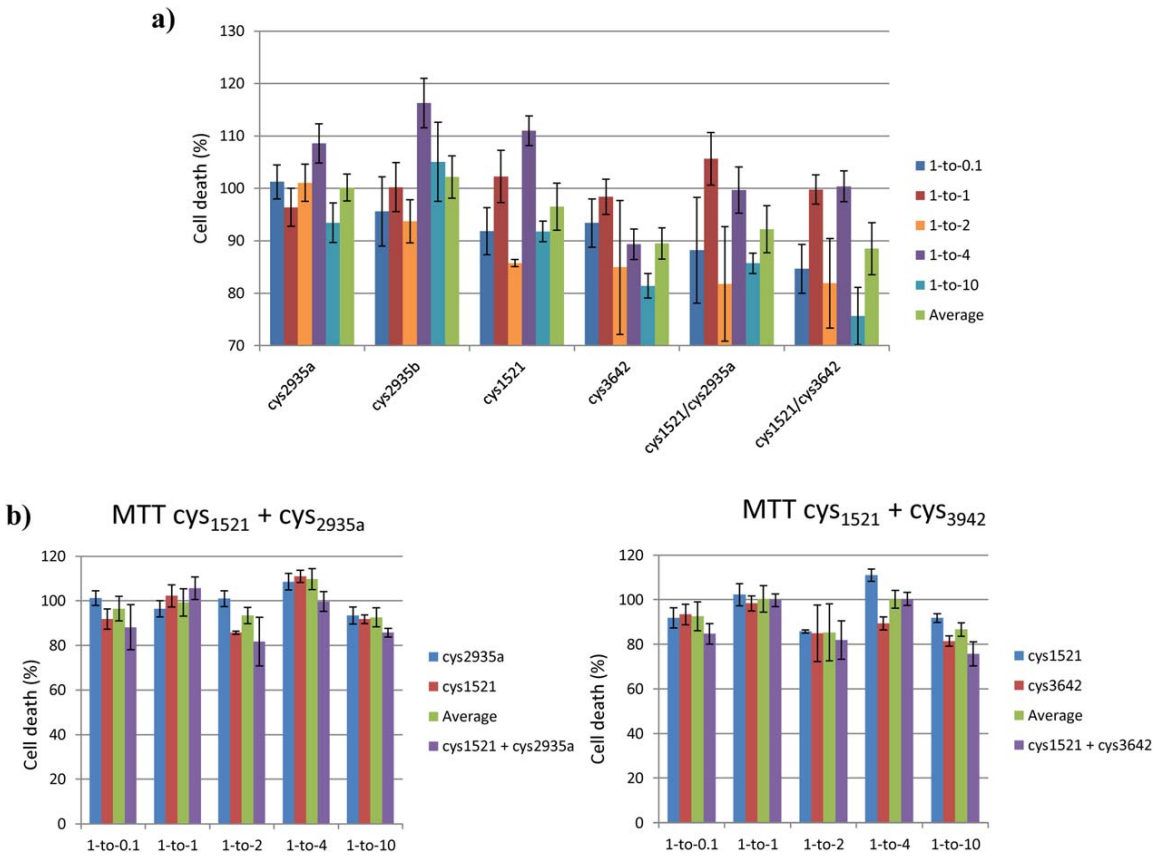

Figure 6. Shown are a) the results from the MTT toxicity assay using $A\beta_{42}$ and selected inhibitors using different molar ratios after 24 h of incubation with PC12 cells. The assay was performed with 10 μM $A\beta_{42}$ and different concentrations of inhibitor, for example, 1:0.1 (1 μM), 1:1 (10 μM), 1:4 (40 μM), 1:10 (100 μM). b) a comparison of the MTT results for individual peptides against those used in combination. All errors are expressed as the standard error of the mean.

toxicity [Fig. 6(b)]. Although reductions in toxicity greater than the average of the component peptides were observed, these were small; 5% for cys_{1521}/cys_{2935a} at 1:10 and 10% for cys_{1521}/cys_{3642} at 1:10. At other molar ratios the errors were either too large or no additional benefits over $A\beta_{42}$ alone were observed. It should be noted that as PCA is undertaken inside bacteria it is possible that intracellular selection of peptides that are nontoxic to *E.coli* may not be as effective when transferred into a mammalian cell system. There, exposure to different off-target interactions and a different protease pool will occur, in addition to the necessity for the peptide to function in the extracellular space, where Aβ is known to aggregate in the brain. This may explain the discrepancy between the effects on growth rates in *E.coli* and efficacy in MTT experiments on peptides incubated with PC12 cells.

Discussion

We have used an intracellular PCA combined with semirational library design to identify peptides that can reverse and inhibit $A\beta_{42}$ aggregation by up to 80% as well as lead to a modest reduction (5–20%) in its toxicity. As a target during bacterial selection, we utilized a double cysteine mutant $A\beta_{42cc}$ (A21C/A30C[7]) that has been shown to lead to the population of pathogenically relevant soluble oligomers in the cytoplasm of an *E.coli* strain that harbors an oxidizing cytoplasm environment.[10,26] An advantage of using PCA with $A\beta_{42cc}$ is that the disulphide bridge forces Aβ into the β-hairpin conformation that is associated with toxicity in AD. The $A\beta_{42cc}$ mutant has been shown to lead to the population of highly toxic oligomers, suggesting that this mutant can be used to improve the stringency of the amyloid-PCA assay. In addition, as oligomers are adopted, we envisage that this conformationally restricted mutant generates an increase in the number of exposed structural epitopes relative to fibrils formed by wild-type $A\beta_{42}$, meaning that more mDHFR activity can be attained within cells harboring binders of this disulphide mutant. To target, the two β-strands either side of the hairpin, we used $A\beta_{15-21}$, $A\beta_{29-35}$, and $A\beta_{36-42}$ as design scaffolds and fully randomized residues at four positions to create three libraries of 160,000 members. All three libraries resulted in the identification of sequences able to bind the target sequence. In the case of wild-type $A\beta_{42}$, it

should be noted that it is possible that the peptide inhibitors may be able to function by stabilizing monomeric $A\beta_{42}$ before it misfolds into the β-hairpin structure, thus preventing conversion into a pathogenic structure. By using the restrained $A\beta_{42cc}$ protein, and because we were unable to identify full length $A\beta_{42}$ binders using many of the same libraries, we infer that the wild-type structure is a poor target for antagonist recognition, possibly due to a lack of well-defined structural epitopes in the nonamyloid or early oligomeric conformations of the molecule. Thus, the generalized approach of using $A\beta_{42cc}$ to screen libraries and generate peptide hits before testing selected peptides on wild-type $A\beta_{42}$ is potentially very exciting.

Combination experiments

As previously noted, we have identified hits from the same 15–21 library that was unable to yield binders for either wild-type $A\beta_{42}$ or $A\beta_{25–35}$ target proteins (unpublished data). The failure to identify binders in these previous PCA screens suggests that the epitope presented was insufficient for effective binding. Thus, we believe that the restricted conformation of $A\beta_{42}$ in the disulphide bridged version represents an improved target for our "recognition-element" based libraries. As the 15–21 library was unable to provide colonies under PCA conditions with $A\beta_{42}$, we instead focused our efforts on the 25–35 region of the molecule. We therefore envisage that the cys_{1521} winner is able to target the first β-strand in the constrained amyloid conformation of $A\beta_{42cc}$, with the cys_{2935} and cys_{3642} libraries targeting the second β-strand. To look for synergy when used in combination, we therefore incubated the cys_{1521} winner with either cys_{2935a} or cys_{3642}. In the case of cys_{1521} and cys_{2935a}, we found a reduction in bound-ThT signal of 20% over the average of the two individual peptides, indicating that there is an added benefit in combining peptides, and that they may occupy different regions within Aβ. MTT data produced large errors, however, improvements in cell viability of 5–10% at some molar ratios were observed, indicating that the combined effect of the inhibitors is greater than the average of the two. In agreement with this, OAF and AFM experiments also suggest that there is an additional benefit in mixing the cys_{1521} and cys_{2935a} peptides.

This study has led to a number of peptides that are capable of preventing assembly of amyloid aggregates as well as breaking down preformed amyloid and further investigation is warranted in the search for molecules that can ultimately slow or even prevent the onset of AD.

Materials and Methods

Mutagenesis and protein engineering

pES300d-$A\beta_{42cc}$-DHFR2 was created using overlap extension PCR with codon changes corresponding to A21C and A30C. These sites have been previously chosen to constrain the peptide into a β-hairpin conformation[7] and are located on nonhydrogen bonded sites between β-strands either side of the hairpin and in close proximity to each other.[27]

Choice of E.coli strain

PCA were undertaken using *E. coli* SHuffle Express cells (New England Biolabs). SHuffle cells have been engineered to possess an oxidative cytoplasmic environment that favors disulphide bond formation. In particular, SHuffle cells have been engineered to lack thioredoxin reductase (*trxB)* and glutathione reductase (*gor)* with an additional suppressor mutation (*ahpC*) which is required to restore viability, allowing the formation of stable disulphide bonds in the cytoplasm. Under these conditions, thioredoxins are in their oxidized state, converting them from reductases to oxidases. Proteins that require disulphide bonds for their folding can, therefore, be oxidized and form stable disulphide bonds within the cytoplasm. This cell line also constitutively expresses a chromosomal copy of the disulphide bond isomerase DsbC. DsbC promotes the correction of misoxidized proteins into their correct form.[10,26]

Single step selection PCA

pES300d-$A\beta_{42cc}$-DHFR2 and pREP4 (Qiagen; for expression of the lac repressor protein) were cotransformed into SHuffle Express cells (New England Biolabs) and plated onto LB agar with the appropriate antibiotics (Kan and Cm). These cells were next made electrocompetent before transformation with the appropriate pES230d-library-DHFR1 library plasmid (*E.coli* XL-1 cells were used for construction and cloning of libraries, as described previously[10,14]). Transformed cells were next plated on three different media; 1/20th of the cells were plated onto LB agar with three antibiotics (Kan, Amp, and Cm) as a positive control of transformation efficiency. A further 1/20th of the solution was plated onto M9 minimal medium agar with 1 μg/ml trimethoprim and the same three antibiotics as a negative control. Finally, the remaining 90% of transformed cells were plated onto M9 minimal agar in the presence of the three antibiotics, 1 μg/ml trimethoprim, and 1 m*M* IPTG (isopropyl-β-D-thiogalactopyranoside), to induce expression of the two DHFR fragment fused peptides). This single-step PCA selection typically led to approximately 50–100 colonies from libraries of 160,000 members, meaning that at least 99% of all library members are removed at this stage owing to their inability to bind $A\beta_{42cc}$ and reduce toxicity.

Competition selection PCA

To increase the selection stringency, growth competition experiments were undertaken. Using this

approach, selected colonies were pooled from the plate and grown in M9 minimal media under selective conditions (containing Kan, Amp, Cm, trimethoprim, and IPTG) and serially diluted over 5–10 passages. Using these sequential rounds of competition selection, subtle differences in growth rate are amplified, increasing the stringency of selection relative to the single-step method. Competition selection, therefore, allows the most effective 1–2 sequences to be isolated from the 50–100 $A\beta_{42cc}$ binders that are initially identified during single step selection. At each passage glycerol stocks were prepared and sequencing results were obtained (GATC biotech, London) for DNA pools as well as individual colonies. For each passage, 50 μL of liquid culture was added to 50 ml of fresh M9 minimal media, resulting in an approximate OD_{600} of 0.01. Cells were incubated at 37°C until an OD_{600} of ~0.4 was reached (typically 2–3 days), before moving to the next passage.

Aβ peptide preparation

$A\beta_{42}$ was purchased as a pure recombinant peptide from rPeptide (Stratech) and was used for all of the experiments described. Prior to use, a quantity of peptide was weighed using an analytical balance before being treated to three rounds of dissolution in hexofluoro-2-propanol (HFIP), sonication, drying, dissolution in trifluoroacetic acid (TFA), sonication and drying, according to the Zagorski protocol,[21] and then aliquoted into appropriately sized batches for subsequent assays and dried via lyophilisation before being dissolved in 10 m*M* potassium phosphate buffer (pH 7.4) to generate a final concentration of 50 μ*M*. TFA/HFIP treatment was used to ensure that amyloid growth always proceeds from the same monomeric state, thus reducing errors in amyloid formation measurements.

Peptide inhibitors

Peptides identified using amyloid-PCA (cys_{1521}, cys_{2935a}, cys_{2935b}, cys_{3642}, and a positive control from the literature, iAβ5[22]), were obtained by Peptide Protein Research (Fareham, UK) as pure lyophilized peptides. Peptides were weighed using an analytical balance and stock solutions of 1 m*M* concentration were subsequently dissolved in ultrapure water. At this concentration (2–200x excess of that used in inhibition and reversal experiments) no aggregation or precipitate was observed. In addition, bioinformatics tools (e.g., Waltz,[28] Amylpred,[29] Pasta,[30] Zyggregator,[31] and Tango[32]) do not predict that any of the peptides contain amyloidogenic sequences or aggregate in isolation. Lastly, CD and ThT experiments on peptide antagonists in isolation demonstrate that these sequences do not bind ThT and form random coil-like species in isolation (see Supporting Information Fig. S1).

Growth competition experiments

To confirm that expression of $A\beta_{42cc}$-DHFR2 fragment fusions impedes the growth rate of *E. coli*, and to ascertain that amyloid-PCA derived peptides fused to the DHFR1 fragment are able to reverse this effect, growth competition experiments were undertaken. These experiments were performed in M9 minimal media in an identical manner to that during the PCA competition selection process. In these experiments (Fig. 2), cells expressed either (i) $A\beta_{42cc}$ control, (ii) $A\beta_{42cc}$ + PCA derived peptide, or (iii) the nontoxic control cJun+FosW. The latter PCA-derived pair is known to form a high affinity interaction, leading to significant growth rates relative to (i).

Circular Dichroism

Far-UV CD spectra were recorded on an Applied Photophysics Chirascan at 20°C using the same samples as for ThT experiments. Spectra were recorded over the 200–300 nm range at a scan rate of 10 nm/min with step size of 1 nm. Spectra were recorded as the average of two scans. Peptide (10 μ*M* in 10 m*M* Potassium Phosphate buffer pH 7.4) was added to a 0.1 cm cuvette (Hellma). Spectra were recorded as raw ellipticity.

Thioflavin T assays

ThT inhibition assays were performed with 50 μ*M* Zagorski treated[21] monomeric $A\beta_{42}$ in 200 μL of 10 m*M* potassium phosphate, pH 7.4, with or without each peptide inhibitor at a concentration of 5 μ*M* (for 1:0.1 molar ratio), 50 μ*M* (for 1:1 molar ratio), 100 μ*M* (for 1:2 molar ratio), 200 μ*M* (for 1:4 molar ratio), and 0.5 m*M* (for 1:10 molar ratio). For the inhibition assays, the target-inhibitor mixtures were incubated together on day zero at 37°C. Single ThT readings were taken on day three at which maximal ThT binding was found. For the reversal assays, 200 μL of 50 μ*M* target was incubated alone at 37°C for 3 days before adding to the required amount of lyophilized peptide. The vortexed target-inhibitor solutions were then incubated at 37°C for a further 3 days, during which time single ThT readings were taken on post-mix Day 3. Experiments were undertaken in duplicate and errors expressed as the standard error of the mean. The ThT assay solution was prepared from a 25× stock containing 500 μ*M* ThT in 250 m*M* Tris, pH 7.4. The stock was aliquoted and kept frozen until required. It was then allowed to thaw at room temperature for 10 min before dilution into the appropriate Tris buffer, giving the required freshly prepared ThT assay solution containing 20 μ*M* ThT in 10 m*M* Tris and buffer at pH 7.4. A total of 2960 μL of the ThT assay solution was then added into 40 μL of each inhibition/reversal assay mixture, thoroughly vortexed and transferred into an appropriate cuvette. The fluorescence of amyloid-bound ThT was measured by

fluorescence spectroscopy using a Cary Eclipse fluorescence spectrophotometer; bound ThT exhibits a new excitation maxima at 450 nm and an enhanced emission maxima at 482 nm.[33]

OAF microscopy experiments

Samples were imaged on a custom built OAF[25] system. The OAF system permits high signal to noise imaging with greater sample depth penetration. Fluorescence imaging was achieved through a 500LP dichroic and clean up filter (Chroma, VT) before entering an Optosplit III triple color image splitter (Cairn, UK), and was detected using an EMCCD camera (Andor DU897, Andor, UK). The emission wavelength range used was 500–565 nm, therefore, both the excitation and emission wavelengths were off peak for ThT, however, the image quality was excellent. All samples were prestained with 10 μM ThT, pipetted onto a clean glass slide, air dried and then imaged in 10 mM potassium phosphate buffer, pH 7.4, supplemented with 100 mM DTT to minimize photobleaching. For consistency and cross-correlation, the same samples were used for inhibition/reversal imaging as those in ThT and CD experiments. In addition, all OAF experiments were performed blind to prevent bias toward any one sample.

AFM experiments

Samples were imaged in noncontact mode using a XE-120 Atomic Force Microscope (Park Systems, South Korea). NSC 15 silicon nitride cantilevers with a spring constant of 40 N/m were used for imaging at a scan rate of 1.0 Hz and a resolution of 256 × 256 pixels. All images were taken at room temperature. The AFM data were taken from inhibitors alone as well as inhibition and reversal experiments, using cys_{1521}, cys_{2935a}, and the $cys_{1521} + cys_{2935a}$ mixture. 5 μL sample was placed on freshly cleaved mica (thickness 0.3 mm). Following adsorption of the protein aggregates (2 min), the mica was washed with 5 mL of double distilled water. Excess water was removed and the samples were dried using a stream of nitrogen gas. Samples were immediately analyzed by AFM.

3-(4,5 Dimethylthiazol-2-yl)-2,5-diphenyltetrazolium bromide cell-toxicity assay

MTT experiments were undertaken using Rat phaeochromocytoma (PC12) cells to assess the effect of the toxicity of $A\beta_{42}$. PC12 cells are known to be particularly sensitive and their use in this assay is well established.[34] The MTT Vybrant® MTT Cell Proliferation Assay Kit (Invitrogen) was used to measure the conversion of the water soluble MTT dye to formazan, which is then solubilized, and the concentration determined by a color change monitored via absorbance measurement at 570 nm. The change in absorbance can then be converted to a percentage MTT reduction which can be used as an indicator of the PC12 cell health in the assay. The assay was performed with 10 μM $A\beta_{42}$ and varying molar ratios of peptide corresponding to 1:0.1 (0.1 μM), 1:1 (10 μM), 1:4 (40 μM), 1:10 (100 μM). PC12 cells were maintained in RPMI 1640 + 2 mM Glutamine medium mixed with 10% Horse Serum, 5% Fetal Bovine Serum, supplemented with a 20 mg/mL Gentamicin. Cells were transferred to a sterile 96-well plate with 30,000 cells per well and experiments performed in triplicate. Briefly, different concentrations of peptides were screened in the presence of 10 μM $A\beta_{42}$. The required volume from peptide and target stock solutions was freeze-dried overnight. The freeze-dried peptide and $A\beta_{42}$ target were resuspended in 100% dimethyl sulfoxide (DMSO), each at 100× stock concentration (i.e., 1, 2, 4, or 10 mM). For example, for the molar ratio 1:1 a total of 5 μL from each of the resuspended inhibitor/DMSO and target/DMSO was mixed in a well of a 96-well preparation plate, thus giving 10 μL of 1:1 mM inhibitor/target concentration ratio in 100% DMSO. A total of 90 μL of RPMI media was added to the 10 μL inhibitor/target mixture (100:100 μM inhibitor/target ratio in 10% DMSO). A total of 10 μL of the 50:50 μM inhibitor/target mixture in 10% DMSO was then dispensed into 90 μL of media/PC12 cells, at final peptide inhibitor and target concentrations of 10 μM. These were incubated for 24 h at 37°C, 5% CO_2, prior to the addition of the MTT dye. A total of 10 μL of the dye was added to each well and incubated for a further 4 h at 37°C, 5% CO_2. A total of 100 μL of the DMSO (stop/solubilization solution) was then added to each well and was allowed to stand for 10 min. The absorbance was measured at 570 nm using a 96-well Versamax tunable microplate reader. Assay values for incubation with buffer were taken as 100% and inhibition of cell function by incubation with buffer containing $A\beta_{42}$ alone taken as 0%. Raw data were then scaled as follows: (raw data point − $A\beta_{42}$ mean)/(buffer mean − $A\beta_{42}$ mean) × 100. The scaled mean for each data set was then plotted with the error given by the standard deviation.

Acknowledgments

The authors acknowledge the use made of the Park Systems XE-120 Atomic Force Microscope which was on loan from the EPSRC (Engineering and Physical Sciences Research Council) Engineering Instrument Pool. The authors wish to thank Dr Miao Yu and Dr Victoria Allen-Baume for excellent technical support throughout the project.

References

1. Lambert MP, Barlow AK, Chromy BA, Edwards C, Freed R, Liosatos M, Morgan TE, Rozovsky I, Trommer B, Viola KL, Wals P, Zhang C, Finch CE, Krafft GA, Klein WL (1998) Diffusible, nonfibrillar ligands derived from Abeta1–42 are potent central nervous system neurotoxins. Proc Natl Acad Sci USA 95:6448–6453.

2. Klein WL, Krafft GA, Finch CE (2001) Targeting small Abeta oligomers: the solution to an Alzheimer's disease conundrum? Trends Neurosci 24:219–224.
3. Haass C, Selkoe DJ (2007) Soluble protein oligomers in neurodegeneration: lessons from the Alzheimer's amyloid beta-peptide. Nat Rev Mol Cell Biol 8:101–112.
4. Walsh DM, Selkoe DJ (2007) A beta oligomers—a decade of discovery. J Neurochem 101:1172–1184.
5. Comery TA, Martone RL, Aschmies S, Atchison KP, Diamantidis G, Gong X, Zhou H, Kreft AF, Pangalos MN, Sonnenberg-Reines J, Jacobsen JS, Marquis KL (2005) Acute gamma-secretase inhibition improves contextual fear conditioning in the Tg2576 mouse model of Alzheimer's disease. J Neurosci 25:8898–8902.
6. O'Nuallain B, Freir DB, Nicoll AJ, Risse E, Ferguson N, Herron CE, Collinge J, Walsh DM (2010) Amyloid beta-protein dimers rapidly form stable synaptotoxic protofibrils. J Neurosci 30:14411–14419.
7. Sandberg A, Luheshi LM, Sollvander S, Pereira de Barros T, Macao B, Knowles TP, Biverstal H, Lendel C, Ekholm-Petterson F, Dubnovitsky A, Lannfelt L, Dobson CM, Hard T (2010) Stabilization of neurotoxic Alzheimer amyloid-beta oligomers by protein engineering. Proc Natl Acad Sci USA 107:15595–15600.
8. Petkova AT, Ishii Y, Balbach JJ, Antzutkin ON, Leapman RD, Delaglio F, Tycko R (2002) A structural model for Alzheimer's beta-amyloid fibrils based on experimental constraints from solid state NMR. Proc Natl Acad Sci USA 99:16742–16747.
9. Hard T, Lendel C (2012) Inhibition of amyloid formation. J Mol Biol 421:441–465.
10. Acerra N, Kad NM, Mason JM (2013) Combining Intracellular selection with protein-fragment complementation to derive Aβ interacting peptides. Protein Eng Des Sel 26:463–470.
11. Acerra N, Kad NM, Griffith DA, Ott S, Crowther DC, Mason JM (2014) Retro-inversal of intracellular selected ABeta interacting peptides: implications for a novel Alzheimers disease treatment. Biochemistry 53:2101–2111.
12. Sharpe S, Yau WM, Tycko R (2005) Expression and purification of a recombinant peptide from the Alzheimer's beta-amyloid protein for solid-state NMR. Protein Expr Purif 42:200–210.
13. Soscia SJ, Kirby JE, Washicosky KJ, Tucker SM, Ingelsson M, Hyman B, Burton MA, Goldstein LE, Duong S, Tanzi RE, Moir RD (2010) The Alzheimer's disease-associated amyloid beta-protein is an antimicrobial peptide. PLoS One 5:e9505.
14. Mason JM, Schmitz MA, Muller KM, Arndt KM (2006) Semirational design of Jun-Fos coiled coils with increased affinity: Universal implications for leucine zipper prediction and design. Proc Natl Acad Sci USA 103:8989–8994.
15. Remy I, Campbell-Valois FX, Michnick SW (2007) Detection of protein-protein interactions using a simple survival protein-fragment complementation assay based on the enzyme dihydrofolate reductase. Nat Protoc 2:2120–2125.
16. Pike CJ, Walencewicz-Wasserman AJ, Kosmoski J, Cribbs DH, Glabe CG, Cotman CW (1995) Structure-activity analyses of beta-amyloid peptides: contributions of the beta 25–35 region to aggregation and neurotoxicity. J Neurochem 64:253–265.
17. Hughes E, Burke RM, Doig AJ (2000) Inhibition of toxicity in the beta-amyloid peptide fragment beta -(25–35) using N-methylated derivatives: a general strategy to prevent amyloid formation. J Biol Chem 275:25109–25115.
18. Hung LW, Ciccotosto GD, Giannakis E, Tew DJ, Perez K, Masters CL, Cappai R, Wade JD, Barnham KJ (2008) Amyloid-beta peptide (Abeta) neurotoxicity is modulated by the rate of peptide aggregation: Abeta dimers and trimers correlate with neurotoxicity. J Neurosci 28:11950–11958.
19. Tjernberg LO, Naslund J, Lindqvist F, Johansson J, Karlstrom AR, Thyberg J, Terenius L, Nordstedt C (1996) Arrest of beta-amyloid fibril formation by a pentapeptide ligand. J Biol Chem 271:8545–8548.
20. Lowe TL, Strzelec A, Kiessling LL, Murphy RM (2001) Structure-function relationships for inhibitors of beta-amyloid toxicity containing the recognition sequence KLVFF. Biochemistry 40:7882–7889.
21. Zagorski MG, Yang J, Shao H, Ma K, Zeng H, Hong A (1999) Methodological and chemical factors affecting amyloid beta peptide amyloidogenicity. Methods Enzymol 309:189–204.
22. Soto C, Kindy MS, Baumann M, Frangione B (1996) Inhibition of Alzheimer's amyloidosis by peptides that prevent beta-sheet conformation. Biochem Biophys Res Commun 226:672–680.
23. Soto C, Sigurdsson EM, Morelli L, Kumar RA, Castano EM, Frangione B (1998) Beta-sheet breaker peptides inhibit fibrillogenesis in a rat brain model of amyloidosis: implications for Alzheimer's therapy. Nat Med 4: 822–826.
24. Kokkoni N, Stott K, Amijee H, Mason JM, Doig AJ (2006) N-Methylated peptide inhibitors of beta-amyloid aggregation and toxicity. Optimization of the inhibitor structure. Biochemistry 45:9906–9918.
25. Kad NM, Wang H, Kennedy GG, Warshaw DM, Van Houten B (2010) Collaborative dynamic DNA scanning by nucleotide excision repair proteins investigated by single-molecule imaging of quantum-dot-labeled proteins. Mol Cell 37:702–713.
26. Levy R, Weiss R, Chen G, Iverson BL, Georgiou G (2001) Production of correctly folded Fab antibody fragment in the cytoplasm of Escherichia coli trxB gor mutants via the coexpression of molecular chaperones. Protein Expr Purif 23:338–347.
27. Mason JM, Gibbs N, Sessions RB, Clarke AR (2002) The influence of intramolecular bridges on the dynamics of a protein folding reaction. Biochemistry 41:12093–12099.
28. Maurer-Stroh S, Debulpaep M, Kuemmerer N, Lopez de la Paz M, Martins IC, Reumers J, Morris KL, Copland A, Serpell L, Serrano L, Schymkowitz JW, Rousseau F (2010) Exploring the sequence determinants of amyloid structure using position-specific scoring matrices. Nat Methods 7:237–242.
29. Frousios KK, Iconomidou VA, Karletidi CM, Hamodrakas SJ (2009) Amyloidogenic determinants are usually not buried. BMC Struct Biol 9:44.
30. Trovato A, Seno F, Tosatto SC (2007) The PASTA server for protein aggregation prediction. Protein Eng Des Sel 20:521–523.
31. Tartaglia GG, Vendruscolo M (2008) The Zyggregator method for predicting protein aggregation propensities. Chem Soc Rev 37:1395–1401.
32. Fernandez-Escamilla AM, Rousseau F, Schymkowitz J, Serrano L (2004) Prediction of sequence-dependent and mutational effects on the aggregation of peptides and proteins. Nat Biotechnol 22:1302–1306.
33. LeVine H, III (1993) Thioflavine T interaction with synthetic Alzheimer's disease beta-amyloid peptides: detection of amyloid aggregation in solution. Protein Sci 2:404–410.
34. Shearman MS, Ragan CI, Iversen LL (1994) Inhibition of PC12 cell redox activity is a specific, early indicator of the mechanism of beta-amyloid-mediated cell death. Proc Natl Acad Sci USA 91:1470–1474.